

Polymorph Evolution Mechanisms and Regulation Strategies of Lithium Metal Anode under Multiphysical Fields

Peichao Zou,[#] Yiming Sui,[#] Houchao Zhan, Chunyang Wang, Huolin L. Xin,* Hui-Ming Cheng, Feiyu Kang,* and Cheng Yang*



Cite This: *Chem. Rev.* 2021, 121, 5986–6056



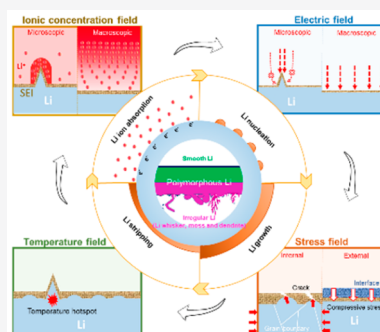
Read Online

ACCESS |

Metrics & More

Article Recommendations

ABSTRACT: Lithium (Li) metal, a typical alkaline metal, has been hailed as the “holy grail” anode material for next generation batteries owing to its high theoretical capacity and low redox reaction potential. However, the uncontrolled Li plating/stripping issue of Li metal anodes, associated with polymorphous Li formation, “dead Li” accumulation, poor Coulombic efficiency, inferior cyclic stability, and hazardous safety risks (such as explosion), remains as one major roadblock for their practical applications. In principle, polymorphous Li deposits on Li metal anodes includes smooth Li (film-like Li) and a group of irregularly patterned Li (e.g., whisker-like Li (Li whiskers), moss-like Li (Li mosses), tree-like Li (Li dendrites), and their combinations). The nucleation and growth of these Li polymorphs are dominantly dependent on multiphysical fields, involving the ionic concentration field, electric field, stress field, and temperature field, etc. This review provides a clear picture and in-depth discussion on the classification and initiation/growth mechanisms of polymorphous Li from the new perspective of multiphysical fields, particularly for irregular Li patterns. Specifically, we discuss the impact of multiphysical fields’ distribution and intensity on Li plating behavior as well as their connection with the electrochemical and metallurgical properties of Li metal and some other factors (e.g., electrolyte composition, solid electrolyte interphase (SEI) layer, and initial nuclei states). Accordingly, the studies on the progress for delaying/suppressing/redirecting irregular Li evolution to enhance the stability and safety performance of Li metal batteries are reviewed, which are also categorized based on the multiphysical fields. Finally, an overview of the existing challenges and the future development directions of metal anodes are summarized and prospected.



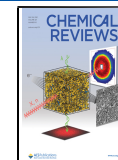
CONTENTS

1. Introduction	5987
2. Fundamentals and Challenges of Li Metal Anode	5988
2.1. Fundamentals of Li Metal Anode	5988
2.1.1. Chemistry and Electrochemistry of Li Metal Anode	5988
2.1.2. Metallurgy of Li Metal Anode	5989
2.2. Challenges of Li Metal Anode	5989
2.2.1. Classification and Definition of Li Polymorphs	5990
2.2.2. Electrochemical Behaviors of Irregular Li	5991
2.2.3. Issues from Irregular Li Formation	5991
3. Theoretical Models and Influencing Factors of Irregular Li Formation	5991
3.1. Ionic Concentration and Electric Fields Influence on Li Metal Evolution	5992
3.1.1. Ionic Concentration Field-Related Models	5993
3.1.2. Electric Field-Related Models	5993
3.1.3. Limitations of Ionic Concentration and Electric Field Models	5994

3.1.4. Influencing Factors on Ionic Concentration and Electric Fields	5995
3.2. Stress Field Influence on Li Metal Evolution	6002
3.2.1. Internal Stress Inside Plated Li Metal	6003
3.2.2. External Stress from Li Metal Surroundings	6005
3.2.3. Influencing Factors on Stress Field	6006
3.3. Temperature Field Influence on Li Metal Evolution	6008
3.3.1. Temperature Field-Related Models	6008
3.3.2. Influence of Temperature on Li Metal Nucleation	6009
3.3.3. Influence of Temperature on SEI Structure	6009

Received: October 9, 2020

Published: April 16, 2021



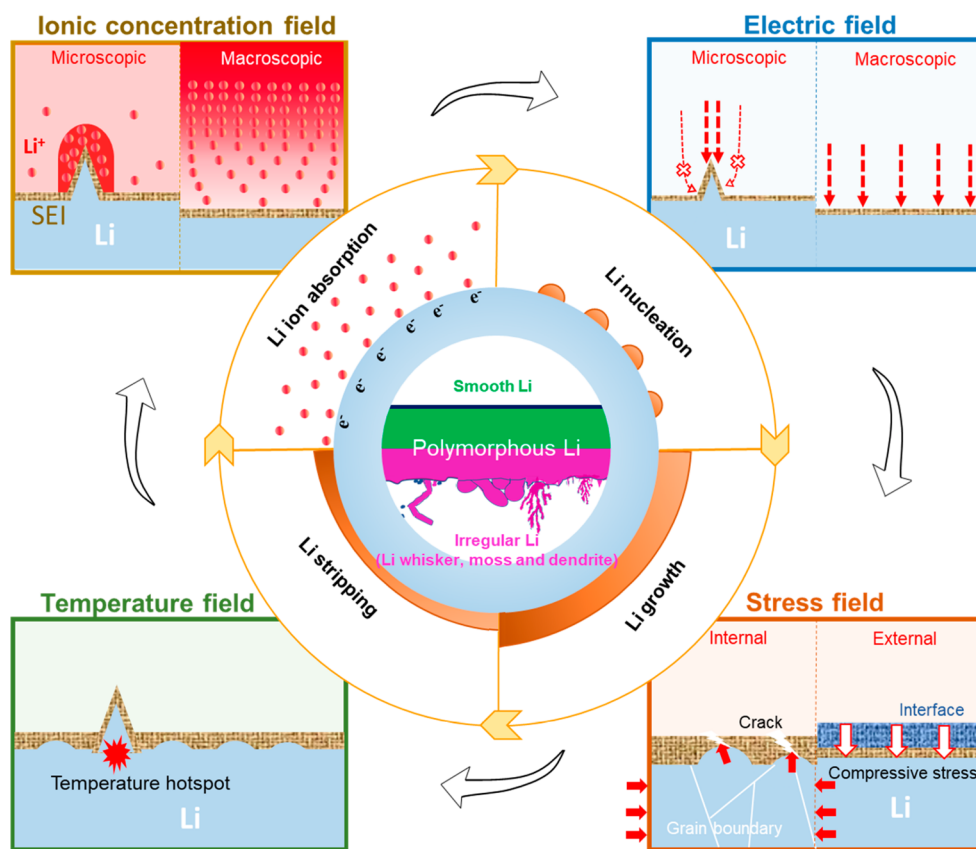


Figure 1. Overview of the connection between multiphysical fields (ionic concentration field, electric field, stress field, and temperature field) and polymorphous Li metal evolution during the entire cycle life.

3.3.4. Influence of Temperature on Li Metal Growth	
3.3.5. Influence of Temperature Homogeneity	
3.4. Connection of Multiphysical Fields on Li Metal Evolution	
4. Li Polymorphs Evolution Management Strategies via Regulated Multiphysical Fields	
4.1. Ionic Concentration Field Regulation	
4.1.1. Reducing Local Reaction Rate	
4.1.2. Uniform and Accelerated Li^+ Diffusion in SEI Layer	
4.1.3. Macroscopic Ionic Concentration Regulation	
4.2. Electric Field Regulation	
4.2.1. Homogenization of Local Electric Field	
4.2.2. Redirection of Macroscopic Electric Field	
4.3. Stress Field Regulation	
4.3.1. Internal Stress Regulation	
4.3.2. External Stress Regulation	
4.3.3. External Applied Pressure Regulation	
4.4. Temperature Field Regulation	
4.4.1. High Working Temperature	
4.4.2. Self-Heating Induced by High Current Density	
4.4.3. Protection at Low Working Temperature	
5. Conclusions and Perspectives	
Author Information	
Corresponding Authors	
Authors	
Author Contributions	
Notes	

Biographies	6046
Acknowledgments	6047
References	6047

6011

1. INTRODUCTION

Reversible energy resources (e.g., sunlight, tide, and wind) are doomed to play crucial roles in the future economy, yet they suffer from instantaneity that compels scientists to find powerful energy storage devices to conserve the electric power derived from them. Lithium ion batteries (LIBs) are undoubtedly one of the most important and successful energy storage devices nowadays, which store and release energy by reversibly converting electric and chemical power.^{1–11} However, the achievable energy density of commercial LIBs almost reaches the ceiling ($\sim 300 \text{ Wh kg}^{-1}$) due to the capacity limitation of conventional intercalation-type anodes, which cannot satisfy the increasing energy/power density demands, particularly in the electric vehicle market.^{12,13} Accordingly, the U.S. Department of Energy (DOE) founded the Battery 500 consortium, aiming to improve the cells' energy density to over 500 Wh kg^{-1} for the application of electric vehicles.¹⁴ From the perspective of anodes, Li metal is considered as the most promising option for next-generation Li-based electrochemical cells, due to its lowest mass density (6.94 g mol^{-1}), volume density (0.534 g cm^{-3}), high theoretical gravimetric/volumetric capacity (3861 mAh g^{-1} , 2061 mAh cm^{-3}), and extremely low standard electrochemical redox potential ($-3.04 \text{ V vs. standard hydrogen electrode, SHE}$) among alkaline metals; all these features endow Li metal batteries (LMBs) (e.g., Li–S battery and Li–air battery)

a higher energy density than commercial LIBs based on graphite anodes.^{4,15,16}

Thus far, a great deal of attention has been attracted to this field with thousands of papers published annually in recent years to accelerate the commercialization of LMBs. Unfortunately, the practical application of LMBs has been plagued by a series of issues, among which the inevitable formation of irregular Li remains one key obstacle. The occurrence of irregular Li is induced by the irregular Li electrodeposition at the interface between deposition substrates and the electrolytes/solid electrolyte interphase (SEI) layer, due to the high electrochemical reactivity and low mechanical strength of Li metal. In principle, irregular Li deposits can be primarily categorized into whisker-like Li (Li whisker), moss-like Li (Li moss), and tree-like Li (Li dendrite), whose morphologies, electrochemical behaviors, formation mechanisms, and corresponding influencing factors vary from each other but deliver close connections. In recent decades, a few theoretical models have been proposed to elucidate the mathematical relationship between irregular Li metal structures and their dominated influencing factors. For instance, the Sand's time model¹⁷ and "space-charge theory"^{18,19} have connected Li dendrite's growth with the cation draining (ion concentration polarization) and electric field aggregation (charge distribution polarization) at deposition sites, respectively, while the occurrence of Li whisker and Li moss has been majorly ascribed to the internal stress accumulation/release and the integrity change of surface-formed SEI layer as influenced by the current density.^{20,21} These models pioneer the mechanistic understanding of polymorphous Li growth and offer valuable guidance to the strategy design for suppressing/delaying/redirectiong irregular Li growth, such as interfacial chemistry regulation,²² electrolyte engineering,²³ nano/microstructural design of Li metal anodes,²⁴ and so forth to eliminate the concentration/electric field distribution polarization and volume change.

Overall, the morphologies of Li polymorphs and their evolution trends are highly dependent on the intrinsic mechanical properties of Li metal and the electrochemical plating conditions (such as current densities, properties of the SEI layer, and temperatures), which are intrinsically related to the influencing factors of multiphysical fields, including the concentration field (majorly connected with the ions transfer in electrolytes), electric field (electron transfer and local electric potential), temperature field (heat), and stress field (associated with the metallurgical properties of Li metal and its surroundings). Despite considerable reviews published in recent years,^{15,16,25–34} few of them have distinguished the properties, formation mechanisms, and regulation principles of Li polymorphs. For instance, different irregular Li patterns are not clearly differentiated and collectively all termed as "dendrites". In addition, both the mechanical and electrochemical properties of Li metal have also been connected much less for discussing the working/failure principles of Li metal anodes. Therefore, the systematic and fundamental understanding of polymorphous Li evolution mechanisms as well as the development of feasible Li metal evolution management strategies are still essential, which are of vital significance for both scientific investigations and industry applications.

In this review, we aim to show a full and clear picture on the formation mechanisms and regulation strategies of polymorphous Li (particularly for irregular Li) in liquid electrolyte based Li metal batteries, specifically from the perspective of multiphysical fields that combine both electrochemical and metal-

urgical effects upon Li metal evolution (Figure 1). First, the distinctive properties and growth processes/mechanisms of polymorphous Li are clarified in detail, and the corresponding influencing factors are also discussed in detail. Second, feasible solutions on delaying/suppressing/redirectiong irregular Li growth are summarized, which can be categorized into four aspects: (1) ionic concentration field regulation, targeted on reducing the local reaction rate, achieving isotropic and accelerated Li⁺ diffusion in the SEI layer, and homogenizing the macroscopic concentration field within the entire anode area; (2) electric field regulation, including the homogenization of local electric field (at local reaction sites) and the redirection of macroscopic electric field (within the entire anode area); (3) stress field regulation, including the internal stress between plated Li metal and external stress from Li metal surroundings; (4) temperature regulation, involving applying a high working temperature, leveraging the self-heating effect induced by a high current density, and related strategies of Li metal protection at low temperatures. Finally, currently remaining challenges of LMBs and some potentially feasible directions are discussed as a reference for future development and large-scale applications. It should be noted that even though all-solid-state LMBs also received much attention lately,^{35–39} they will not be covered too much in this work since it differs from liquid-electrolyte-based LMBs on mechanisms and corresponding problems as focused in this review.

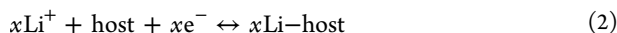
2. FUNDAMENTALS AND CHALLENGES OF LI METAL ANODE

Although Li metal anode has a series of impressive properties, it has to overcome some serious problems (including the irregular Li formation, the "dead Li" accumulation, the thickened SEI layer formation, and so forth) before its commercialization. All these issues are closely correlated to the chemical, electrochemical, and metallurgical properties of Li metal. Fundamental understanding of these properties is helpful to interpret the evolution behaviors of Li metal anode in LMBs. Herein, we first summarize the chemical, electrochemical, and metallurgical properties of Li metal, followed by discussing the classification/definition and the electrochemical behaviors of different Li patterns in the Li metal anode, along with the introduction of the issues caused from irregular Li evolution.

2.1. Fundamentals of Li Metal Anode

2.1.1. Chemistry and Electrochemistry of Li Metal Anode.

A typical LMB consists of a Li metal anode, a sulfur/air/intercalation-type cathode, and a separator soaked with liquid electrolyte in between. The key difference between LMBs and conventional LIBs lies in the energy storage chemistries: Li metal is a hostless anode, presenting the deposition/dissolution mechanism (eq 1), while the anode materials for LIBs are of host-type and follow the Li-(de)intercalation mechanism (such as graphite and Li₄Ti₅O₁₂), alloying mechanism (e.g., Si, Ge, and Sn) or conversion mechanism (particularly for transition metal oxides, nitrides sulfides and phosphides) during the charge/discharge processes (eq 2).⁴⁰ A reversible dissolution reaction will occur during the Li stripping process. Based on the working mechanisms described in eqs 1 and 2, the distribution and migration of charges (Li ions and electrons) play essential roles in the working of Li metal anodes. Thus, optimizing the ion migration and electron distribution behaviors are two basic tasks in LMBs electrochemistry, as it does in LIBs.



Owing to the elimination of host materials, intrinsically small atomic radius, and low volume density of metallic Li, Li metal anode exhibits extremely high gravimetric and volumetric capacities, which exceed those of most other LIB anodes. In addition, Li metal anode displays a low standard reduction potential (-3.04 V vs. SHE), which is far beyond the stability window of most electrolytes; consequently, the electrolyte will be reduced to form a SEI layer on the Li metal surface at the working conditions. Generally, the SEI layer is formed from the decomposition of electrolyte during the initial electrochemical cycle in the lower potential range (below $1 \text{ V vs. Li}^+/\text{Li}$ for carbonate-based solvents) for the anode materials of LIBs.⁴¹ For Li metal anode, due to its extremely high chemical reactivity, the surface SEI layer can also be formed as long as Li metal contacts with the electrolyte. In practical situations, the Li plating/stripping redox reaction often initiates with dozens or hundreds millivolt potential deviation due to the existence of non-equilibrium polarization potential (*i.e.*, overpotential). Meanwhile, analogous to other alkali metals, such as sodium (Na) and potassium (K), Li metal has very high chemical reactivity, which enables it to not only react with O_2 , H_2O , N_2 , and CO_2 in air or dissolved gases in electrolytes but also reduce the liquid electrolytes in cells to form a SEI layer on its surface.⁴²

2.1.2. Metallurgy of Li Metal Anode. The plating/stripping behavior of Li metal anode is regarded as an electrochemical metallic deposition/dissolution process. The “hostless” Li metal anode naturally presents a dramatic volume expansion/shrink characteristic during the plating/stripping process, which far exceeds those of other anode materials (*e.g.*, nearly “zero-strain” for $\text{Li}_4\text{Ti}_5\text{O}_{12}$, $\sim 400\%$ for Si, $\sim 370\%$ for Ge, $\sim 300\%$ for Sn, and $\sim 10\%$ for carbonaceous anodes).⁴³ The distinguished features bring some issues regarding the growth orientation and stress produced inside the anode material or in contact with other components of cells, which are fundamentally related to the metallurgical and mechanical properties of Li metal.

As known, Li is a soft metal with the Young’s modulus of $\sim 10^9 \text{ Pa}$ and the yield strength of $0.4\text{--}0.9 \text{ MPa}$ in the bulk state^{44,45} at room temperature. Notably, the strong variance of the yield strength value of Li bulk metal reported in the literature could be attributed to different microstructures, nonequilibrium defect concentrations, size, and impurity concentrations.⁴⁶ In addition, since Li possesses a very high atomic mobility in comparison to other metals like Zn and Ni owing to its low melting point (180.5°C), it enables the conduction of diffusional creep in a short time.²¹ Therefore, for bulk Li metal, multiple slip systems could be easily activated with a small stress.

In general, the mechanical properties of Li metal are dependent on sample dimensions, temperature, and crystallographic orientations, which could significantly influence the Li metal evolution in Li metal anodes. For example, regarding the dimension effect, nanomechanical experiments conducted by *in situ* scanning electron microscope (SEM) show that micro-meter-sized Li attains an extremely high yield strength of 105 MPa at room temperature.⁴⁷ More recently, *in situ* deformation experiments in transmission electron microscopy (TEM) reveal that with the diameter of Li whisker decreasing to the submicrometer regime, its yield strength increases to as high as 244 MPa .⁴⁸ This significant size effect on the strength of Li metal could be explained by dislocation nucleation-governed

plasticity, which has been universally observed in small-scale single crystalline metals.^{49,50} By using the AFM technique, Zhang *et al.*⁴⁸ figured out that the critical stress (buckling point) shows a distinctive negative correlation with the whisker radius, following eq 3,

$$\sigma_m \approx E^{1/3} \left(\frac{k}{d} \right)^{2/3} \quad (3)$$

where the σ_m stands for the critical stress, E denotes the Young’s modulus, k is the AFM cantilever stiffness, and d represents the radius of the Li whisker. Simultaneously, the critical buckling stress also clearly differs between growth directions of the Li whisker, including the $\langle 001 \rangle$, $\langle 112 \rangle$, $\langle 110 \rangle$, and $\langle 111 \rangle$. Overall, the values of σ_m range from tens to 130 MPa , which are higher than the ones reported in the literature.^{47,48,51–54} Furthermore, the correlations between the Young’s modulus, yield strength of the Li whisker with its radius and growth direction are also revealed by recording the stress-strain curve under a constant rate of 10^{-3} s^{-1} . To be specific, the Young’s modulus of the Li whisker is calculated to be from 2.7 to 21 GPa , while the reported values in the literature for bulk polycrystalline Li metal are between 4.3 and 8 GPa . Similarly, the derived yielding strength varies from 12.2 to 244 MPa , which is much higher than the recorded ones ($0.4\text{--}0.9 \text{ MPa}$).^{45,48}

In terms of the temperature impact, it is found that the yield strength of Li whiskers significantly reduces at elevated temperature: its value for microsized Li pillars with different diameters at 363 K decreases by a factor of ~ 3.5 in comparison to that at room temperature.⁴⁷ The phenomenon could be explained by the fact that elevating temperature can trigger the cross-slip and dislocation climb, where the dislocation movement is no longer confined to slip planes that exhibit the largest resolved shear stress.⁵⁵ At low temperature, the Li metal is expected to undergo several phase transitions: (1) from body-centered-cubic (bcc) to hexagonal structure below 72 K without cold work and (2) from bcc to faulted face-centered-cubic (fcc) below 110 K under cold work.^{56,57} Besides, Li metal shows a strain hardening phenomenon below room temperature, which conversely does not appear at room temperature.^{57,58}

Crystallographic orientation is another critical factor that has a significant influence on the mechanical properties of Li metal. Owing to the anisotropy in the elastic properties of Li metal, the mechanical properties of Li crystals vary significantly with different orientations; for instance, $\langle 111 \rangle$ -oriented Li crystal has a much smaller shear modulus than that of a $\langle 100 \rangle$ -orientated crystal, thus showing a lower possibility of dendrite formation over it.⁴⁷

Aside from the relationship with mechanical properties, the inherent defects of Li metal are also correlated to the Li deposition homogeneity, thus influencing the morphological evolution behaviors. Grain boundaries, as an important class of structural defects in polycrystalline Li anodes, exhibit a higher interfacial energy than grain sites due to the distorted atomic arrangements (bond lengths and angles).⁵⁹ Consequently, grain boundaries would be preferential sites for SEI precipitation, Li atom diffusion driven by internal stress, and Li stripping after SEI breakdown during the cycling.^{21,60,61} All these facts are supposed to facilitate irregular Li deposition over the thermodynamically favored planes (*i.e.*, $\{110\}$ planes).²¹

2.2. Challenges of Li Metal Anode

Despite their intriguing features on enabling powerful metal batteries, Li metal anodes have to overcome a series of

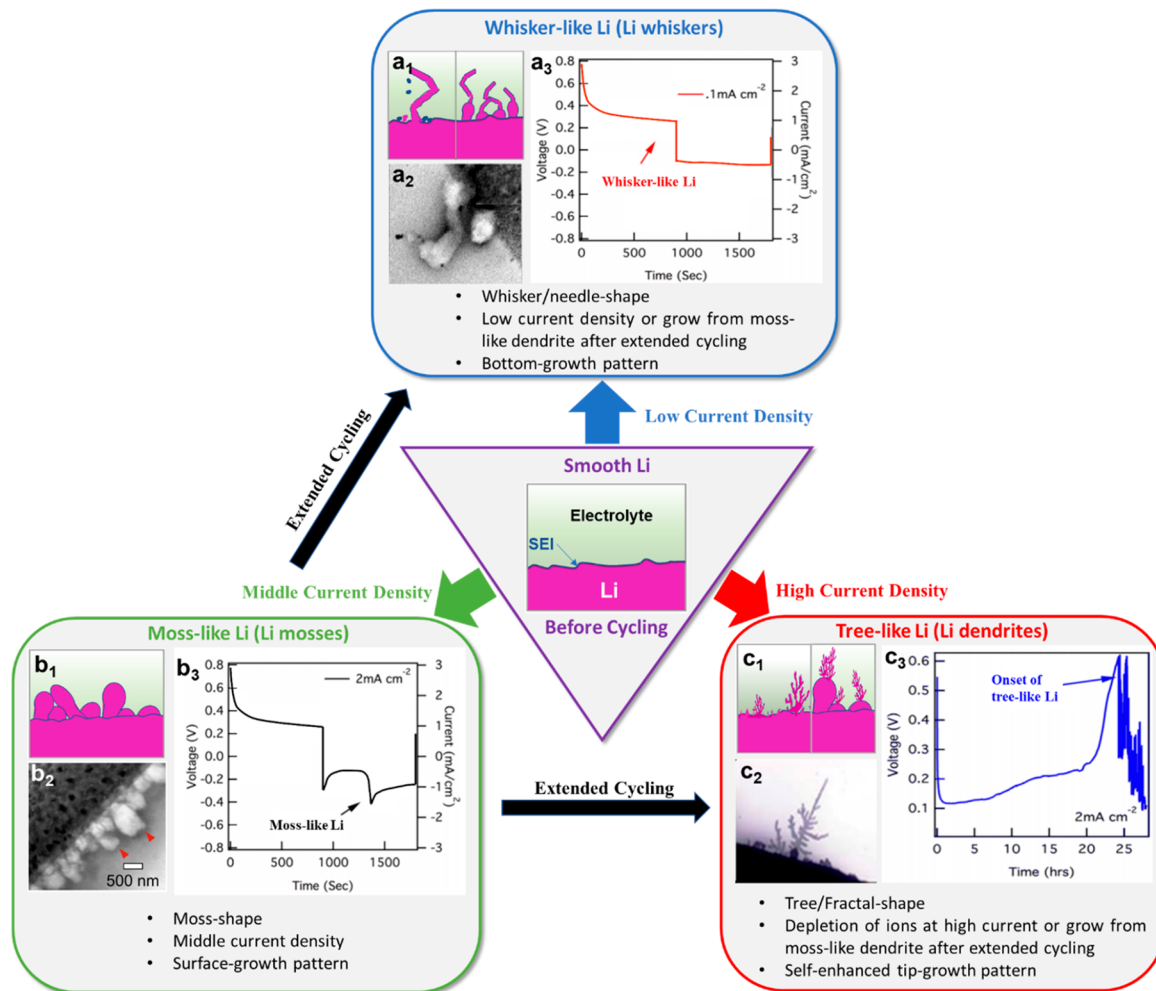


Figure 2. Comparison of polymorphous lithium formation pathways: (a₁, b₁, and c₁) schematic morphologies, (a₂, b₂, and c₂) real microscopic images, and (a₃, b₃, and c₃) featured voltage profiles of whisker-like, moss-like, and tree-like Li formation. The possible morphology transition of different Li deposits during cycling is also revealed by arrows. Adapted with permission from ref 16. Copyright 2014 Royal Society of Chemistry. Adapted with permission from ref 20. Copyright 2018 Elsevier. Reproduced with permission from ref 74. Copyright 1976 Elsevier. Adapted with permission from ref 73. Copyright 2017 Elsevier. Adapted with permission from ref 84. Copyright 2017 American Chemical Society.

challenges before commercialization, *e.g.*, the large volume change, the formation of porous Li deposition layer, and the parasitic thickening of solid-electrolyte interface (SEI) layer, followed by severe irregular Li formation and “dead Li” accumulation that jeopardize the delivered electrochemical performance and even bring about safety issues.¹⁵ These issues are primarily correlated to the inherent chemical, electrochemical, and metallurgical characteristics of Li metal as discussed in section 2.1, including the high reactivity, “hostless” feature, and low mechanical strength. Ideally, the Li metal electroplating is expected to occur evenly and densely over substrates, affording a smooth Li morphology. However, Li metal plating often exhibits an irregular and porous pattern (namely, forming Li whiskers, Li mosses, or Li dendrites) in practical situations, which majorly accounts for the rapid capacity fading and remains the bottleneck for the commercialization of LMBs. Worse still, the tendency for polymorphous Li evolution cannot be fully inhibited after initiation during repeated Li plating/stripping processes, particularly for tree-like Li dendrites due to both their thermodynamically and kinetically favorable evolution nature.⁶² All these issues will be comprehensively discussed in the following parts.

2.2.1. Classification and Definition of Li Polymorphs.

As mentioned above, polymorphous Li deposits in Li metal anodes can be mainly divided into film-like Li (smooth Li), whisker-like Li (Li whisker), moss-like Li (Li moss), tree-like Li (Li dendrite), and their derivates. It is essential to mention that whisker-like, moss-like, and tree-like Li patterns are collectively termed as Li dendrites in many publications, which is ambiguous. In the field of crystallography and metallurgy, dendrite refers to the tree-like structure of crystals growing as material crystallizes.⁶³ Therefore, to clearly define different irregular Li deposits, it is necessary to distinguish tree-like Li from whisker-like Li and moss-like Li for the community of battery.

(1) Film-like Li is the ideal Li morphology in Li metal anode, which shows a dense structure (~4.85 μm thick at an areal capacity of 1 mAh cm^{-2}) and smooth surface (without protuberances or with a low surface roughness). Typically, the film-growth is realized by vapor deposition based methods (such as chemical/physical vapor deposition),^{64,65} which is mainly dependent on the surface energy and lattice mismatch between substrates and growing films.⁶⁶ In the metal electrodeposition

- process, thin-film electrodeposits can also be achieved if the single crystalline new phase (epilayer) exhibits a correlated orientation with the substrate and low residual stresses, such as copper (Cu) and platinum (Pt).^{67–69} However, the Li metal evolution process in Li metal anode is far more complicated, and it is controlled by many factors (multiphysical fields). This is also the reason why smooth film-like Li morphology is hard to achieve in practical Li metal anodes. In the battery community, dendrite-free or protuberance-free are also widely used to describe the smooth Li morphology.
- (2) Whisker-like Li (Li whiskers) grows simultaneously along both the length and diameter directions without significant branching (Figure 2a₁,a₂), while the growth in the length direction is remarkably faster than in the diameter direction. In some papers, the words like Li filaments and Li needles are also used to define such Li structures.^{70,71}

- (3) Tree-like Li (Li dendrites) grows in all directions with typical multiple branches (Figure 2c₁,c₂), which are the most widely used Li morphology mode for Li metal evolution simulations. In addition to Li dendrites, some other terms have also been used to describe such branched Li structures, *e.g.*, dendritic Li, ramified Li, and bushlike Li.⁷²
- (4) Moss-like Li (Li mosses) often has smaller lengths but larger diameters (Figure 2b₁,b₂), in comparison with Li whiskers and Li dendrites.

In addition, the Li metal deposits may also present some other morphologies, such as particulate, nodulelike, and microwirelike Li,³⁰ while it is difficult to clearly define and separate them from each other. For example, some Li deposits are macroscopically moss-like, while their microscopic morphology is still whisker-like or tree-like. In general, whisker-like Li, moss-like Li, and tree-like Li are three of the most observed irregular Li deposit patterns. Therefore, in this review, the morphological, metallurgical, and electrochemical distinctions of these three Li patterns are discussed and compared.

2.2.2. Electrochemical Behaviors of Irregular Li. Aside from the morphological distinctions of different irregular Li structures, they also emerge under different conditions and exhibit distinct evolution behaviors (Figure 2).^{16,20,73,74}

- (1) The occurrence of Li whiskers is typically triggered under low currents, which is usually accompanied by a slight increase of the potential in the galvanostatic Li//Li symmetric cells and their growth will stop after a finite period (Figure 2a₃).^{70,75}
- (2) At a relatively higher current, irregular Li deposition will follow the surface-growth mechanism and present moss-like patterns. Unlike Li whiskers, Li mosses are supposed to have a tremendous amount of exposed fresh Li metal and faster deposition rate due to the higher current, which result in characteristic potential decay in the galvanostatic V-t plots in Li//Li symmetric cells (Figure 2b₃).^{76,77}
- (3) When further increasing the current to the critical value predicted by Sand's time model, the salt will be depleted near the anode surface, and then the tree-like Li dendrites with the tip-growth pattern will be initiated. In the current-constant symmetric cell test, it usually exhibits an abnormal voltage profile (Figure 2c₃). What make the Li dendrites most lethal toward the cell's performance and safety are the self-enhancing growth mode and consid-

erably large surface area.^{20,28,78,79} Furthermore, whisker-like and moss-like dendrites are more commonly observed than tree-like dendrites in experiments.^{80,81}

2.2.3. Issues from Irregular Li Formation. Once the irregular Li evolution emerges, it will incessantly trigger structural/morphological abnormality and further aggravate the performance decay, which can be achieved through¹⁵

- (1) Massive consumption of electrolyte to form thick SEI film on the dendrite surface, resulting from the high reactivity and large surface area of irregular Li structures. Besides, the repeatable breaking and reformation of SEI film due to the large volume change will further promote the depletion of electrolyte.
- (2) “Dead Li” formation due to the breaking of irregular Li structures from the root followed by the transition of Li metal anode from a dense structure to a porous structure, in which the isolated “dead Li” particles are electrochemically inert due to the coverage of SEI film and barely contribute to the capacity, leading to considerable Li loss.
- (3) Accompanied by the electrolyte decomposition and SEI formation in the above issues, Coulombic efficiency and cyclic stability will be deteriorated and the resistance of Li⁺ ion diffusion will increase with the accumulation/thickening of the SEI layer. Furthermore, the issues brought by irregular Li appearance will conversely aggravate the irregular Li evolution and lead to a vicious circle until the failure of cells.¹⁵
- (4) In addition, the emergence of irregular Li structures also brings about safety concerns. In a severe situation, when the irregular Li deposits penetrate the separator and reach the counter electrodes (as revealed by the isolated “black spots” visible on both sides of the separator or solid electrolyte), an internal short circuit will occur, resulting in the death of cells or even thermal runaway in the highly flammable organic electrolytes.¹⁵ In fact, the application of Li metal anode in commercial batteries could be dated back to the late 1980s, realized by Moli Energy; however, it was the frequent safety accidents, like explosions and fires occurring on the cells, that forced the company to abandon that project, and then the Li metal anode was rapidly replaced by the safer and more stable graphite anode.^{4,82,83}

3. THEORETICAL MODELS AND INFLUENCING FACTORS OF IRREGULAR LI FORMATION

As demonstrated in the former section, three types of well-defined irregular Li structures present distinct characteristics and growth formats, though their occurrences are all extremely detrimental to the stability of Li metal anodes. Particularly, the sharp tips of Li dendrites and Li whiskers are susceptible to penetrating the separator and short-circuiting the cells when contacting with the counter electrodes. Unveiling the formation mechanisms of various irregular Li structures from the perspective of multiphysical fields would be critical to properly guide the smooth Li plating. In the following sections, the specific initiation mechanisms of the above-mentioned three types of irregular Li structures will be demonstrated from the points of the ionic concentration field, electric field, stress field, and temperature field; some key influencing factors such as the electrolyte composition, SEI layer, and initial nuclei states will also be introduced to show their relationships with the physical

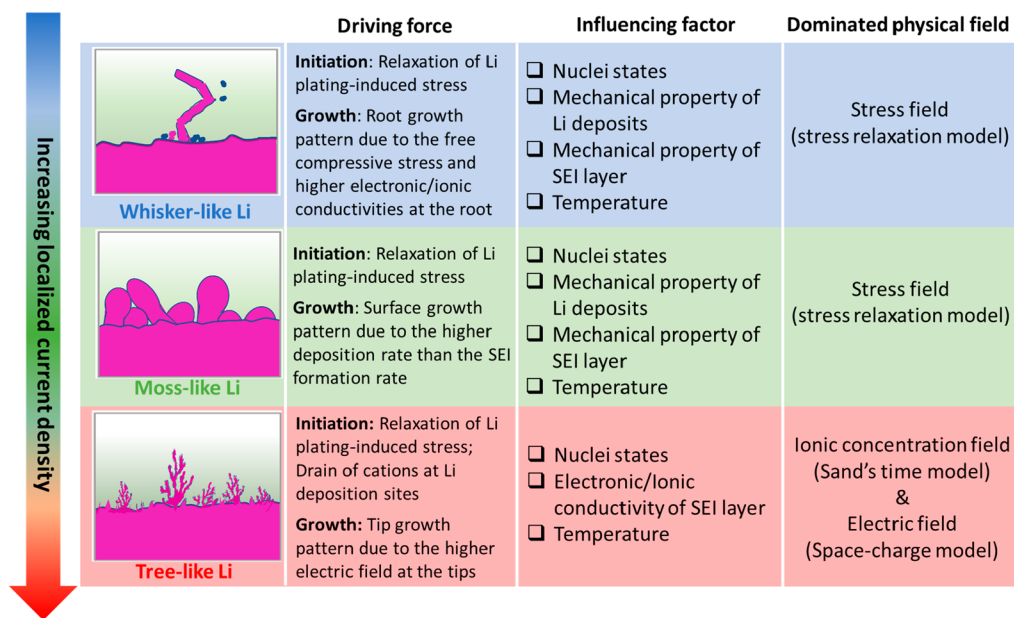


Figure 3. Summary of the driving force, influencing factor, and dominated physical fields for the formation of whisker-like, moss-like, and tree-like Li deposits.

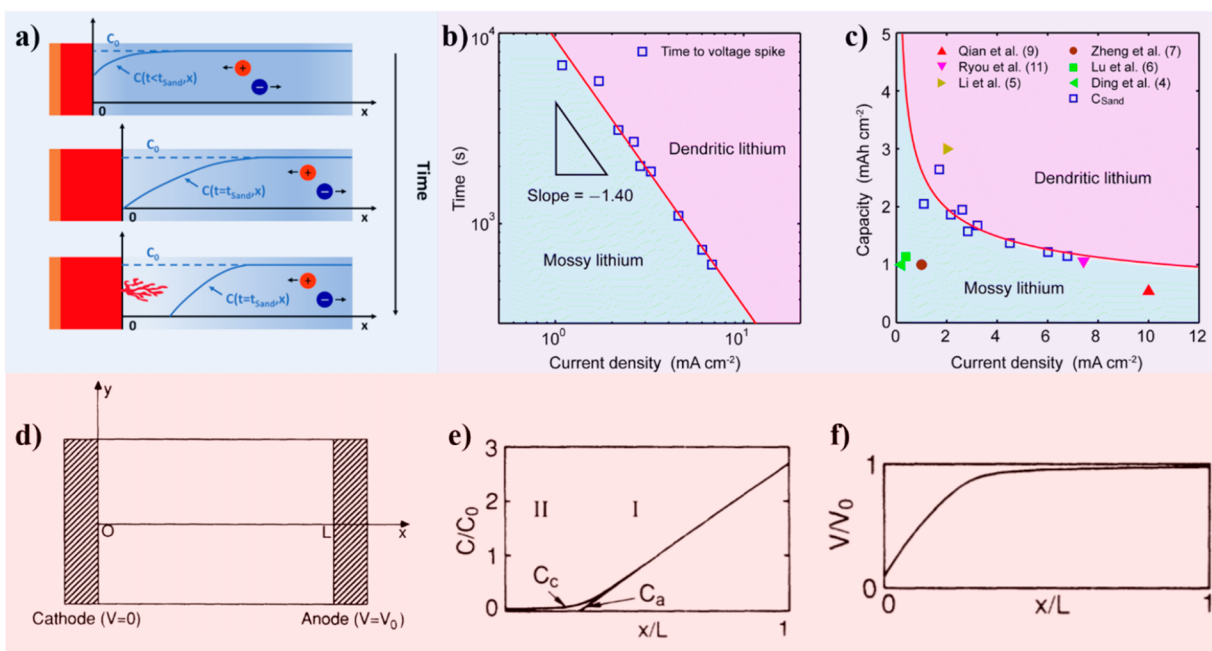


Figure 4. The origins of tree-like dendrite growth. (a) Schematic of tree-like dendrite growth mechanism due to draining of cations on the electrode surface as a function of time.²⁸ (b, c) Curves of Sand's time (b) and Sand's capacity (c) variance as a function of current density. Reproduced with permission from ref 28. Copyright 2016 Royal Society of Chemistry. (d–f) Schematic illustration of simulation-based symmetrical cell setup (d), calculated cation/anion concentration distribution (e), and voltage distribution (f) within the cell. Reproduced with permission from ref 18. Copyright 1990 American Physical Society.

fields and the evolution trends of Li deposits, as summarized in Figure 3.

3.1. Ionic Concentration and Electric Fields Influence on Li Metal Evolution

It is well accepted that the distribution of ionic concentration field and electric field has direct connection with the transition between steady deposition and tree-like Li dendrite growth. In retrospect, a series of theories were presented to predict the Li dendrite formation, among which the most famous two are the

Sand's time model¹⁷ and space-charge theory.^{18,19} Many factors are taken into consideration within these theories, for instance, the current density, mobility of both cations and anions, and salt concentration in electrolytes, etc. Nevertheless, the real situation is far more complexed than it is supposed in the models. First, the naturally produced SEI layer and its characteristics, such as compositions, homogeneities, mechanic strength, and so forth, have great impact over the distribution of both ionic concentration and electric fields over the anode surface. In addition, the different initial nucleation states, as affected by the

experimental conditions, substrate properties, and electrolytes, also change the local salt concentration or electric field distribution on the anode surface, thus influencing the growth pattern of Li metal anode. Herein, both the merits and limitations of the ionic concentration and electric fields-dominated models, as well as the influencing factors will be categorized and introduced in the following parts.

3.1.1. Ionic Concentration Field-Related Models. In a simplified situation of electrodeposition, solvated Li^+ migrates toward the anode direction under the electric field, then gets adsorbed via the electric double layer effect on the electrode surface, experiences the desolvation process, and finally undergoes the continuous reduction reaction to Li metal and accumulation over the anode.⁸⁵ For metals like copper (Cu), silver (Ag), and zinc (Zn), ramified products (tree-like dendrites) are broadly observed during their electrodeposition processes and the phenomenon is assumed to be correlated to the salt concentration gradients within electrolytes.¹⁸ As reported by Sand *et al.* in 1901, the dendritic growth of Cu during electrodeposition from the mixture of copper sulfate and sulfuric acid is controlled by the salt concentration near the electrode surface.¹⁷ During the deposition process, cations and anions transfer along the reverse directions, with cations accumulating near the anode and anions accumulating near the cathode; simultaneously, the cations are constantly consumed during the metal deposition process and the salt concentration on the anode surface decreases as a function of time. If the salt concentration on the anode surface turns to zero, the deposition will transform from the steady deposition mode to the self-amplified tree-like dendrite growth mode (Figure 4a). The critical time for dendrite initiation, also known as the Sand's time, can be derived with eq 4.⁸⁶

$$t_c = \pi D \frac{Z_C^2 F^2 C_{C0}^2 (\mu_A + \mu_C)^2}{4J^2 \pi_A^2} \quad (4)$$

in which μ_A and μ_C represent the mobilities of anions and cations, respectively, D stands for the ambipolar diffusion constant and its value equals $(\mu_A D_C + \mu_C D_A)/(\mu_A + \mu_C)$, D_C and D_A are, respectively, the diffusion constants of anions and cations in the electrolytes, Z_C is the cation's charge number, F is the Faraday constant, C_{C0} represents the initial concentration of cations, and J stands for the current density.

In 2001, Brissot *et al.* proposed another model to simulate the tree-like dendrite growth process in LMBs.⁸⁷ In this model, the overall salt content in the cell is considered a constant value since the cathode releases Li^+ to compensate for the loss on the anode side during the charging process. With the anions moving toward the cathode, a linear-changing Li-salt concentration gradient appears after polarization as shown in eq 5,^{86,87} which relates to the current density (J), ambipolar diffusion constant (D), mobilities of anions (μ_A) and Li^+ (μ_{Li^+}) separately.

$$\frac{\delta C}{\delta x} = \frac{J \mu_A}{FD(\mu_A + \mu_{\text{Li}^+})} \quad (5)$$

Hence, the Li-salt concentration on the anode surface can be expressed by eq 6, in which the concentration change (ΔC_+) is demonstrated in eq 7,

$$C_+ = C_0 - \Delta C_+ \quad (6)$$

$$\Delta C_+ = \frac{\mu_A}{\mu_A + \mu_C} \frac{Jl}{FD} \quad (7)$$

where l represents the diffusion distance of cations and $l = \sqrt{t_D D_C}$, and t_D is the diffusion time of the cations. If the surface concentration of $\text{Li}^+(C_+)$ is reduced to zero, the critical diffusion time on the distance l can be derived, which displays the same format with Sand's time model in eq 3.^{86,88} In this theory, the significances of both cation and anion behaviors on dendrite growth during Li plating are highlighted. To better track the dendrite growth and set the critical working conditions for Li metal anode in real application, Sand's time can be further transformed to Sand's capacity by multiplying the current density (Figure 4b,c).²⁸ Similarly, when the accumulated plating capacity exceeds the critical value at the working current density (red curve), the originally steady deposition will immediately transit to uncontrollable tree-like dendrite deposition.

To sum up, the initiation of tree-like dendrites is due to the draining salt concentration on the electrode/electrolyte interface brought by limited diffusion capability of Li^+ . Two models introduced above could be used to predict the critical conditions influencing the tree-like dendrite appearance in an ideal case.

3.1.2. Electric Field-Related Models. Chazalviel *et al.* introduced a so-called "space-charge theory" with an emphasis on the anions' influence during the charging process, where the tree-like Li dendrites originate from the locally aggregated electric field.^{18,19} In this model, anion depletion along with Li^+ accumulation near the anode creates a concentrated space charge and strong electric field, thus inducing the dendritic growth. To support the theory, the simulations are conducted for both the ion concentration and electrostatic potential in the dilute electrolytes within symmetrical cells (Figure 4d–f). When the consumption rate of Li^+ (reaction rate) overpasses the provision rate (mobility of Li^+), the tree-like dendrite growth will be triggered and the concentration gradient in cells is supposed to follow eq 4 with the curve shown in Figure 4e. Meanwhile, the voltage gradient within the cells follows the curve displayed in Figure 4f, where region I refers to the quasi-neutral region and region II indicates the space-charge region. Clearly, there remains certain amounts of space charge, distinguished from the depleting salts on the anode surface, thus creating a large local electric field and triggering the dendrite formation.

Later on, Chazalviel *et al.* also predicted the growth rate of dendrites through the equation of $v_a = -\mu_a E_0$, in which μ_a is the mobility of anions in electrolyte and E_0 is the electric field intensity in the neutral region of the electrolyte.^{18,19} However, the constant-growth-rate theory was refuted by Newman *et al.* since they demonstrated that the distribution of ionic concentration and electric fields on dendrite tips continuously varied during the growth.⁸⁹ According to them, the growth rate would also change with time, as estimated to be $v_{\text{tip}} = \frac{J_n V}{F}$, where v_{tip} is the growth rate over dendrite tip, J_n is the tip current density, V is the molar volume of Li metal, and F is the Faraday constant.⁸⁹ Furthermore, this equation also indicates that the dendrite growth can be effectively hindered by reducing the current density on the tip, which will be discussed in detail in the following section.

Remarkably, all aforementioned mechanisms, no matter of the ionic concentration field-dominated or electric field-dominated ones, set up the connections of tree-like dendrite formation with diffusion-controlled salt depletion on the electrode surface, and their estimated critical conditions on dendrite growth are quite close. Accordingly, several factors are correlated to the Li plating behavior, including the mobilities of both cations and anions in

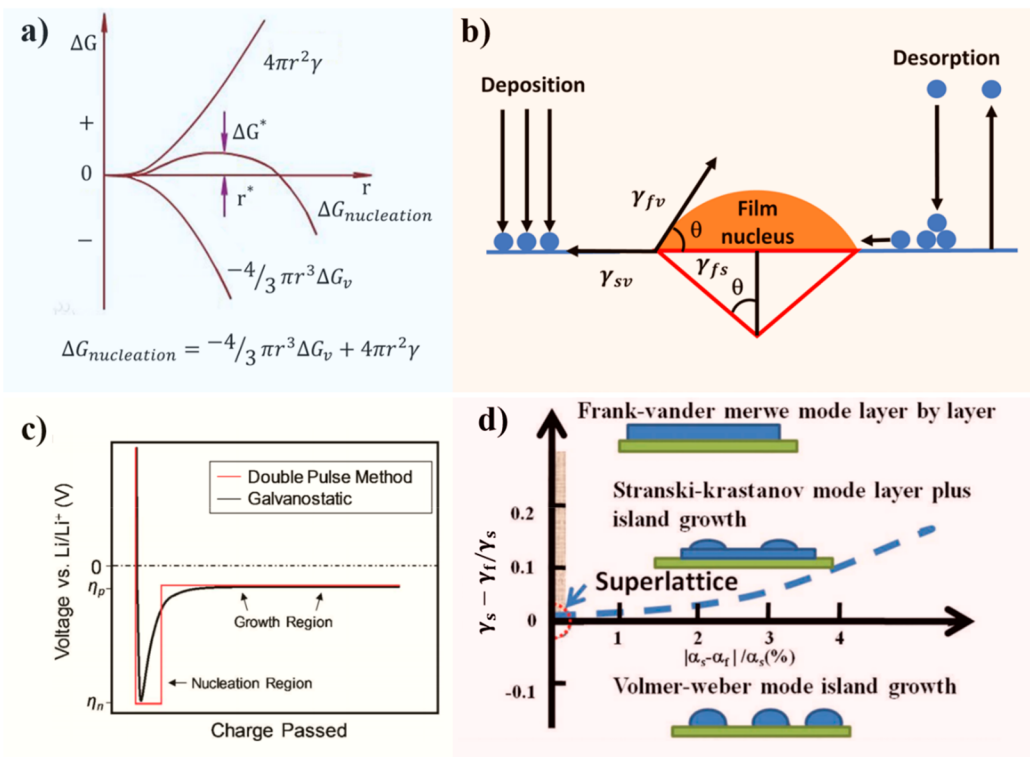


Figure 5. Li metal nucleation thermodynamics. (a) Homogenous nucleation energy curve as a function of the nuclei radius. Reproduced with permission from ref 94. Copyright 2017 American Chemical Society. (b) Schematic diagram of the heterogeneous nucleation and related parameters.^{66,97} (a, b) Redrawn after the reference. (c) Schematic voltage–charge curve of typical Li plating under galvanostatic charging. Reproduced with permission from ref 94. Copyright 2017 American Chemical Society. (d) Regions of three nucleation modes in coordination with the lattice mismatch (x axis) and the surface energy differences (y axis).⁹⁷ (d) Redrawn after the reference.

electrolyte, initial concentration of salts, and current densities, which have all been proven by experiments.^{30,90–92}

3.1.3. Limitations of Ionic Concentration and Electric Field Models. The above-mentioned theories provide a solid understanding for the growth mechanism of tree-like metal dendrites. Unfortunately, the derived mathematical models fit well for the electrodeposition behaviors of metals such as Zn, Ag, and Cu but lack sufficient accuracy on predicting the Li dendrite evolution.²⁸ For instance, in the early report on Li/polymer electrolyte cells, the relationship between dendrite growth initiation time and current density followed a similar trend with the Sand's time equation, but the deviation happened at the low current density areas.⁸⁷ In other words, dendrite growth occurred at a low current density, where it was not expected to take place according to the classical Sand's time prediction due to the limited concentration variance.^{28,76,93} Furthermore, whisker-like Li and moss-like Li are more commonly observed than tree-like Li dendrites in experiments,^{80,81} while their appearance cannot be well explained by the above ionic concentration/electric field models. Hence, there are more aspects necessary to consider if we want to fully understand and predict the evolution of different Li structures in practical situations.

The above-mentioned deviations between theoretical predictions and experimental observations can be ascribed with the following two reasons:

- (1) The first point is that the theories and derived mathematical models simplify the ionic concentration field and electric field to be a 2D distribution along with the distance to the Li metal anode and ignore the

inhomogeneity of the ionic concentration field and electric field over the anode surface in real cases. In fact, there are some variables (e.g., SEI layer and nuclei states) in Li metal anode that may result in the local aggregation of Li⁺/electron and the acceleration of Li⁺ depletion, thus enhancing the possibility of dendrite growth at these sites (namely, hotspots). The earlier emergence of dendrites is affected by every stage of Li plating, among which the nucleation stage should receive the most attention. Perfecting the nuclei states (e.g., morphology, size, and distribution density) is expected to set a solid foundation for steady plating behavior. In the next section, how the nuclei state affects the further deposition pattern and the influential factors on the nuclei state will also be systematically summarized and introduced.²¹ Besides, the composition, structure, and even the mechanical properties of SEI layer also relate to the distribution of salt concentration and electric field around electroplated Li metal, thus influencing the evolution behavior of the Li metal.

- (2) The trigger of tree-like dendrites requires a localized zero cation concentration around deposition sites (often under high rates or in dilute electrolytes), which is more critical than those of whisker-like and moss-like Li structures (see sections 3.2 and 3.4). In practical situations, most Li metal anodes are cycled under mild conditions, thus Li whiskers and Li mosses can be mostly observed rather than Li dendrites. However, the growth mechanisms of Li whiskers and Li mosses cannot precisely be explained by the ionic concentration field and electric field models.

This is because the ionic concentration and electric field models are mainly based on the electrochemical parameters of electrodeposited metal yet ignore its metallurgical properties: the solid-state atomic mobility, crystal structure, and mechanical properties of Li metal, which have strong impacts on the plating morphology via the mechanical deformation. Meanwhile, unlike Zn, Cu, and Ag metals, Li metal is covered with a SEI layer,^{4,15} which will pose a compressive stress on Li metal; conversely, the accumulation of internal stress during plating can break the SEI layer and influence the distribution of ionic concentration and the electric field. The stress-related contents will be discussed in section 3.2.

3.1.4. Influencing Factors on Ionic Concentration and Electric Fields. As summarized above, the ionic concentration field and electric field based models are usually employed to simulate the evolution of tree-like Li dendrites, implying that Li dendrite formation is highly dependent on the ionic concentration field and electric field within the whole Li metal anode area, including the Li metal layer, SEI layer, electrolyte, and separator. In this section, we will focus on two major influencing factors (*i.e.*, Li nucleation states and SEI layer properties) and discuss how these two factors affect the ionic concentration and electric fields and how these two fields further influence the morphology of Li deposits. It is also worth mentioning that the formation of Li whiskers and Li mosses are also susceptible to the ionic concentration and electric fields; therefore, the discussion about the influences of nucleation states and SEI layer properties on these two fields in this section is not limited to tree-like Li dendrite formation only. It is difficult to clearly differentiate the influence of these two factors from the case of Li dendrite formation to the cases of Li whisker and Li moss formation. Nevertheless, to clarify the relationship between the influencing factors with Li morphologies, some dominated effects toward specific irregular Li formation will be highlighted in this section, *e.g.*, the cell operation rate. Similarly, some other stress-related influencing factors for the formation of Li whiskers and Li mosses will be introduced later in section 4.

3.1.4.1. Influence of Nucleation States. Typically, the plating of Li metal in rechargeable cells starts with heterogeneous nucleation on the surface of pristine Li metal or other non-Li substrates. The features of substrate, such as component, size, morphology, and surface chemistry, all have direct impacts on the distribution of concentration/electric fields around substrates, thus influencing the Li nucleation and subsequent growth behavior. In this part, basic thermodynamic and electrochemical analysis for both homogeneous nucleation and heterogeneous nucleation will be first introduced; subsequently, detailed influences on the nucleation process from diverse nucleation substrates, electrolyte systems, and cell operation conditions will be discussed.

(1) Thermodynamic Analysis of Homogeneous Nucleation

Before discussing the heterogeneous nucleation case during Li plating process, the simpler homogeneous nucleation will be introduced first. According to the classical nucleation theory, with the decreasing potential, the Li metal nucleation starts with the local composition fluctuation and energy fluctuation at the anode/electrolyte interface and ends with the emergence of embryos at some supersaturation sites through overcoming the nucleation barrier. Notably, the nucleation energy ($\Delta G_{\text{nucleation}}$) is the sum of its volume energy change and surface energy change to form a spherical nuclei with a radius of r (Figure 5a).⁹⁴ When the differential of the $\Delta G_{\text{nucleation}}$ equals zero, the critical

radius (r_C) for thermodynamic favored nuclei can be derived as eq 8.

$$r_C = -\frac{2\gamma}{\Delta G_V} \quad (8)$$

where ΔG_V stands for the free energy per volume, and γ is the surface energy between the Li particle and the electrolyte. Embryos with a radius larger than the critical value will survive, while the smaller embryos will dissolve into the electrolytes. In an equilibrium state, the potential for Li deposition is -3.04 V (vs SHE). However, an overpotential (η) is always observed for Li nucleation as predicted by the Butler–Volmer equation, which means lower potential is needed to initiate the nucleation process. The ΔG_V is correlated to the deposition overpotential and can be expressed as^{95,96}

$$\Delta G_V = \frac{Fl\eta_l}{V_m} \quad (9)$$

where V_m is the molar volume of Li, and F is the Faraday's constant. Then the r_C is further derived as⁹⁴

$$r_C = \frac{2\gamma V_m}{Fl\eta_l} \quad (10)$$

From eq 10, it can be implied that r_C is negatively proportional to the value of η_l ; in other words, the size of particles can be adjusted through tuning the overpotential for nucleation.

(2) Thermodynamic Analysis of Heterogeneous Nucleation

In the practical situation of galvanostatic plating, Li metal deposition starts from the heterogeneous nucleation (Figure 5b). Three interfaces coexist after the nucleation process, including the film–vapor (fv), substrate–vapor (sv), and film–substrate (fs). The contact angle θ indicates the lithiophilicity of the substrate. The equilibrium of the interface tension and the contact angle is expressed by Young's equation (eq 11).^{66,97}

$$\gamma_{sv} = \gamma_{fs} + \gamma_{fv} \cos \theta \quad (11)$$

For heterogeneous nucleation, the substrate serves as the catalyst for Li^+ deposition since it can significantly reduce the nucleation energy barriers. The critical nucleation energy is derived as⁹⁷

$$\Delta G_c = \frac{16\pi\gamma_{fv}^3}{3\Delta G_V^2} \left(\frac{2 - 3 \cos \theta + \cos \theta^3}{4} \right) \quad (12)$$

When θ is 0° , there will be no barrier for nucleation and the nuclei will be evenly deposited over the substrate; instead, when θ is 180° , the nuclei will be of spherical shape, resembling homogeneous nucleation.⁹⁷

(3) Connection between Nucleation Energy Barrier and Substrate Lithiophilicity

The energy barrier for Li nucleation on different substrates is closely connected with the lithiophilicity of the substrate, which can be reflected electrochemically. Typically, in the case of Li plating at a constant current density, the voltage will rapidly drop to a value lower than 0 V vs. Li^+/Li (the overpotential for Li embryo nucleation on substrate (η_n)) and then increases to a plateau with a higher value (the overpotential for Li growth (η_p) over formed Li nuclei), as shown in Figure 5c.⁹⁴ The difference between two characteristic overpotentials ($\eta_p - \eta_n$) partially reflects the nucleation energy barrier, namely, the lithiophilicity of the substrates.⁹¹ If $\eta_p - \eta_n$ is close to zero, it indicates that the

substrate is lithophilic and there is nearly no energy barrier for Li nucleation on the substrate. Besides, the more positive the value of $\eta_p - \eta_n$ is, the less lithophilic the substrate is and the higher the energy barrier is for Li nucleation. In some works, the individual η_p is directly applied to evaluate the superiority of substrates for convenience: a high absolute value of η_p indicates poor lithophilicity of the substrates for hosting Li metal. In DFT simulations, the binding energy between atomic Li and substrate is another critical indicator for the substrate lithophilicity. Here, the binding energy only indicates the interaction strength between substrates and Li in the atom state, and it does not involve the formation of chemical bonds. It is generally defined as follows with the unit of eV:

$$E_{\text{bind}} = E_{\text{total}} - E_{\text{Li atom}} - E_{\text{substrate}} \quad (13)$$

where the E_{bind} represent the binding energy, E_{total} is the total energy of the substrate bound with the adsorbed Li atom, $E_{\text{Li atom}}$ stands for the energy of the Li atom, and the $E_{\text{substrate}}$ is the energy of the substrate bound.⁹⁸ The calculated binding energy should be of a negative value; the more negative binding energy demonstrates the better lithophilicity of the substrate.

In principle, the lithophilicity of the substrate relates to its physicochemical properties, such as the extent of lattice mismatch between substrate with the Li atom. As shown in Figure 5d, there are three different growing formats, distinguished by the surface energy difference between Li deposits and substrate ($\gamma_s - \gamma_l/\gamma_s$) and the lattice mismatch ($|a_s - a_l|/a_s$). When there is trace lattice mismatch between the substrate and nuclei and the substrate's surface energy is higher than that of the deposit, the plating process will follow the Frank–Vander Merwe mode that a smooth film-like morphology will be achieved for the deposits.^{99,100} To note, a higher surface energy of substrate is demanded to trigger the flat film and island growth (the Stranski–Krastanov mode) with the increment of lattice mismatch (see the blue dashed line), or the deposits will merely form the isolated islands over the substrate (the Volmer–Webber mode).^{66,97} Taking Cu as an example, it shows the fcc crystal structure with an atom radius of around 1.28 Å, while Li is of the bcc crystal structure with an atomic radius of around 1.52 Å. The massive difference in lattice structure results in the poor lithophilicity of Cu and the large overpotential for Li nucleation on its surface.¹⁰¹ Furthermore, the plating will primarily occur on the formed nuclei due to the closer surface energy and lattice structure, thus aggravating the inhomogeneity of the Li⁺ concentration and the electric field over the electrode. According to the Sand's time model, the nuclei spots with a higher local current density will present a shorter time for dendrite initiation. This fact partially accounts for the lower critical current density for practical dendrite formation than the Sand's model prediction. Even if the initial salt concentration is high, concentrated current over these spots still has the chance to overpass the critical current density and induce the formation of Li dendrites.

Besides, the lithophilicity of the substrates is also correlated to the charge density (electronic interaction strength) between the Li atom and the substrate.^{102,103} For example, the nonpolar structure of the metallic substrates (*i.e.*, Cu) and pristine graphite with dominant sp² carbon partially accounts for their insufficient binding energy with the Li atom.¹⁰² In comparison, the introduction of nitrogen-containing functional groups, such as pyridinic nitrogen and pyrrolic nitrogen, could significantly improve the lithophilicity of the graphene layer. The DFT

calculation reveals that due to the lattice difference between the graphene layer and Li metal, as the local charge density between pyrrolic nitrogen and Li atom is increased, the strong interaction between Li and N atoms is expected to reduce the strong nucleation barrier and thus will promote the homogeneous Li nucleation/plating.¹⁰² More specific introduction will be given in the following section.

(4) Influence of Nucleation Substrates

Ideally, the Li metal is expected to nucleate densely and evenly over the substrate, which will minimize the chance of irregular Li initiation in the following stages. Nevertheless, the real situation of nucleation distinctly varies between different type of substrates (*e.g.*, Li metal, non-Li metal, and carbonaceous materials).

(i) Pristine Li Metal Substrate

Li metal is a primary substrate for nucleation. Although there is no concern for nucleation overpotential when using a Li metal substrate, its initial morphology and surface roughness can also change the distribution of concentration and electric field nearby. The connection between Li nucleation/growth on Li metal substrate with ionic concentration/electric fields is unveiled by Suzuki *et al.* using the phase-field modeling method.¹⁰⁴ Specifically, the Li⁺ ions and electric field tend to concentrate around the sharp tips with a lower radius of curvature ("tip effect"), as indicated by the density of the contour line (Figure 6). The ionic concentration difference on the electrode surface brings in another type of overpotential called concentration overpotential (η_c), which could be approximated via eq 14 and eq 15:¹⁰⁴

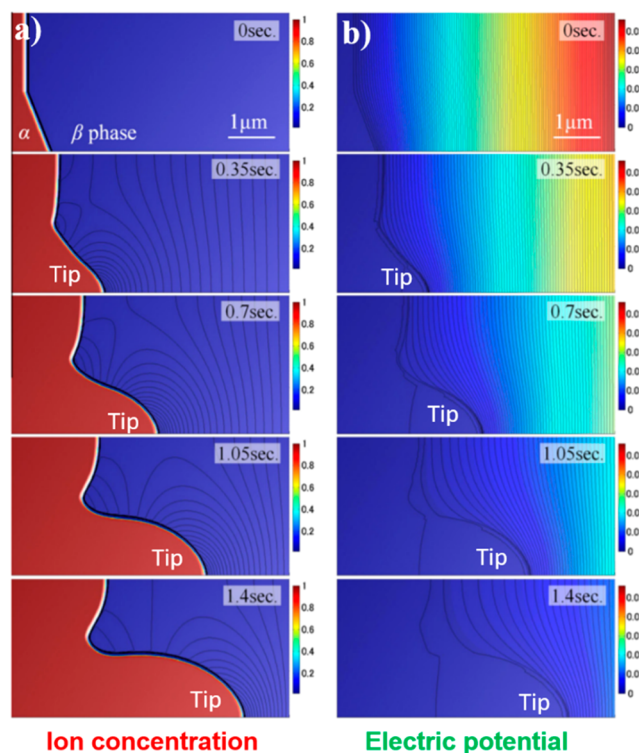


Figure 6. Connection between Li nucleation/growth on the Li metal substrate with ion concentration and electric potential. (a, b) Growth behavior simulation of phase α with a protrusion on the surface with distribution of (a) the metal ion concentration and (b) electric potential. Reproduced with permission from ref 104. Copyright 2010 Elsevier.

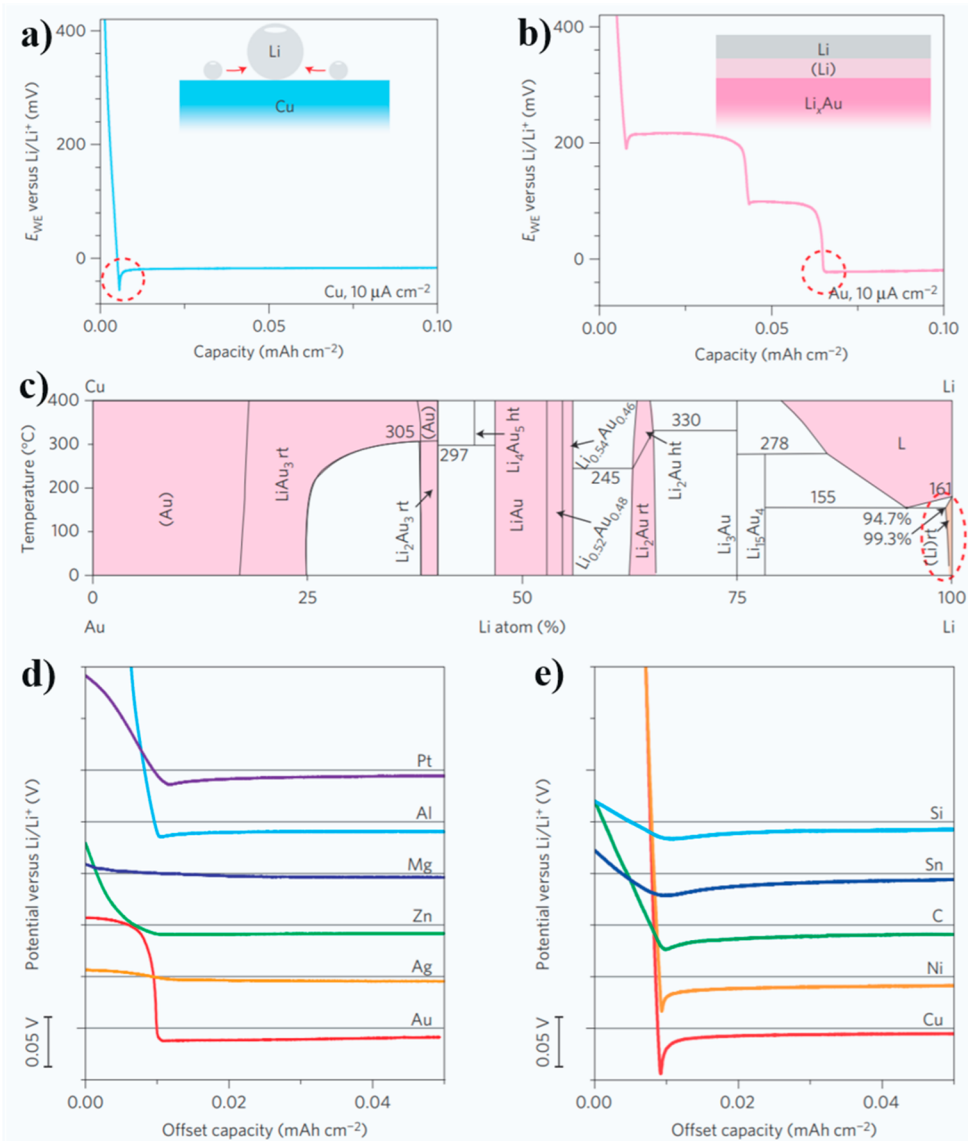


Figure 7. Li nucleation overpotential over varied non-Li metallic substrates. (a, b) Voltage–capacity profile of Li deposition over (a) Cu substrate and (b) Au substrate at the constant current density of $10 \mu\text{A cm}^{-2}$; insets: schematic diagrams of Li nucleation process. (c) Binary phase diagram between Au and Li, where the dashed line marked area is assumed to be the composition for low overpotential plating. (d,e) Voltage–time profiles of different non-Li metallic substrates during Li deposition at the rate of $10 \mu\text{A cm}^{-2}$. Reproduced with permission from ref 101. Copyright 2016 Springer Nature.

$$\eta_c = \varphi_r - \varphi_\infty \quad (14)$$

$$\varphi = \varphi_0 + \frac{RT}{nF} \ln[\text{Li}^+] \quad (15)$$

where φ_r and φ_∞ represent the electric potential at the place with a radius of r and a flat place, respectively; φ_0 stands for the standard potential of the half reaction of Li^+ reduction, $[\text{Li}^+]$ is the concentration of Li^+ on the surface. It can be inferred from the Nernst equation (eq 15) that increasing the concentration leads to a higher potential for the reaction; therefore, the sharper tips with a low radius of curvature are more kinetically favored for Li plating than the flat place, owing to the larger η_c (Figure 6). Furthermore, the concentration polarization will be more severe as the deposition continues, thus aggravating the growth inhomogeneity.¹⁰⁴ This evidence well elucidates the “tip-induced” and “self-amplified” growing tendency of tree-like Li dendrite.

(ii) Non-Li Metallic Substrates

As mentioned above, the commonly used Cu substrate exhibits a large Li nucleation energy barrier due to the distinctive surface energy and lattice structure with Li metal (Figure 7a). Accordingly, the Au substrate possessing the fcc structure with an atomic radius of 1.44 \AA shall exhibit a large Li nucleation energy barrier as well; however, it delivers a negligible nucleation energy barrier with close nucleation potential and plating potential as shown in Figure 7b. This is due to the occurrence of the alloying process before Li metal plating; concretely, Au is able to alloy with Li at multiple compositions as indicated by the Au–Li binary phase diagram (Figure 7c), where the alloy can contain trace amounts of Au and almost all Li.¹⁰¹ The Li–Au alloy possesses a similar lattice structure with pure Li metal, thus eliminating the nucleation energy barrier. Such a mechanism also fits for other metals such as Sn, Zn, Mg, Ag, Al, inorganic materials such as Si, and some oxide materials such as SiO_2 and ZnO that can react with Li to form Li oxide and the corresponding metal (see Figure 7d).^{27,100,101,105} Moreover,

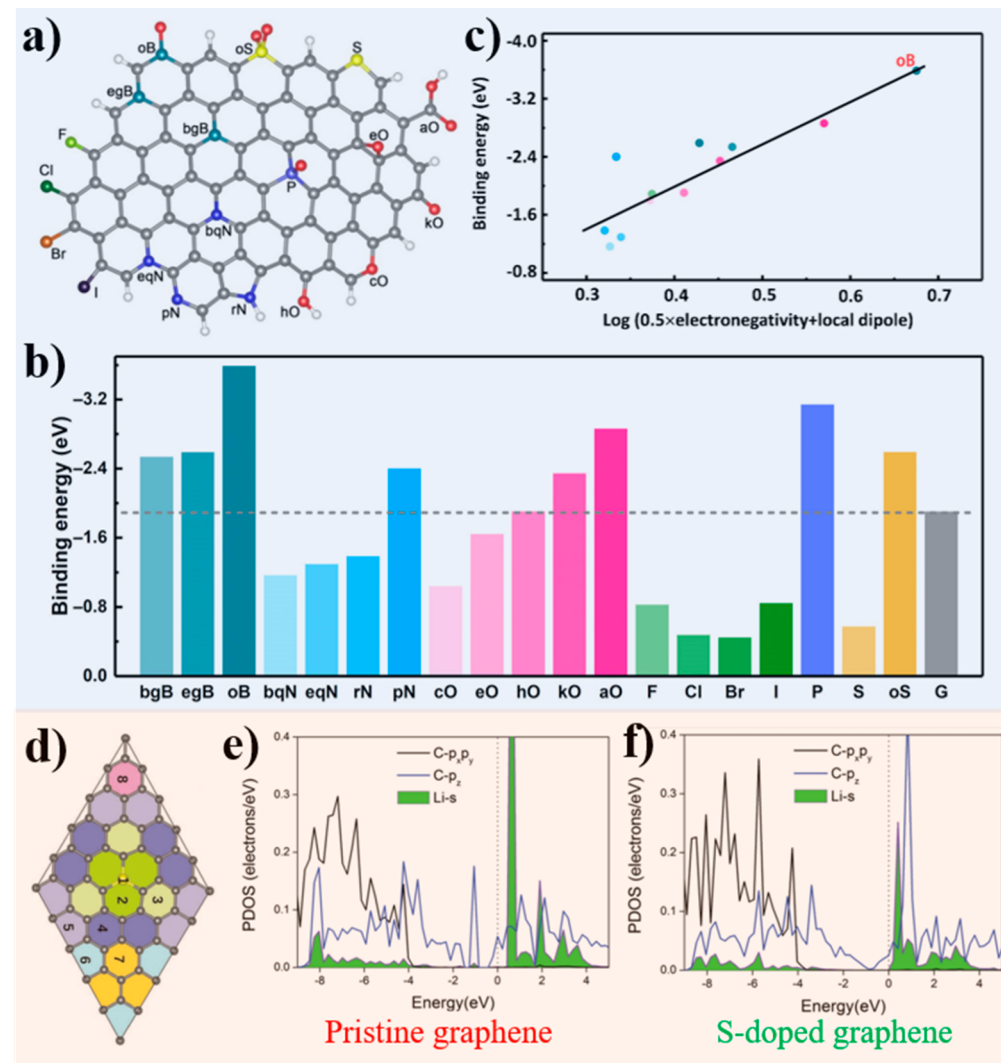


Figure 8. Li ions absorption on surface-doped carbonaceous substrates. (a) Schematic illustration of multiple doping structure over graphene nanoribbons.⁹⁸ (b) Binding energy calculated between single-doping graphene nanoribbons and bare graphene nanoribbons with one Li atom.⁹⁸ (c) Proposed correlation between binding energy and electronegativity + local dipole. Reproduced with permission from ref 98. Copyright 2019 AAAS. (d) Top view of S-doped graphene with the adsorption sites categorized by numbers and colors. (e,f) Partial density of states for (e) pristine graphene and (f) S-doped graphene with one Li⁺ cation adsorbed separately. Reproduced with permission from ref 109. Copyright 2018 Wiley-VCH.

since Au has a lower Li nucleation energy barrier than Cu (Figure 7e), the Li nuclei is more uniformly distributed over the Au substrate, which benefits the growth of preferential moss-shape Li instead of the whisker-shape Li in the Cu case; this is also related to the stress accumulation and SEI layer formation that will be discussed later.⁷³ Another thing that should be emphasized is that the nucleation substrate will be Li metal rather than the original metallic hosts (or carbon-based ones discussed in the following part) if the plated Li is not fully stripped in the former cycle; in this case, the influencing factors convert to the initial morphology and surface roughness as discussed in the above section.

(iii) Carbonaceous Substrates

In addition to the metallic substrates, carbonaceous materials (*e.g.*, graphite, graphene, and CNT) are also common substrate candidates to host Li metal. As discussed above, pristine graphitic materials usually exhibit poor lithiophilicity due to the intrinsically nonpolar structure of sp² carbon and substantial lattice mismatch between graphene and Li metal.^{106,107} These features bring strong polarization and a large energy barrier for

Li nucleation over it; thereafter, sparse nuclei over the substrate and high possibilities for dendrite growth are expected to occur as discussed above. Furthermore, the involvement of surface defects (*e.g.*, heteroatoms, functional groups, topological defects, and vacancies) in carbonaceous substrates can significantly reduce the nucleation energy barrier and enhance the lithiophilicity via localizing their surface electrons or directly providing the electrons; the modification benefits the flat nucleation by decreasing the nucleation energy and possibly homogenizing the Li⁺ flux near the anode surface, thus eliminating the concentration polarization at the adsorption stage.^{94,98,102} Pyridinic nitrogen, for example, presents strong electronic interaction with the Li atom, thus promoting the charge depletion between the Li atom and carbon; this partially leads to the elevated binding energy for pyridinic nitrogen-doped graphene host (-4.26 eV) relative to that of the pristine graphene host (-3.64 eV).¹⁰² Besides, the pyridinic nitrogen contains one lone pair of electrons without incorporation into the conjugated π bond, which are expected to become an electron donor and act as a Lewis base to absorb free Lewis acid

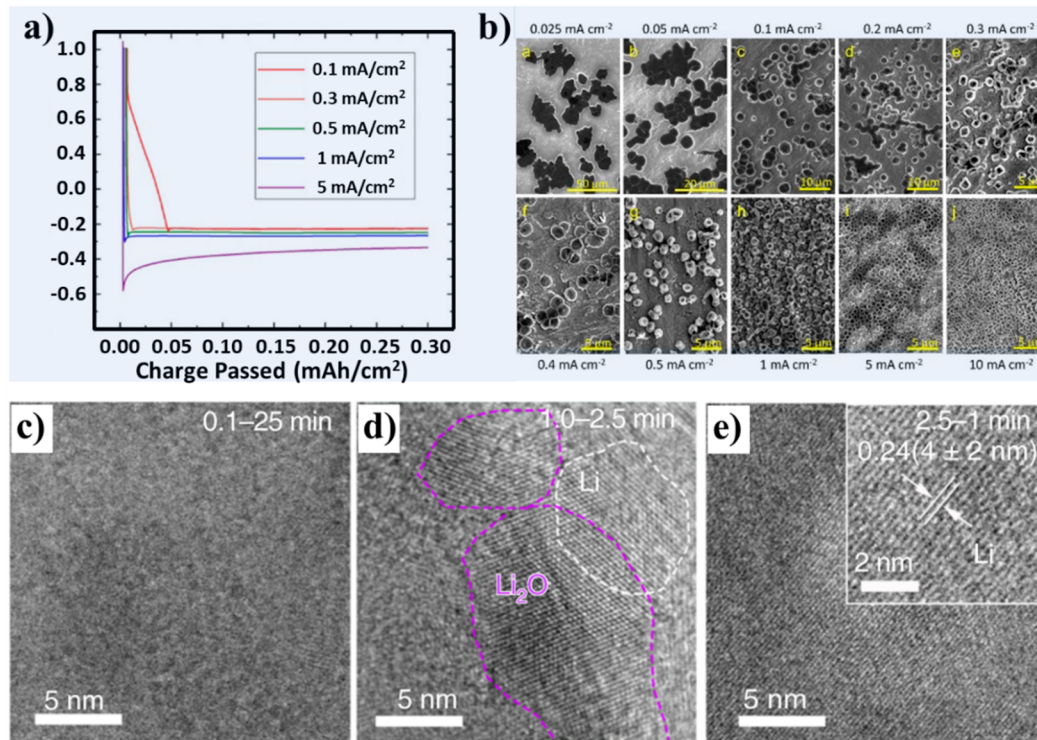


Figure 9. Influence of cell operation rate on Li nucleation. (a) Galvanostatic discharging curves under different working temperatures for the same deposition capacity of 0.3 mAh cm^{-2} . (b) SEM images of Li nuclei deposited at different current densities with a total areal capacity of 0.1 mA h cm^{-2} . Reproduced with permission from ref 94. Copyright 2017 American Chemical Society. (c–f) Cryo-TEM images of the Li deposits at (c) 0.1 mA cm^{-2} for 25 min, (d) 1.0 mA cm^{-2} for 2.5 min, and (e) 2.5 mA cm^{-2} for 1.0 min. Reproduced with permission from ref 112. Copyright 2020 Springer Nature.

Li^+ in the electrolytes.¹⁰⁸ Furthermore, these features endow pyridinic nitrogen-doped carbon high lithiophilicity and a substantial decrement of nucleation overpotential relative to bare graphene substrates, as observed in the galvanostatic electrochemical plating test at a current density of 0.05 mA cm^{-2} .¹⁰²

Furthermore, the factors that influence the lithiophilicity of the functional groups (e.g., electronegativity of atoms, local dipole, and charge transfer) are also comprehensively discussed by Zhang *et al.*⁹⁸ Based on the first principle calculation, the binding energies between Li with over 20 types of doping elements on graphene nanoribbons (GNRs) are derived (Figure 8a); the results indicate that bgB, egB, pN, kO, and aO single-doped graphene nanoribbons exhibit higher Li atom binding energy than bare GNRs (Figure 8b). The first and well-accepted factor that contributes to the enhanced Li^+ affinity is the electronegativity of sites brought by doping/functional groups.⁹⁸ For instance, the high binding energy with Li atom for aO-GNR can be ascribed to several reasons: (i) O atom itself has large electronegativity (3.44) and (ii) the doping has one pair of electrons that act as a Lewis base to absorb Li^+ . The theories also fit for the situation of kO and pN doping. In contrast, other O- or N-containing doping/functional groups such as bqN, eqN, and cO only contain the odd electrons, which negatively influence their electronegativities and their binder energies with Li atoms. It is worth mentioning that halogen atoms, particularly the F atom, exhibit large electronegativity (3.98 for F) but present even poorer binding energy than bare GNRs. This phenomenon might relate to the chemical state difference between halogen doping and N/O containing doping; specifically, N and O doping can effectively delocalize π electrons from carbon substrate, while halogen atoms reversely

feedback the electrons to carbon substrates by forming p- π conjunction. Meanwhile, carbon substrates with a relatively large halogen atom doping such as Cl, Br, and I will also damage their binding energy with Li atoms. For B-based doping (e.g., bgB or egB), the situation is opposite to that of O and N: the B atom (2.04) has lower electronegativity than the C atom (2.55), and the B-based doping can convert the adjacent carbon atoms to electronegative; furthermore, sites near the bgB or egB single doping will be preferential for deposition.⁹⁸ The second factor for the enhanced Li^+ affinity is the local dipole which is formed by both the doping and doped carbon atom.⁹⁸ The local dipole would induce the dipole force and a dipole around absorbed Li^+ . The stronger local dipole it is, the larger binding energy it will be between the substrate and Li^+ . The proposed binding energy correlation with dipole intensity and the value of electronegativity is shown in Figure 8c. Inspired by the thought, binary B-O doping on GNRs with both large electronegativity and large dipole intensity is expected to exhibit the optimum lithiophilicity.⁹⁸

The traditional adsorption and nucleation mechanism mentioned above lies on the direct interaction between Li^+ with the host atom, where the sites possessing the highest binding energy/adsorption ability with Li^+ are preferential for local Li deposition. An exception for such a mechanism is the S dopant, which replaces one carbon atom in the hexagonal carbon ring in the graphene crystal.¹⁰⁹ The expected adsorption site in the traditional mechanism should be the center of the ring (site 2 in Figure 8d); however, the simulation results indicate that Li^+ prefers to adsorb on neighboring sites (site 4 marked in Figure 8d), which means the effective adsorption area gets expanded by applying the type of dopant. To count, altogether four reasons may account for such abnormal phenomenon: (1)

one excess electron remained after the S atom forms δ and π bonds with the surrounding carbon atoms through hybridization, which may prevent the S atom from taking extra electrons and force the Li^+ transferring to the neighboring sites, (2) the incorporation of the S atom also interferes with the π -bonding states in the graphene crystal: both the intensity of hybridization and the amount of hybridization states for S-doped hosts get increased relative to those of pristine counterparts, as shown in the partial density of states (Figure 8e,f), (3) the amount of adsorbed Li^+ over S-doped graphene has direct connection with the electronic structure of graphite substrates, in turn, affecting the subsequent deposition potential. According to the simulation results, utmost six well-dispersed sites are energy-favored for adsorption before the potential decreases to negative value, which significantly expands the lithophilic ranges over substrates, and (4) the S-doped graphene maintains the low surface diffusion barrier for Li^+ equal to that of pristine graphite counterpart, which also contributes to the enhanced lithophilicity in the broader area.¹⁰⁹

(5) Influence of Cell Operation Rate

As known, the size and distribution of nuclei are coinfluenced by the diffusivity of Li^+ in electrolyte and cell operation rate. The former parameter and correlated factors (*i.e.*, working temperature, salt concentration, and composition of electrolytes) will be mentioned in other sections. Herein, we will discuss the role of the cell operation rate in the nucleation stage and further the impact on the subsequent growth stage.

The cell operation rate is closely correlated to the applied current density of the cells. Decreasing the current density leads to a low reaction rate and guarantees a relatively sufficient Li ion compensation time, which is effective to reduce the concentration polarization and nucleation overpotential (Figure 9a),⁹⁴ further reducing the possibility of tree-like dendrite formation. Consequently, Li metal prefers to further deposit on the initially formed small Li nuclei due to the lower energy barrier, affording larger, sparse nuclei on the substrate surface, in accordance with eq 9 and experimental results (Figure 9b). In contrast, at a higher current density, the nuclei tend to be smaller in size and more densely distributed since Li-ion diffusion is limited. It should be mentioned that the ether-based electrolyte (1 M LiTFSI in 1,3-dioxolane (DOL)/dimethyl ether (DME), 1:1 vol/vol, with 1 wt % LiNO_3) is widely applied in the works, in order to obtain the nearly circular Li deposits for convenient size-measurement.¹¹⁰

Generally, the densely and uniformly distributed small nuclei, formed under high current densities, are beneficial for the subsequent formation of a regular and smooth Li deposition layer, owing to the enlarged electroactive sites and homogeneous concentration and electric field distributions.¹¹¹ However, these advantages are usually outweighed by the disadvantages resulting from a high current density. According to the Sand's time model, increasing current density or reducing diffusion capability may aggravate the dendrite formation. Furthermore, small nuclei present a large surface area, thus consuming more electrolytes to form the SEI layer; the decreasing salt concentration in the electrolyte will also trigger the dendrite growth.⁹¹ Therefore, it is unable to affirm whether the nuclei states produced under different current densities are positive or negative unless all the facts are comprehensively considered.

In addition, the nanostructure configuration of nuclei is also dependent on the cell operation rate, specifically the effective current density. With the assistant of cryogenic transmission

electron microscopy (cryo-TEM), it was revealed that a disorder-order phase transition (DOPT) would occur with increased current density and deposition time during Li nucleation and growth.¹¹² As shown in Figure 9c–e, a higher applied current density results in a larger cluster size and higher degree of crystallinity in electrochemically deposited Li. Compared with crystalline Li metal, the glassy Li metal avoids the epitaxial growth into irregular patterns but supports the multidimensional growth into large grains with higher density, lower porosity and tortuosity, less reactivity, and better microstructure interconnections. These fancy features of glassy Li metal can substantially minimize the volume expansion, reduce the side reaction between Li and the electrolyte, and maintain an effective electronic and ionic network or percolation pathway. Consequently, a higher electrochemical reversibility would be expected for the glassy Li.

3.1.4.2. Influence of SEI Layer Properties. Differing from the electrodeposition of Ag, Zn, and Cu metals, the distinct SEI layer formation on the Li metal anode makes it much more complicated to manage the Li metal evolution during long-term cycling. Generally, the SEI layer can be formed as long as the Li metal is in contact with the electrolyte or formed from the electrochemical decomposition of the electrolyte. Several models have been proposed to demonstrate SEI formation on the Li metal anode, including the Peled model,^{42,113} the mosaic model,^{114,115} and the Coulombic interaction mechanism.^{116,117} During Li plating, Li ions pass through the SEI layer first and then are reduced to deposit between the SEI layer and the pristine Li metal. The SEI layer blocks the electron conduction but permits Li^+ ion transport from the bulk electrolyte to the surface of Li metal electrode, which hinders the continuous reaction between the electrolyte and fresh Li metal beneath the SEI film. Therefore, the SEI layer can adjust the distribution of Li ions from the bulk electrolyte to the Li anode and the electron around the Li anode. The properties and stability of the SEI layer are closely related to the ionic concentration field (ion diffusion) and electric field (charge transfer) near/at the reaction interfaces, thus influencing the Li metal nucleation/propagation kinetics and further the Li metal morphology. An ideal SEI layer shall have the following features: high electronic resistivity, high Li-ionic conductivity and permeability, strong mechanical stability, as well as appropriate thickness with a compact structure.^{118–120}

(1) Compositional and Structural Homogeneity of SEI Layer

The specific components and structures of the SEI layer strongly depend on the electrolyte composition. One pioneering work demonstrates that the SEI layer contains inorganic components (such as Li_2O , LiOH , LiF , and Li_2CO_3) decomposed from the anions in electrolytes and organic components (*e.g.*, ROLi, RCOOLi, ROCOLi, RCOO₂Li, and ROCO₂Li, where R represents alkyl groups) derived from the solvents in electrolytes.¹²¹ Compared with the inorganic components, organic components are more electrochemically stable but more cation-transfer resistive.¹²² Furthermore, it was previously deemed that inorganic components are mainly distributed in the inner part while organic components exist on the outer surface.¹²³ In contrast, the SEI layer in both the plane direction and the thickness direction are inhomogeneous because of the multiple reduction reactions and the formation-dissolution-reprecipitation mechanism, and the distributions of different components are highly dependent on the electrolyte systems. Recently, cryo-electron microscopy techniques have

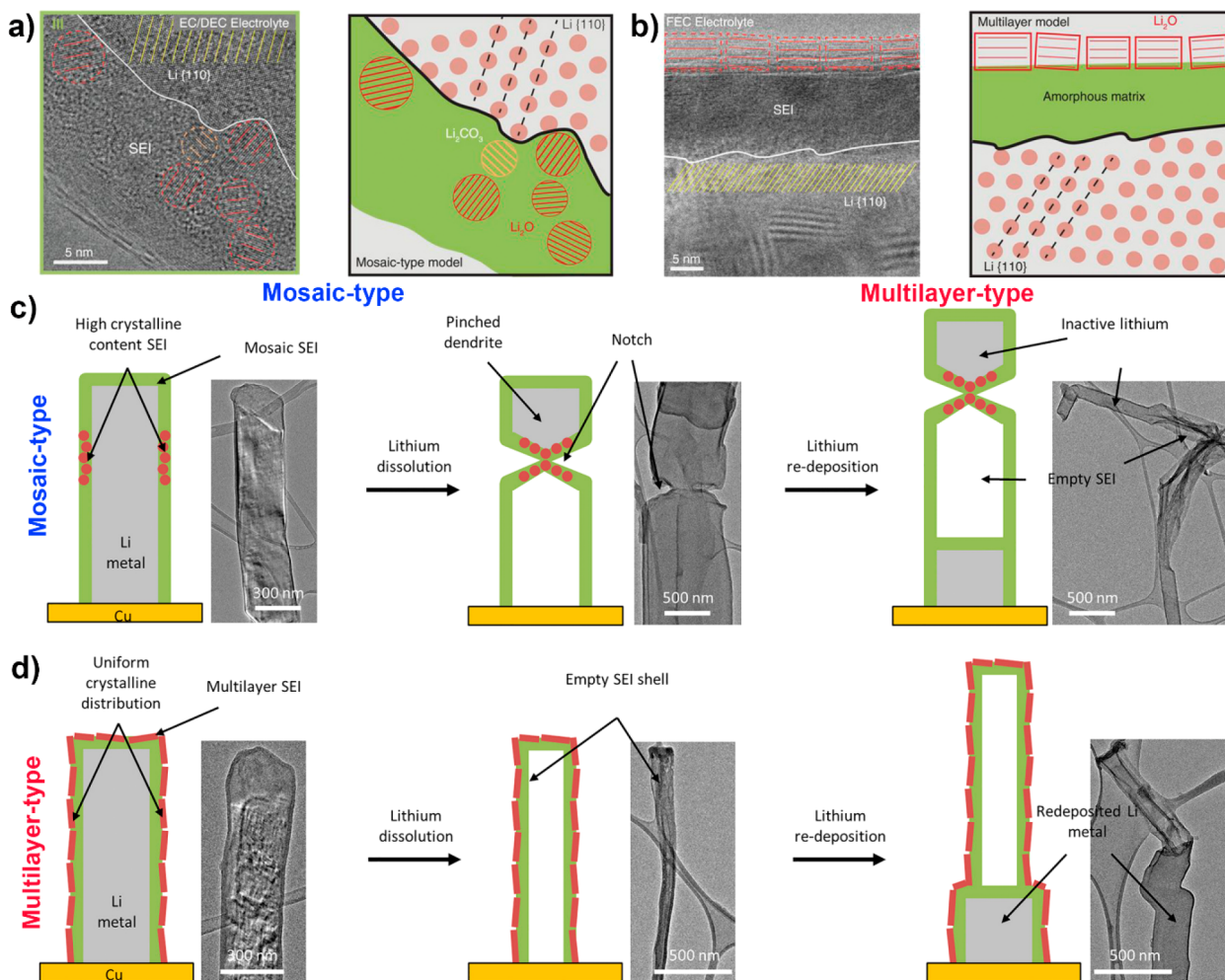


Figure 10. SEI structure in different electrolyte systems. (a,b) Atomic resolution image and schematic of the observed mosaic-type SEI structure (a) and multilayered SEI structure (b) formed on the Li metal (whisker in this work) in EC–DEC electrolyte without and with FEC additive, respectively. Reproduced with permission from ref 124. Copyright 2017 AAAS. (c) Nonuniform Li stripping through mosaic-structure SEI and (d) uniform Li stripping through multilayer-structure SEI. Reproduced with permission from ref 125. Copyright 2018 Elsevier.

been used to identify the spatial distribution of organic and inorganic components in the SEI layer.¹²⁴ As shown in Figure 10a, the as-formed SEI film in the widely used carbonate-based electrolyte (ethylene carbonate–diethyl carbonate (EC–DEC)) resembles the mosaic structure, where the SEI film presents a heterogeneous distribution of inorganic components and organic components (amorphous part). In the carbonate-based electrolyte with 10 vol % fluoroethylene carbonate (FEC), the as-formed SEI is more ordered and appears to have a multilayer structure, where the inner layer appears to be an amorphous polymer matrix and the outer layer is examined to be the inorganic component (Figure 10b).¹²⁴

In principle, the composition and homogeneity of the SEI layer will influence the morphology of Li deposits by influencing both the plating and stripping kinetics. For example, in the above-mentioned two distinctive SEI structures (mosaic and multilayer structures), localized Li dissolution occurs quickly through the regions of high crystallinity in the mosaic SEI; in contrast, uniform Li stripping is observed for the more ordered multilayer SEI and this is favorable for suppressed Li loss and enhanced cycling stability (Figure 10c,d).¹²⁵ Based on all these results, it is implied that crystalline grains within the SEI film must be distributed evenly such that the spatial ion diffusion does not vary significantly. More discussion about the

relationship between SEI chemistry/composition, Li diffusivity, and Li morphology will be present in the Ionic Conductivity of SEI Layer part later, which is from the point of Li ion transfer within the SEI layer.

(2) Electronic Conductivity of SEI Layer

The ideal SEI layer should allow fast Li-ion penetration but block electron tunneling. Hence, low electronic conductivity (*i.e.*, the transference number of electrons approaches to zero) should be considered as a key parameter for the SEI layer to suppress irregular Li formation, which is consistent with the observations in solid-state batteries that high electronic conductivity is the culprit for the Li protuberance penetration in solid-state electrolytes.¹²⁶ In the real SEI layer, the inorganic layer can only facilitate Li^+ transport (*i.e.*, the transference number of Li^+ ($t_+ = 1$)), while the organic layer can also be penetrated by both solvents and anions (*i.e.*, the transference number of anions ($t_- > 0.5$)).^{127,128} As a result, the electrolyte will be immediately attacked once electrons tunnel from the Li metal anode through the inorganic layer to the interface of the inner and outer layers, leading to incessant growth of the SEI. Therefore, the capability of the inorganic SEI components to block electron conduction plays a critical role in stabilizing the SEI, and the properties (*e.g.*, composition, distribution, and immunity) of the inorganic phase are all key to the

protection function of the SEI.¹²⁹ However, the electric conductivity of the native SEI is hard to manage, due to the facts that^{34,129} (1) the native SEI is heterogeneous due to the multistep formation mechanism; (2) the evolution of SEI are dynamic and continuous during cycling, resulting in variable microstructure and properties; (3) the electronic conductivity of the ionic crystals in the SEI (*e.g.*, Li halide) may be increased by the local excessive heating caused by uneven plating currents. Therefore, the native SEI layer with inhomogeneous electric conductivity is easy to trigger irregular Li formation. To mitigate the above challenges, introducing artificial electron tunneling barriers (AETB, *e.g.*, atomic crystal nanodiamond particles) into the native SEI layer to construct the AETB-embedded SEI layer might be a more effective way to maintain the low electron conductivity of SEI layer; meanwhile, the influence on electric field can be easily adjusted by the number of AETB.¹²⁹

(3) Ionic Conductivity of SEI Layer

In bulk electrolyte, the Li^+ conductivity can reach 10^{-2} S cm^{-1} ,¹³⁰ in comparison, Li-ion migration through the SEI layer is much more sluggish. Regarding the Li-ion diffusion mechanism through the inorganic layer, there are also some controversies in different models. In the model called the “multicomponent, multilayer structure”, it is deemed that ions can diffuse through the grains (individual components of the SEI) and the grain boundary formed between those individual components.¹³¹ Another model called “two-layer-two-mechanism diffusion” considers the inner layer as one structured sublayer, where ions diffuse through it via the knock-off mechanism.¹³² To further explore the charge-transfer behavior (especially ion migration) in different inorganic components and boundaries, DFT numerical simulations have been widely adopted and approved as a valuable tool. As evidenced by Peled *et al.*,¹³³ Christensen and Newman,¹³⁴ and Leung and Jungjohann,¹³⁵ transport of Li ions through the film via vacancies, interstitials, and grain boundaries are all important factors. Mashayek *et al.* demonstrate that Li ion diffusion in the grain boundary, formed between major inorganic components of the SEI film, is generally faster than that in the neighboring crystalline regions within the grain interiors.¹³⁶ Moreover, it is revealed that the LiF/LiF, $\text{Li}_2\text{O}/\text{Li}_2\text{O}$, and LiF/ Li_2O grain boundaries are the most stable configurations. In addition, the fastest Li diffusion rate is observed for the heterogeneous LiF/ Li_2O grain boundary, relative to the homogeneous LiF/LiF and $\text{Li}_2\text{O}/\text{Li}_2\text{O}$; this is because Li multatom coordination inside the grain boundary is a very favorable structure, which makes the multatom hopping mechanism more advantageous than any other mechanism.

Basically, the SEI layer with a higher and isotropic ionic conductivity allows faster Li ion transportation and lower concentration gradient polarization, thus enabling smooth plating/stripping behavior even at high working current densities. The importance of ionic conductivity of the SEI layer was unveiled by a diffusion–reaction competition mechanism.¹³⁷ Specifically, the SEI layer with low ionic conductivity retards the Li ion diffusion, thus accelerating the Li ion depletion beneath it; the process is diffusion-controlled. Because the initial Li nucleation sites evolve into bumps distributed on the current collector and the bottom edges of Li bumps are unable to capture Li ions under the electric field, insufficient Li ions tend to gather on the tips and trigger the irregular Li deposition.¹³⁸ When the SEI layer exhibits high ionic conductivity, Li ions will migrate onto the surface of anode with faster kinetics. As a result, the rate-determining step of Li

deposition transits to the reaction-controlled one, and the number of Li ions beneath the SEI remarkably increases even on the edges of Li nucleation bumps. Then the conversion of Li ion to Li atom can occur uniformly on Li nucleation bumps, leading to spherical Li deposition.¹³⁷

Furthermore, the influence of Li transport in the SEI layer toward the morphology of Li deposits has also been visualized by an *in situ* AFM-TEM study. It was found that when the experiment was conducted in $\sim 10^{-2}$ mbar CO_2 to form the SEI components of Li_2O and Li_2CO_3 on the deposited Li metal surface, the Li^+ ions are preferentially reduced and locally deposited at the Li particle–SEI interface, leading to the sprouting of a Li whisker from the initially formed Li particle nuclei, as the SEI is sluggish in transporting Li ions (particularly compared with self-diffusion of Li metal). In contrast, when the Li deposition was performed in a N_2 environment, the deposited Li slowly and continuously expands from the side surfaces, manifesting a surface-growth mode with a protuberance-free morphology; this is because lithium nitrides (*for example*, Li_3N) are presumably introduced inside the SEI, where Li_3N is a much better Li^+ conductor than Li_2CO_3 and Li_2O .¹³⁹ To validate above findings from the *in situ* experiments in practical coin cells, an “electrolyte-poison” experiment was designed, in which EC (or EMC) was added in baseline electrolyte (1 M LiFSI in DME) to reduce the ionic conductivity of the SEI layer. Experimental results show that a pure monolithic Li morphology is primarily observed during deposition in baseline electrolyte, while the introduction of EC will lead to mixed morphologies of monolith and whisker or even pure whiskers.¹³⁹ Similar phenomena are also observed when using a series of electrolytes with different $\text{LiNO}_3/\text{LiTFSI}$ ratios, which construct the SEI layer with a diffusion kinetics gradient.¹³⁷ Here, the partial substitution of routine TFSI⁻ anion to NO_3^- generates LiN_xO_y and Li_3N in SEI, thus enhancing the ionic conductivity of SEI. In the baseline electrolyte without LiNO_3 , almost all Li deposits present whisker-like morphology, while the spherical Li deposition appeared with increasing the proportion of LiNO_3 . The experimental results are consistent with the aforementioned diffusion–reaction competition mechanism. In other words, when using the solvents to produce decomposed products with a higher ionic conductivity, the possibility of an irregular Li appearance will be significantly reduced.¹³⁹

To conclude, the electronic/ionic mitigation behavior inside the SEI layer changes with different compositions and structures of the SEI layer, and any local variations in the SEI layer can cause a significant anisotropic diffusivity of electrons or Li ions across the SEI and ion concentration polarization beneath the SEI layer, thus leading to nonuniform Li delivery.^{137,140} To address this issue, artificial SEI coating films with a uniform composition and structure have been intensively investigated (see a detailed discussion in section 4.3.1).

3.2. Stress Field Influence on Li Metal Evolution

Like ionic concentration field and electric field, the stress field around the metal anodes also has a great impact on the deposition pattern of Li metal. The evolution of three types of irregular Li structures, including tip-growth Li dendrites, bottom-growth Li whiskers, and surface-growth Li mosses, are all closely correlated to the stresses inside the cells. Tuning the intensity and distribution of stress applied on Li metal may not only accelerate or suppress the growth of irregular Li but also induce the morphological transition between polymorphous Li deposits. These are correlated to the fact that Li metal has a very

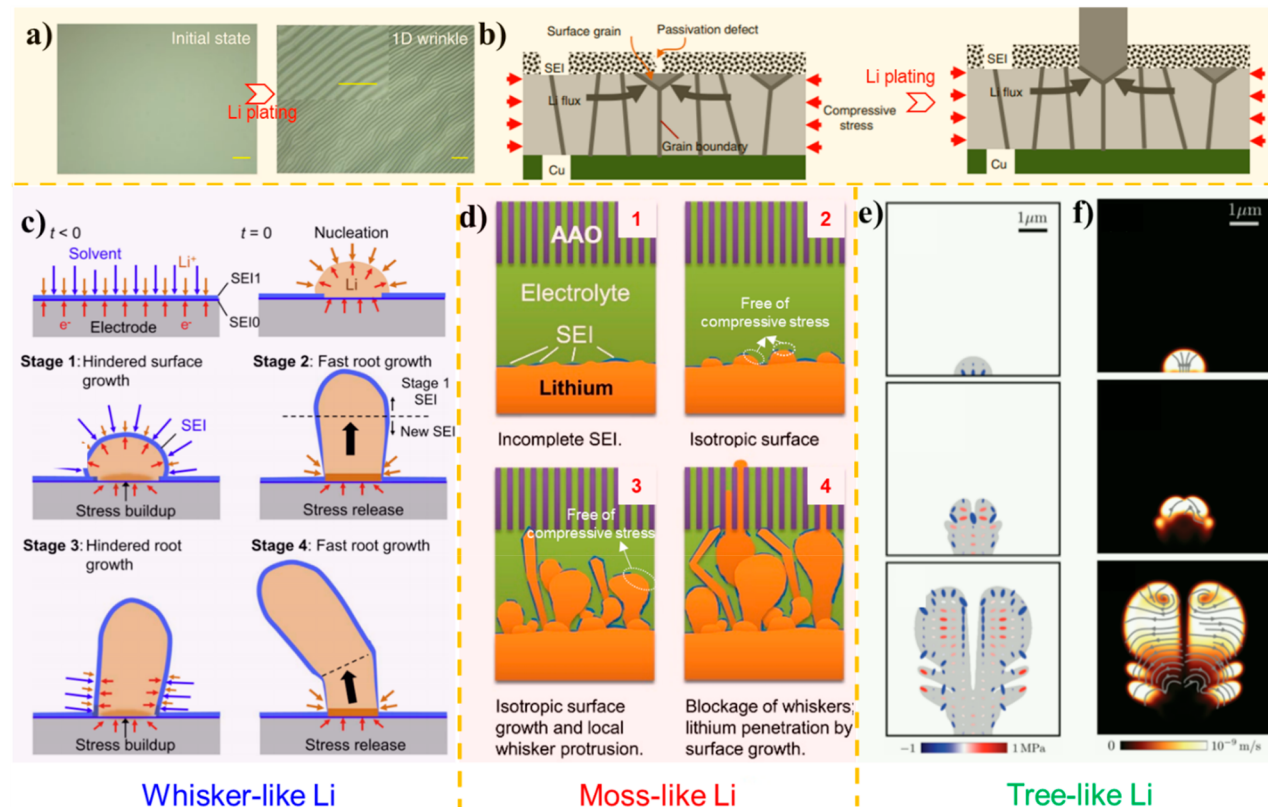


Figure 11. Origins of internal stress generation and polymorphous Li formation. (a) Direct observation of internal stress induced by the plating process through the wrinkle that appeared over 200 nm Cu@PDMS substrates, where all scale bars (including that in inset) represent 100 μm . (b) Schematic diagram of stress-driven whisker growth model proposed by Wang *et al.* Reproduced with permission from ref 21. Copyright 2018 Springer Nature. (c) Schematic diagram of the whisker-like Li growth process proposed by Li *et al.* Reproduced with permission from ref 73. Copyright 2017 Elsevier. (d) Schematic explanation of moss-like Li growths due to the incomplete SEI layers interrupted by the increased current density and heterogeneous distribution of internal stress. Reproduced with permission from ref 20. Copyright 2018 Elsevier. (e,f) Evolution of (e) stress and (f) plastic displacement rate within tree-like Li deposits with time from 0 s (upper) to 1200 s (middle) and to 4800 s (below) at a current density of 1 mA cm^{-2} . Reproduced with permission from ref 153. Copyright 2019 Royal Society of Chemistry.

low hardness and poor mechanical strength as mentioned in section 2.1, making its nucleation/growth susceptible to the surrounding stress deviations. To count, the stresses can be categorized into internal stress and external stress. Internal stress is the stress between the plated Li metal derived from the dramatic volume change during the plating process and inhomogeneous deposition rate, while external stress is the compressive stress generated from the neighboring solid interfaces (*e.g.*, SEI and separator). In the following subsections, the originalities of these two types of stresses and their connections with polymorphous Li growth will be discussed in-depth.

3.2.1. Internal Stress Inside Plated Li Metal. The residue compressive stress induced by the plating process exists in the plated Li metal, namely, the internal stress, can be directly observed through a control experiment by applying a soft Cu@PDMS substrate (Figure 11a)²¹ or soft Sn foil substrate.¹⁴¹ Such a type of internal stress is also broadly observed in other materials with high atomic mobilities (*i.e.*, Ag, Cu, and Au) that grow in the Volmer–Webber mode.^{21,142,143} The migration of Li atoms through grain boundaries under nonequilibrium growth conditions is blamed for the appearance of such stress.¹⁴⁴ Upon the stress effect, Li deposits may evolve into irregular structures with different morphologies.

3.2.1.1. Stress-Driven Li Whisker Growth. It is known that residue stress in the thin film leads to the growth of whiskers with

a preferential crystallographic orientation along $\langle 111 \rangle$.^{124,145–148} Similarly, the deposition-induced stress is also one important driving force for Li whisker growth, but the situation is more complicated and more factors should be taken into consideration in the case of Li plating, particularly the SEI layer.^{21,149}

In a pioneering model proposed by Yamaki *et al.*, it is assumed that the inhomogeneous Li deposition on the anode under the influence of the SEI layer initially results in gradual accumulation of stress.⁹³ Afterward, the SEI layer breaks up so as to release stress and Li metal sticks out in the shape of whiskers. The speculation was further proven valid via a mathematical model, in which the whiskers exist when the surface tension of Li metal is higher than the creep strength of bulk Li to allow effective mass transfer of Li metal but is lower than the creep strength of whiskers to maintain the shape. Instead, if the surface tension of Li metal overpasses the creep strength of whiskers, the deposited Li metal is supposed to appear as a particle shape.⁹³ Later on, a more comprehensive stress-driven Li whisker growth model is proposed by Wang *et al.* (Figure 11b).²¹ Since the plated film typically possesses a relatively dense body with low volume for vacancy or holes, the stress is hard to release inside the body but concentrates over some spots (*e.g.*, grain boundary¹⁴⁹ and crystalline impurities^{150,151}). Additionally, the Li metal surface is passivated by the SEI layer, where the bottom inorganic salts of SEI attach closely to the Li metal surface. If the SEI layer is rigid

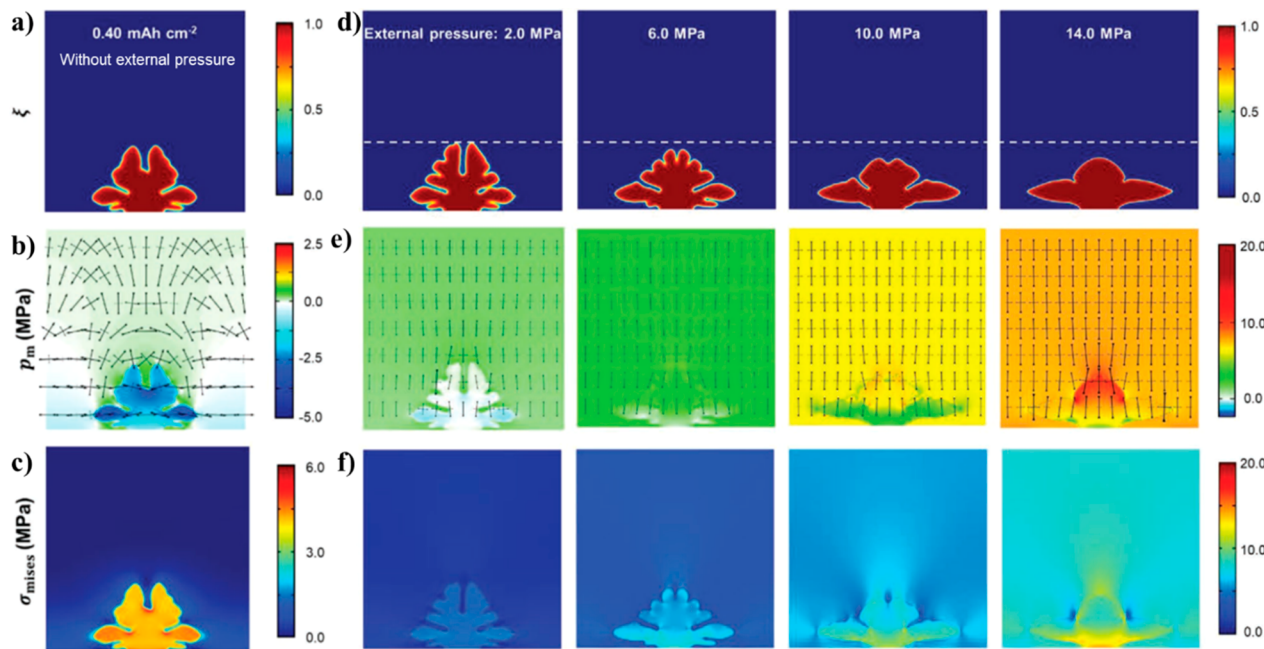


Figure 12. Influence of external stress on Li dendrite shapes. (a–c) Simulated results of Li dendrites in the absence of external pressure at a plating capacity of 0.40 mAh cm^{-2} . (d–f) Simulated results of Li dendrites under the external pressure ranging from 2.0 to 14.0 MPa. Specifically, (a, d) dendritic morphology, (b, e) principle stress and hydrostatic pressure, and (c, f) von Mises stress evolution. Reproduced with permission from ref 163. Copyright 2018 Wiley-VCH.

enough, it will be very hard for the pressure to release freely. However, the SEI layer is usually inhomogeneous as mentioned above and some parts contain the defects such as pinholes or vacancies, where the stress relaxation is most probable to occur. The growth rate of the whisker is given by $v_w = JV_{\text{Li}}/\pi r^2$, in which r is the whisker radius, V_{Li} is the molar volume of Li, and J is the Li flux (mol s^{-1}) that is influenced by the compressive stress. As known, the compressive stress can promote the diffusion of Li^+ . Upon compressive stress, if the growth rate of the whisker is higher than the uniform Li deposition rate ($v_p = jV_{\text{Li}}/F$, where j is the plating current density, F is Faraday's constant), Li probably protrudes out in the whisker form, otherwise it will maintain a uniform deposition. Notably, when the compressive stress overpasses the yield strength of Li metal, localized creep of Li will occur over the defective regions and Li whiskers growth will be strengthened.^{21,47} Furthermore, when the compressive stress is large enough to break the SEI layer, pinholes will be created in the SEI layer that offer the routes for whiskers growth.^{73,93}

In another model, the significance of the SEI layer toward Li whisker growth is further highlighted, as illustrated in Figure 11c.⁷³ At the initial stage, Li nuclei overcame the overpotential to form on the substrate surface and are rapidly covered with the SEI layer due to their high reactivity. With the plating process continuing, the stress simultaneously accumulates at the bottom of the deposits. Once the stress reaches a threshold, the SEI layer will be broken to enable the pressure release, and the subsequent Li metal deposition will be preferentially triggered at the fresh root due to the free compressive stress and better electronic/ionic conductivity, where the newly plated Li metal is prone to evolve into Li whiskers. After the full relaxation of stress, the whisker growth stops and the SEI film will resume covering onto the surface of freshly exposed Li. In the next Li plating cycling, stress is supposed to accumulate again and induces the next-round whisker growth. Notably, due to the constant change of the interface/boundary state (e.g., SEI)⁷³ and the existence of

crystalline defects (e.g., dislocation, grain boundary, and weak point on the SEI layer),²⁷ the relaxation direction of the dominant stress also changes accordingly; in turn, the growing redirection of the whisker is induced as observed in multiple works.^{73,75,93,152} Furthermore, in Li whisker growth cases, the Li plating current density should be below a critical value, where the rate of Li deposition is much slower than the rate of SEI formation and complete coverage of robust SEI can be achieved; otherwise, moss-like Li or even tree-like Li will be triggered.²⁰

3.2.1.2. Stress-Driven Li Moss Growth. Analogous to the growth mechanism of whisker-like Li, the moss-like Li growth is also majorly dependent on the internal stress. However, the moss-like Li growth typically occurs at a current density higher than whisker-like Li but lower than tree-like Li, at which the deposition rate exceeds the SEI formation rate.²⁰ In this case, the anode surface is usually covered with the incomplete SEI layer. At those sites without (or with poor) SEI protection, the Li^+ polarization and electric field aggregation are more dramatic because of the locally higher electric conductivity and free of compressing stress from the SEI layer; in these parts, the deposition rate will be faster than that at SEI-well-covered parts and the Li metal deposits will follow the regular surface-growth mode to grow into moss-like morphology (Figure 11d).²⁰ At the sites covered with an unbroken SEI film, the internal stress would still possibly accumulate in the following plating process and have the chance to break the SEI layer at certain points, then the Li metal will also protrude out in whisker morphology. This explains why the mixture of whisker-like Li and moss-like Li can be observed in practical situations.

3.2.1.3. Stress-Driven Li Dendrite Growth. As stated in section 3.1, the initiation of tree-like Li dendrite is primarily under the joint impact of an ionic concentration field (salt depletion) and electric field (charge aggregation); in fact, its evolution has a close relationship with internal stress as well.¹⁵³ According to the simulation results from Garcia *et al.*, the

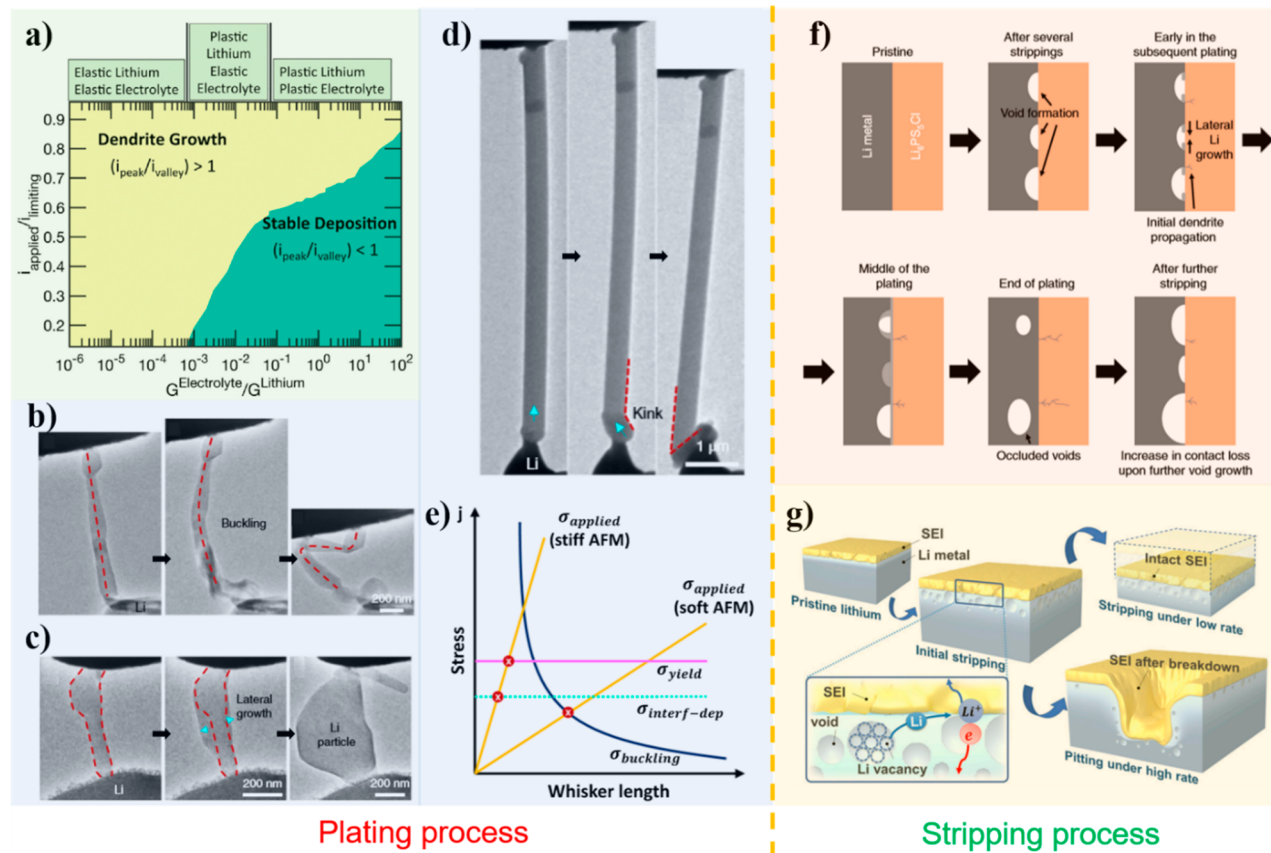


Figure 13. Influence of external stress on the Li metal plating/stripping process. (a) A phase map of Li deposition format as a function of the normalized current density $i_{\text{peak}}/i_{\text{valley}}$ and normalized shear modulus of polymer electrolyte $G_{\text{Electrolyte}}/G_{\text{Li}}$ which also stands for the compressive stress over the Li anode. Reproduced with permission from ref 164. Copyright 2017, Royal Society Chemistry. (b–d) TEM images of (b) the buckling process of the Li whisker, (c) the cessation of axial direction growth but expansion in the lateral direction of the Li whisker, and (d) the kinking process of the Li whisker. (e) Numerical relationships of several scenarios of the Li whisker under stress, in which the pink line, blue line, dashed line, and yellow line stand for critical yielding stress, buckling stress, cessation of axial direction growth stress, and applied force from the AFM cantilever as a function of the whisker length separately. The “ \times ” markers represent the intersection of the applied force curve of the AFM cantilever and the critical stress lines, which demonstrate the state of the whisker at the load state. Reproduced with permission from ref 138. Copyright 2019 Springer Nature. (f) Schematic illustration of voids evolution at different testing conditions in the liquid electrolyte case. Reproduced with permission from ref 166. Copyright 2019, Springer Nature. (g) Schematic illustration of the Li cycling process in the solid electrolyte case with voids formation and dendrite growth as the stripping current density exceeds a critical value. Reproduced with permission from ref 165. Copyright 2018 National Academy of Sciences.

deposition promotes the appearance and accumulation of stress within the tip of the dendrite since the inflection stage even below the critical current density (transition from reaction-controlled to diffusion-controlled at 10 mA cm^{-2}).¹⁵³ As shown in Figure 11e,f, the inhomogeneous distribution of compressive stress in the dendrite determines the nonuniform deposition on the surface, which will further lead to the plastic flow of the Li atom to release the internal stress and cause the bifurcation of the tip into secondary branches. Afterward, the ionic concentration and electric fields induce the preferential growth over the tips, and the macroscopic tree-like morphology of the dendrite is derived. Overall, at a low rate (such as 0.1 mA cm^{-2}), the internal stress favors the surface-growth pattern and the deposits are supposed to develop into planar morphology.^{73,153,154} At a higher current density (1 mA cm^{-2}), the reaction rate becomes the dominant factor, and the stress will accumulate at the tip since the deposition rate is faster than the stress relaxation rate.^{28,93,153} Then the stress forces the atom to flow through bulk Li metal and split the tip into tree-like branches. When the current density exceeds the critical one (10 mA cm^{-2}), the tree-like dendrite formation is determined by both the diffusion-restriction and the internal stress. Nevertheless, the rapid

deposition rate at the tip inhibits the stress relaxation process, so the stress majorly influences the derivation of lower branches.^{153,155} Here, above the critical current densities, localized zero ion concentration around plated Li metal occurs, and the tree-like dendrite growth can also be explained by the Sand's time theory (concentration field-based model as discussed in section 3.1.1).

3.2.2. External Stress from Li Metal Surroundings.

There are different sources of external stress toward the Li metal, primarily coming from the SEI layer, solid-state electrolyte, and separator. These external stresses also exert great influences on the evolution of polymorphous Li as an internal stress does.¹⁵⁶ According to García *et al.*'s calculation, external compressive stress on the Li metal anode can interfere with the irregular Li development, in which a larger compressive stress helps increase the critical current density of Li dendrite initiation and hinders the formation of Li dendrites.¹⁵⁷ Even the growth pattern can be transited from coexistence to the base-growth-dominated one when the external stress accumulates for a critical time (t_c).^{28,157} One explanation as suggested by Monroe and Newman *et al.* ascribes the irregular Li suppression and flat deposition morphology to the elastic and more importantly plastic

deformation of the Li metal on the anode, which is in accordance with some experiment results based on polymer electrolyte and separators.^{44,158–162} More recently, the mechanism for the impact of external pressure (stress) on Li dendrites is revealed and quantified by a mechano-electrochemical phase field model. As shown in Figure 12, compared with the case without externally applied pressure, the morphology of Li dendrites tends to be relatively smooth and dense with less branches when the external pressure increases from 2.0 to 14.0 MPa. In addition, the shaped Li dendrites tend to have higher mechanical instability.¹⁶³

Moreover, the phase map of the Li deposition format is drawn as a function of applied current density and normalized shear modulus, in which the normalized shear modulus is an indicator of the amount of compressive stress over the Li metal (Figure 13a).¹⁶⁴ Accordingly, another factor that contributes to the suppression of irregular Li growth lies in the reduced reaction rate at the Li protuberance tips, in comparison to the valleys by enhancing the compressive stress from polymer electrolytes.¹⁶⁴ These factors are supposed to play roles on suppressing irregular Li initiation and growth throughout the whole cycling process.

Specifically, the existence of external stress will impact both the Li plating process and the Li stripping process. During the Li plating process, the tip/front of the Li protuberances has close contact with the external pressure; therefore, it will undergo the direct physical suppression from the forces. The growth of Li whiskers under an external pressure is supposed to contain four scenarios, as observed through an atomic force microscope with an environmental transmission electron microscope (AFM-ETEM), including (i) buckling of the Li whisker (Figure 13b), (ii) cessation of whisker elongation along the axial direction but expanding laterally instead (Figure 13c), (iii) kinking of the Li whisker, in other words, changing growing direction when reaching the critical stress (Figure 13d), and (iv) yielding of the Li whisker; the numerical relationship of these scenarios are shown in Figure 13e.¹³⁸ According to the Euler equation (eq 16), where the E stands for the elastic constant of the Li metal, I stands for the minimum second area moment for the cross-section of the whisker, L is the length of the whisker, and μ is a constant depending on the load condition of the whisker), the critical yielding value of Li whisker in the first scenario is calculated to be around 85 MPa, which fits well with the data collected from experiments. The second and third scenarios occur when the whisker stays in a thermodynamically-stable state. Nevertheless, the calculated value of the critical stress $\sigma_{\text{interf-dep}}$ from eq 17 (where γ represents the surface energy of the Li whisker, s stands for the perimeter of the whisker, A represents the contact area, the dL is the unit length increment of the whisker, σ is the compressive stress over the whisker, U is the applied potential on the interface, M_{Li} and ρ_{Li} stand for the molar mass and mass density of Li metal, respectively, and F is the Faraday constant) is over 14.8 GPa, which is about a hundred times larger than the measured value (\sim 13 MPa). According to Zhang *et al.*, the large gap between theory and reality may relate to the resistance of ionic transfer in the SEI layer: nonzero ionic current through the SEI layer when transiting from axial growth to lateral expansion, and the value of U in reality is not as high as the external applied potential.¹³⁹ In the fourth scenario, the measured critical yielding value for the Li whisker is around 100 MPa, which is consistent with the yielding strength of the submicron-scale Li particle reported previously in the literature.^{47,139}

$$F_{\text{cr}} = \frac{\pi^2 EI}{\mu^2 L^2} \quad (16)$$

$$\sigma_{\text{interf-dep}} = U \frac{\rho_{\text{Li}} F}{M_{\text{Li}}} - \gamma \frac{s}{A} \quad (17)$$

From the perspective of the stripping process, the stress impact over the irregular Li evolution is less direct in comparison to that in the plating process. The new scenario is correlated to the voids formation during the Li stripping process, which has been observed in both the liquid-electrolyte system (between Li metal and the SEI layer) and in an all solid-state system (on the interface between Li metal and the solid-state electrolyte).^{165,166} The formation of the voids is partially due to the uneven dissolution on the Li metal surface at a high cycling rate, particularly at certain sites like slip lines and grain boundaries and further the accumulation of vacancies on the interfaces.¹⁶⁵ The voids in both cases are detrimental to the cell performances. In the liquid-electrolyte system, the voids may result in the detachment of Li metal from the passivation layer above it, in turn, more electrolytes will be reduced by freshly exposed Li metal and the original SEI layer will lose function (Figure 13g).¹⁶⁵ For the solid-electrolyte system, the emergence of voids makes part of the Li metal lose contact with the solid electrolyte and slightly increases the polarization during the stripping process (Figure 13f). Due to the fact that Li metal prefers to deposit at the interface between voids and the solid electrolyte, some parts of the voids will be healed as evidenced by decreasing polarization while the remaining parts will be occluded within the Li metal and the voids will reappear and expand in the next stripping process, accompanied by constantly increasing polarization.¹⁶⁶ Moreover, the appearance of voids in both cases are supposed to aggravate the tree-like dendrite growth. According to Bruce *et al.*, the applied external stress (e.g., from solid electrolyte) on the Li metal anode can hinder the advent of Li dendrites. Specifically, the soft Li metal is easy to creep under external stress.^{166,167} Voids on interphases are formed since the rate of stripping is faster than the rate of Li metal replenishment, which includes the Li solid-state diffusion and Li metal creep: $J_{\text{Li diffusion}} + J_{\text{Li creep}} < J_{\text{Li+migration}}$, where J stands for the Li ion flux. Therefore, increasing the compressive stress over the Li metal anode enables better replenishment by accelerating the Li^+ diffusion rate and further suppresses the formation of Li dendrites.¹⁶⁶ For instance, in the Li//LiPS_xCl_y/Li solid-state testing cells, the critical plating current density for dendrite production significantly increase from 0.2 mA cm^{-2} under 3 MPa pressure to 1 mA cm^{-2} under 7 MPa pressure.¹⁶⁶

3.2.3. Influencing Factors on Stress Field. **3.2.3.1. Mechanical Properties of Li Deposits.** As detailed in section 2.1.2, the mechanical properties of the Li metal are dependent on the metallurgical structure (e.g., crystallographic orientations), morphology, dimensions, and temperatures, which are closely associated with the stress field generated inside/around the Li deposits. To avoid repeated discussion, we only highlight some major conclusions here: (1) dimension effect, micrometer-sized Li attains a high yield strength of 105 MPa at room temperature,⁴⁷ while its yield strength increases to as high as 244 MPa with the diameter of Li whisker decreasing to the submicrometer regime;⁴⁸ (2) crystallographic orientation effect, $\langle 111 \rangle$ -oriented Li crystal has a much smaller shear modulus than that of a $\langle 100 \rangle$ -orientated crystal, thus showing a lower possibility of dendrite formation over it;⁴⁷ (3) temperature effect, the yield strength of Li whiskers significantly reduces at

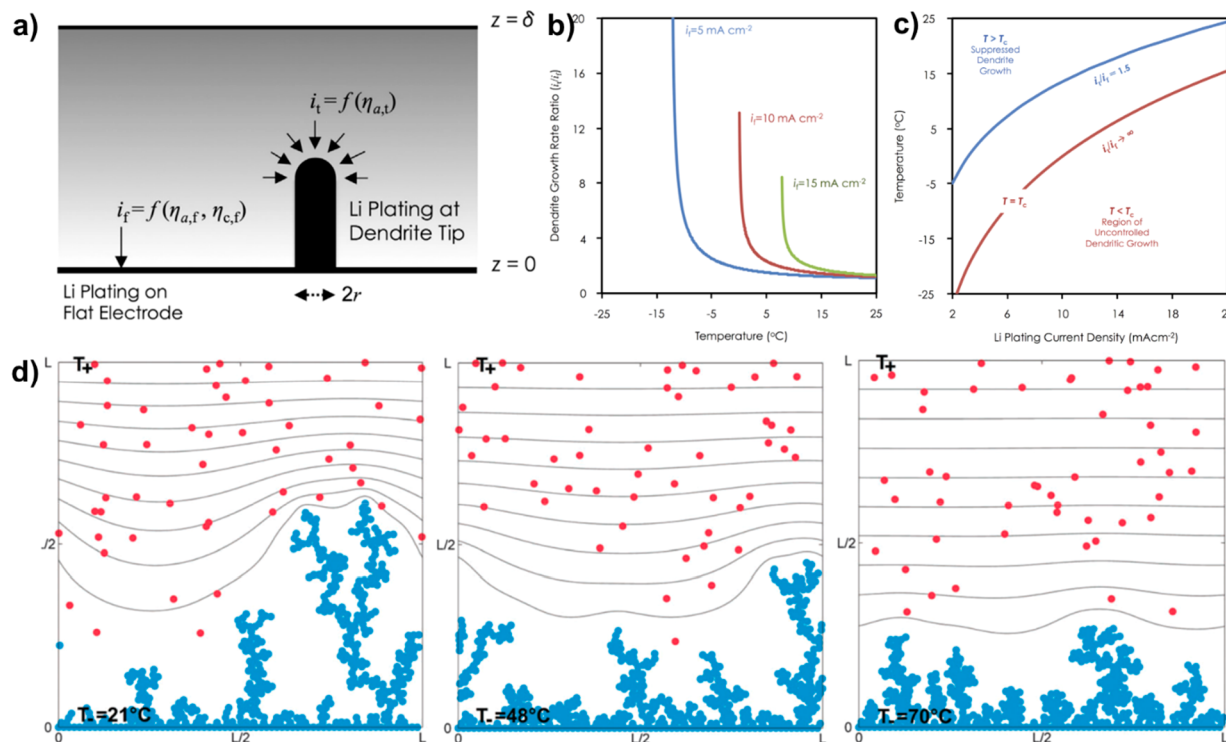


Figure 14. (a) Schematic of the model setup (a flat electrode surface with electrodeposited lithium). (b) The ratio of the current density at the dendrite tip (i_t) to that at the flat electrode surface (i_f) plotted as a function of the system temperature. (c) Variation of the dendrite growth rate ratio i_t/i_f with the temperature and Li plating current density. Comparison of the voltage hysteresis of the Zn/rGO anode with different thicknesses of the rGO layer. Reproduced with permission from ref 170. Copyright 2014 Elsevier. (d) Results of CG-MC calculations including both Li^+ transport and Li^0 thermal relaxation. Reproduced with permission from ref 172. Copyright 2015 Royal Society of Chemistry.

elevated temperature: its value for microsized Li pillars with different diameters at 363 K decreases by a factor of ~ 3.5 in comparison to that at room temperature.⁴⁷ Above size, temperature, and crystallographic orientation effects imply that applying an external stress which is slightly higher than the yield strength of bulk Li metal may not be enough to suppress irregular Li growth; all of these facts should be taken into consideration in regards to smoothening of the Li plating through an externally applied stress.

In addition, the nuclei shape of Li deposits will also influence the surface stress, which follows the Young–Laplace equation as described below:

$$\Delta P = \gamma \left(\frac{1}{R_1} + \frac{1}{R_2} \right) \quad (18)$$

where the ΔP is the pressure difference on the Li surface, γ is the surface tension (or surface energy) of the Li surface, and R_1 and R_2 are the radius of the curvature of the studied Li deposits with two orthogonal directions. With a smaller radius (larger curvature) and a constant surface tension on the less lithiophilic substrates, the as-formed Li particles have a larger pressure difference over the surface. If the stress is larger than the Li creep strength, some protrusions will be formed in order to release the pressure, probably damaging the SEI layer and inducing irregular Li formation.⁹³

3.2.3.2. Mechanical Properties of SEI Layer. Since the SEI layer is in intimate contact with the as-plated Li metal, the stress field around nucleation substrates or Li deposits is also dependent on the mechanical properties of the SEI layer (e.g., Young's modulus). In general, the naturally formed SEI layer is structurally fragile and compositionally heterogeneous. Due to

the dramatic volume change of the Li metal during long-term cycling, it will bring about large mechanical deformation. If the SEI layer cannot withstand this deformation, it will be repeatedly broken and reformed, during which polymorphous Li formation may be triggered (Figure 11). Meanwhile, it is not favorable to release the plating-induced stress if the SEI layer is too rigid. Hence, the SEI layer with a proper mechanical strength is of key importance to inhibit irregular Li growth. In a pioneering theoretical work done by Monroe *et al.*, they considered a solid polymer electrolyte (SPE) in contact with a Li metal electrode and performed a linear stability analysis of the deformation at the interface, in which the linear elasticity was used to simulate the stresses generated at the interface due to small deformations.¹⁶¹ They found that the dendrite growth decays with time if the SPE holds a shear modulus twice time higher than that of the Li dendrite (10^9 Pa).¹⁶¹ Another work demonstrated that the irregular Li growth can also be terminated if the SEI layer maintains a tension stress over 0.2 N m^{-1} .⁹³

Another issue caused by repeated Li plating/stripping is the potential formation of cracks and pinholes inside the SEI layer. These defective sites are mechanically favorable for stress release that further act as the extremely sporadic nucleation sites (namely, hotspots) for Li deposition,^{94,168} giving rise to irregular Li growth. Li *et al.* demonstrated that a pinhole-free Li_3N film can dramatically prevent continuous electrolyte consumption during battery cycling and promote protuberance-free and uniform Li plating underneath, which displays a strong contrast with the porous Li_3N film.¹⁶⁹ Thus, it is highly desirable to have a homogeneous and defect-free SEI layer, which can be potentially achieved by using the modified electrolyte (see

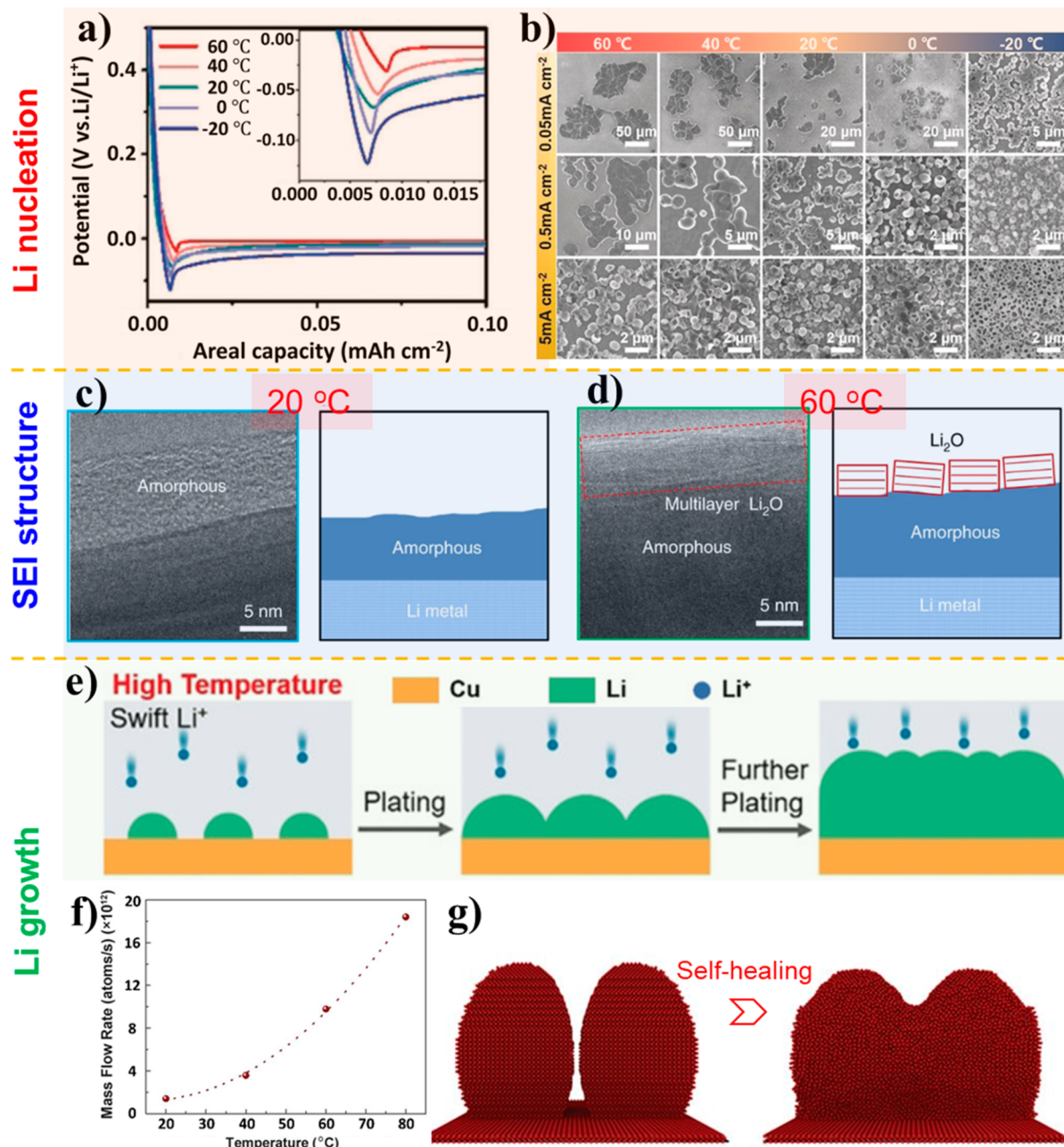


Figure 15. Influence of temperature on Li nucleation, SEI structure, and Li growth. (a) Chronoamperometric comparison of Li nucleation at varied temperatures at 0.05 mA cm^{-2} . (b) SEM images for Li nuclei morphology at varied current densities and temperature conditions with the capacity limitation of 0.1 mAh cm^{-2} . Reproduced with permission from ref 91. Copyright 2015 Springer Nature. (c,d) Emergent SEI nanostructure formed at (c) 20°C and (d) 60°C , in which the as-characterized Li metal was deposited in DOL/DME/LiNO₃ electrolyte using 1 M LiTFSI salt at a rate of 1 mA cm^{-2} with a capacity of 0.4 mAh cm^{-2} . Reproduced with permission from ref 174. Copyright 2019 Springer Nature. (e) Schematic illustration of Li growth pattern at high temperature. Reproduced with permission from ref 173. Copyright 2019 Wiley-VCH. (f,g) MD simulation results of (f) mass flow rate changes of Li atoms as the function of working temperature and (g) healing process of Li dendrite during heating. Reproduced with permission from ref 169. Copyright 2018 AAAS.

discussion in section 4.1.2 and 4.3.2.1) or introducing artificial SEI layers (see the discussion in section 4.3.2.2).

3.3. Temperature Field Influence on Li Metal Evolution

The temperature field inside batteries, majorly influenced by external surroundings and internal Ohmic heating, has an impact over almost every stage of Li metal evolution by influencing the ionic conductivity in electrolytes, atomic transfer within bulk Li metal, and the composition and physical properties of the SEI film. In addition, the temperature distribution homogeneity on

the anode surface which is dependent on the host thermal conductivity also has a direct connection with the Li deposition sites. In the following parts, we will discuss the temperature related models and elucidate the influence of temperature on the above circumstances one by one.

3.3.1. Temperature Field-Related Models. To bridge the relationship of Li metal evolution with the temperature field, Akolkar developed a mathematical model to quantify the protuberance growth rate during Li electrodeposition at subambient temperature.¹⁷⁰ As shown in Figure 14a, a flat

electrode with one electrodeposited Li whisker onto its surface is set as the model background. The key point of this model is to evaluate temperature effects on whisker growth rate via the ratio (i_t/i_f) of the whisker tip current density (i_t) and flat electrode current density (i_f). At steady state, the concentration at the outer edge of the boundary layer ($z = \delta$) is equal to the bulk concentration (C_0). At the electrode surface ($z = 0$), the concentration gradient is proportional to the deposition flux. By constructing the dependence of the bulk concentration (C_0), the fraction of the Li plating current density with respect to the system limiting current ($i_{L,f}$) and the cathodic charge transfer coefficient (α_c), the whisker growth rate ratio (i_t/i_f) can be analytically expressed as¹⁷⁰

$$\frac{i_t}{i_f} = \left\{ -\frac{1}{bC_0} \ln \left[e^{-bC_0} + \frac{i_f}{i_{L,f}} (1 - e^{-bC_0}) \right] \right\}^{-\alpha_c/n} \quad (19)$$

where $b = 2.856 \text{ M}^{-1}$. At lower temperature, the viscosity of the nonaqueous electrolyte will be increased, thus lowering the effective diffusion coefficient; in addition, the SEI layer formed on the electrode surface will be thinner, which provides an effectively larger cathodic transfer coefficient. Therefore, it can be deduced that the ratio $\frac{i_t}{i_f}$ increases with decreased temperature. When inserting the temperature effects on the diffusion coefficient and the charge-transfer coefficient via the temperature dependence of the Arrhenius equation and the Tafel expression, the concise analytical equation of this model can be derived:^{170,171}

$$\frac{i_t}{i_f} = \left\{ -\frac{1}{bC_0} \ln \left[e^{-bC_0} + \frac{i_f(1 - t_+)b\delta}{nFa_0 \exp \left\{ \Delta_1 \left(\frac{1}{T_0} - \frac{1}{T} \right) \right\}} \right] \right\}^{-(a_c^0/n) \exp(\Delta_2(\frac{1}{T_0} - \frac{1}{T}))} \quad (20)$$

($b = 2.856 \text{ M}^{-1}$; a_0 , diffusion pre-exponent; T_0 , reference temperature; n , electron transfer number; F , Faraday constant; t_+ , Li^+ transference number; a_c^0 , cathodic charge-transfer coefficient; $\Delta_1 = E_D/2R$; $\Delta_2 = -E/R$; E_D , solution phase diffusion activation energy; E , SEI-phase diffusion activation energy; R , gas constant).

Based on eq 20, the temperature dependence of dendrite growth rate (i_t/i_f) at different plating current densities is plotted as curves in Figure 14b. It can be noticed that the ratio i_t/i_f is small ($i_t/i_f \rightarrow 1$) at all operating current densities when the temperature is ambient ($\sim 25^\circ\text{C}$); however, as the temperature decreases, the ratio i_t/i_f gradually increases until a critical temperature is reached. Near the critical temperature, the dendrite growth rate ratio increases exponentially with decreasing temperature on account of the retarded diffusion and the accelerated surface reaction; thereafter, the current density dependence of the critical temperature (T_c) at which uncontrolled dendritic growth initiates and the ratio $i_t/i_f \rightarrow \infty$ is displayed in Figure 14c.

To explore the Li dendrite behaviors above ambient temperature, coarse-grained dynamical Monte Carlo (CG-MC) computations were used to deal with both Li^+ transport in the electrolyte and thermal relaxation of Li^0 electrodeposits at various temperatures.¹⁷² In this model, the combined diffusional and migrational Li^+ displacements were calculated using Li^+ diffusion coefficients and mobilities, which are codependent on

the local electric field and temperature fields. The simulation results show that it is less likely to form dendrites at high temperature than at low temperature (Figure 14d), majorly due to the high mobilities of Li atoms and Li ions under high temperatures. In addition, runaway growth of electrolytic Li dendrites could be better controlled by increasing the mobility of Li atoms on the solid than by increasing the mobility of Li^+ ions in the electrolyte. Therefore, directly enhancing interfacial Li-atom diffusion (such as by implanting extrinsic defects in Li metal) could potentially suppress dendrite growth.

3.3.2. Influence of Temperature on Li Metal Nucleation. Similar to the cell operation rate as discussed in section 3.1.4.1, tuning the working temperature of Li metal anode can regulate the nuclei size and distribution at the nucleation stage as well.⁹¹ Generally, increasing the temperature enhances the Li^+ mobility, which contributes to reduced concentration polarization and nucleation overpotential (Figure 15a); thereby, larger and sparser nuclei on the substrate surface can be experimentally observed at elevated temperatures, while the nuclei tend to be smaller in size and more densely distributed at a lower working temperature (Figure 15b). In terms of independent nucleation states, low temperature is more beneficial for stable Li plating than high temperature. Nevertheless, the conclusion may change when taking the ionic mobility into consideration. Dropping the temperature interferes with the diffusion of ions in electrolytes (e.g., $1.05 \times 10^{-5} \text{ cm}^{-2} \text{ S}^{1-}$ at 60°C vs $3.4 \times 10^{-6} \text{ cm}^{-2} \text{ S}^{1-}$ at 20°C and $6.1 \times 10^{-7} \text{ cm}^{-2} \text{ S}^{1-}$ at -20°C in the electrolyte of 1 M LiPF_6 in 1:1 vol/vol EC-DMC) and through the SEI layer,^{173,174} which is more likely to give rise to concentration polarization and induce irregular Li metal morphology in the following plating process. Therefore, all these factors should be comprehensively considered on evaluating the temperature impact in practical situations.

3.3.3. Influence of Temperature on SEI Structure. Decomposition of Li salts and solvents is an intricate, multistep, and multielectron process, while temperature can affect the rate of each individual reaction by influencing the rate-determining steps and thus the properties of reaction products (namely, the SEI layer).¹⁷⁵ For example, at a low temperature (e.g., -80°C), the SEI formed in the DOL/DME electrolyte system was found to be thinner, chemically and structurally distinctive, and less resistive in comparison to that formed at room temperature. The thinner SEI is mainly due to the low reaction rate at low temperature.¹⁷⁵ Wang *et al.*¹⁷⁴ found that in additive-free carbonate electrolytes (1.0 M LiPF_6 in 1:1 vol/vol EC-DEC), the SEI film remains amorphous with embedded inorganic nanoparticles at both 20 and 60°C , but the SEI grows thicker and Li deposits become more nonuniform at 60°C than at 20°C , resulting in worse cycling stability of Li metal anode in higher temperature. In ether-based electrolytes (DOL/DME) with/without LiNO_3 or carbonate electrolytes with an FEC additive, an amorphous polymeric SEI is formed at 20°C (Figure 15c), which is soluble in the electrolyte and fractures during cycling, leading to limited passivation of the Li metal and continuous SEI formation and mechanical instability. Conversely, high-temperature operation (60°C) in these electrolytes is demonstrated to be beneficial for cycling stability of Li metal anode, owing to the formation of more stable SEI structure: a highly ordered layered SEI (Figure 15d). The stable SEI layer effectively passivates the anode and maintains mechanical stability during cycling, thus inhibiting later-cycle SEI formation and leading to much better cycling stability.

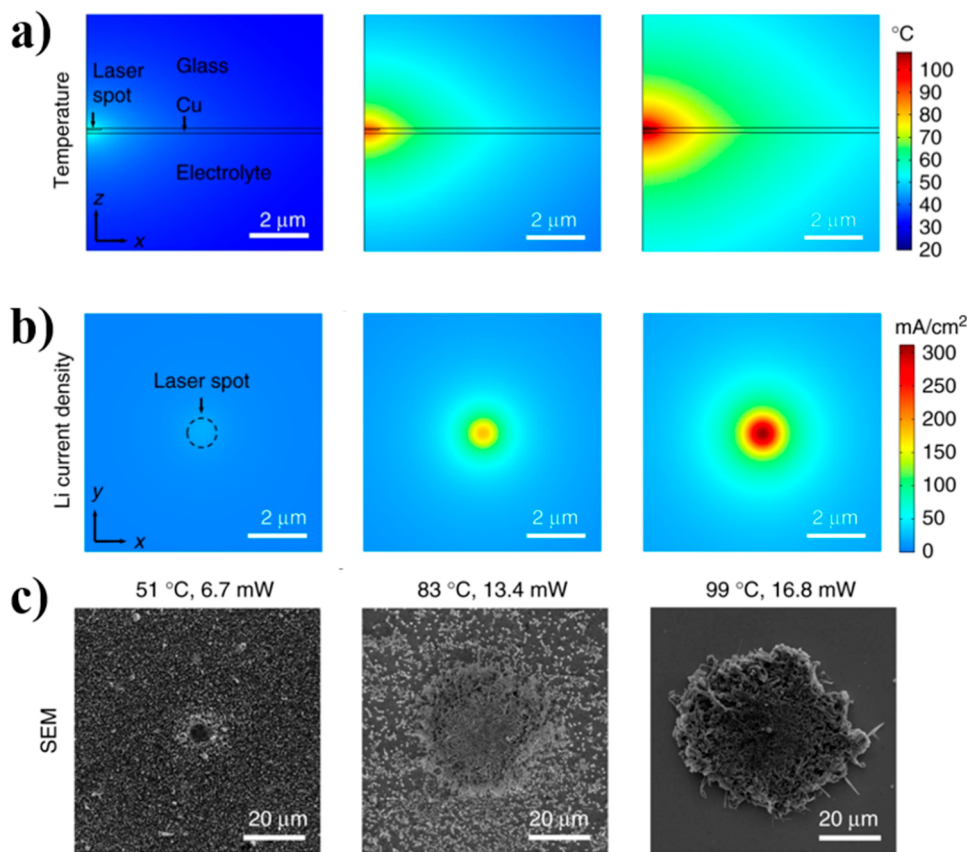


Figure 16. Influence of temperature homogeneity on Li metal evolution. (a) Simulated temperature distribution (cross-sectional view), (b) the simulated deposition rate as indicated by current density (top-down view), and (c) SEM images of Li deposition in the situation of a hotspot temperature of 51 °C at a laser power of 6.7 mW (left), 83 °C at 13.4 mW (middle), and 99 °C at 16.8 mW (right) separately. Reproduced with permission from ref 173. Copyright 2019 Springer Nature.

Similarly, the beneficial effect brought by elevated temperature is also observed in the DOL/DME or EC/DEC/FEC electrolyte systems. Besides, it is worth mentioning that large and islandlike Li nuclei is prone to form at elevated temperatures (consistent with other works,¹⁷³ as shown in Figure 15b), which decreases the electrode/electrolyte contact area and thus relieves the formation of the SEI film.

Unfortunately, the formation mechanisms of observed SEI structures in various temperature and electrolyte conditions remain elusive in the above works. In one contribution, Matthew *et al.* correlated varied SEI properties to the solvation environment around Li^+ at different temperatures through using nuclear magnetic resonance (NMR) and molecular dynamics simulations.¹⁷⁶ They found that the addition of small amounts of cyclic carbonate solvents, such as FEC and EC, into ether (DOL/DME)-based electrolytes can stabilize Li deposition/stripping and substantially increase CE in half cells at the working temperature down to $-60\text{ }^\circ\text{C}$. This benefits from the richer inorganic species (LiF , Li_2CO_3) in the SEI layer by using FEC-containing ether electrolytes. More specifically, FEC is preferred over DOL to solvate with Li^+ in the first solvation shell and facile to be reduced to form LiF and Li_2CO_3 particularly at low temperatures.

3.3.4. Influence of Temperature on Li Metal Growth. Owing to distinct nucleation characteristics and SEI structures of the Li metal anode under different temperatures, the as-grown Li metal shows different morphologies. In ether-based electrolytes, due to the stabilized organic/inorganic bilayer formed at a

high temperature ($60\text{ }^\circ\text{C}$), Li metal presents a relatively smooth morphology;¹⁷⁴ therefore, the electrodeposition of Li on the Cu surface exhibits a higher Coulombic efficiency at elevated temperatures than that at room temperature. In carbonate-based electrolyte, the trends in electrochemical behavior of Li metal anode cycled at 0, 25, and $60\text{ }^\circ\text{C}$ are shown to be significantly different from the results in ether electrolyte. Low temperature is demonstrated to increase Coulombic efficiency and extend cycle life through lowering the chemical reactivity of Li metal, because it is believed that higher temperatures lead to unstable SEI formation, poor Coulombic efficiency, and electrolyte degradation.¹⁷⁷

Aside from the beneficial effect on improving the Li^+ ionic diffusion in electrolytes,^{173,174} increasing temperature is also able to accelerate the Li atomic diffusion in bulk Li metal (Figure 15f),^{169,172} thus smoothing the surface of the plated Li metal and blocking the parasitic dendrite propagation. At an elevated temperature, more swift Li^+ migration allows fast Li^+ replenishing from the electrolyte to the anode surface, which contributes to the steady and uniform Li deposition (Figure 15e).¹⁷³ In addition, based on MD simulations, the Li atoms preferentially diffuse from the tip of two protuberance to the valley in between, induced by a surface energy difference at the places (like the Ostwald ripening process). Therefore, facilitated diffusion of Li atoms under high temperature ($>40\text{ }^\circ\text{C}$) is expected to turn the dispersed and sharp Li deposits into interconnected and flattened morphology, showing a self-healing effect (Figure 15g).¹⁶⁹

3.3.5. Influence of Temperature Homogeneity. The aforementioned positive effects of elevated temperature on protuberance suppression are based on the uniform distribution of temperature on the anode surface. However, the temperature effect may be reversed if temperature is not uniformly distributed in the anode, particularly when certain points have a higher temperature than other parts. In this case, the local reaction rate will be dramatically increased due to the enhanced Li^+ diffusion capability and electrochemical kinetics (Figure 16a,b).¹⁷³ Then the irregular deposition will occur over the Li metal anode surface and accelerate the failure of cells (Figure 16c). It should be mentioned that the temperature homogeneity is dependent on the thermal conductivity on the reaction interface between the Li metal and the electrolyte. The thermal energy typically prefers to accumulate on the spots with low thermal conductivity and promotes the transfer of Li atoms as confirmed by heat transfer simulation.¹⁷⁸ Overall, enhancing the temperature is an effective way to suppress dendrite evolution, but its uniformity on the anode surface is also an essential point for consideration.

3.4. Connection of Multiphysical Fields on Li Metal Evolution

In LMBs, the roles of multiphysical fields are not independent in the galvanic plating/stripping process of Li metal; instead, they closely interact with each other and their intensity/distribution jointly influences the morphology evolution of the Li metal anode. The importance of the multiphysical fields varies in the production of polymorphous Li (e.g., Li whiskers, Li mosses, and Li dendrites), which is displayed in Figure 17. Accordingly, the

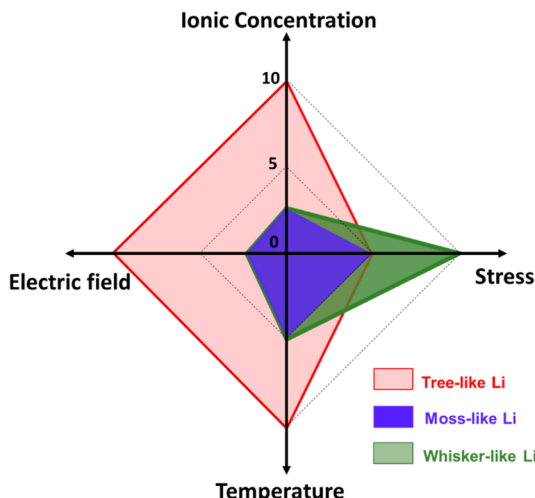


Figure 17. Radar plot illustrating the dominated influencing physical fields for the growth of different irregular Li structures. Note that 0, 5, and 10 are arbitrary units, which are just used for comparison.

connection of multiphysical fields on Li metal evolution are concluded as below:

- (1) Ionic concentration and electric fields have the most intimate relationship among the physical fields since the electric field serves as the guidance for Li^+ diffusion and their distribution typically follow the same trend.
- (2) In general, ionic concentration and electric fields are the determining factors on the appearance of tree-like Li dendrite: the depletion of Li^+ and remaining charges around the anode surface breed the irregular pattern, as

separately suggested by Sand's time model and the space charge model. Beyond the theoretical models, there are many factors, such as the SEI layer characteristics and nucleation states, with the involvement of the other two physical fields, stress and temperature fields, that may alter the local ionic concentration/electric field distribution and influence the critical current density of the tree-like dendrite appearance in practical situations. Specifically, the lithophilicity of conductive substrates, environment temperature, and charging rates have a direct impact on the size, distribution density/homogeneity of nuclei, and on the ionic concentration/electric field distribution in the subsequent growth stage. The mechanical property (cycling stability against internal stress), electric/ionic conductivity, and component homogeneity of the SEI layer are the key issues on determining local Li^+ and electron dispersions near/on the anode surface, and these characteristics of the SEI layer are normally regulated by electrolyte components and environment temperature.

- (3) In comparison with tree-like dendrite formation, the presence of Li mosses and Li whiskers is principally related to the stress field, containing the destruction of the SEI layer and the relaxation of Li metal deposition-induced internal stress. Their morphology difference is supposed to originate from the relative rate between galvanic Li metal deposition and SEI reproduction, with moss-like Li formed at a higher current density (faster deposition rate) and whisker-like Li formed at a lower current density (faster SEI reproduction rate).
- (4) The temperature field majorly influences Li^+ ion diffusion and the distribution of the ionic concentration field further; therefore, the tree-like dendrite formation is more susceptible to the temperature field than the whisker-like and moss-like Li structures. Besides, the temperature field also affects the Li atom transfer rates within the Li metal and the properties of the SEI on the Li metal surface, which are associated with the internal/external stress field during Li metal evolution. Under this consideration, all three irregular Li structures, particularly the whisker-like Li and moss-like Li, will be affected.

4. LI POLYMORPHS EVOLUTION MANAGEMENT STRATEGIES VIA REGULATED MULTIPHYSICAL FIELDS

As mentioned above, multiphysical fields (involving the ionic concentration field, electric field, stress field, and temperature field) work together to guide Li metal plating and determine whether it will evolve into an irregular pattern or not as well as which form of irregular pattern it will evolve into. Accordingly, through elaborately manipulating all these physical fields and related influencing factors, it is feasible to manage the Li plating process and mitigate irregular Li formation during long-term cycling, in turn, improving the overall electrochemical performances and the safety of cells. In this section, we will review some typical irregular Li delay/suppression/redirection strategies from the point of multiphysical fields regulation, aiming at better unveiling their intrinsic mechanisms. It should be noted that in some references we cited in this section, the irregular Li patterns are not specifically clarified and they are all generally termed as "dendrites". To avoid possible inaccurate interpretation, "dendrites" are also used to describe some indistinguishable irregular Li patterns here as it does in the original references, which does not merely refer to the tree-like Li structure. On the

Ionic Concentration Field Regulation

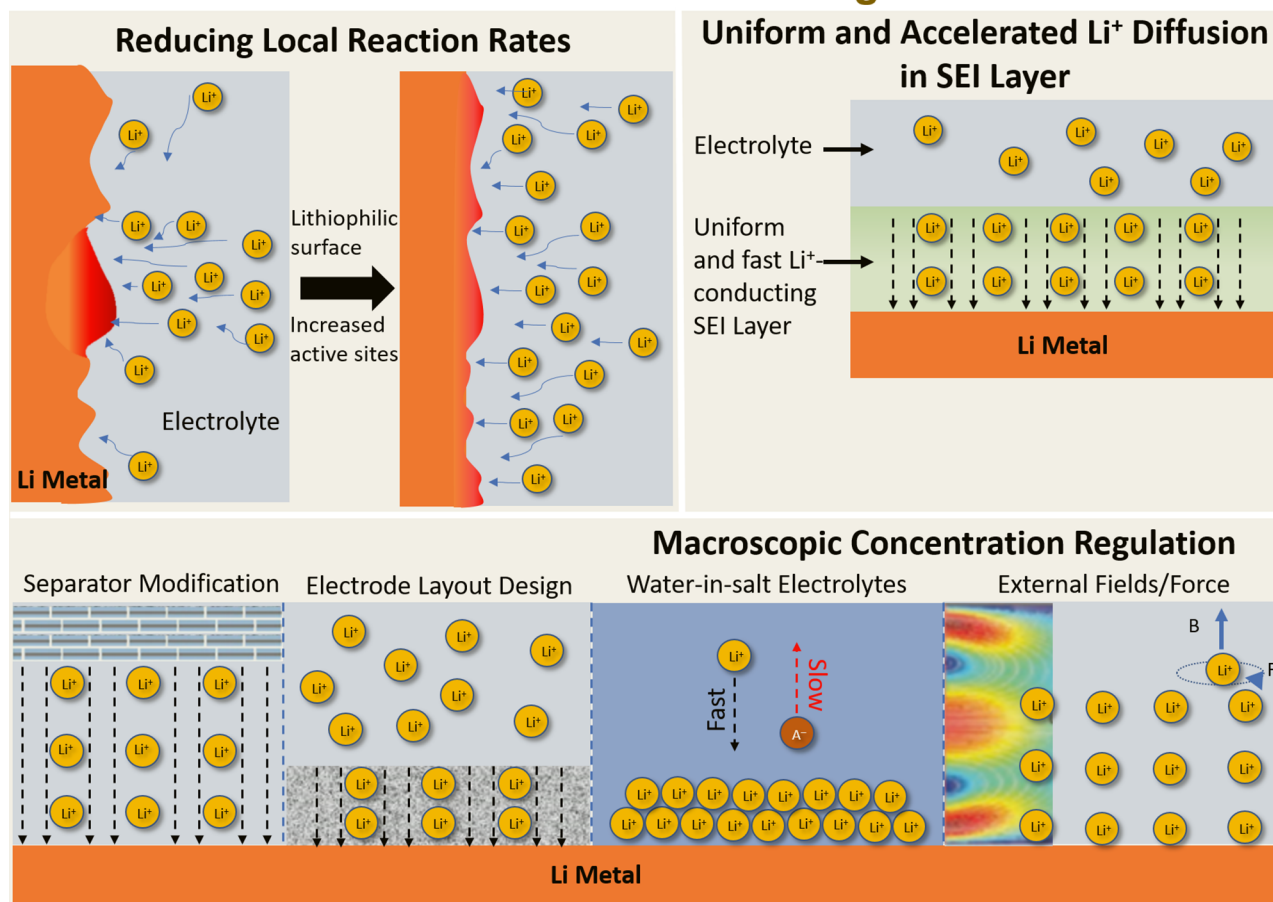


Figure 18. Overview of ionic concentration field regulation strategies for the management of Li metal deposition.

other hand, some works discussed in the section focus on mitigating irregular Li formation and promoting smooth Li formation, rather than exploring the irregular Li formation mechanism; therefore, it is for simplification purposes to use the word “dendrites” to represent irregular Li deposits that are usually observed in the control cases.

4.1. Ionic Concentration Field Regulation

According to the Sand’s time model, the appearance of tree-like dendrite is blamed for the depletion of salts on the anode surface, which results from the inequivalent provision of Li resources (Li ion mobility in electrolytes) relative to the reaction rate (local current density at nucleation sites). Meanwhile, the incorporation of other factors such as the SEI layer, surface roughness, and inherent stress results in significant shrinkage of the electrochemical-active area followed by the formation of hotspots on the anode surface, which further aggravates the concentration polarization and accelerates the dendrite production. Based on these facts, several feasible and well-accepted routes on regulating the salt concentration distribution around the anode surface are proposed to avoid the tree-like Li dendrite formation (Figure 18). For example, the pressure on the Li^+ transfer can be reduced through reducing the local current density, which is viable by enlarging the electrochemical-active area. Additionally, some other strategies such as enhancing the Li^+ mobility (*e.g.*, via tuning the SEI composition and structure) and macroscopically homogenizing the Li^+ concentration (*e.g.*, via applying a modified separator, porous

dielectric/insulating skeleton with strong Li^+ affinity, highly concentrated electrolytes, and external forces/fields) are feasible to guarantee the prompt supply of Li^+ resources even at high rates. Herein, the strategies for suppressing dendrite formation from the point of ionic concentration field regulation will be comprehensively discussed with the most-updated progress.

4.1.1. Reducing Local Reaction Rate. In common cells with a very thin separator or electrolyte layer, the theoretical limiting current density (before the Sand’s time) can be $\sim 100 \text{ mA cm}^{-2}$; therefore, the practical current densities ($< 10 \text{ mA cm}^{-2}$) is not expected to trigger diffusion limitation if the applied total current is uniformly distributed over the entire geometrical area of the anode surfaces.¹⁷⁹ However, recent studies of failure mechanisms in rechargeable metal batteries showed that metal penetrations were self-confined within a few isolated micro-channels of the porous separator^{180,181}; this implies that the local current density at some spots that enable the penetration can be several orders of magnitude higher than the geometrically averaged current density and may even be higher than the system-specific limiting current density.¹⁷⁹ Under the circumstances, minimizing the local reaction rate on the anode surface is anticipated to delay the dendrite formation since it enables the prompter compensation of Li^+ and further avoids the severe polarization brought by the concentration gradient. To count, the reaction rate is codetermined by the external current intensity and effective electrochemical-active area. Solely limiting the external current intensity does not meet the increasing demand on fast charging; hence, a critical strategy on

reducing local current density depends on increasing the electrochemical-active areas on anode surface. Herein, related strategies will be comprehensively discussed with the sub-categories of planar electrodes and highly porous electrodes, combined with the specific examples and the supporting electrochemical performances in corresponding cells. Furthermore, the inherent problems of some methods followed by feasible solutions will also be detailed in the following sections.

4.1.1.1. Planar Conductive Substrates. For planar conductive substrates, the initial nucleation states, such as the nuclei morphology, size, and distribution, have direct connection with the overall electrochemical-active area and further influence the subsequent propagation process, as well-discussed in section 3.1. An ideal image of the deposition layer shortly after initial nucleation is supposed to be densely packed and evenly distributed over the whole surface. Therefore, perfecting the nucleation process is expected to be a powerful way to prohibit dendrite growth: the key point for a pristine Li metal substrate is to guarantee the evenness of the surface, and for non-Li-metal substrates (*e.g.*, metallic ones and carbonaceous ones), this is accomplished by enhancing the surface lithiophilicity of the substrates. In this section, progress made on expanding the electrochemical-active area by optimizing the host's surface properties will be summarized and discussed in detail. It should also be noted that the surface lithiophilicity modification for non-Li hosts is also well-applied for 3D conductive current collectors, which will be principally introduced in the next section; here, we only cover the cases of planar electrodes.

For the Li metal substrate, the lithiophilicity variance usually originates from its surface roughness, which determines the preference of deposition sites and concentration distribution. Due to its soft nature, Li metal foil made by extrusion or roll pressing may have cracks even before its use in batteries.^{182–184} Therefore, to enable a uniform plating behavior over Li metal foils, its surface should be made as smooth as possible. Accordingly, three general methods are developed to fulfill the intention, including mechanical polishing⁶¹, chemical polishing^{185–188}, and electrochemical polishing^{182–184}.¹⁸² Through the mechanical method, Li foil can be polished by silicon carbide paper in acetone in seconds; afterwards, dendrite-free deposition on the polished Li metal surface was observed at a current density of 1 mA cm^{-2} , albeit the inherent defects (*e.g.*, dislocation); cracks will reappear during cycling and deteriorate the cycling efficiency.⁶¹ Regarding the chemical polishing methods, Li metal is usually immersed into different solvents/electrolytes to smoothen the surface through certain chemical reactions. For instance, Li metal can react with the aromatic hydrocarbon in naphthalene in its tetrahydrofuran solution to improve the smoothness, and the uniformity of the electric/ionic conductivity is simultaneously enhanced by removing the natively formed layer over pristine Li metal during the process.¹⁸⁸ Benefitting from the steady and even deposition pattern, the polished Li metal anode delivers an improved cycling efficiency, with a high average Coulombic efficiency of 92.6% relative to that of 85.1% for pristine Li metal in the symmetric cell and a high Coulombic efficiency of 99.5% for over 350 cycles in the $\text{LiFePO}_4//\text{polished Li metal full cell}$. Lastly, the electrochemical polishing methods typically depends on the anodic dissolution of Li metal to smooth the surface under the protection of the SEI layer.¹⁸⁴ For instance, a two-step electrochemical polishing method is designed, where the pristine Li metal first undergoes the anodic dissolution to remove part of the defects and then experiences the cathodic

deposition to further smoothen the surface. To note, the *in situ* formed uniform SEI layer in 1 M LiTFSI in 1:1 vol/vol DME/DOL electrolytes at the anodic dissolution stage not just assists the surface-polishing process but also contributes to more stable plating/stripping in the cycling process afterward.¹⁸⁴

Additionally, pristine Li metal foil can also be replaced by or combined with other highly lithiophilic substrates like Au,¹⁸⁹ Ag^{189,190}, Na^{191,192}, Sn¹⁹³, Li_9Al_4 ¹⁹⁴ and so forth as planar substrates for Li deposition. For example, Ag nanoparticles could be uniformly dispersed over the Li metal surface by treating it with Ag-containing electrolytes (AgTFSI/DME + FEC), where the Ag^+ reacts with active Li metal to produce the fine and abundant Ag nanoparticles layer. Meanwhile, the consumed Li metal will be turned into Li^+ , which will further bind with F^- released from the FEC additive to form a robust and uniform LiF coating over the anode surface. The synergistic effect of enhanced lithiophilicity and a uniform composite coating film on the anode surface can efficiently remove the concentration polarization of Li deposition, resulting in a significantly lower overpotential of 5.5 mV than that of 68.9 mV for pristine Li metal counterparts and an enhanced CE of 97.5% in comparison to that of 77.6% for bare Cu substrates.¹⁹⁰ However, one limiting factor of the above strategies on improving substrate's lithiophilicity is the effectiveness duration. Except for the nucleation optimization, the one-time lithiophilic sites do not have a constant contribution on dendrite suppression in the following plating stage; in other words, they have a great chance to lose their function after being blocked by the inactive Li accumulation layer in long-term cycling.¹⁹⁵ To ameliorate the problem, Yuan *et al.* introduced the $\text{NaMg}(\text{Mn})\text{F}_3@\text{C}$ nanocubes over Cu foil as composite substrates for Li deposition, where the $\text{NaMg}(\text{Mn})\text{F}_3$ can slowly but constantly release Na^+ , Mg^{2+} , Mn^{2+} , and F^- into electrolytes.¹⁹⁵ Due to the higher redox potential for these metal ions than Li^+ , they will deposit prior to the Li metal and serve as a lithiophilic substrate while the F^- is supposed to *in situ* form a LiF layer on the Li metal surface to guide a homogeneous deposition. Benefiting from the spansule-like releasing nature, the composite substrate significantly expands the lifespan of the Li metal anode to over 1000 h at the rate of 1 mA cm^{-2} and a cycling capacity of 1 mAh cm^{-2} in the half cell test with an average Coulombic efficiency of ~98%.

4.1.1.2. 3D Porous Conductive Substrates. To achieve a large electrochemical-active area for Li plating, an effective way is to adopt the 3D porous conductive substrates, including pristine Li metal, non-Li metal, and carbonaceous materials-based ones, which have received a lot of attention in recent years. Here, the 3D porous substrates exhibit some other attractive features for hosting the Li metal anode, from the aspects of stress field and ionic concentration field, *i.e.*, (1) enhanced rate capability as a benefit from the open and fast ion diffusion channels and (2) the effective relaxation of internal stress brought by Li plating.^{15,196} Nevertheless, high-surface-area substrates also exhibit some inherent drawbacks that hinder their further development and broad application, including the high preparation cost and increased electrolyte dosage for much more SEI production, *etc.* In this section, the progress made so far on 3D porous conductive substrates to reduce local current density will be summarized, followed with discussion about the confronted problems and corresponding solutions.

(1) Patterned Li Metal Substrates

Li metal can be designed into different structures to increase its surface area. The first way is to load spherical Li metal

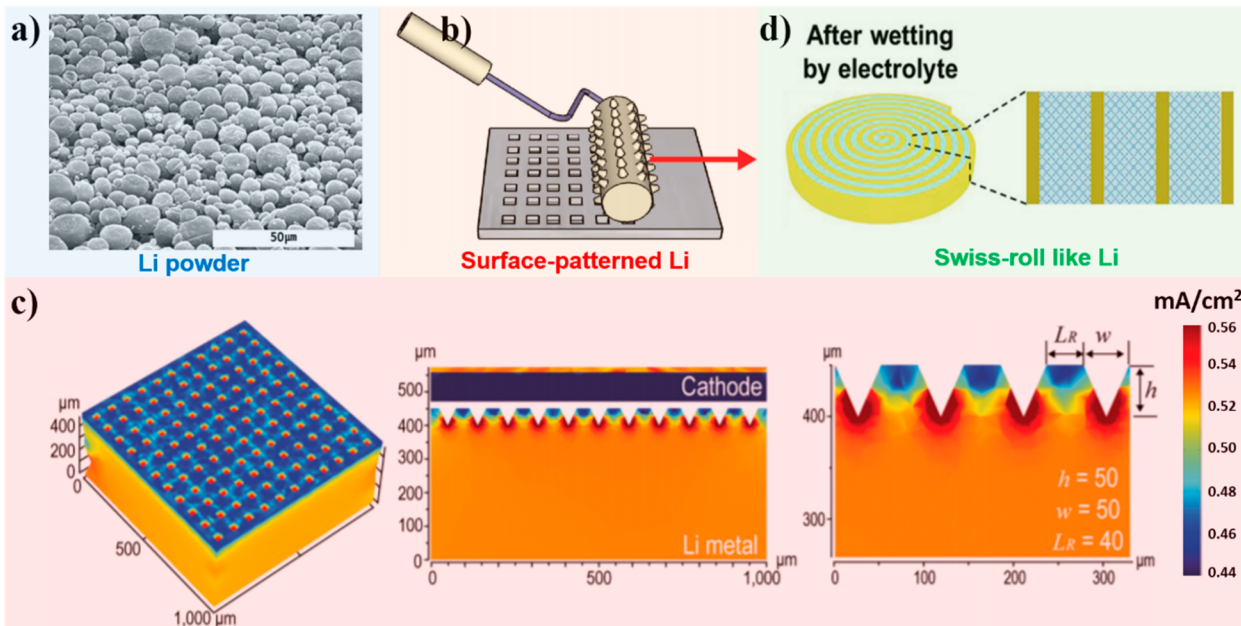


Figure 19. 3D design of pristine Li metal substrates. (a) SEM image of spherical Li particles. Reproduced with permission from ref 198. Copyright 2008 Elsevier. (b) Schematic diagram of the process of making surface-patterned Li metal by a microneedle roller. Reproduced with permission from ref 201. Copyright 2014 Wiley-VCH. (c) Current density of the optimized pattern on the Li anode ($h = 50 \mu\text{m}$, $w = 50 \mu\text{m}$, $L_R = 40 \mu\text{m}$) as simulated by the finite element method. Reproduced with permission from ref 196. Copyright 2016 Wiley-VCH. (d) Schematic illustration of the process of making the Swiss-role like Li anode, in which the yellow part is Li metal and the blue part stands for the nonconductive framework. Reproduced with permission from ref 203. Copyright 2019 Wiley-VCH.

powders over the current collector instead of using a dense Li metal foil.^{197–200} The improvement on dendrite suppression is noticeable in comparison to the Li metal foil that the particles' shape is well-preserved after cycling. Notably, Li powder prepared by Kong *et al.* (Figure 19a) is free of dendrite growth when cycling at a high current density of 5 mA cm^{-2} for 250 cycles.²⁰⁰ However, only the very top of the Li is used for cycling, which is a waste of resources. In addition, the preparation process of Li powder is costly and complicated.²⁰¹ Thereafter, a facile, cheap, and scalable mechanical method is reported to increase the surface area of the Li metal anode; specifically, a microneedle roller was employed to make a regular, repeatable microsize hole-array pattern over the Li metal surface by a rolling process (Figure 19b).²⁰¹ This method efficiently improves the cycling stability: 85% capacity retention after 150 cycles at a rate of 7 C for pretreated lithium metal anode, in comparison to 85% retention after 70 cycles for a pristine one. Furthermore, with the help of the finite-element simulation method, the optimum size of the surface pattern is derived with the current density concentrating at the tip of the inverted pyramid-shape pattern (Figure 19c).¹⁹⁶ The optimized pattern significantly inhibits the dendrite growth and increases the stability from 43.9% of the initial capacity after 250 cycles to 88.7% of the initial capacity after 450 cycles at the rate of 0.5 C. However, the hole-array structure also has some intrinsic drawbacks. As reported by Zhang *et al.*, the hole is easy to be filled with “dead Li” derived from the Li dendrite stripping in the previous cycling.²⁰² The poor electric conductivity between isolated particles (“dead Li”) and the large resistance on Li^+ diffusion is assumed to block the reactions and significantly improve the potential hysteresis on Li plating/stripping. In comparison, the distribution of “dead Li” over an originally even and smooth Li metal is sparser, thus showing less effect on the reaction polarization.

Another method to increase the surface area of Li metal is by coiling Li metal with a thin layer of porous nonconductive membrane to fabricate a Swiss-roll like composite structure (Figure 19d), where the nonconductive membrane has good wettability toward electrolytes.^{203,204} For one thing, the upright surface of the Li metal separated by a nonconductive membrane significantly dissipates the local current density. For another, a porous membrane can effectively suppress the volume change during the cycling process due to its rigid structure. When applying the $12 \mu\text{m}$ -thick nanoporous polyethylene (PE) film and $50 \mu\text{m}$ -thick Li metal foil-composite anode, the Li//Li symmetry cells deliver improved electrochemical performances over the bare Li metal foil-based ones, such as the decrement of potential hysteresis from 98, 146, 295, and 450 mV to 46, 73, 166, and 241 mV at rates of 0.5, 1, 3, and 5 C, respectively. Moreover, the composite anode allows stability working at a high current density of 5 mA cm^{-2} for over 200 cycles, which is also far more superior than the Li foil counterpart.²⁰⁴ In another work, porous glass fiber (SiO_2) is applied to separate Li foil instead of using the PE membrane.²⁰⁵ It was found that SiO_2 has great affinity with Li^+ due to its polar structure, which helps homogenize Li^+ concentration within the framework. With the unique structure and composition, the Li//coiled Li asymmetry cells exhibit stable cycling at a current density of 1 mA cm^{-2} and an areal capacity of 1 mAh cm^{-2} for over 1000 h. Furthermore, the full cells composed of the coiled Li as the anode and $\text{Li}_4\text{Ti}_5\text{O}_{12}$ as the cathode exhibit a large capacity ($\sim 150 \text{ mAh g}^{-1}$), high Coulombic efficiency ($\sim 100\%$) at a high rate of 5 C, and long life of over 2500 cycles without obvious performances decay. In contrast, full cells with bare Li foil as the anode fail after merely 500 cycles on the same conditions.²⁰³

(2) Non-Li Metallic Substrates

Despite the low energy barrier for Li nucleation, the pristine Li metal substrate is not an ideal choice due to the limited ratio of

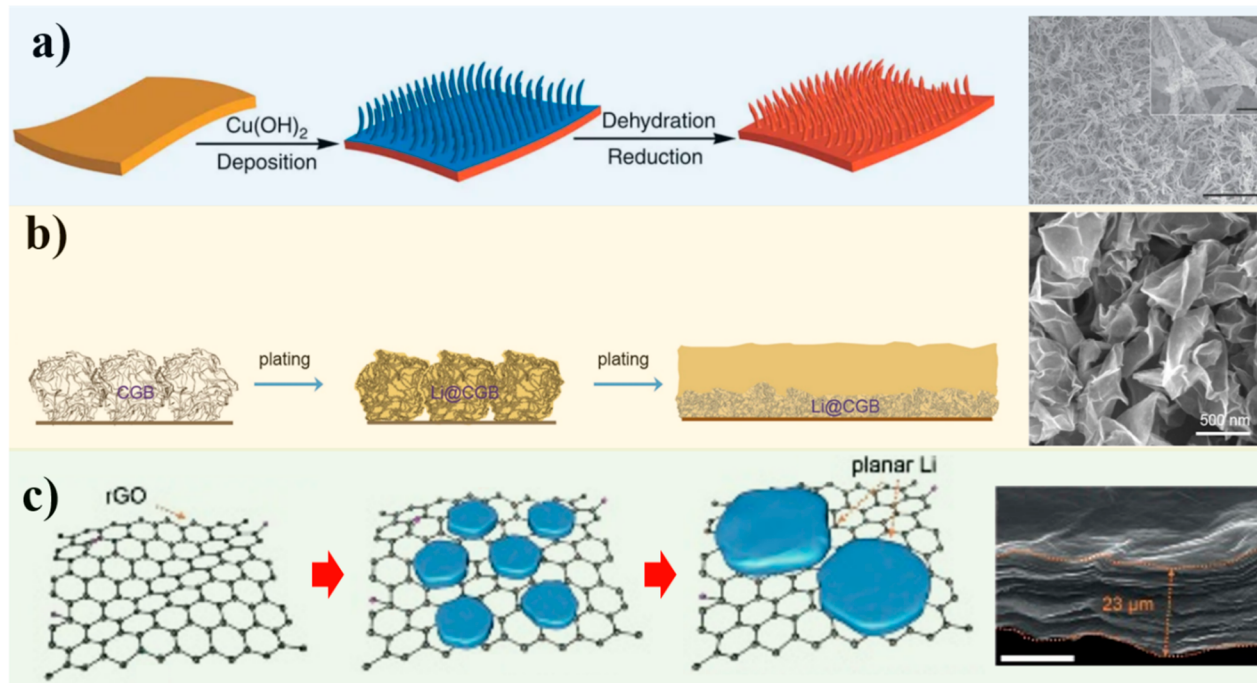


Figure 20. 3D design of non-Li conductive substrates. (a) Schematic illustration of the preparation process for 3D porous Cu hosts (left) and the SEM image of the as-obtained Cu substrate (right). Reproduced with permission from ref 91. Copyright 2015 Springer Nature. (b) Schematic illustration of the Li deposition manner over the crumpled graphene balls (left) and the SEM image of as-obtained crumpled graphene balls. Reproduced with permission from ref 30. Copyright 2018 Elsevier. (c) Schematic illustration of the Li deposition manner on the rGO substrate (left) and the cross-sectional SEM image of as-obtained rGO (right). Reproduced with permission from ref 99. Copyright 2019 Wiley-VCH.

Li usage in the overall mass and limited surface area. In this regard, some alternative 3D porous substrates (non-Li metals and carbonaceous materials) are explored. In this part, we will focus on metallic substrates, while progress about using carbonaceous substrates will be discussed in the next part.

Typically, metals like Cu, Ni, and stainless steel have been widely used as metal hosts due to their high anodic stability, high electric conductivity, and chemical inertness toward Li⁺. These metallic substrates can be fabricated with high surface areas to dissipate the local areal current density and mitigate concentration polarization. For example, a 3D Cu foil is synthesized through the process as shown in Figure 20a⁹¹; specifically, the nano Cu(OH)₂ arrays are formed on planar Cu foil in the first stage, and then they undergo the dehydration and reduction process to obtain the Cu arrays over Cu foil. The 3D Cu foil not just decreases the overpotential but also extends the asymmetric Li//Li@Cu cell life to over 600 h at 0.2 mA cm⁻² without a short circuit, indicating effective suppression of dendrite growth. Besides, a 3D metallic membrane based on stacked and interconnected Cu nanowires is also applied as a substrate for the Li metal anode due to its large surface area.²⁰⁶ It is able to accommodate up to 7.5 mAh cm⁻² of Li metal and delivers a low overpotential of 40 mV with a high average Coulombic efficiency of ~98.6% in the first 200 cycles at the current density of 1 mA cm⁻². For Ni metal, it can be fabricated into the nickel foam with a large surface area. The composite anode made by dipping nickel foam into molten Li delivers a relatively stable performance in the symmetric cell test, albeit with a relatively large overpotential of 200 mV at 5 mA cm⁻² after 100 cycles in carbonate electrolytes.²⁰⁷

(3) Carbonaceous Substrates

Despite the giant potential in stabilizing Li metal nucleation/growth, metallic substrates have to face a big problem: their

relatively large mass density hampers the energy/power densities by decreasing the ratio of active mass in the cells. Besides, some metallic hosts (e.g., Cu) face chemical stability problems, such as the corrosion by HF gas originated from decomposition of LiPF₆-based electrolytes and the potential oxidation for nanostructured Cu.^{15,24} In this regard, lightweight carbonaceous materials have been proven as more promising candidates for Li metal hosts than the non-Li metallic hosts counterparts due to their excellent chemical inertness resulting from delocalized π electrons within nanosheets.²⁰⁸ Meanwhile, the carbonaceous materials also present other advantages, including superior mechanical strength and high electric and thermal conductivities.^{209,210}

Thus far, intensive studies have been conducted to explore 3D carbonaceous substrates for lithium metal anode, involving graphene, carbon wood, carbon felt, graphite nanotube, carbonized metal–organic frameworks (MOFs), and so forth. For instance, a carbonaceous host with a high surface area is made by fabricating a reduced graphene oxide (rGO) host into a crumpled ball powder through the aerosol-assisted capillary compression method (Figure 20b).²¹¹ Based on N₂ adsorption–desorption isotherms, the surface area of the material is estimated to be 382 m² g⁻¹ and a pore volume of 1.8 cm³ g⁻¹. The fabricated anode delivers an average Coulombic efficiency of 97.5% for over 700 cycles at 0.5 mA cm⁻² and 0.5 mAh cm⁻². An unstacked graphene framework with a high surface area of 1666 m² g⁻¹, large pore volume of 1.65 cm³ g⁻¹, and great electric conductivity of 435 S cm⁻¹ is proven effective on controlling dendrite growth: improving the average Coulombic efficiency to ~93% at the current density of 2 mA cm⁻² and accumulation capacity of 5 mAh cm⁻² in comparison to the bare copper foil counterpart.²¹² More recently, an rGO film with a limited surface area of 13.96 m² g⁻¹ is also reported as a substrate



Figure 21. Surface lithiophilicity enhancement of 3D substrates. (a) Schematic illustrating the plating behavior difference over Ag particle-coated CNF and bare CNF. Reproduced with permission from ref 219. Copyright 2017 Wiley-VCH. (b) Schematic illustration of the fabrication process for the MgO particle modified carbon framework. Reproduced with permission from ref 214. Copyright 2018 Elsevier. (c) Schematic illustration of fabrication process for ZnO coated brass alloy and the corresponding atom distributions before and after the heating process. Reproduced with permission from ref 221. Copyright 2019 American Chemical Society.

for a Li metal anode.⁹⁹ What is unique for the reported rGO is that the distance between the two carbon hexagons along zigzag directions in the graphene plane (4.92 Å) approximates the distance between two adjacent Li atoms within the (110) crystallographic plane, with a lattice mismatch of merely 0.8%. Under the circumstances, Li metal is expected to follow the Frank–Vander Merwe mode and deposit epitaxially in the plane format (Figure 20c). Taking advantage of the homogeneous nucleation and controlled growth pattern, rGO-Li symmetry cells deliver a much improved Coulombic efficiency (99% at 1 mA cm⁻² and 1 mAh cm⁻², 98% at 2 mA cm⁻² and 2 mAh cm⁻²) and reduced plating overpotential (31.2 mV at 1 mA cm⁻²) than the copper foil-based counterparts.⁹⁹

(4) Surface Lithiophilicity Enhancement of 3D Substrates

As comprehensively discussed in section 3.1.4.1, the surface lithiophilicity of host materials is considerably crucial at the nucleation stage. Unfortunately, the common metallic materials and pristine carbonaceous materials mentioned above suffer from poor affinity to Li metal, which is related to their surface energy, lattice structure, and the surface polarity features. This hampers the steady Li plating and increases the risk for dendrite growth. To improve the lithiophilicity of the conductive hosts, several effective surface-engineering solutions have been proposed.

The most facile way in tuning the lithiophilic property of the hosts is to coat or disperse some low-nucleation-overpotential-substances on their surface, including the Li-alloying materials (e.g., Au¹⁰¹, Ag¹⁰¹, Mg¹⁰¹, Zn²¹³) and oxides (e.g., MgO²¹⁴, ZnO^{105,215–218}) as mentioned in section 3.1.4.1. For example, Ag particles are randomly deposited on carbon nanofibers (CNF) through reducing AgAc by electric joule heating (Figure 21a). The overpotential for Li nucleation over the composite anode is negligible, with an absolute value of merely 25 mV at a rate of 0.5 mA cm⁻² and a capacity of 1 mAh cm⁻², which are far superior to those for bare CNF.²¹⁹ Besides, MgO particles can also be evenly dispersed on the wall of 3D porous graphite paper in the similar way by calcinating Mg(OH)₂ particles, which are performed via reaction between NH₃ gas and Mg(NO₃)₂ in ethanol (Figure 21b).²¹⁴ The anode material presents a low nucleation overpotential of merely 10.3 mV and plating

overpotential of 36.1 mV at a current density of 1 mA cm⁻². In addition, there are also some unique methods to fabricate the lithiophilic coatings over hosts. Heating brass mesh (Zn–Cu alloy) at 300 °C in air produces a compact and even ZnO layer on the surface, which is ascribed to the atom diffusion on the surface driven by the Gibbs free energy decrement of the oxidation reaction (Figure 21c).^{211,220,221} By applying the anode, the lithiophilic property gets improved a lot and the cells are able to stably run for 500 cycles at the current density of 2 mA cm⁻².

In terms of graphitic carbon materials, a routine method to improve the surface lithiophilicity is to delocalize the electrons within nanosheets by incorporating defects or heteroatom doping, as discussed in the nucleation part (section 3.1.4.1). In regular planar graphite, the carbon atoms within one graphene layer share a delocalized π electron and the whole body exhibits an electrical neutrality, which results in the poor wetting for Li deposits. In contrast, the delocalized π electrons can be partially localized by the curved surface of the graphite particle in a spherical shape; thereafter, the electronegativity of the carbons will be increased (Figure 22a). To note, if the graphite substrate is prelithiated, π electrons delocalization will be strengthened through the deviating electrons from carbon to Li and the electronegativity will be further improved.²²² In addition, rGO, synthesized by reducing the graphene oxide, has rich defects and small amounts of functional groups (e.g., carbonyl, alkoxy) on the surface, which endows it far better lithiophilicity than regular graphitic carbon materials.^{30,223–225}

It is widely adopted that graphite contains two types of planes: a basal plane with a well-ordered comblike structure and an edge plane with rich defects, which possess distinctive electrochemical properties.^{226,227} Increasing the ratio between the edge plane and the basal plane has proven to be an effective way to improve graphite substrate's lithiophilic properties (Figure 22b).²²⁸ Specifically, after eliminating the influence of surface functional groups and Li preformed graphite intercalation compounds, the change on the electron distribution by tuning the ratio of the two types of planes is considered the key reason for the improvement. The existence of the edge plane is supposed to disturb the uniform electron distribution in the

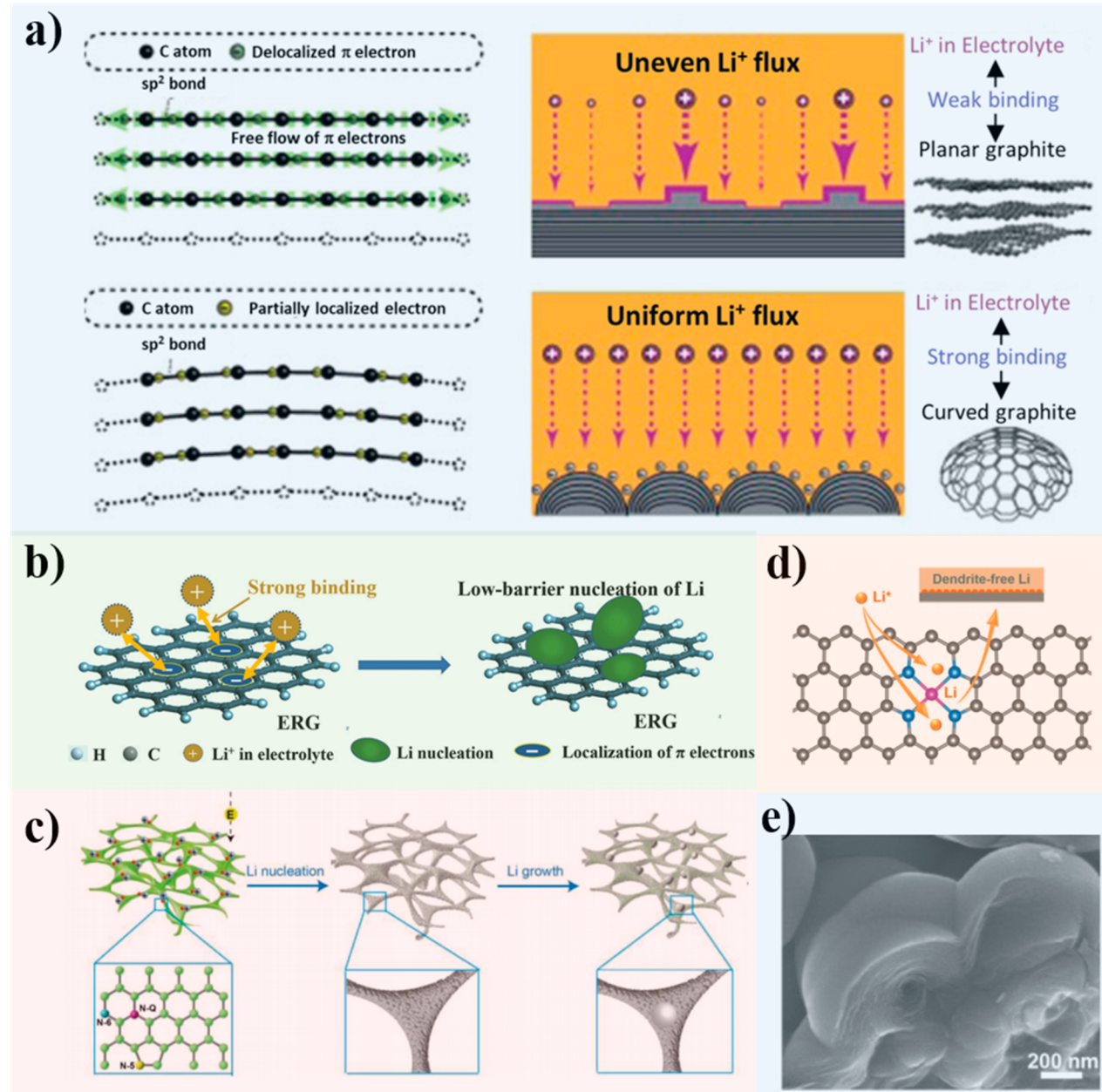


Figure 22. Surface lithiophilicity enhancement of carbonaceous substrates. (a) Schematic illustration of the electron distribution in both planar graphene sheets and deformed/curved graphene sheets and their influences on Li⁺ adsorption and Li nucleation. Reproduced with permission from ref 222. Copyright 2017 American Chemical Society. (b) Schematic illustration of the strategy on using edge-rich graphene (ERG) and its function. Reproduced with permission from ref 228. Copyright 2018 Wiley-VCH. (c) Schematic illustration of the structure of the nitrogen-doped graphene framework and the deposition manner over it. Reproduced with permission from ref 231. Copyright 2018 Wiley-VCH. (d) Schematic illustration of the CoNx-doped carbon structure and the preferential sites of plating, in which pink, blue, and gray balls represent the elements Co, N, and C separately. Reproduced with permission from ref 232. Copyright 2019 Wiley-VCH. (e) SEM image for the spherical disklike carbon. Reproduced with permission from ref 222. Copyright 2017 American Chemical Society.

basal plane and induce its inhomogeneous localization according to Clar's aromatic sextet theory. This property allows the attraction of more Li⁺ ions and decreases the nucleation overpotential with increasing the ratio of the edge plane.²²⁸

When mentioning lithiophilic dopants/functional groups on the carbonaceous framework surface, nitrogen-based groups are the most frequently investigated ones, while O- or S-based ones are scarcely reported.^{109,229,230} Zhang *et al.* demonstrated that rich and various types of nitrogen-based functional groups (*i.e.*, pyridinic nitrogen (pnN), pyrrolic nitrogen (prN), and quaternary nitrogen (qN)) are attached on the graphene surface

by annealing it at 600 °C within an ammonia gas atmosphere. The nitrogen-doped graphene framework exhibits a nucleation potential as low as 0.36 eV at a rate of 1 mA cm⁻²; the assembled cells can remain stable working at 2 mA cm⁻² for more than 50 cycles with a high Coulombic efficiency of 98%.¹⁰² Besides, the nitrogen-doped carbon framework (Figure 22c) can also be obtained through carbonizing the melamine foam; the XPS spectrum reveals that the functional groups are also composed of pnN, prN, and qN.²³¹ Remarkably, in that study, a superior lithiophilicity is achieved for the substrates, with a plating overpotential of merely 25 mV at 3 mA cm⁻²; it contributes to a

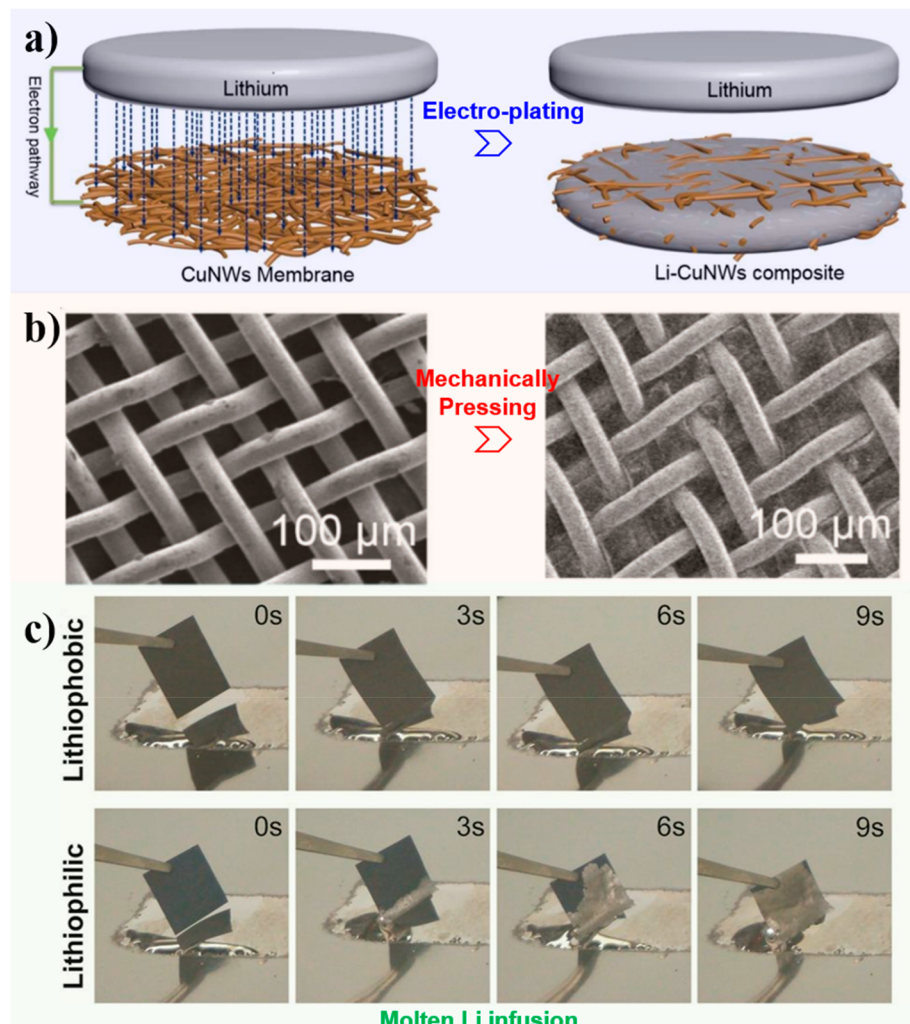


Figure 23. Preparation methods for composite Li metal anode based on 3D substrates. (a) Schematic of Li electroplating in the 3D Cu nanowires membrane. Reproduced with permission from ref 206. Copyright 2016 American Chemical Society. (b) SEM images of Cu mesh before (left) and after (right) being mechanically pressed with Li metal. Reproduced with permission from ref 239. Copyright 2017 Wiley-VCH. (c) Time-lapse images of the molten Li infusion process in lithiophilic substrates. Reproduced with permission from ref 240. Copyright 2015 National Academy of Sciences.

fairly stable/recyclable plating/stripping process with 99.6% Coulombic efficiency at 2 mA cm⁻² and 2 mAh cm⁻² for 300 cycles, 99.4% Coulombic efficiency when increasing the areal capacity to 6 mAh cm⁻² for 150 cycles, and 99.1% when increasing to 8 mAh cm⁻² for 140 cycles. In another work, CoN_x doping is dispersed in the carbon crystal structure and successfully tailors the electronic distribution by forming a Co—N_x—C bond with the substrates, as demonstrated in Figure 22d.²³² Dropping of the overpotential absolute value suggests the enhancement of host wettability toward Li. Furthermore, the material supports superior electrochemical performance: a high Coulombic efficiency of 99.2% for over 400 cycles at a rate of 2 mA cm⁻² and an areal capacity of 2 mAh cm⁻² and 98.2% Coulombic efficiency for 200 cycles at 10 mA cm⁻² and 2 mAh cm⁻². Lastly, both the curving surface and the prelithiation to form the LiC_x compound can trigger the delocalization of electrons and then the increment of electronegativity of the carbonaceous hosts. Growing spherical disklike carbon granules with nanogaps in between over nickel foam guarantees the large surface area (see Figure 22e). The improvement of lithiophilicity is not difficult to observe due to the higher nucleation/

plating overpotential, more stable cycling, and long lifespan in comparison to the bare nanofiber counterpart.²²²

However, the incorporation of the aforementioned defects in the graphene structure not just effectively enhances the host's lithiophilicity but also brings about a negative impact, that is the acceleration of electrolyte reduction, followed by the SEI thickening over heteroatom-doped sites²³³ and lower Coulombic efficiency throughout cycling²³⁴ as reported in related works.^{235,236} Besides, it is further revealed that the SEI layer formed over defect-containing rGO nanosheets possess poorer stability than that formed over defect-free GO nanosheets (abbreviated as df-G), which results in the constant consumption of electrolytes (*e.g.*, SEI-stabilizing additives) and formation of a thicker and less protective SEI layer. Furthermore, the SEI layer on rGO also suffers from a more seriously inhomogeneous composition/structure, which will worsen the nonuniformity of Li-ion distribution and speed up the appearance of the Li dendrite around some hotspots.¹⁰⁹ Overall, the real contribution of introduced defects in carbonaceous materials to overall performances of LMBs depends on the situation: it is positive when applied for homogenizing the Li⁺ concentration/electric field over 3D-

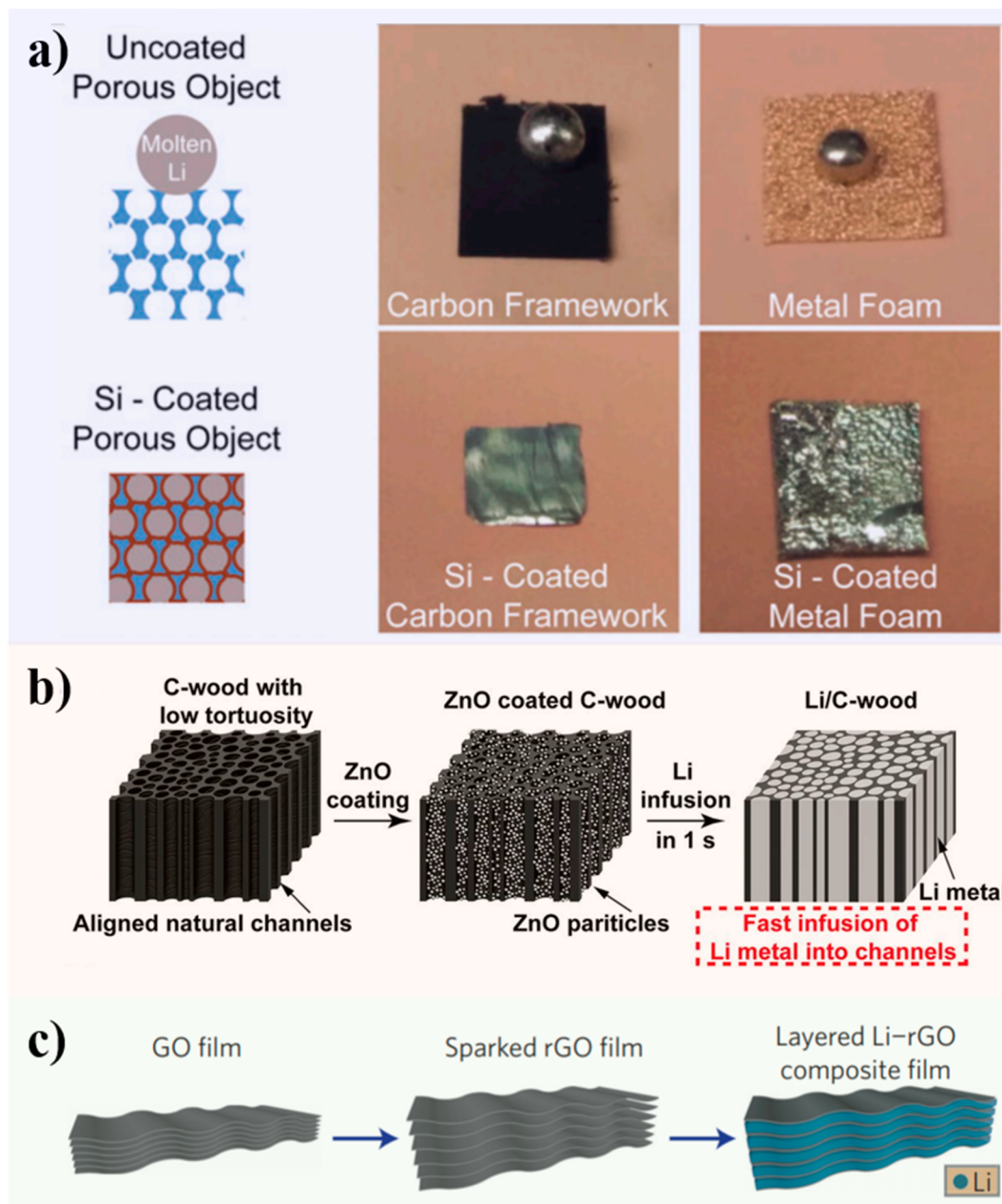


Figure 24. Strategies toward improving molten Li lithiophilicity of 3D substrates. (a) Schematic illustration and photos of molten Li wetting behavior over the uncoated lithiophobic framework (i.e., carbon, metal foam) and Si-coated lithiophilic framework. Reproduced with permission from ref 240. Copyright 2015 National Academy of Sciences. (b) Schematic illustration of fabrication process for the Li/C-wood composite electrode. Reproduced with permission from ref 215. Copyright 2017 National Academy of Sciences. (c) Schematic illustration of the fabrication process of Li-rGO composite material. Reproduced with permission from ref 223. Copyright 2016 Springer Nature.

conductive hosts, while it is negative when applied to coat the planar hosts.

(5) Compositing Methods for Li Metal and 3D Substrates

When using the above-mentioned non-Li materials as the substrates, it needs to prestore Li metal inside these porous substrates to obtain composite Li anodes for further application in the full cells, which can be realized via several routes, including the electroplating, mechanical rolling, and molten Li infusion methods. Different compositing methods for Li metal and 3D substrate show differential effects on reducing the effective current density.

First, Li metal can be encapsulated in conductive hosts through the conventional electrodeposition method; this is usually applied in a coin-cell configuration where conductive hosts serve as the working electrode and Li metal foil is used as the counter electrode (Figure 23a). By controlling the electroplating conditions, the loading capacity of the Li metal can be well-manipulated. In addition, the as-obtained composite Li metal can be porous with a massive exposed electrochemical surface area for Li metal plating/stripping as long as the hosts are not fully filled with Li metal, which will then be truly effective in lowering the local reaction rate. This method has been employed as a major method for constructing a host-based Li metal anode.

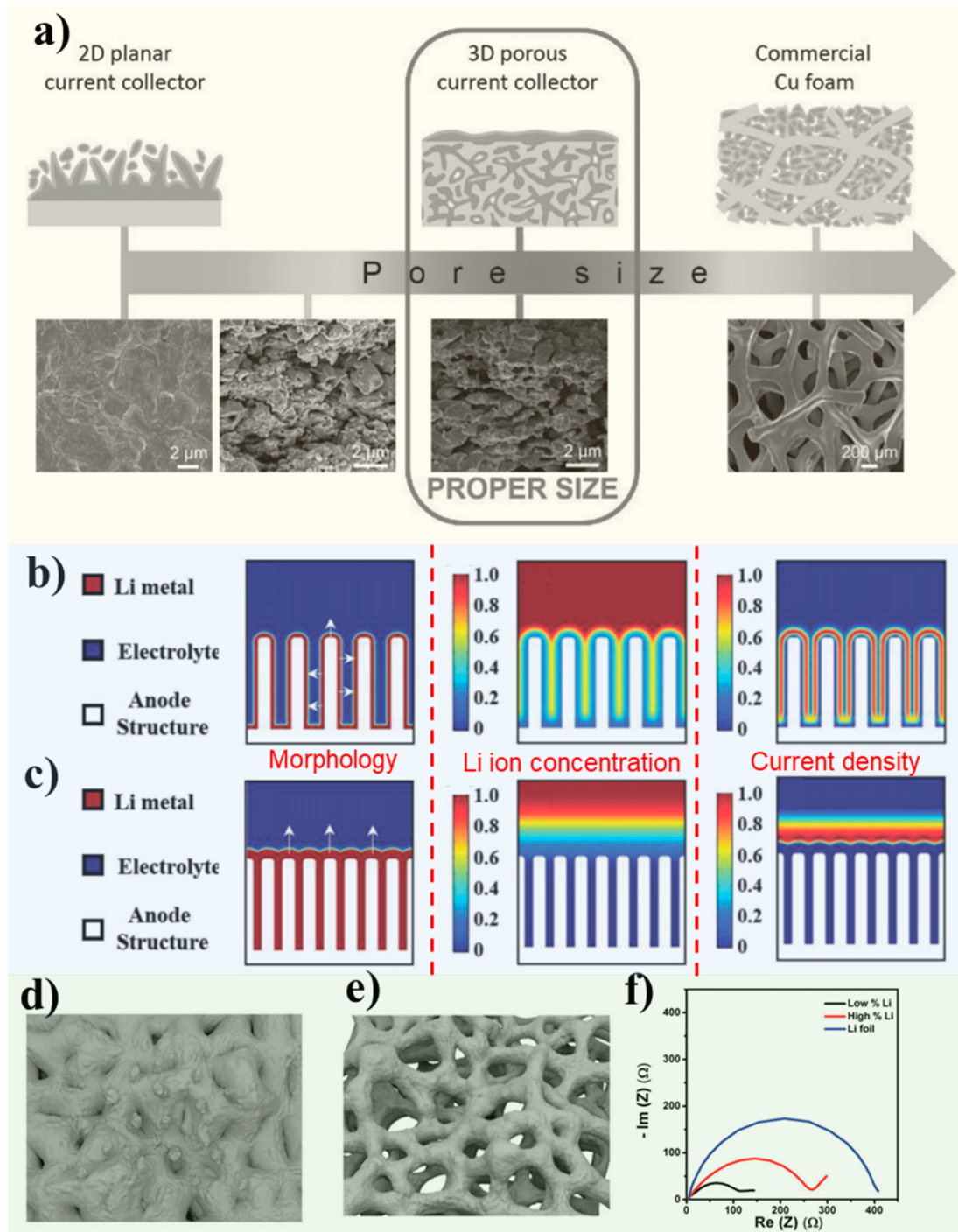


Figure 25. Importance of pore size and porosity of 3D Li anodes. (a) Principle of designing the 3D current collector for an Li metal anode. Reproduced with permission from ref 92. Copyright 2016 Wiley-VCH. (b,c) Simulated Li deposition morphology (left), Li-ion concentration distribution (middle), and normalized current density distribution (right) for the (b) spaced Li nanotubes and (c) closed Li nanotubes. Reproduced with permission from ref 247. Copyright 2019 Wiley-VCH. (d–f) Structure morphologies of Li foam under (d) high coverage and (e) low coverage, and (f) corresponding EIS spectra for Li foil, Li foam under high Li coverage, and Li foam under low coverage after 15 cycles. Reproduced with permission from ref 216. Copyright 2018 Wiley-VCH.

Unfortunately, this method can hardly be adopted for practical application because of its operation complexity. Specifically, the composite electrode has to be withdrawn from the prelithiated cell and assembled into another cell with cathode material for practical use. Another long-lasting obstacle that the electro-deposition fabrication method inherits is the preferential deposition of Li metal around the top layer while the remaining

bottom parts remain hollow during the process, as reported by many works.^{203,204,206,237,238} With the increment of the deposition capacity, the plating area gradually moves downward at a lower current density, following the top-down deposition manner (see some discussion in section 4.2.2.1).²⁰⁶ In this case, the electrochemical active area is largely shrunk and the substrates lose function on dissipating the current density,

which obviously deviates from the primary intention on designing the porous conductive skeleton. According to Yu *et al.*, this phenomenon is ascribed to the competition between the Li deposition rate (electron transfer rate) and Li⁺ diffusion.²⁰⁶ This problem can be solved by tuning the surface lithiophilicity of conductive hosts. For example, when randomly dispersing lithiophilic Au particles over rGO hosts, the sites of Li plating expand from the top layer to the whole body; consequently, the fabricated anode can deliver a high Coulombic efficiency of 98% after 200 cycles with a constant cyclic capacity of 2 mAh cm⁻², which far surpasses that of bare rGO or Cu hosts.²³⁷

Regarding the mechanical rolling method, soft Li foils are usually pressed with 3D substrates (particularly for metallic ones) to afford dense Li composite anodes. For example, copper mesh is mechanically pressed into the Li plate and the composite is directly used as an anode in LMBs (Figure 23b).²⁰⁷ It is worth mentioning that the options for the substrates are very limited as the substrates are required to exhibit high mechanical strength. Moreover, the as-composited Li metal anodes are usually very dense, which partially sacrifice the large-surface-area advantage of 3D substrates. Lastly, compared with the electroplating method, it is more difficult to adjust the loading capacity of Li metal in the composite anode by using the mechanical pressing method.

Infusing molten Li metal inside the porous hosts is another way to fabricate porous Li metal anodes. This method simplifies the fabrication process and expands the range of treated hosts. Unlike the electrodeposition method, there is no demand on the hosts' electric conductivities for the strategy; instead, the key demand lies on the good surface wettability/lithiophilicity of the host materials toward the molten Li metal in order to achieve fast infusion and an even/smooth Li metal layer (Figure 23c).²⁴⁰ Nevertheless, similar to the mechanical pressing method, the molten Li infusion method is weak in controlling the loading capacity of the Li metal, and the as-composited Li anode usually has a dense structure, which weakens the host's capability of dissipating the current density. Thus, far, several methods are designed to modify the hosts' surface lithiophilicities. The first way is by coating or dispersing some low nucleation overpotential substances on the host surface, including the Li-alloying materials such as Zn,²⁴¹ Ag^{219,242}, Si²⁴⁰, and oxides such as ZnO^{215,243}, Al₂O₃²⁴⁴, Co₃O₄²⁴⁵, and SnO₂²⁴⁵. When contacted with the molten Li metal, the decorated materials on the hosts will react with it and form a Li-rich alloy on the top layer, which exhibits strong lithiophilicity, and the byproduct of Li₂O in the case of oxide decoration, which contributes to an effective SEI layer above for guiding the homogeneous plating.^{211,240} It has been proven that both the lithiophobic metal and carbon framework have significant improvement in Li-affinity capabilities after surface coating a thin layer of Si by the CVD method.²⁴⁰ Figure 24a displays a schematic illustration and photos of the improvements with molten Li placed on different hosts, in which the coated samples will be immediately rinsed by Li metal while the uncoated samples stay unwetted. Similarly, the inner wall of the aligned channels within porous wood-carbon is randomly dispersed with ZnO particles, thus presenting excellent lithiophilicity (Figure 24b).²¹⁵ As a result, the large surface area with excellent lithiophilicity allows the decrement of overpotential to less than 90 mV at 3 mA cm⁻² and an extended life of symmetric cells (130 h at 3 mA cm⁻²) than the pristine Li metal counterparts.²¹⁵ Another route to enhance lithiophilicity depends on the large binder energy for surface defects²²³, functional groups^{223,246}, and dopants²⁹ on carbona-

ceous materials with Li metal. For instance, dense graphene oxide (GO) film undergoes a so-called "sparked" process by getting contact with the molten Li; subsequently, molten Li not only reduces the GO into rGO but also significantly enlarges its surface area by triggering the formation of a nanogap between the nanosheets; the rich functional groups on the rGO surface conversely guarantee the high enough lithiophilicity due to their relatively large binding energy with Li metal (*e.g.*, 3.080 eV for carbonyl groups and 2.974 eV for alkoxy vs 1.983 eV for bare graphene) (Figure 24c).²²³ The material effectively cuts plating overpotential to ~80 mV at 3 mA cm⁻² and guarantees the stable cycling for at least 100 cycles at the current density of 3 mA cm⁻².²²³

Overall, the diverse choices of fabricating porous Li metal anodes based on 3D conductive substrates indeed present some potentials on replacing pristine Li metal as the anode. Much evidence has consolidated their feasibility on suppressing dendrite growth and improving cell performance through the synergistic effects of dissipating local current density and enhancing surface lithiophilicity. Nevertheless, there are some vital issues that need extra attention before discussing their future commercialization. First, the pore size and porosity of the hosts and as-prepared Li metal anodes should be carefully controlled since they are closely related to the functions of the electrode structure.^{92,216} For instance, a highly porous Cu framework (Figure 25a) with the proper pore size between 200 nm and 2 μm and evenly distributed TiO₂ nanotube arrays with an average diameter of ~70 nm and interspace around 125 nm are proven to have much better electrochemical performances than more compact counterparts.^{92,247} It is demonstrated that if the pores are too small, the porous host cannot effectively confine the growth of deposited Li and most of the Li metal will be deposited on the surface of the current collector (particularly the conductive hosts), as it does on a conventional planar current collector. In other words, the porous structures lose their functions on homogenizing Li concentration and dissipating local current density, as evidenced by the COMSOL simulation results (Figure 25b).²⁴⁷ Meanwhile, Zhu *et al.* also explored the effect of Li coverage, namely, the porosity of Li metal anode on the electrochemical performance in their works.²¹⁶ It is revealed that hollow Li foam under low coverage (Figure 25d) has better charge transport, lower impedance, and long-term cycling stability than that with the highly covered Li (Figure 25e) and bare Li foil counterparts, owing to the facilitated electrolyte diffusion channels, increased charge carrier, and ionic mobility from its significant porosity as reflected in Figure 25f.²¹⁶ Overall, the porous substrates shall have good wettability of electrolyte and abundant open pore space for Li accommodation and electrolyte penetration. More essentially, Li metal should not completely fill the hosts, otherwise it will block the electrolyte diffusion pathway throughout the anode, decrease electrochemical-active sites, and enhance the possibility of dendrite formation after long cycling. Another special issue for 3D porous conductive hosts is the enhanced electrolyte consumption on forming the SEI layer brought by the larger electrochemical-active area, which not only negatively influences the Coulombic efficiency of the cells but also increases the risks of dendrite appearance.^{15,196}

4.1.2. Uniform and Accelerated Li⁺ Diffusion in SEI Layer. As previously stated in section 3.1.4.2, Li ions would go through the SEI films before being reduced to the Li atom; therefore, microscopic Li ion transportation inside the SEI layer is a key influencing factor for Li metal plating. Functionalizing

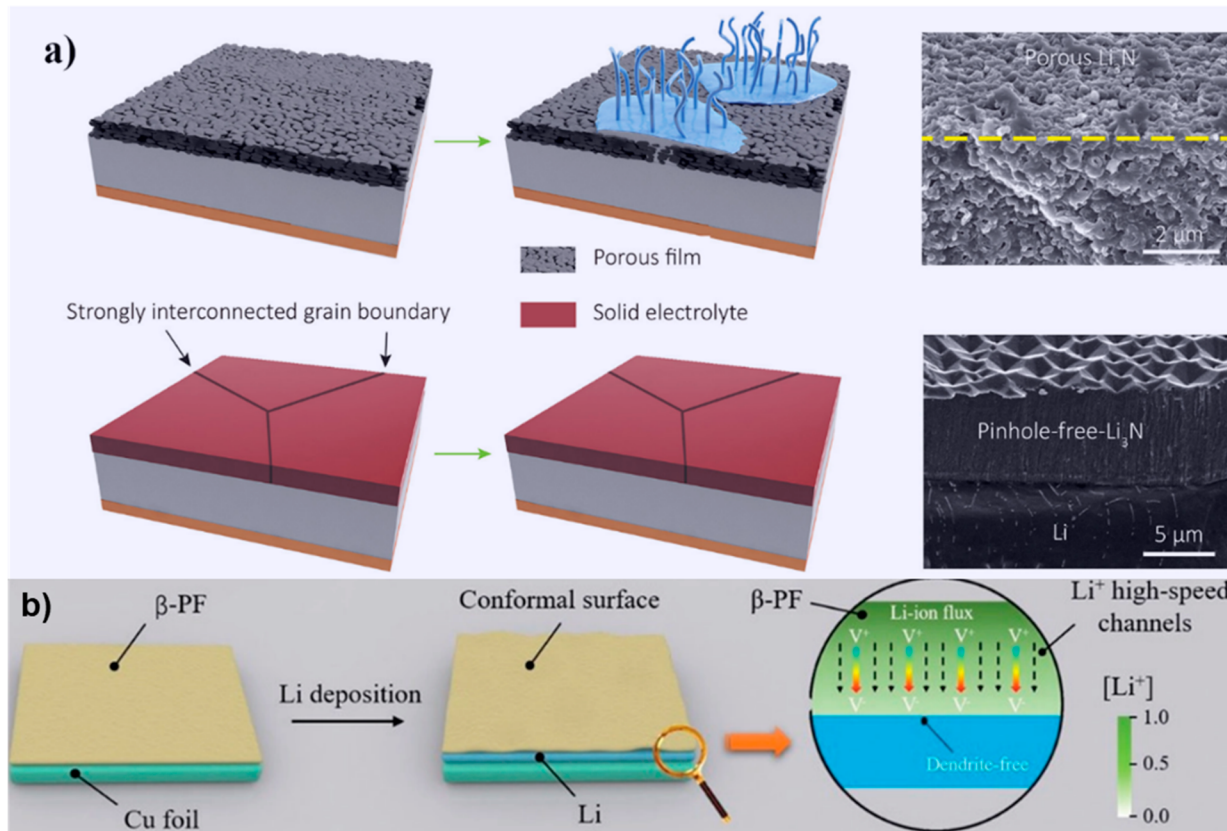


Figure 26. Strategies toward isotropic and accelerated Li⁺ diffusion at the Li anode surface. (a) Schematic and SEM images of Li metal anodes coated with porous Li₃N film (up) and dense, pinhole-free Li₃N film with strongly interconnected large grains (bottom). Reproduced with permission from ref 169. Copyright 2018 American Chemical Society. (b) Schematic illustration of Li deposition on Cu foil with β-PF film modification, serving as the Li-ion pump to regulate the uniform distribution of Li ions. Reproduced with permission from ref 254. Copyright 2019 Wiley-VCH.

SEI films with the isotropic ion transportation property can reduce the concentration polarization, thus suppressing dendritic growth. Accordingly, single-component artificial SEI films have been designed, featuring less defects and higher structural uniformity compared with the naturally formed SEI layer. These artificial SEI films can be mainly divided into the inorganic ceramic-based ones and polymer-based ones (also see some discussion in the stress field regulation part in section 4.3.2.2). It should be noted that some electrochemically stable inorganic materials, such as Al₂O₃, SiO₂, and ZnO, are the most common ones,^{245,248} yet these materials suffer from poor interfacial ion transportation as their intrinsic ionic conductivity is relatively poor. In contrast, some other single-component films using LiF, Li₃N, or Li₃P are more promising,²² as these components present superior ion-transportation ability. For example, Li₃N is an excellent material for Li metal protection with a high ionic conductivity (up to 10⁻³ S cm⁻¹) and low electronic conductivity (<10⁻¹² S cm⁻¹);²⁴⁹ however, the grain sizes of Li₃N are generally small (<160 nm),^{250,251} thus easily affording an anisotropic ion transportation behavior through the crystal or along the boundary, making the grains interconnection too weak to suppress the Li metal dendrites. To solve the above challenges, a stable, mechanically strong, dense, and pinhole-free α-Li₃N interface layer on Li metal is designed (Figure 26a), which promotes superior electrochemical performance.¹⁶⁹ Benefiting from the isotropic Li ion migration inside the pinhole-free interface layer, full cell based on a Li₃N-protected Li anode can stably run for over 500 cycles, which is far superior over that based on a bare Li anode. Another approach for the

migration homogenization of Li ions within SEI layer is to redistribute the Li ion flux above/near the SEI layer, such as introducing parallelly aligned holey 2D materials (*i.e.*, MgO nanosheets) closely on the Li metal anode surface to form multilayer SEI.²⁵² The holey nanosheets outside the SEI can redistribute the Li-ion flux in the electrolyte because of the evenly distributed and smaller-sized (<50 nm) pores, which are different from the irregular pores with sizes between 50 and 800 nm in a commercial Celgard 2500 separator. Of note, the size of the pores on the 2D materials should be large enough to support rapid Li-ion migration.

Reinforcing the dynamic Li-ion migration inside the SEI layer is also helpful to mitigate the concentration polarization. In principle, improving the content of highly ionic-conductive components inside the SEI films has been verified as an effective solution. Inspired by this concept, a variety of electrolyte additives, including FEC, VC, and SEI-forming salts (*e.g.*, LiNO₃, Li₃PO₄, LiFSI) have gained massive popularity since they are favorable for the formation of thermodynamically stable and highly ionic-conductive LiF, Li₃N, or Li₃P components.^{27,253} In the second, leveraging LiF-, Li₃P-, and Li₃N-containing single-component or hybrid artificial SEI films is a more direct way to fulfill this goal as addressed above.^{120,169} Lastly, equipping SEI films with a self-built driving force for ion migration is also considered an effective approach. Following this motivation, Huang's group reported a multifunctional artificial SEI layer based on piezoelectric polyvinylidene fluoride (PVDF), as shown in Figure 26b.²⁵⁴ During Li metal deposition, compressive stress is created on the piezoelectric PVDF film,

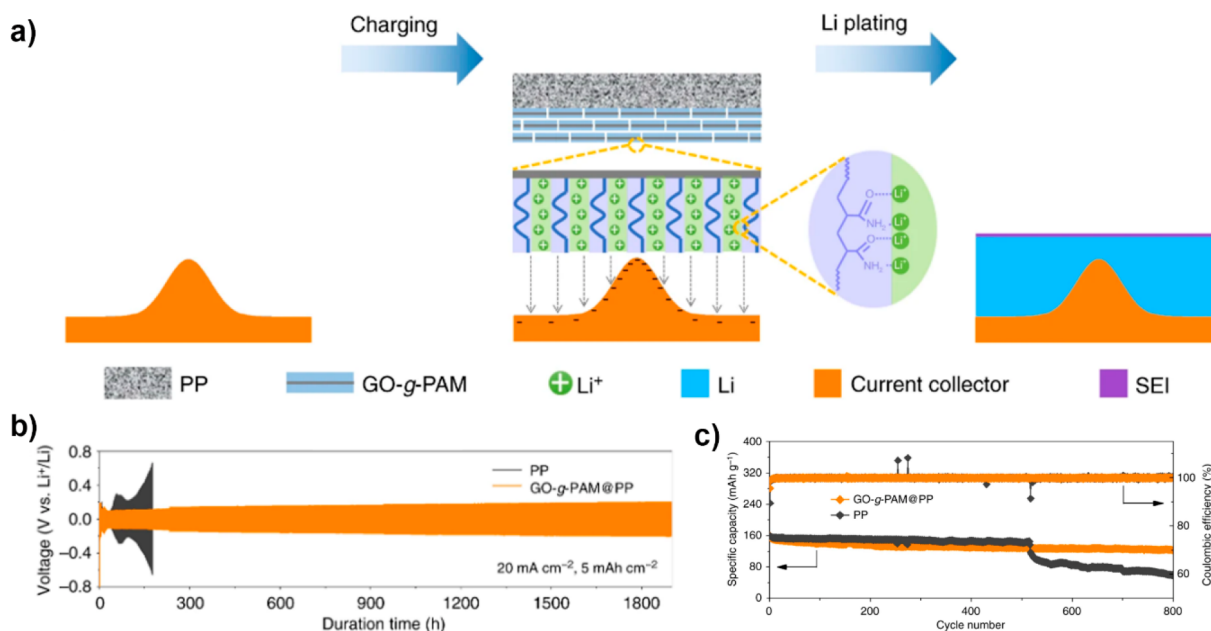


Figure 27. Separator modification toward uniform macroscopic Li ion flux. (a) Schematic diagram of Li deposition on Li electrode with microscopic surface roughness, where the separator is modified with polyacrylamide (GO-g-PAM@PP). (b) Voltage–time profiles of Li plating/stripping processes with a cycling capacity of 5 mAh cm^{-2} at 20 mA cm^{-2} in symmetric Li//Li cells with GO-g-PAM@PP. (c) Long-term cycling stability of Li// $\text{Li}_4\text{Ti}_5\text{O}_{12}$ cells with GO-g-PAM@PP separator at a current density of 3C ($1\text{C} = 175 \text{ mA g}^{-1}$). Reproduced with permission from ref 262. Copyright 2019 Springer Nature.

which further induces a piezoelectric field with a direction pointing from the cathode to the anode; driven by the piezoelectric field, Li ions migration will be accelerated through the PVDF film in the same direction, presenting a “Li-ion pump” effect. This effect is also applicable to other energy storage systems, such as supercapacitors^{255,256} and LIBs.^{257–259}

Of interest, all of the above-mentioned functionalized protective layers offer extra benefits for suppressing Li dendrite growth through the physical shield effect (see more discussion in the stress regulation part in section 4.3.1).

4.1.3. Macroscopic Ionic Concentration Regulation

Homogenizing the Li^+ concentration within the whole electrolyte-filled areas is also an essential method to relieve the Li^+ agglomeration effects around hotspots and avoid the salt depletion on the anode surface. To achieve the above goal, a series of macroscopic concentration regulation strategies have been developed based on modifying the components in cells (including the separator modification, high concentration electrolyte, and electrode layout design) and applying external fields. In the following sections, the most-updated progress made so far on these methods will be separately introduced and discussed.

4.1.3.1. Separator Modification

As revealed by the Li-ion transport dynamics study in isolated electrolyte microchannels using the glass capillary cells, concentration polarization is highly dependent on the geometry of the channels; specifically, a positively deviated Sand's time scaling exponent can be used to infer a converging penetration area through the electrolyte, while a negatively deviated scaling exponent suggests that diffusion limitation can be avoided in expanding channels, namely, the eradication of tree-like dendrites.¹⁷⁹ This result suggests that separators with expanding ionic conduction structures can not only homogenize macroscopic Li-ion flux at the interface between the Li metal anode and separator but also delay the local concentration depletion at the electrode surface,

which is feasible to avoid the fatal tree-like dendrites. Noted that such separator modification is especially beneficial for a dense Li metal anode like commercial Li chips; instead, if 3D porous Li metal anodes are used, the enhancement of uniform Li ion flux will be weakened due to the longer diffusion distance from the counter electrode to the internal part of the porous anode, compared with the dense anode.

Furthermore, constructing lithiophilic separators with strong Li-ion affinity have received much attention; correspondingly, polydopamine²⁶⁰, metal–organic framework (MOF) materials²⁶¹, and polyacrylamide-grafted graphene oxide (GO-g-PAM) nanosheets²⁶² are studied as coatings over commercial separators. For instance, Wu's group²⁶² developed functional porous bilayer composite separators by simply blade-coating polyacrylamide-grafted graphene oxide molecular brushes onto commercial polypropylene separators. This modified separator enables molecular-level homogeneous and fast Li ionic flux on the surface of electrodes because of the lithiophilic feature of hairy polyacrylamide chains with a large quantity of polar functional groups (C=O and N–H), as shown in Figure 27a. Remarkably, Li metal anodes working in the conditions present an unprecedented stability of more than 1900 h cycling at an ultrahigh current density of 20 mA cm^{-2} (Figure 27b). Moreover, the cell with the GO-g-PAM@PP separator retains 77% of the initial capacity with a steady Coulombic efficiency of nearly 100% over 800 cycles, which is superior to that with pristine PP separator (Figure 27c). Tu *et al.* developed a sandwich-type composite separator by laminating a nanoporous $\gamma\text{-Al}_2\text{O}_3$ sheet with high porosity between macroporous poly(vinylidene fluoride-co-hexafluoropropylene) (PVDF-HFP) polymer layers.²⁶³ This vertically aligned pore configuration enables a uniform and rapid Li^+ ion diffusion from the bulk electrolyte to anode surface. In another work, a polydopamine-treated PE separator was reported for LMBs.²⁶⁰ It turns out that the polydopamine coating offers PE surface excellent

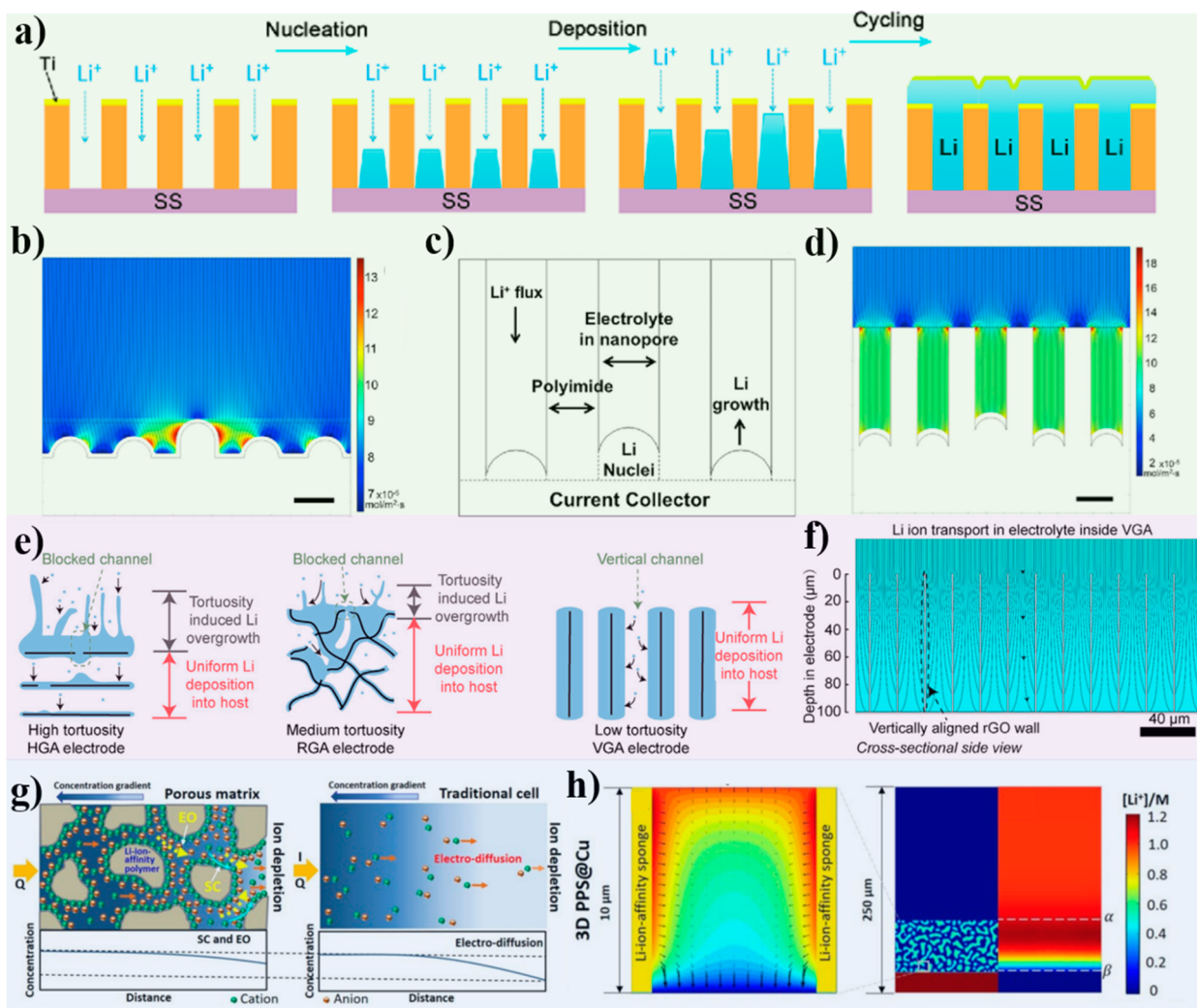


Figure 28. Electrode layout design toward uniform macroscopic Li ion flux within the entire anode area. (a) Schematic illustration of the Li deposition pattern over the anode with a vertically aligned nanochannel coating.¹³⁰ (b) Simulation of Li⁺ concentration distribution for a bare electrode.¹³⁰ (c) Simulation cell geometry of the anode with a nanochannel coating.¹³⁰ (d) Simulation of the Li⁺ concentration distribution for the anode with a nanochannel coating of 3.5 μm in height. Reproduced with permission from ref 130. Copyright 2016 American Chemical Society. (e) Schematics of Li deposition in horizontally aligned rGO (left), randomly arranged rGO (middle), and vertically aligned rGO (right). (f) Simulation of Li-concentration distribution in low-tortuosity vertically aligned rGO. Reproduced with permission from ref 266. Copyright 2020 Elsevier. (g) Schematic illustration of electrokinetic effects within the 3D PPS framework under an electric field (left) and the ions movements in regular cells under an electric field (right). Reproduced with permission from ref 270. Copyright 2018 Springer Nature. (h) Simulated Li⁺ distribution under a constant current density within the PPS framework at the scale of $10 \times 10 \mu\text{m}^2$ (left), initial phase morphology at the scale of $250 \times 250 \mu\text{m}^2$ (middle), and Li⁺ distribution at the scale of $250 \times 250 \mu\text{m}^2$ (right). Reproduced with permission from ref 270. Copyright 2018 Springer Nature.

lithiophilicity and increases the uptake electrolyte amount, owing to the strong affinity for surface polar functional groups to Li ions; the properties help homogenize macroscopic Li ionic flux on the surface of Li metal anode. As expected, adopting the modified separator helps improve the cycling stability. In addition, Shang and co-workers prepared an ultrathin graphdiyne (GDY) (10 nm) film with inherent atomic-level cavities as a coseparator, where the GDY sheet was proven to be an atomic semipermeable filter to enable the homogeneous migration of atomic Li.²⁶⁴ Similar macroscopic cation regulation mechanisms can also be achieved by anchoring the biomolecule (collagen hydrolysate)²⁶⁵ and biofilm (*Escherichia coli*)²⁶² on separators, which simultaneously induce a deionization shock inside the separator and spread cations on the anode to promote uniform electrodeposition.

4.1.3.2. Electrode Layout Design. Homogenizing the Li-ion flux within the whole anode area can be realized via designing the electrode layout or modifying the electrode with Li-attracting dielectric or insulating hosts. For example, the polyimide membrane with nanochannels is coated on the surface of the current collector (Figure 28a).¹³⁰ As a benefit of the confined Li⁺ flux within independent channels, the hotspots can only receive the Li⁺ sources in the channels above rather than the whole electrolytes close to the anode surface. As a result, the self-amplified growing pattern of Li dendrite will be relieved and a more homogeneous deposition is expected to occur during the charging process, which have been proven by the COMSOL simulation results (Figure 28b–d), and enhanced the cyclic stability in the half cell tests. Another thing that should be noted is that the size of the channel can also affect the performance; specifically, channels with sizes up to micrometers do not exhibit

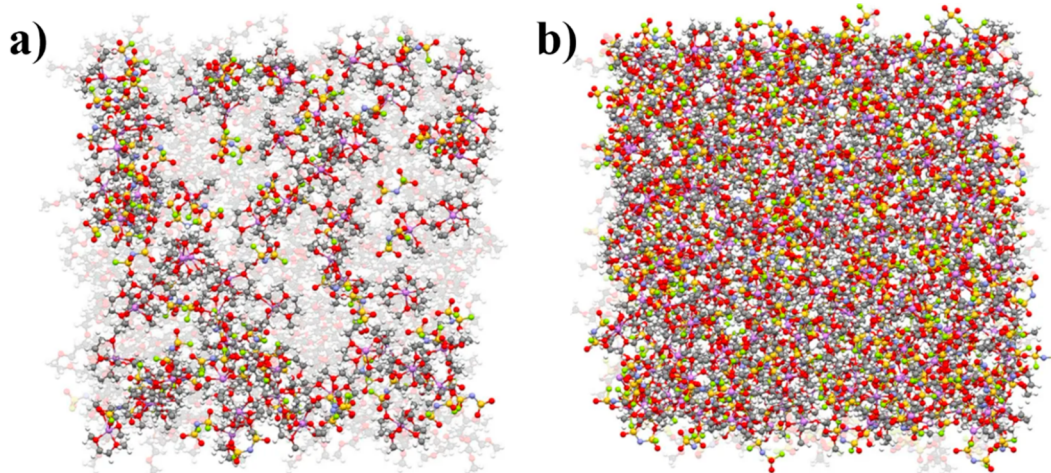


Figure 29. MD simulation results for coordination state of ions and solvents in (a) 4 M LiFSI/DME electrolyte and (b) 1 M LiFSI/DME electrolyte, respectively, in which purple, red, blue, yellow, and green dots stand for the elements of Li, O, N, S, and F, respectively and the uncoordinated DME solvent is in light gray. Reproduced with permission from ref 276. Copyright 2015 Springer Nature.

the dendrite suppression capability anymore.¹³⁰ In another work, three types of hosts, vertically aligned, horizontally aligned, and random rGO electrodes with a tortuosity of 1.25, 4.46, and 1.76, respectively, were designed.²⁶⁶ It is demonstrated that high electrode tortuosity causes higher current density on the top surface of the electrodes, resulting in severe inhomogeneous Li deposition and fast-degraded cycling performance; in contrast, low electrode tortuosity in the vertically aligned rGO host enables homogeneous Li transport and uniform Li deposition across the host (Figure 28e,f). As a result, the low-tortuosity, vertically aligned rGO electrode achieved a high CE of ~99.08% under high-capacity and high-current-density cycling conditions (5 mAh cm^{-2} , 5 mA cm^{-2} in ether electrolyte for 150 cycles). In comparison, the high-tortuosity rGO electrodes exhibited a severe 80 mm-thick upper overgrowth of dendrites after a single plating step, rapid anodic CE decay from 98.6% to 90% after only 24 cycles. Furthermore, parallelly aligned holey MgO nanosheets on a Li metal anode were reported to simultaneously redistribute the Li-ion flux in the electrolyte and in the solid-electrolyte interphase, which allowed uniform Li-ion distribution as well as fast Li-ion diffusion for reversible Li plating and stripping.²⁵² The MgO-protected Li anodes could achieve a high Coulombic efficiency of $\approx 99\%$ and ultralong-term reversible Li plating/stripping over 2500 h at a high current density of 10 mA cm^{-2} .

Compared with the physical confinement effect for Li-ion flux from the electrode layout design, equipping nonconductive hosts with abundant functional polar groups on their surface seems better at redistributing the ionic concentration due to the strong chemical attraction forces toward Li^+ ²⁶⁷ similar to the separator modification as discussed above in section 4.1.3.1. Such strong chemical affinity between polar groups and Li^+ ions is effective on immobilizing Li^+ ions within the whole anode area, presenting a so-called spatial confinement effect. Meantime, the highly porous structure allows the free penetration of electrolytes and provides adequate volume for Li accommodation.²⁶⁸ These features of 3D nonconductive hosts are favorable for macroscopic homogenization of ion flux and the smooth Li plating. Furthermore, the electrochemical-active area in nonconductive hosts is dramatically reduced, which can minimize the electrolyte consumption for massive SEI formation. Another advantage for nonconductive hosts is that Li metal plating often

follows a bottom-up pattern in them rather than an undesired top-down pattern as reported in some 3D conductive hosts; therefore, the ion flux confinement functionality can last for a long time until the host is fully filled by Li metal, making it less possible for dendritic evolution (see more explanation in section 4.2.2). For example, it demonstrates that oxidized PAN-based 3D nonconductive host contains rich polar functional groups such as $\text{C}=\text{N}$, $\text{C}-\text{N}$, $\text{C}=\text{O}$, and $\text{O}-\text{H}$ on its surface.²⁶⁹ When hotspots appear over the surface of plated Li metal, the host can effectively ameliorate the Li^+ concentrating effect nearby and change the dendrite morphology to a pancakelike shape. Porous polymelamine-formaldehyde (PMF) is also designed as an insulating host for Li accommodation, where the surface functional groups (*i.e.*, amine and triazine) are evidenced to have excellent attraction toward Li^+ through the simulation of DFT.²⁶⁷ By applying Cu-PMF composite anode, the cells achieve an average Coulombic efficiency of 94.7% for 50 cycles at the fast rate of 10 mA cm^{-2} . Besides, glass fiber is a popular group of nonconductive hosts for LMBs.^{203,205} For instance, Zhang *et al.* fabricated a 3D glass fiber cloth, which contained rich $\text{Si}-\text{O}$, $\text{O}-\text{H}$, and $\text{O}-\text{B}$ polar groups, and directly used it as hosting material.²⁰⁵ The material contributes to a relative smooth deposition, together with an average Coulombic efficiency of $\sim 90\%$ for 40 cycles at the current density of 10 mA cm^{-2} and areal capacity of 2 mAh cm^{-2} . Additionally, one work that needs to be mentioned is done by Wang *et al.*, where the electrokinetic effect is proven helpful for promoting the homogeneity of Li^+ concentration.²⁷⁰ Basically, the polyethylenimine (PEI) sponge used in this work has a large amount of functional groups (amine and ether) to attract and dissipate Li^+ as the regular nonconductive hosts do. Furthermore, the functional groups also induce the formation of an electric double layer near the surface with a high zeta potential of $\sim 42 \text{ mV}$. Under the influence of an electric field, the *in situ* formed double layer will bring some beneficial effects: electrokinetic surface conduction and electroosmosis (Figure 28g);^{271–274} these effects will lead to a high enhanced Li^+ diffusion capability within the nonconductive framework and further promote the Li^+ homogeneity within the hosts. As a confirmation of the electrokinetic surface conduction's existence, the ionic conductivity of Li^+ is measured to be the value of $9.62 \times 10^{-5} \text{ S cm}^{-1}$ at 25°C , which is higher than the PEI film counterpart. The

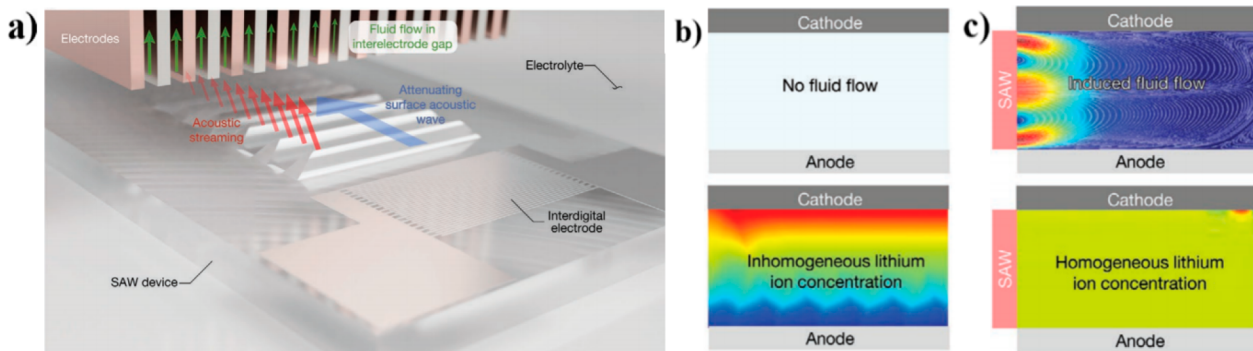


Figure 30. Implementation of the external acoustics force toward uniform macroscopic Li ion flux. (a) Schematic illustration of the acoustic wave-integrated cell configuration and working mechanism. (b,c) Simulation results of fluid flow (upper) and concentration distribution (down) for (b) traditional LMBs and (c) acoustic wave-integrated LMBs. Reproduced with permission from ref 285. Copyright 2020 Wiley-VCH.

synergetic effects of electrokinetics and strong Li^+ -adsorption ability from surface functional groups on Li^+ -concentration homogenization are demonstrated through simulation results in Figure 28h. As a result, the material delivers remarkable working stability/reversibility at both high current density and areal capacity, such as an average CE of 99.1% for 800 cycles at 2 mA cm^{-2} and 2 mAh cm^{-2} , 99% CE for 450 cycles at 4 mA cm^{-2} and 4 mAh cm^{-2} , and 97.8% CE for 150 cycles at 20 mA cm^{-2} and 4 mAh cm^{-2} .²⁷⁰

4.1.3.3. Highly Concentrated Electrolytes. According to the Sand's time model, increasing the initial salt concentration in electrolytes is a feasible method to postpone the dendrite initiation; however, the concentration of electrolytes in general cases is very low (<1.2 M) due to the limited solubility of salts in paired solvents.²⁷⁵ Under this circumstance, a series of highly concentrated electrolytes (abbreviated as HCEs) or so-called “solvent in salt” electrolytes are reported. First, using HCEs can help to homogenize the Li ion flux within the whole electrolyte-filled area because the Li-ion source is much more sufficient than that of diluted electrolyte; in other words, the chances of salt depletion near the anode surface will be largely reduced. Furthermore, in HCEs, more anions and solvents are closely confined in the Li^+ primary solvation layer. For instance, in 4 M LiFSI/DME electrolyte, ~3% anions are uncoordinated and ~6% Li^+ are solvated as simulated by the MD method (Figure 29a).²⁷⁶ In comparison, these two values for 1 M LiFSI/DME electrolyte are 60% for the amounts of both uncoordinated anions and nonfully solvated Li^+ (Figure 29b). Therefore, they typically exhibit a high Li^+ transference number ($\mu_{\text{Li}^+}/(\mu_A + \mu_{\text{Li}^+})$) (e.g., 0.73 for 7 M LiTFSI in DOL/DME (1:1 vol/vol)), thus avoiding the draining of Li salts near the anode surface.²⁷⁵ Also, the SEI will be majorly contributed from the decomposition of anions in electrolytes; common F-contained anions (e.g., FSI^-) in HCEs result in LiF-richer SEI layers with a robust structure, superior ionic conductivity, and homogeneous supply of Li^+ , thus stabilizing the Li deposition.^{270,277,278} With the collective influence of these issues, the Cu//Li asymmetric cells using the 4 M LiFSI/DME electrolyte deliver superior electrochemical performances, with an average Coulombic efficiency of 98.4% in 1000 cycles at the high current density of 10 mA cm^{-2} . However, simply asserting that higher concentration leads to greater performances of cells is not appropriate. Increasing the salt concentration to 5 M for the LiFSI/DME electrolyte dramatically decreases the ionic conductivity (1.7 ms cm^{-1} vs. 5.7 ms cm^{-1}), which does harm to the rate performance of

cells.²⁷⁶ Besides, increased cost of the cells should also be taken into concern when utilizing such a great amount of expensive -imide salts. Furthermore, even though the highly concentrated ether-based electrolytes exhibit significantly improved anodic stability, they still suffer from the poor stability toward oxidation; consequently, they are unable to be applied in high-voltage LMBs, which jeopardizes the energy density of the cells and overshadows their further development and application.

Until recent years, it is realized that some cosolvents or diluents added into the electrolytes can help ameliorate the problems of HCEs.^{279–284} The feasible diluents should meet several demands, including (i) a wider electrochemically-stable potential range than original HCEs, (ii) insolubility for the salts in the electrolytes to maintain the coordination between original salt and solvent in HCEs, and (iii) miscibility with the original solvents and Li^+ -solvent solvates to form a homogeneous liquid.²⁷⁹ In one work, the cosolvent 1,3-dioxolane (DOL) is added into the high-concentration ionic liquid electrolytes which are composed of Li bis(fluorosulfonyl)imide (LiFSI) salt and glycol dimethyl ether (G4) solvent to form the diluted electrolytes LiFSI-2G4-50 vol % DOL, where the number 2 refers to the molar ratio of G4 to LiFSI.²⁸⁰ Consequently, compared to highly concentrated counterparts, the diluted ionic-liquid electrolytes exhibit higher ionic conductivity ($4.82 \times 10^{-3} \text{ S cm}^{-3}$), lower viscosity (2.98 mPa s), and wider electrochemical-stable potential range (>5.5 V). Meanwhile, the solvation state of Li^+ in pristine HCEs still maintains after mixing with diluents. Therefore, half-cell based on the LiFSI-2G4-50 vol % DOL electrolytes can achieve a superiorly high Coulombic efficiency of 99.98% for over 450 cycles at a high rate of 5 mA cm^{-2} with a cycling areal capacity of 12 mAh cm^{-2} .²⁸⁰ In another work, the bis(2,2,2-trifluoroethyl) ether (BTFE) is also applied as the diluent for the HCEs (LiFSI/dimethyl carbonate (DMC)), thus decreasing the saturated concentration of LiFSI to merely 1.2 M.²⁷⁹ The DFT and *ab initio* molecular dynamics (AIMD) calculations further confirm the preferred interaction of Li^+ to DMC solvent than to BTFE solvent, so the addition of BTFE will not have a negative impact on the ion–solvent coordination in the electrolytes. In the Li//Cu half-cell test, high Coulombic efficiencies of over 99.4% and 98.9% at the rate of 1 mA cm^{-2} and 3 mA cm^{-2} separately are realized by applying the diluted electrolytes (1.2 M LiFSI/DMC-BTFE (1:2, mol/mol)). SEM images demonstrate that the plated Li metal maintains the nodule morphology even at a high rate of 10 mA cm^{-2} and exhibits a much denser Li deposition film than that in conventional electrolytes.

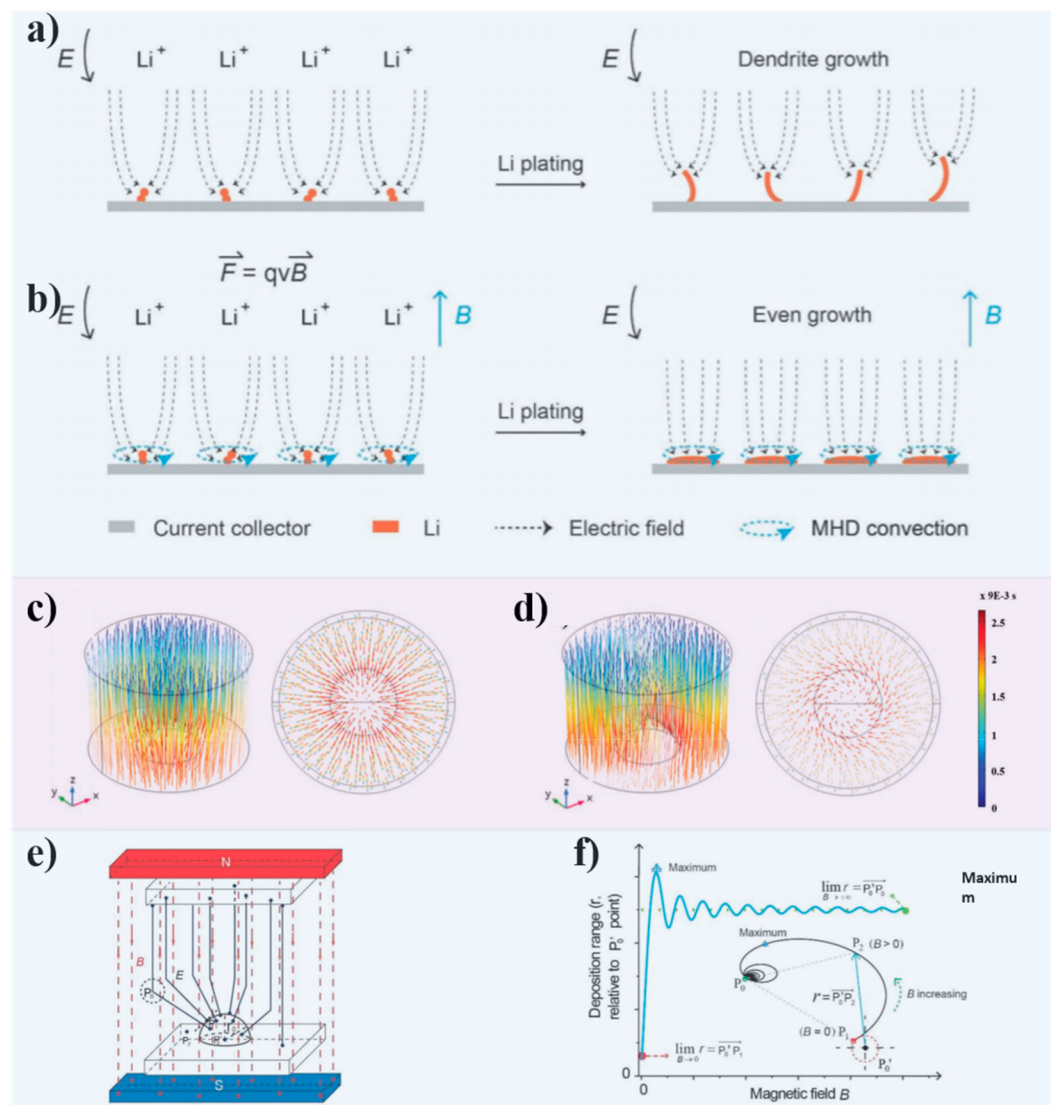


Figure 31. Implementation of the external magnetic field toward uniform macroscopic Li^+ ion flux. (a,b) Schematic illustration of (a) dendrite growth with Li^+ concentrating around the tip and (b) dendrite suppression under a magnetic field with Li^+ homogenizing near the anode surface. Reproduced with permission from ref 287. Copyright 2019 Wiley-VCH. (c,d) COMOSOL simulation results of time-dependence Li^+ transfer trajectory during Li deposition (c) with an external magnetic field (intensity, 350 mT) and (d) without an external magnetic field. Reproduced with permission from ref 286. Copyright 2019 Wiley-VCH. (e) Schematic illustration of the Li plating process under the collective influence of electric and magnetic fields and (f) simulation results of the deposition radius with an increasing intensity of the magnetic field. Reproduced with permission from ref 287. Copyright 2019 Wiley-VCH.

In addition, recent literature demonstrates that introducing inert diluent solvent into HCEs can potentially improve the solvation coordination of Li^+ relative to the undiluted counterparts. For instance, adding cosolvent 1,1,2,2-tetrafluoroethyl-2,2,3,3-tetrafluoropropylether (TTE) into highly concentrated LiFSI/DMC electrolytes is effective on strengthening the bond between Li^+ and anions and conversely reducing the solvation degree of Li^+ by DMC solvent. As a result, the SEI layer formed on the anode surface contains more inorganic LiF , thus improving the Li metal plating morphology.²⁷⁸ To summarize, the emerged diluted HCEs not only inherit the superior properties of HCEs on suppressing dendrite growth but also overcome the intrinsic shortcomings of HCEs by cutting the cost and improving the ionic conductivities and favor the stable plating of Li metal anode in the long run.

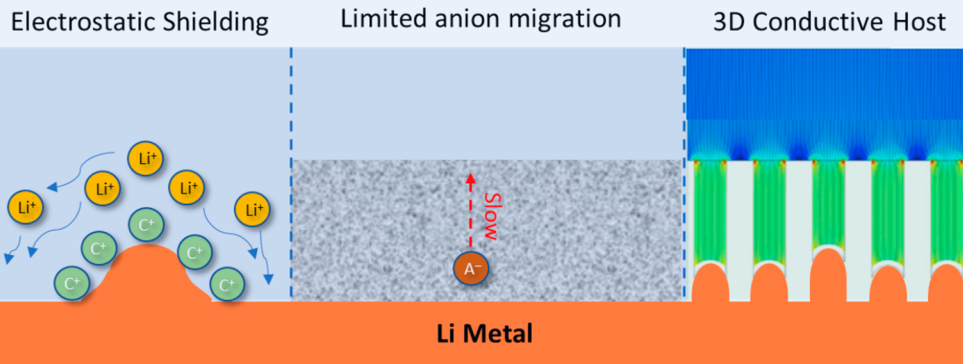
4.1.3.4. External Fields/Forces. In order to homogenize the salt concentration on the Li metal surface, external power could

also be utilized, such as the acoustic forces²⁸⁵ from ultrasonic-wave devices and the Lorentz forces^{286,287} from magnetic fields. Appropriate forces are expected to improve the distribution uniformity of dominated ionic concentrations and electric fields, namely, removing the local hotspots, thus promoting an even and dense Li plating with high efficiency. In the following section, the progress made so far in this field is comprehensively reviewed.

Ultrasound has been widely used in fluid stirring and ion homogenization in common electrolyte preparations and the chemical vapor deposition method. It could also be a powerful tool for reducing the ion inhomogeneous distribution and local depletion in the Li metal plating process.²⁸⁵ Huang *et al.* designed a special cell configuration (Figure 30a) with an average fluid flow rate of 1 m s^{-1} , and simulation results proved the concentration homogenization effect of it (Figure 30b,c).²⁸⁵ The acoustic wave-integrated Li/Cu half cells could work

Electric Field Regulation

Homogenization of Local Electric Field



Redirection of Macroscopic Electric Field

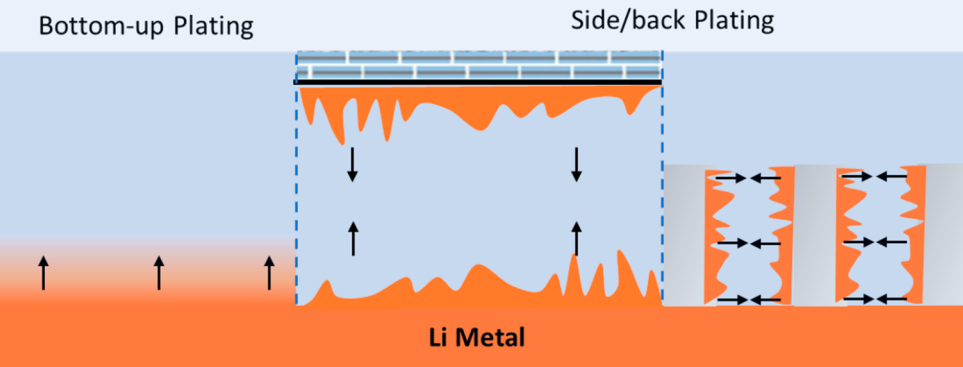


Figure 32. Overview of electric field regulation strategies for the management of Li metal deposition.

stably at a high current density of 6 mA cm^{-2} in conventional carbonate electrolytes (1.0 M LiPF_6 in 1:1 vol/vol EC/DEC) with an overpotential around 100 mV. In addition to the free notorious Li dendrite, a much denser deposition layer (from 9.1 to $5.3 \mu\text{m}$) and reduced porosity (from 46.7% to 8.5%) for wave-integrated Li//Cu half cells in comparison to nonacoustic wave counterparts at 1 mA cm^{-2} and 1 mAh cm^{-2} also demonstrate the good practicality of the method.

External magnetic field could also help regulate the Li growing morphology by influencing the macroscopic distribution of Li^+ . As known, the tip of Li dendrite is surrounded by larger amounts of Li^+ as well as a stronger electric field than the other parts of the hosts, which promote its rapid and self-enhancing growth toward the separator (Figure 31a). With the interruption of the magnetic field perpendicular to the current collectors, the Li^+ can be removed from the hotspots (e.g., dendrite tip) and homogenized near the surface of anode material under the effect of the Lorentz force (Figure 31b), as supported by the simulation of the time-dependent Li^+ transfer trajectory (Figure 31c,d).^{286,287} The impact of the magnetic field is further simulated by finite element analysis: suppose that a dendrite appears over the surface and concentrates Li^+ around the tip, the magnetic field will dissipate the Li^+ until they deposit in the area with a radius of r ; the simulation results also demonstrate that the radius of Li^+ plating increases to the maximum, then decreases to a nearly constant value as the intensity of the magnetic field increases (Figure 31e,f). For practical use, a small piece of permanent magnet with a magnetic intensity of around

0.6 mT is assembled in the Li//Li@Cu coin cells. The improvement on electrochemical performances is noticeable: the magnet-containing cells deliver an average Coulombic efficiency of 98.3% at a current density of 0.25 mA cm^{-2} and areal capacity of 0.5 mAh cm^{-2} for 180 cycles, while nonmagnetic cells present a significant performance decay after 60 cycles. When further increasing the cycling capacity and rate to 1 mAh cm^{-2} and 1 mA cm^{-2} , the magnet-containing cell exhibits a relatively stable voltage hysteresis of merely 20 mV for over 400 h; in contrast, the nonmagnetic control cell fails after merely 120 h.²⁸⁷

In another case, an external magnetic field with an intensity of 350 mT is directly applied to the cells and the ferromagnetic CoNi alloy is coated over the Cu current collector to enhance the magnetic field effect.²⁸⁶ Consequently, in a half cell test with Li metal as the counter electrode, the Coulombic efficiency for the nonmagnetic field cells quickly drops below 70% after 242 cycles, while cells under a magnetic field could maintain ~96% Coulombic efficiency after over 360 cycles at a rate of 0.5 C. Besides, at a current density of 1 mA cm^{-2} and cycling capacity of 1 mAh cm^{-2} , cells under a magnetic field deliver a stable overpotential for over 300 cycles while the nonmagnetic field cells quickly fail after 170 cycles. Furthermore, the full cell based on the LiFePO_4 cathode and the Cu/CoNi anode present superior cyclic stability and rate capability under a magnetic field, with 132 mAh g^{-1} retained after over 300 cycles at a rate of 0.5 C and 97 mAh g^{-1} delivered at a high rate of 4 C.²⁸⁶ All in all, even though the overall performance of the cells with an external

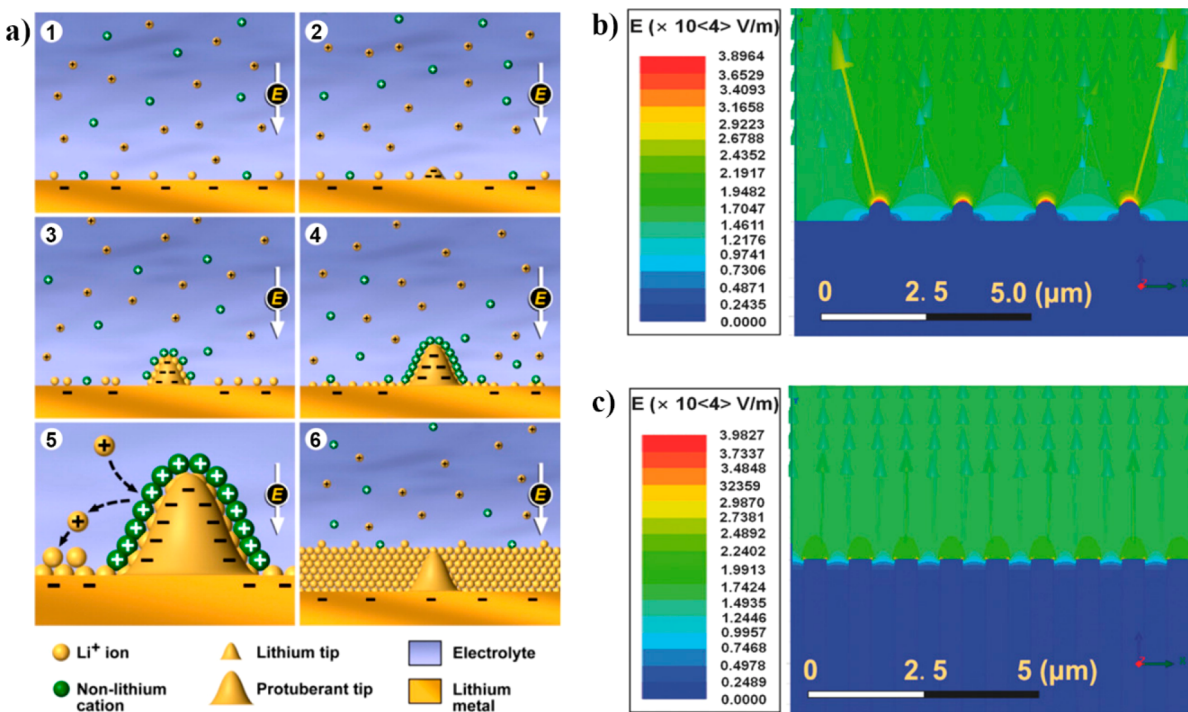


Figure 33. Local electric field regulation at the reaction interface. (a) Illustration of the Li deposition process (step 1 to step 6) based on the self-healing electrostatic shield mechanism using cesium or rubidium ions as electrolyte additives. Reproduced with permission from ref 293. Copyright 2013 American Chemical Society. (b,c) Simulation models of electric field values of (b) a bare Li anode and (c) a TiC/C/Li nanowire array anode after Li nuclei formation. Reproduced with permission from ref 36. Copyright 2017 Wiley-VCH.

magnetic field are still unable to meet the demands of actual application at the current stage, the method is still promising due to its facile availability, broad resources in nature, and more critically, its feasibility on suppressing dendrite growth and enhancing electrochemical performance.²⁸⁷

4.2. Electric Field Regulation

As discussed in section 3.1, an uneven electric field distribution at different deposition sites is regarded as one of the major driving forces for Li dendrite growth.^{288,289} In addition, the growth speed of Li metal is highly dependent on the intensity of the electric field, while the growth direction of the Li metal is associated with the direction of the electric field. It should be noted that practical situation is more complicated since many other factors (*e.g.*, SEI layer, electrode structure) shall affect the electric field distribution, thus making it harder to effectively inhibit the irregular Li growth. In this section, we will primarily highlight the influence of local electric field homogeneity and macroscopic electric field direction on Li deposition and then review electric field regulation strategies regarding these two aspects. Here, the local electric field is referred to as the electric field around local active sites. For comparison, the macroscopic electric field is defined as the one within the whole anode area or the cell. Correspondingly, strategies on homogenizing the local electric field aim at inhibiting dendrite initiation, which contains the electrostatic shielding effect with cation additive, limiting anionic migration, and adopting a 3D conductive host; the regulation of the macroscopic electric field is majorly used for Li deposition redirection, thus postponing the penetration of the separator and the failure of cells, which involves regulated bottom-up Li plating and side/back Li plating as summarized in Figure 32.

4.2.1. Homogenization of Local Electric Field.

Generally, the dendritic growth at certain active sites is closely

related to the homogeneity of the local electric field. The electric field intensity around the protruded nuclei tip is excessively stronger than that at the bottom or the smooth base surface, known as the “tip effect”.³⁶ This phenomenon can also be explained by the “lightning rod theory”: the density of electric charge is significantly increased at the point of the largest curvature.^{290–292} Then, driven by the electric field, the Li⁺ ion flux is preferentially adsorbed on the protruding nuclei, thus facilitating the self-amplified dendrite growth. To eliminate the formation of the local space charge aggregation and the locally enhanced electric field, several strategies have been proposed, including the electrostatic shielding effect, limiting anionic migration, and adopting a 3D conductive host.

4.2.1.1. Electrostatic Shielding Effect. Introducing cation additives with a reduction potential lower than the Li reduction potential can automatically restore the irregular deposition through the so-called electrostatic shield effect. A pioneering work depends on the cesium or rubidium ions added into the electrolyte.^{293,294} As shown in Figure 33a, during Li deposition, these additive cations are preferentially adsorbed over the initial growth tip of the protuberances without reduction, forming a positively charged electrostatic shield. This forces Li⁺ to deposit in adjacent regions and eliminates the irreversible dendrite growth in LMBs. Later on, some other metal ions, such as calcium, strontium, barium, and N-methyl-N-butylpiperidinium, present a similar effect on inhibiting dendrite growth.^{295,296} Nevertheless, the Li deposition CE in the electrolytes is still far from satisfaction. The contained solvents, salts, and additives need careful optimization to achieve better performance.

4.2.1.2. Limiting Anionic Migration. As indicated in the space-charge model, anion depletion and cation accumulation on the Li metal surface produce a space charge region with an intense electric field, thus triggering the rapid dendritic growth.

Therefore, eliminating the concentration polarization is regarded as an ideal approach to avoid the local-enhanced electric field and to ultimately achieve the dendrite-free deposition. This concept is also consistent with the Sand's time theory that Sand's time (τ_s) tends to be prolonged with improved cationic mobility or reduced anionic mobility. The strategies on facilitating cationic migration have been discussed in the former ionic concentration field regulation part (section 4.1); here, we will only introduce the strategies about limiting the anion migration so as to reduce the space charge and local electric field intensity. First, developing high concentration electrolytes (HCEs) is a choice, as also reviewed in section 4.1.3.3. The high transmittance number of HCEs depends on the incredibly low anions mobility inside them, which helps inhibit rapid anion depletion at the anode side and thus relieve the locally enhanced electric field; these facts are beneficial for controlling the deposition morphology. Another promising method is by designing an electrolyte with immobilized anions. As demonstrated by Archer's group, immobilizing even a small fraction (10%) of anions can dramatically improve the uniformity of Li deposition, in comparison to the case of using routine liquid electrolytes.^{90,297} Specifically, the stability of the Li metal surface under electrodeposition with immobilized anions in the electrolyte is directly associated with improved electrolyte conductivity at the metal electrode.²⁹⁷ For a cation diffusivity of $10^{-7} \text{ cm}^2 \text{ s}^{-1}$ in a 1 M total cation concentration with 10% fixed anions in a cell with 1 mm interelectrode spacing, the current density at which is 0.35 mA cm^{-2} and the corresponding overpotential is 72 mV. In comparison, the improvement in conductivity is seen very strongly at a high overpotential of 144 mV, where a 10% tethered anion electrolyte shows a 13% improvement in conductivity over a salt electrolyte, while a single ion conductor has 45% more conductivity compared to a salt electrolyte.

4.2.1.3. Adopting 3D Conductive Hosts. According to the former discussion, massive electrochemical-active sites endow a locally reduced effective current; therefore, the local electric field around the Li nuclei will be weakened and no hotspots or "tip effect" can be found on the surface of the Li nuclei (Figure 33b).³⁶ To achieve this goal, numerous efforts have been dedicated to developing 3D conductive hosts for the Li metal, e.g., carbon-based materials^{212,223,298–300}, MXene (Ti_3C_2), and metallic scaffolds^{91,92,206,239}. Since we have introduced the progress about using 3D conductive hosts in section 4.1.1.2 in detail, we will only cover several different examples in this section with the highlight on discussing the electric field regulation. For instance, Liu *et al.* developed self-supported TiC/C core/shell nanowire arrays as skeletons and confined hosts for molten Li, where the electric field streamlines exhibited more uniform distribution and no hotspot or tip effect could be found on the surface of Li nuclei (Figure 33c), resulting in a low hysteresis of less than 85 mV beyond 200 cycles at 3 mA cm^{-2} .³⁶ Yang *et al.* reported a graphitic carbon nitride ($\text{g-C}_3\text{N}_4$)-coated Ni foam for Li metal anode; the microelectric field formed in tri-triazine units of $\text{g-C}_3\text{N}_4$ are demonstrated to create numerous Li nucleation sites, which is supposed to guide uniform deposition of Li metal in the charging process.¹³⁹ As a result, the Li metal anode based on the $\text{g-C}_3\text{N}_4@\text{Ni}$ foam shows an ultralong lifespan up to 900 h with a low overpotential of $<15 \text{ mV}$ at 1.0 mA cm^{-2} and a cycling capacity of 9.0 mAh cm^{-2} .

Despite the feasibility in lowering the current and electric field intensities from 3D conductive hosts, the electron distribution within these 3D nanostructured scaffolds might not always be

homogeneous and there potentially exists strong electric field polarization either locally or macroscopically, especially when these hosts are quite thick. As mentioned in section 4.1.1.2, the intensity of the electric field within 3D scaffolds gets stronger as the distance gets shorter toward the cathode, thereby the Li metal tends to nucleate and grow on the top surface of the 3D porous conductive hosts. This phenomenon has been observed in many systems, such as the copper nanowire membrane²⁰⁶, the nickel nanowire membrane³⁰¹, carbon paper³⁰², the pristine reduced graphene oxide film²³⁷, and etc. Such Li plating behavior results in insufficient utilization of the host space and increases the chances of dendrite growth, particularly at a high cycling rate and capacity. Therefore, apart from homogenizing the local electric field around the active sites, the regulation of the macroscopic electric field on the anode side is also critically important to the deposition homogeneity and stability of the Li metal (see detailed discussion below in section 4.2.2). For instance, Yang's group demonstrated that *in situ* formation of the ionic-conductive Li_2O layer on the surface of the 3D Ni nanowire scaffold cannot only facilitate Li^+ transportation but also render a more homogeneous electric field strength distribution throughout the entire anode, thus realizing a spatially uniform Li plating.³⁰¹ Owing to the aforementioned features, a very low voltage hysteresis ($\sim 55 \text{ mV}$ during 200 cycles) with enhanced cycling stability of more than 150 cycles at 3 mA cm^{-2} is achieved. When coupling with LiFePO_4 cathode, the as-assembled full cell can stably run for over 300 cycles with minimal capacity degradation and an average Coulombic efficiency of 99.9% at 1 C. Another solution is to modify the 3D conductive host with one lithiophilic surface at the top side and another lithiophobic surface by loading lithiophilic nanoparticles (e.g., gold or zinc oxide) on the bottom surface, so as to disperse the surface-concentrated electric field and guide spatially heterogeneous Li deposition.³⁰² Despite the improvement in these works, the control on completely spatially uniform Li plating may be lost when the battery is cycling under some other critical conditions where the balance between electrochemically dominated deposition and uniform electric field distribution-induced Li plating (or the lithiophilic seed-induced Li plating) is broken.

4.2.2. Redirection of Macroscopic Electric Field. The homogenization of the local electric field plays a major role in determining whether Li metal is easy to evolve into dendrite at local electrochemical active sites or not, while the distribution of the macroscopic electric field determines the growth direction of the Li metal. Therefore, regulating the distribution of the macroscopic electric field would also exert an influence on the Li metal plating/stripping behavior. By controlling the direction of the macroscopic electric field within the entire anode area, both Li metal morphology and growth direction can be well manipulated, holding the purpose to improve the safety level. In the following sections, we will summarize two distinctive Li plating patterns (bottom-up and side/back Li plating) and the corresponding strategies to realize the redirection of the macroscopic electric field.

4.2.2.1. Bottom-Up Li Plating. Typically, the self-built electric field inside sandwich-type cells presents a parallel-allied pattern perpendicular to the anode current collector/sePARATOR, thus guiding the bottom-up plating of the Li metal. However, the bottom-up Li plating may easily evolve into an uncontrolled pattern and induce dendritic formation during long-term cycling once the surface morphology becomes irregular, such as on conventional Li metal foils. Therefore, fixing and stabilizing the

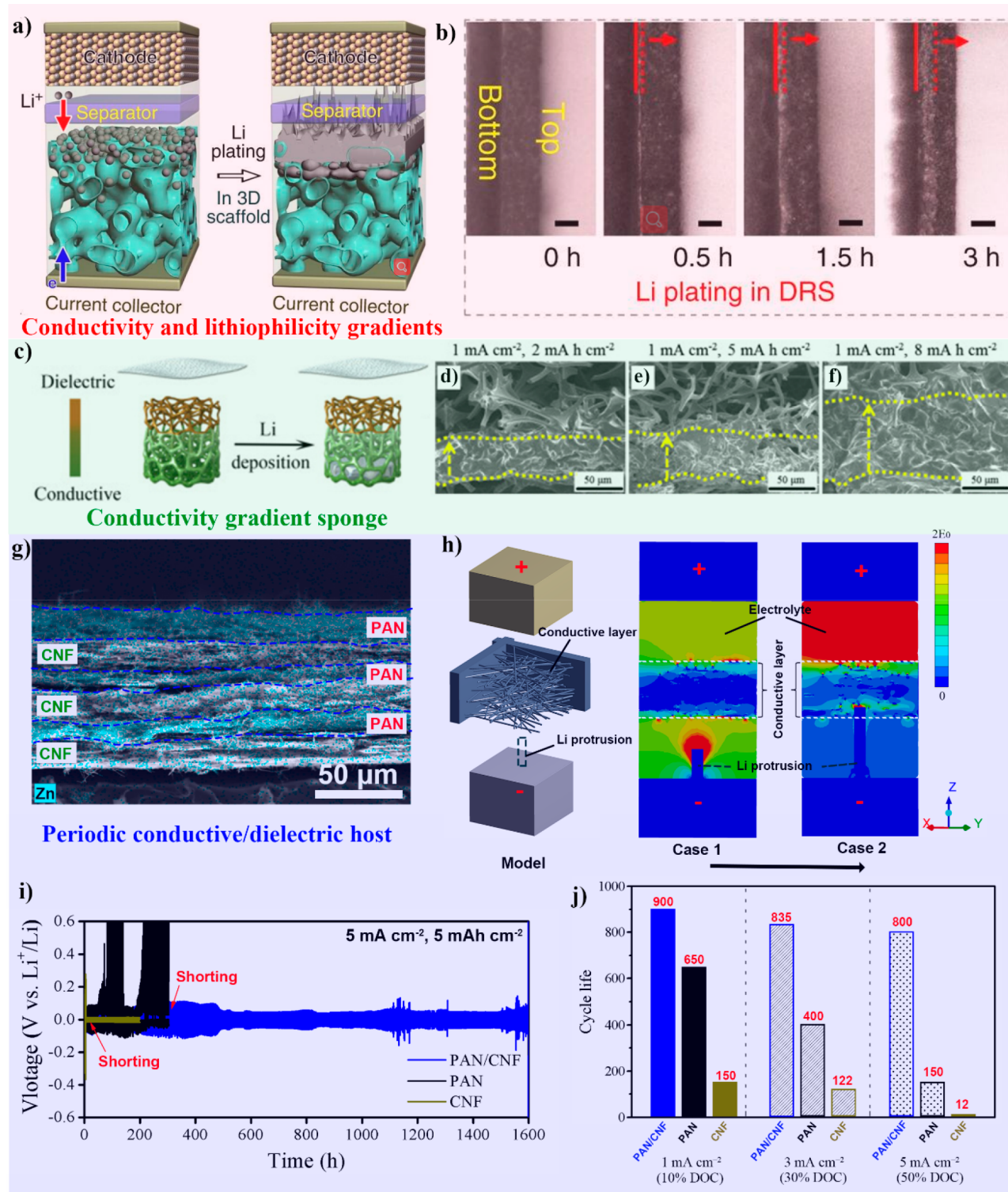


Figure 34. Bottom-up Li plating strategies. (a) The bottom-up Li deposition in a deposition-regulating scaffold (DRS) anode. (b) Optical microscopy images of the cross section of the DRS, which show the Li-plating process over time (the red arrow indicates the direction of Li growth). Reproduced with permission from ref 304. Copyright 2019 Springer Nature. (c) Schematic illustration of Li metal deposition behavior in a conductive-dielectric gradient sponge (CDG-sponge): “bottom-up” deposition without dendrite formation. (d–f) Cross-sectional SEM images of the CDG-sponge after depositing (d) 2 mA h cm^{-2} , (e) 5 mA h cm^{-2} , and (f) 8 mA h cm^{-2} of Li at 1 mA cm^{-2} . The regions deposited with Li metal are highlighted by arrows and dotted lines. Reproduced with permission from ref 238. Copyright 2020 Elsevier. (g) A Zn element distribution mapping image within periodic PAN/CNF indicates the structure of alternately stacked PAN and CNF. (h) Simulation model of the domain setup (left) and electric field distributions in periodic host-based Li metal from the bottom electrode to the top electrode along the Z-axis of the system (middle and right). From case 1 to case 2, the dendrite keeps growing and propagates to keep in touch with the conductive layer ahead. (i) Voltage–time profile of different Li metal anodes at 5 mA cm^{-2} with a plating/stripping capacity of 5 mAh cm^{-2} . (j) Comparison of cycle life of Li@PAN/CNF electrode with Li@PAN and Li@CNF electrodes at different DOD. Reproduced with permission from ref 307. Copyright 2020 Wiley-VCH.

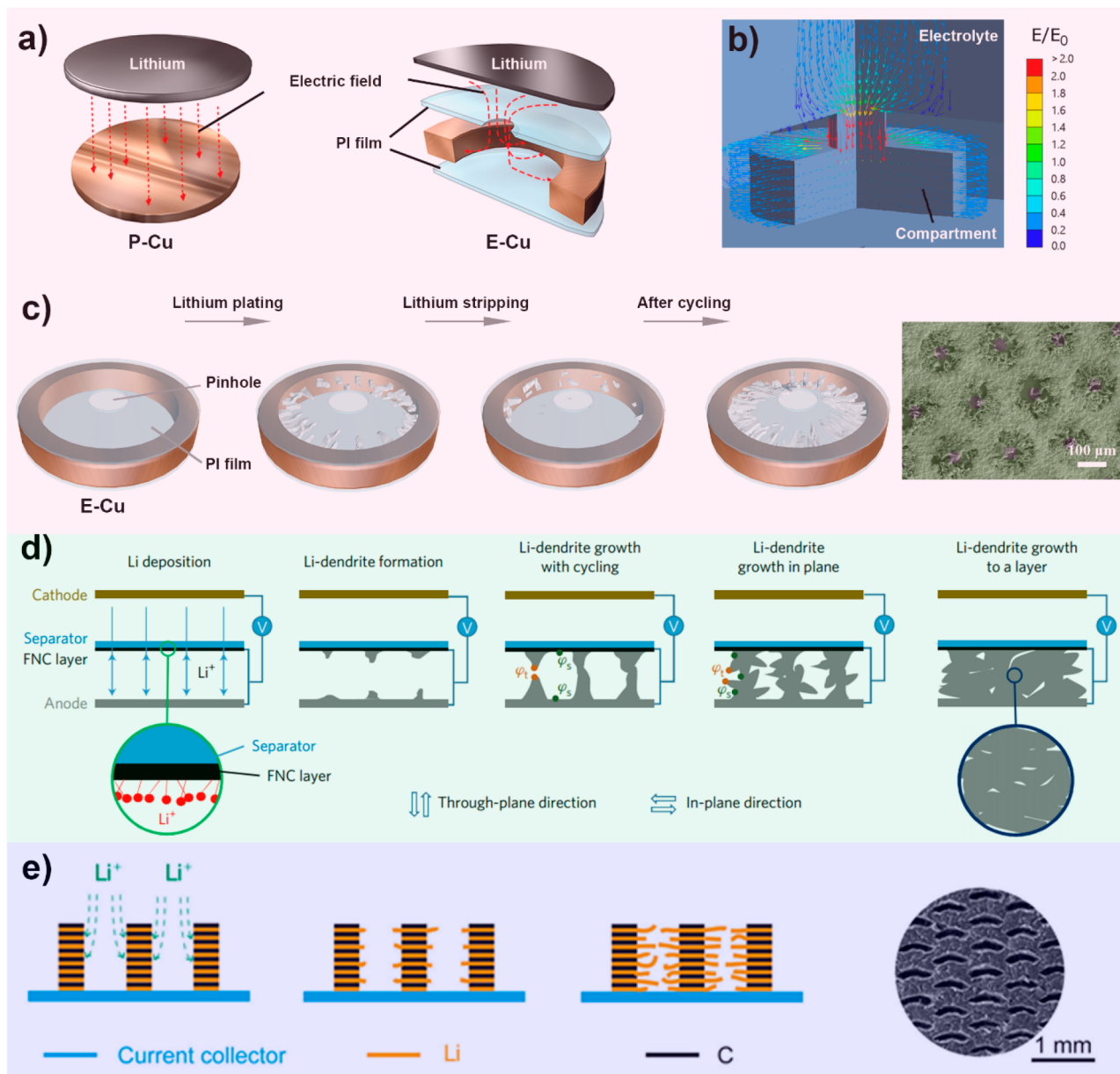


Figure 35. Side/back Li plating strategies. (a) Schematic illustration of the electric field distribution in planar Cu (P-Cu) and microcompartmented Cu (E-Cu). (b) Simulated result of the electric field distribution in E-Cu. (c) Schematic illustration of the evolution of Li anode structure based on E-Cu during Li plating/stripping (left) and SEM image of E-Cu after Li deposition at 0.5 mA cm^{-2} with 2 mAh cm^{-2} (right). Reproduced with permission from ref 81. Copyright 2018 Springer Nature. (d) A functionalized nanocarbon (FNC)-based cell using a FNC-coated separator. The detailed structure of the separator can be seen in the inset at the left-hand side of the schematic. Li dendrites formed on both surfaces of the Li anode and the FNC thin film simultaneously growing toward each other driven by the potential difference between the tip and the base, stopping growth along the through-plane direction when dendrites from two opposite directions meet, restarting growth along the in-plane direction (as indicated in the figure) and, finally, growing into a Li dendrite layer (the right-hand side of the panel). Reproduced with permission from ref 62. Copyright 2017 Springer Nature. (e) Schematic illustration of Li deposition in P-rGO/Li electrode (left) and SEM image of P-rGO/Li anodes obtained by absorbing molten Li into the patterned rGO films (right). Reproduced with permission from ref 309. Copyright 2018 Elsevier.

bottom-up deposition pattern is critical for dendrite control. The most effective way is to composite Li metal with a stable 3D host. As mentioned in section 4.2.1.3, Li deposition in fully conductive hosts suffers from the surface-dominated growth issue, rather than the bottom-up pattern. Instead, employing dielectric hosts or gradient/periodic hosts have been proven as effective avenues to realize stable “bottom-up” Li deposition.

In terms of fully dielectric hosts, glass fiber²⁶⁹ and some polymeric nanofiber membranes^{280,303} have been developed. Within fully dielectric hosts, as electrons cannot transfer through

the dielectric parts, Li metal plating can only be initiated on the limited electrochemical-active area (from the bottom current collector, such as Cu foil and stainless steel sheet), which is not beneficial for high-rate cycling. To reduce the nucleation and deposition polarization within dielectric hosts, various seed materials are proposed to enhance the affinity of these matrixes with Li metal or Li ions, which is helpful for achieving a uniform microscopic ionic concentration field, as discussed in section 4.1.3.2. In comparison, 3D hosts featured with gradient or periodic conductivity/lithiophilicity characteristics can provide

a more electrochemical-active area for simultaneous Li nucleation/propagation, in comparison with fully dielectric hosts. Therefore, superior performance can be achieved when cycling under both high current densities and high capacities. To illustrate, Pu and co-workers reported a conductivity/lithophilicity gradient host by electrically passivating the top of a porous nickel scaffold and chemically activating the bottom of the scaffold (Figure 34a).³⁰⁴ Within this gradient structure, the unsafe deposition mode was overridden with the bottom-up plating, because the insulating coating in the top region shuts off the electron conduction in the anode/separator region whereas the Au coating lowers the nucleation overpotentials at the bottom (Figure 34b). At spatial and temporal scales, this gradient structure, to some extent, could reduce the probability of the dendrite-induced short circuits. Experimental results show that excellent properties can be obtained at an extremely high current density (10 mA cm^{-2}), high capacity (up to 40 mAh cm^{-2}), and low temperatures (down to -15°C). Li *et al.* fabricated a conductive-dielectric gradient framework structure by introducing a conductive nickel nanolayer with thickness-dependent gradient structure on a dielectric porous melamine sponge via a simple magnetron sputtering process (Figure 34c).²³⁸ As demonstrated by an electric field simulation, the electric field distribution within the gradient sponge is dominated at the bottom area due to higher electric conductivity, and this uniform area is wider than that in the fully conductive sponge. Therefore, Li metal plating inside the scaffold presents a desired bottom-up deposition pattern (Figure 34d–f). The symmetric cell based on the electrode presents stable Li metal deposition/dissolution for 780 h with a low overpotential (<20 mV) at 1 mA cm^{-2} , better than those based on a fully conductive sponge and a fully dielectric sponge. In addition, Zhang *et al.* developed a lithophilic-lithophobic gradient structure by dripping carbon nanotubes (CNT) with various ZnO loadings layer by layer onto Li foil.²⁴¹ Peng's group reported a 3D porous lithophilic-lithophobic-lithophilic dual-gradient (Cu–Au–ZnO–PAN–ZnO) current collector³⁰⁵ and a gradient Si-modified carbon paper³⁰⁶ as the hosts for the Li metal. Benefiting from the unique gradient feature, bottom-up Li metal plating with suppressed dendrite growth is obtained in those works. More recently, Yang's group reported a periodically conductive/dielectric lamella scaffold (periodic CNF/PAN) for hosting the Li metal anode (Figure 34g), which can also realize a “bottom-up” Li plating pattern.³⁰⁷ More interestingly, even if uneven Li metal deposition occurs inside this periodic host, its parasitic propagation can be blocked by the overhead conductive layers as they are electrically equipotential for rehomogenizing the local electric field around the Li protrusion (from case 1 to case 2 in Figure 34h), thereby automatically smoothing the subsequent Li metal plating (noted as “self-correction” behavior). By employing such a unique host, dendrite-free Li plating/stripping with a high Coulombic efficiency can be achieved even at 5 mA cm^{-2} and an ultrahigh cycling capacity of 15 mAh cm^{-2} , and a maximal cumulative plating capacity of 4000 mAh cm^{-2} with a Li utilization of 50% realized, superior to solely conductive CNF-based and solely dielectric PAN-based counterparts (Figure 34i,j).

4.2.2.2. Side/Back Li Plating. An ideal Li anode shall be dendrite free, yet dendrite growth cannot be practically avoided during prolonged cycling. Therefore, an ultimately safe LMBs solution might have to consider the presence of a number of irregular Li deposits, no matter when, where, and how these irregular Li grow from the anode.^{62,81} In this context, directing

irregular Li growth toward the direction with less harm, by torturing the self-built electric field distribution, has been reported to tackle the irregular Li formation issue. For instance, Yang's group developed a microcompartmented array host for accommodating laterally grown deposits (Figure 35a), where the electric field is simulated to exhibit a lateral pattern inside the host (Figure 35b) and thus guides the Li deposits towards lateral growth within the interior compartments (side plating).⁸¹ Instead of suppressing/delaying irregular Li growth, this technology modulates the Li growth direction: from perpendicular to parallel to the separator (Figure 35c), thus prolonging the safe operation life of the batteries. Numerical simulation also demonstrates that ~60% reduced stress from the protruded Li deposits can be achieved in the compartmented host, as compared with that in the planar Cu current collector. Similarly, a coiled Li anode with a unique upright structure could also guide inner/side growth of the Li metal, so as to improve the battery safety level.²⁰³

Another feasible strategy to redirect Li growth is reported by coating the separator with functionalized nanocarbon with immobilized Li^+ ions.⁶² In this structure, the functionalized nanocarbon film is electrically connected to the Li metal electrode through the tabs, thus affording an equal-potential layer. As shown in Figure 35d, during cycling, the Li deposits grow toward each other simultaneously from both the functionalized nanocarbon layer on the separator (back plating) and the Li metal anode; when the Li deposits meet, the growth changes direction rather than penetrating the separator, then a dense Li layer is formed between the separator and the Li anode. As a result, a long stable cycle life (>800 cycles with 80% retention of the initial capacity) and improved efficiency (>97%) was fulfilled in a Li//LiFePO₄ coin cell. Such a side-plating configuration has also been proven an effective solution to avoid internal short circuits from zinc dendrites.³⁰⁸

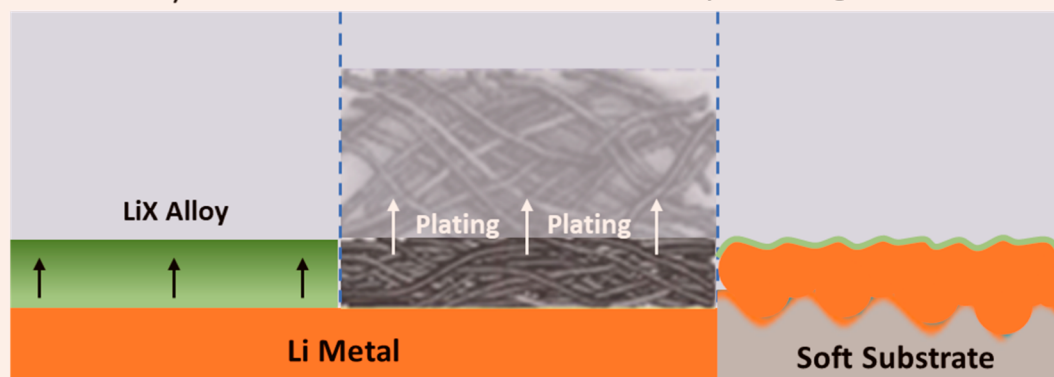
Even though regulating a side/back Li plating pattern can improve the battery safety level to some extent, the Li metal may still grow in dendritic morphology, which is not desirable for high CE since it is easier to form “dead Li” from dendrites than a smooth Li metal structure. To eliminate the dendrite formation while maintaining a side-plating pattern, a patterned reduced graphene oxide (P-rGO)/Li composite anode was developed, where the electric field is detoured to the edges of the patterned anodes (Figure 35e).³⁰⁹ Due to the electric field regulation effect, Li initially nucleates at the rough edges of the voids in the patterned anodes and grows horizontally and centripetally to fill the empty space. On the other side, high-surface-area graphene has been widely studied as an excellent Li metal host to suppress the dendritic growth.^{212,223,310} As a result, the symmetric cell with P-rGO/Li anodes could be cycled for more than 2 000 h and is able to maintain a stable plating and stripping voltage profile at the current density of 10 mA cm^{-2} . Moreover, a dendrite-free Li anode based on vertically oriented Li–copper–Li arrays is also developed.³⁰⁶ Such vertically oriented arrays not only regulate the electric field to realize gradual deposition along the in-plane direction but also act as a “dam” to guide the regular plating of Li, thus efficiently buffering the volume change of the Li anode even under an ultradeep stripping/plating capability up to 50 mAh cm^{-2} , high rate capabilities (20 mA cm^{-2}), and long cycle life (2000 h).

To summarize, redirecting the macroscopic electric field distribution can manipulate the morphology and growth direction of Li metal anode, and improve the stability and safety level of the cell. Most efforts have been focused on

Stress Field Regulation

Internal Stress Regulation

LiX Alloy Anode



External Stress Regulation

SEI/Artificial Interface Layer

Separator Modification

SEI/Artificial Layer

Li Metal

External Pressure on Cells

Cathode

Li metal anode

Figure 36. Overview of stress field regulation strategies for the management of Li metal deposition.

achieving bottom-up or side/back Li plating patterns. It is also expected that Li plating can be controlled in any direction as long as a specific anode structure is designed, based on electric field regulation knowledge. For reference, we can introduce “defective sites” on the anode surface through microneedle surface treatment²⁰¹ and the stamping technique¹⁹⁶, aiming to utilize the “lightning rod theory” to selectively direct the Li plating and stripping processes for dendrite growth control. Another possible strategy is to construct hosts with an elaborately designated structure for the Li metal anode. In such kind of hosts, Li metal prefers to deposit at some local specific sites that have a stronger current density (or electric field). For example, a porous Cu current collector with vertically aligned microchannels is reported for Li metal anodes, within which Li is successfully deposited into the channels by regulating the current density distributions.³¹¹ As demonstrated by current density distribution analysis, the current density within the microchannels is significantly larger than that on the upper surface of the porous Cu, thus resulting in preferential nucleation of Li inside the mouth of the channels.

4.3. Stress Field Regulation

Stress is another key physical field that influences the evolution of Li metal. If the overwhelming stress that inherits in plated Li metal cannot be well released, it is probable to trigger catastrophic irregular Li growth, particularly whisker-like and moss-like Li. Meanwhile, the evolved Li metal deposits shall have physical contacts with other rigid components in cells, such as the SEI layer and separator, which will affect their evolution pattern. In these regards, numerous efforts have been made to regulate the stress for stable Li plating and stripping, either on the solely Li metal anode or inside the whole battery. In this section, we will review some related strategies from the point of internal stress regulation, external stress regulation, and external applied pressure regulation, as summarized in Figure 36.

4.3.1. Internal Stress Regulation. As discussed in section 3.2, the Li-plating/stripping cycle inevitably results in a large volume change of the Li metal; the internal tensile stress between plated Li metal is supposed to build up during the process and induces the evolution of Li mosses and Li whiskers (Figure 11). Meanwhile, the accumulated internal stress may also threaten the structural stability of substrates, thus influencing the evolution pattern of Li deposits. Therefore, the stiffness/flexibility of substrates where Li electrodeposits

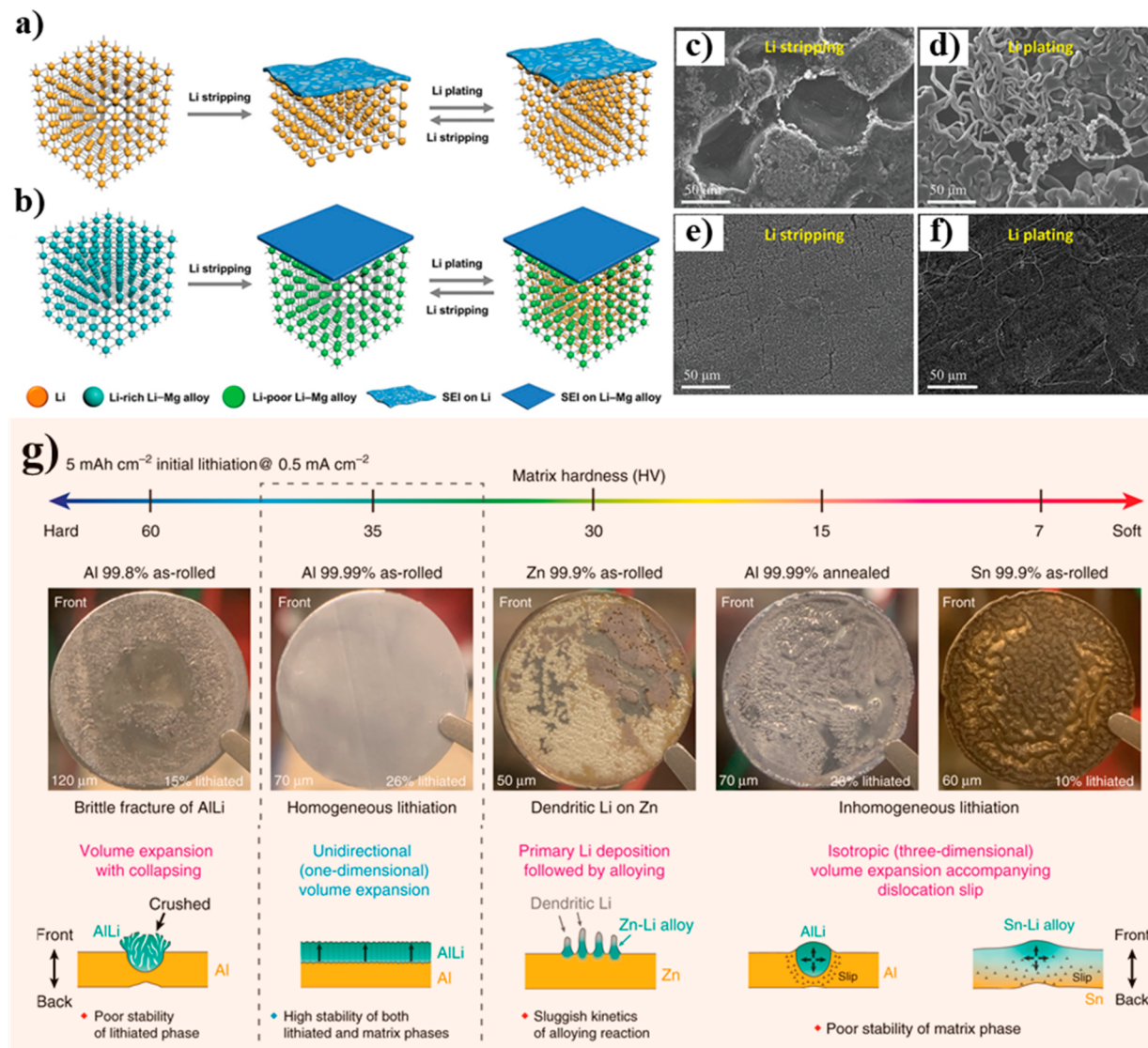


Figure 37. LiX alloy anodes for internal stress regulation. (a,b) Schematic structure illustration in the bulk and at the surface for Li (a) and Li-Mg alloy (b) anodes during the Li stripping/plating process. (c–f) SEM images of Li and Li-Mg alloy after (b,e) Li stripping and (c,f) following Li plating at 0.5 mA cm⁻² for 24 h in Li//Cu and Li-Mg//Cu coin cells. Reproduced with permission from ref 315. Copyright 2019 Wiley-VCH. (g) Photographs of various metallic foils with different hardness after lithiation of 5 mAh cm⁻² and corresponding schematic illustrations of the lithiation process. Reproduced with permission from ref 141. Copyright 2020 Springer Nature.

strongly determine whether the internal stress can be promptly released and further influence the shape of solid Li deposition.

4.3.1.1. LiX Alloy Anode. The “hostless” deposition feature of bare Li metal anode is considered as a key factor of its failure. Specifically, intense internal stress formed inside the Li deposits may force the soft metal to deform, thus destroying the SEI layer and triggering irregular Li growth. Alternatively, applying LiX alloy can solve the problems, where the X component in the alloy functions as the host to withstand the internal stress from Li atom insertion.

Of note, electrochemical alloying chemistries involve two distinctive mechanisms: (1) solid-state reaction, where no phases or structure change occurs, and (2) addition reaction, where the phase structure of LiX alloy differs from that of the pristine X host.³¹² Materials that follow the former mechanism (*i.e.*, Mg, Ag, and amorphous Si) are ideal hosts for the strategy on alleviating the negative impact from internal stress in lithium metal anode since they have better reaction kinetics. For

instance, Li_xAg ($x = 4.7\text{--}20$), as a solid-solution-based metal alloy, involves highly reversible phase changes of the alloy at potentials of -0.015 to $\sim+0.015$ V (vs Li⁺/Li), respectively.³¹³ Furthermore, the mechanism supports the fast diffusion of Li atoms (diffusion coefficient of 10^{-8} cm² S⁻¹ in Li_xAg vs 5.7×10^{-11} cm² S⁻¹ in bulk Li metal) formed on the anode surface throughout the whole body so that the plating occurs homogeneously inside the alloy anode instead of concentrating on the surface to form bulk Li metal.^{313,314} Due to the rigid host and the homogeneous dissipation of Li atoms, the problems brought by the internal stress in plated bulk Li metal are removed, as reflected by the much reduced volume change and relieved irregular Li growth. For example, it is reported that the Li–Mg alloy anode well maintains the SEI structure and uniform surface morphology after cycling while the bulk Li metal anode displays a severe structure change, thus destroying the SEI layer and producing tremendous amounts of irregular Li deposits (Figure 37a–f).^{315,316} When used in a Li–S cell, Li–Mg alloy

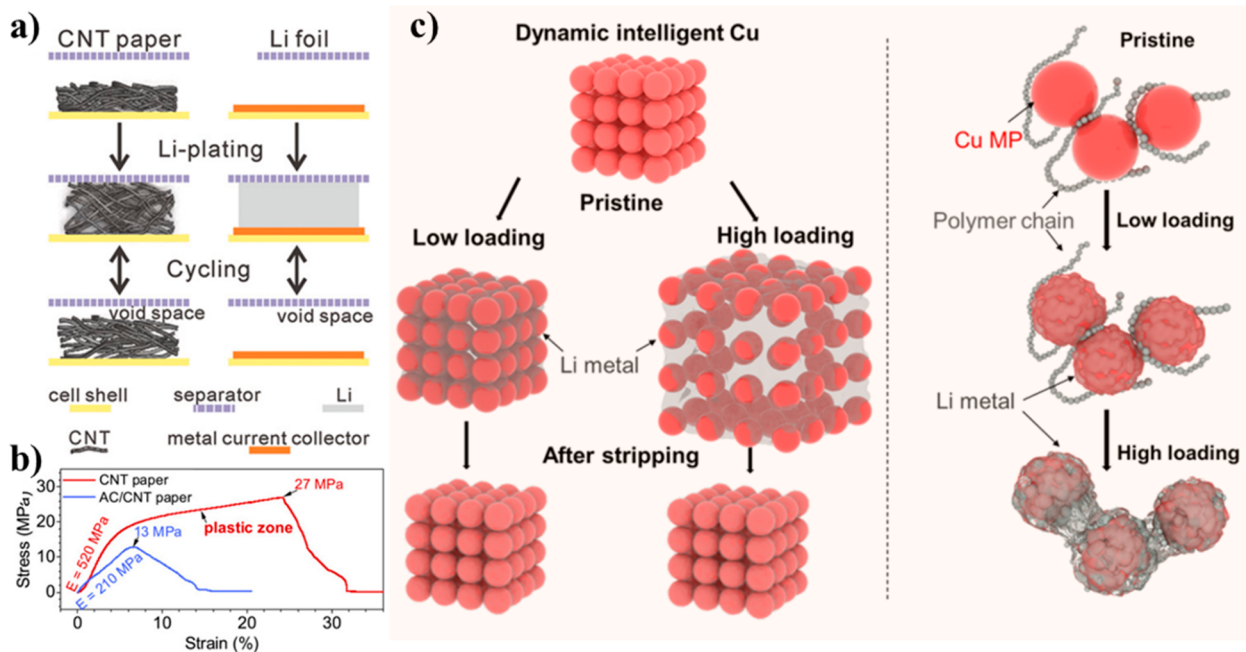


Figure 38. Electrode layout design toward stress release. (a) Schematic of volume expansion Li/CNT and Li metal foil as an electrode during Li-stripping/plating. (b) Tensile stress–strain curves of CNT and AC/CNT papers. Reproduced with permission from ref 321. Copyright 2018 Elsevier. (c) Illustration of the Li plating and stripping process on the dynamic intelligent Cu substrate (left) and schematic of the interaction among the Cu microparticles varied before and after Li plating (right). Reproduced with permission from ref 320. Copyright 2020 American Chemical Society.

shows much improved stability with a discharge capacity of 606.5 mAh g⁻¹ after 200 cycles, relative to that of 433.6 mAh g⁻¹ capacity remaining for bulk Li metal anode.³¹⁵ Besides, the Li_xAg ($x = 4.7\text{--}20$) alloy is demonstrated to deliver an average Coulombic efficiency of $99.5 \pm 0.2\%$ when cycled at 1 mA cm⁻² and 1 mAh cm⁻² for 200 cycles in a half cell and a high initial Coulombic efficiency of 98.6% in a Li₂₀Ag//LiFePO₄ cell.³¹³

In the practical application of the strategy, there are several issues that should be noted. First, in the alloy anode, the matrix material should also be counted as an active mass to calculate the theoretical gravimetric capacity (eq 21).³¹³ The theoretical capacity of Li₂₀Ag alloy anode, for instance, is calculated to be 1661 mA h g⁻¹. Besides, the hardness of alloy matrix should be carefully controlled (Figure 37g), so as to balance the stress between alloyed parts and unalloyed matrix to achieve a smooth Li deposition.¹⁴¹ Only if the strengths of both sections are comparable to each other (e.g., rolled Al), the high structure stability can be maintained during the first lithiation (i.e., Li plating process). This is because the resultant alloyed parts cannot deform the matrix; therefore, the chemical potential of the unalloyed part remains unchanged everywhere in the matrix. However, if the matrix is too soft or too hard, the strength unbalance of the matrix and alloyed parts will lead to poor stability of either the alloyed parts or the matrix phase.¹⁴¹

$$\text{theoretical capacity} = 3860 \text{ mAh g}^{-1}$$

$$\times \frac{(x - y) \times M_{\text{Li}}}{x \times M_{\text{Li}} + 1 \times M_{\text{Ag}}} \quad (21)$$

4.3.1.2. Electrode Layout Design. Employing 3D porous substrates for hosting Li metal has been proven robust enough to withstand the tensile stress induced by the Li metal volume change. Among them, stiff substrates made of both carbon and metal are generally excellent candidates, yet they are not favorable for stress release.³¹⁷ In comparison, soft substrates can

relax the build-up stresses, leading to the smooth filmlike electrodeposition. Accordingly, some other studies have been paid on developing soft substrates for the Li metal anode, aiming to combine the merits of both the 3D design and stress releasing function. For example, a 3D soft Cu/PDMS substrate is developed for addressing the Li whisker issue via the surface wrinkling-induced stress relaxation mechanism as they proposed (also see discussion in section 3.2.1);²¹ this hypothesis was further verified by computational analysis.³¹⁷ Wen *et al.* adopted a flexible carbon microtube skeleton to serve as a soft and conductive “air cushion” for the Li metal anode, which can release the Li plating-induced internal stress due to its excellent compressibility.³⁰⁹ As a result, the as-composited electrode maintains a steady and high CE (~98%) for nearly 1400 h with a high areal capacity (10 mA h cm⁻²). Ji *et al.* reported a robust and expandable CNT paper substrate for the Li metal anode, which is a perfect candidate host for releasing the internal stress to withstand the huge volume change (Figure 38a) due to its high Young’s modulus (210 MPa) and tensile strength (13 MPa) as well as a long elastic deformation zone (Figure 38b).³¹⁸ Furthermore, the as-composited Li/CNT electrode retains practical areal and gravimetric capacities of 10 mAh cm⁻² and 2830 mAh g⁻¹ (vs. the electrode mass), respectively, with 90.9% Li utilization for 1000 cycles at the current density of 10 mA cm⁻². To further dissipate the stress generated during Li uptake–release, a pulley binder (polyrotaxane-incorporated poly(acrylic acid)) with extraordinary elasticity is reported to reinforce the integrity of a CNT network.³¹⁹ Owing to the high stretchability and elasticity without breaking of the polymer film, mechanical stress exerted on the polymer network can be effectively released, substantially improving the cyclability in both Li//Cu asymmetric cells and Li//LiFePO₄ full cells.

Aside from the adoption of soft substrates, employing intelligent substrate that can dynamically accommodate the volume change is also feasible to release stress and guide dense

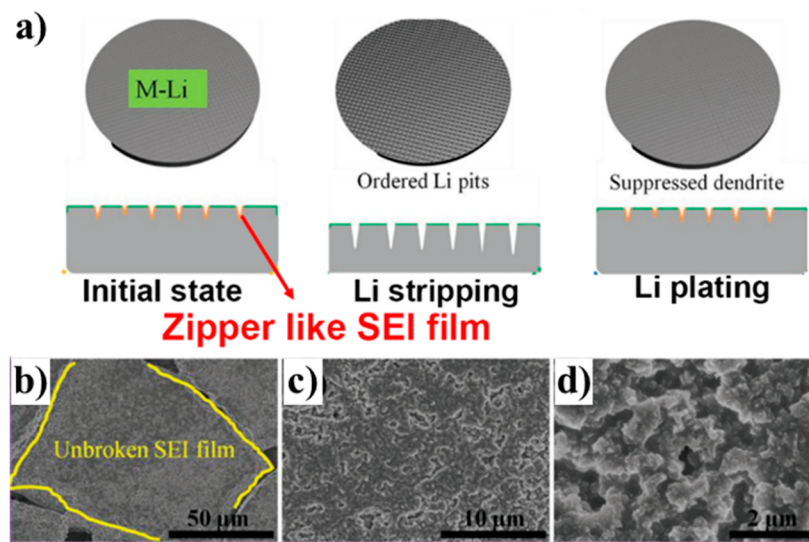


Figure 39. SEI layout design toward stress release. (a) Schematic diagram of M-Li protection mechanism for a zipperlike SEI film. (b–d) SEM images of M-Li wafers after 100 cycles at the Li stripping state under different magnifications. Reproduced with permission from ref 333. Copyright 2018 Wiley-VCH.

Li plating; for example, by changing the packing density of the assembled particles of the substrate (Figure 38c).³²⁰ The anode based on the dynamic intelligent Cu (DfCu) substrate presents excellent long-term plating/stripping efficiency at cycling rates up to 10 mA cm^{-2} . Specifically, it realizes a high Coulombic efficiency of 99.6% after 800 cycles at the current density of 1 mA cm^{-2} with a deposition capacity of 1 mAh cm^{-2} ; in contrast, the anode based on planar Cu quickly fails due to the short-circuiting within 200 cycles. Another approach to release internal stress is through the architecture design of the Li metal anode. For instance, an Archimedean spiral Li metal anode using a 2D Cu coil substrate and highly elastic poly(styrene-ethylene-butylene-styrene) (SEBS) is designed, which makes the anode stretchable.³²¹ Upon being stretched, the 2D Cu coil exhibits excellent extendibility due to the hierarchical spiral structures. Once the stress is released, the extended SEBS rubber exerts a contraction force onto the small microdomains, allowing the whole electrode to recover its original shape and dimension.

4.3.2. External Stress Regulation. Apart from the internal stress inside the Li metal, there exist some other stresses (external stress) on the intimate interfaces between the Li metal and the SEI layer, electrolyte, and separator. To modulate the impact of external stress on Li metal evolution, dominated investigations have been focusing on the SEI layer reinforcement, anchoring the Li metal anode with robust and artificial passivation layers, and separator modifications. In the following parts, we will discuss the external stress regulation strategies from the above three categories.

4.3.2.1. SEI Reinforcement. To regulate Li plating behavior, much effort has been devoted to reinforce the SEI layer so that it could withstand a large tensile stress on the interface. Electrolyte engineering is considered a practical and promising route, which has been broadly studied in both LIBs and LMBs. Notably, the composition and structure of SEI layer are highly dependent on the electrolyte composition, including the solute, solvent, and additive (see discussions in section 3.1.4.2). Primarily, a family of additives with higher reduction voltages than solvents and salts have been widely employed to strengthen the interfacial SEI layer on Li metal. In retrospect, VC^{322–324} and FEC^{325,326} have been widely used for stabilizing graphite-based anodes in LIBs.

These conventional additives are also transferred into LMBs with intercalation-type cathodes using a carbonate electrolyte, in hope of inheriting their beneficial features demonstrated in graphite-based LIBs.^{23,327,328} For LMBs using an ether-based electrolyte, such as Li–S batteries and Li–O₂ batteries, LiNO₃ additive is proven feasible on smoothing the Li metal plating.³²⁹ When LiNO₃ is present in the electrolyte, it will be reduced to insoluble but stable Li_xNO_y species on the Li metal, thus passivating the Li electrodes. Besides, the enriched inorganic components in the SEI layer by introducing some additives in the electrolytes may account for the performance enhancement since they exhibit better mechanical strength (such as a high module of 65 GPa for LiF) and ionic conductivity than those of the polymeric components in the SEI layer. For example, the addition of FEC into the electrolytes can extend the cycling lifetime of the Li metal anode, resulting from richer LiF in the SEI layer.^{330,331} Besides, increasing the concentration of F-containing salt can also improve the cycling performance of Li metal anodes. Specifically, when increasing the Li bis-(fluorosulfonyl)imide (LiFSI) concentration to 10 M in carbonate electrolytes, the higher F content in the interphases leads to better suppression performance on Li metal dendrite, demonstrated by a high Li plating/stripping Coulombic efficiency of ~99.3%.²⁷ Furthermore, many other methods can be also used to achieve the fluorinated SEI layer for stable Li metal batteries.³³²

Similar to the Li metal layout design for internal stress release (section 4.3.1), a more recent strategy takes advantage of the structural geometry to design the SEI layer so that the overwhelming stress can be facilely released with minimized SEI breaking. For demonstration, a mechanical rolling method was adopted to produce the array pattern on the Li surface, which will induce a zipperlike SEI film formation on the surface (Figure 39a).³³³ Such a unique SEI layout is favorable for uniformly releasing the stress, thus minimizing the broken regions of the SEI film and enhancing the cycling stability of the Li metal anode (Figure 39b–d).

4.3.2.2. Artificial Interface Layer. Even functionalized with electrolyte additives, the naturally formed SEI layer on the Li anode surface is still too vulnerable to withstand large

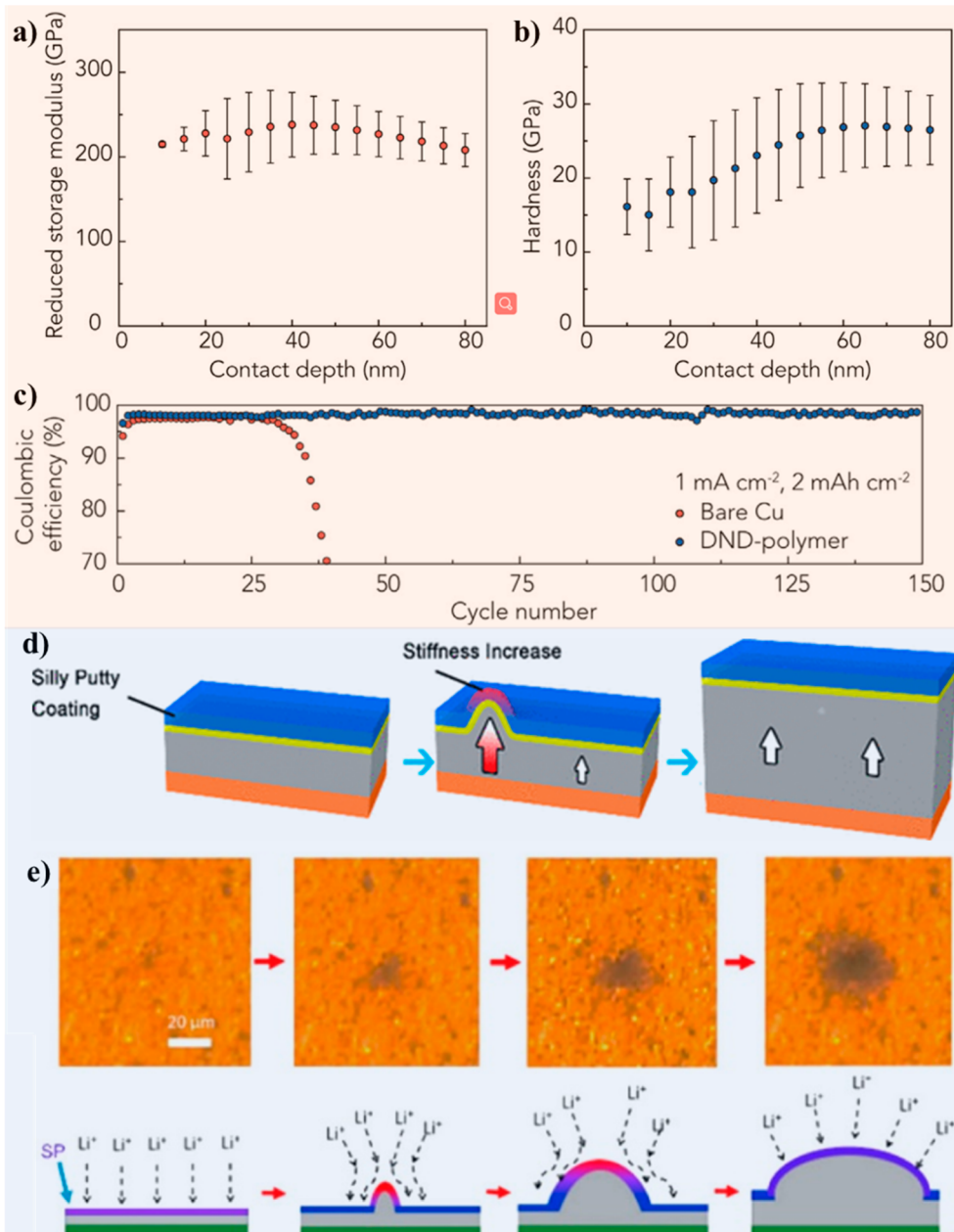


Figure 40. Reinforced interface layer for Li metal anode. (a and b) Reduced storage modulus (A) and hardness (B) of double-layer nanodiamond (DND) via nanoindentation measurements. (c) Long-term cycling CE of bare Cu and DND-polymer electrodes at a current density of 1 mA cm^{-2} and a capacity of 2 mAh cm^{-2} . Reproduced with permission from ref 337. Copyright 2018 Elsevier. (d) Schematic diagram shows the covered dynamically cross-linked polymer (SP) can eliminate SEI cracking and potential catastrophic dendritic growth. (e) Series of optical microscope images depicting the Li metal deposition process on SP-coated Cu. (bottom) Schematic of Li deposited on SP-coated Cu. The red color in the SP coating represents the local dynamic stiffening. Reproduced with permission from ref 334. Copyright 2017 American Chemical Society.

deformation during Li plating/stripping; the cracked and deformed SEI layer will increase the chances of irregular Li growth. In this regard, artificially constructing a stable and robust film on the lithium metal surface (so-called artificial SEI layer) is designed to restrain deformation and protect the Li metal anode from dendritic evolution. So far, void-free and functionalized ceramic nanoparticles (*e.g.*, SiO_2 and Al_2O_3)^{78,334,335}, carbonaceous/two-dimensional nanomembranes (*e.g.*, graphene, BN, and MoS_2)^{154,336–339}, polymeric films^{140,340}, organic–inorganic hybrid layers, and Li-rich salt/alloy films^{124,169,341–343} have been intensively investigated as artificial interphases in tandem via physical and chemical

approaches. All these artificial interphases serve as a physical barrier to restrain dendrite growth and block their further penetration through the separator. It should be also noted here that the artificial interphases may also serve to homogenize and accelerate ion transportation inside (section 4.1.2), particularly the Li-rich salt/alloy films and organic–inorganic hybrid layers.

(1) Inorganic Ceramics Layers

Inorganic ceramics layers are one of the most attractive artificial layers because of their high mechanical strength. As known, high modulus coatings or interphases are effective for suppressing irregular Li growth.¹⁶¹ Following this concept, physical methods, such as atomic layer deposition (ALD)^{78,248}

and sputtering²⁴⁵, have been developed to coat an Al₂O₃, SiO₂, ZnO layer onto the surface of the Li metal anode. For example, Li metal anodes coated with Al₂O₃ thin layers (2–20 nm) via the ALD method or radiofrequency magnetron sputtering present enhanced cycling performance and depressed irregular Li formation.^{78,245,342,344} It is explained that the Al₂O₃ thin film can act as a passivation layer to prevent side reactions between Li metal and electrolytes from the very early stage. Besides, the Al₂O₃ exhibits a low binding energy with Li metal to form a Li–Al–O–se'd based ionic-conducting layer, which greatly negates the metallic Li surface layer interface impedance and heightens the adhesion to the Li metal. More importantly, the as-obtained Al₂O₃ films (20 nm) exhibit a Young's modulus as high as 6.4–14.3 GPa, which is significantly higher than that of Li metal (4.9 GPa); hence, it is sufficient to restrain irregular Li growth.²⁴⁵ Among all materials, diamond has an ultrahigh modulus (>200 GPa) and electrochemical inertness, making it a prime candidate for Li stabilization. Motivated by this idea, an ultrastrong double-layer nanodiamond (DBD) interphase has been successfully developed for Li metal (Figure 40a,b).²⁴⁸ Thanks to its exceptional mechanical strength, the nanodiamond interface results in a dense Li deposition morphology with effective dendrite suppression; additionally, a high Coulombic efficiency of >99.4% is obtained at 1 mA cm⁻² (Figure 40c), and more than 400 stable cycles are realized in prototypical Li–S cells with limited lithium, corresponding to an average anode Coulombic efficiency of >99%.

(2) Polymeric Films

Polymeric films have much better flexibility than inorganic ceramic layers, which makes them ideal candidates for accommodating the volume change and releasing tensile stress. One of the pioneering works show that a soft, viscoelastic polymer coating with extreme softness and intrinsic polymer flow can also be utilized to improve the electrode uniformity.¹⁴⁰ This is different from the cases using high-modulus coatings or interfaces as artificial SEI layers to mechanically suppress irregular Li growth. Benefiting from the highly viscoelastic polymer, a flat and dense lithium metal layer can be obtained at a high current density of 5 mA cm⁻², with a stable cycling Coulombic efficiency of ~97% for more than 180 cycles at the current density of 1 mA cm⁻². Another work demonstrates that a dynamically cross-linked silly putty polymer is potentially an excellent “adaptive” interfacial layer for Li metal anodes (Figure 40d,e).³³⁴ Such a polymer can reversibly switch between its “liquid” and “solid” states in response to the rate of Li growth to provide uniform surface coverage and dendrite suppression, respectively, thereby enabling the stable operation of Li metal electrodes. The dynamic stiffening of silly putty introduces a new concept of the “smart” Li anode for solving the notorious problem of nonuniform deposition of Li metal. Subsequently, polymeric films such as poly((N-2,2-dimethyl-1,3-dioxolane-4-methyl)-5-norbornene-exo-2,3-dicarboximide)³⁴⁵, poly(dimethylsiloxane) (PDMS)³⁴⁰, Polyurea³⁴⁶, and Li poly(acrylic acid) (Li-PAA)³³⁷ are developed in tandem.

It should be noted that the Li metal deposition size and morphology are strongly influenced by the chemical and mechanical properties of soft polymeric coatings: low surface energy of the coating polymer promotes larger deposits with smaller surface areas.³⁴⁷ This may be explained by a reduced interaction between the coating and Li metal surface and thus an increase in the interfacial energy. Furthermore, high dielectric constant polymers are also found to increase the exchange

current and contribute to larger Li deposits due to the decreased overpotentials at a fixed current density.

(3) Carbonaceous Materials and Two-Dimensional Membranes

Carbonaceous materials and two-dimensional membranes with excellent chemical and mechanical stabilities as well as high mechanical strength are also promising artificial interphases to protect the Li metal. For instance, Zheng *et al.* demonstrate that coating the Li metal anode with a monolayer of interconnected amorphous hollow carbon nanospheres is helpful to isolate the Li metal deposits and facilitate the formation of a stable SEI film; the improvements relate to its excellent chemical stability and high Young's modulus of ~200 GPa.¹⁵⁴ With the protection of the carbon nanospheres layer, irregular Li does not form up to a current density of 1 mA cm⁻², and the Li plating/stripping Coulombic efficiency improves to ~99% for more than 150 cycles in the Li//Cu configuration, which is better than that of the bare unmodified samples which show rapid Coulombic efficiency decay in fewer than 100 cycles. It should be noted that the top surface of evaporated carbon is highly insulating due to rich tetrahedral bonding, otherwise Li metal plating would be initiated on the top of the carbon layer, losing the protection of the artificial interphase. In addition, the graphitic regions of carbon would initially be lithiated and form a stable SEI on the top of the carbon nanospheres. Similarly, 2D BN³³⁸ and graphene materials³³⁶ are also proposed as a mechanically strong interface layer onto the Li metal surface, owing to their strong intralayer bonding. The in-plane elastic stiffness of the single atomic layer corresponds to Young's modulus approaching 1.0 TPa for both graphene and h-BN, which is over 2-orders of magnitude higher than that of Li metal (4.9 GPa).³³⁸ Owing to the excellent interfacial protection of 2D layers, smooth Li metal deposition without dendritic and mossy Li formation is realized. Furthermore, under the protection of the artificial SEI, the Li metal anode presents stable cycling for over 50 cycles with a Coulombic efficiency ~97% in organic carbonate electrolyte at the current density and areal capacity up to the practical value of 2.0 mA cm⁻² and 5.0 mAh cm⁻², respectively.

(4) Li-Rich Salt/Alloy Films

Li-rich salt/alloy films typically have much higher ionic conductivity than the above-mentioned ceramic and polymeric interface layers, which makes them closer to the natural SEI layer on the function perspective. Moreover, some inorganic components existed in native SEI (Li₂CO₃, 68 GPa; LiF, 65 GPa; Li₂O, 141 GPa) show higher mechanical strengths than Li metal.³³⁸ Therefore, artificially introducing compact and homogeneous Li-rich salt/alloy layers on the Li metal anode can suppress irregular Li growth. For example, surface fluorination treatment using a fluoropolymer as a solid and nontoxic fluorine source is reported for the formation of the LiF-rich passivation layer on Li metal.¹²⁴ The surface LiF layer enables dendrite-free and stable cycling for over 300 cycles at the current densities up to 5 mA cm⁻². Likewise, the artificial Li₃N-rich layer with outstanding ionic conductivity, excellent interface stability, and high mechanical strength is also constructed on the Li metal anode using surface nitridation treatment.^{169,348} In addition, many other Li salts interfaces are also studied. For instance, the artificial Li₃PO₄ SEI layer can be stable in the electrolyte and during cycling in Li//LiFePO₄ battery systems without a breakage/repair mechanism.³⁴² Owing to the chemical stability in organic electrolytes, high Li⁺ conductivity, high Young's modulus (around 10–11 GPa), and homogeneous composition of the Li₃PO₄ layer, Li dendrite growth is

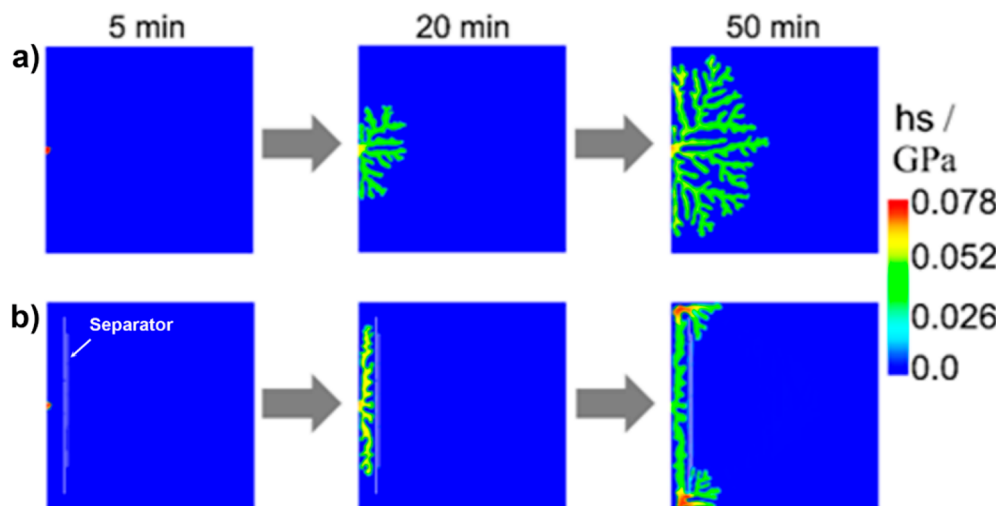


Figure 41. Hydrostatic stress as obtained in the present PFM calculations. (a) Stress development for the case without the barrier layer. (b) Results for the case where spacing within the barrier layer are 15 nm and the sides have spacing bigger than 25 nm. Reproduced with permission from ref 355. Copyright 2018 Wiley-VCH.

suppressed and reduced corrosion of bulk Li is achieved. Similarly, Li salt films (e.g., Li_4SiO_4 ³⁴¹, Li_3PS_4 ³⁴³, and Li_2TiO_3 ³⁴⁹) are also investigated.

Furthermore, *in situ* formation of surface films comprised of Li-based compounds ($\text{Li}_{13}\text{In}_3$, LiZn , Li_3Bi , or Li_3As)/ LiCl is demonstrated as an effective approach to prevent irregular Li formation.³⁴⁸ These composite alloys exhibit much higher Li diffusion coefficients than Li metal, while the resistive nature of the insulating LiCl component in the alloy layer can inhibit reduction of Li ions on the surface. Impressively, the Li-compounds-protected Li is stabilized to sustain electrodeposition over 700 cycles of repeated plating/stripping at a practical current density of 2 mA cm^{-2} , and a 1500 cycle-life is realized for a cell paired with a $\text{Li}_4\text{Ti}_5\text{O}_{12}$ cathode. Later, Archer's group took advantage of an ion-exchange chemistry performed in a carbonate electrolyte to rapidly deposit conformal coatings of Sn onto Na and Li electrodes. Sn–Li and Sn–Na anodes exhibit vastly reduced interfacial impedance and much higher exchange current in liquid electrolytes, attributed to the utilization of a combination of metal electrodeposition and alloying for hybrid charge storage and fast interfacial charge transport. However, the influence of mechanical strength of these Li-based compounds is still unclear, which needs be further studied.

(5) Organic–Inorganic Hybrid Layers

Organic–inorganic hybrid layers are another group of promising artificial films, featured with favorable ionic conductivity and excellent flexibility. In such a hybrid structure, the “hard” inorganic moiety helps to suppress irregular Li and improve the ionic conductivity, while the “soft” organic moiety serves to enhance the toughness. A routine method to introduce organic–inorganic hybrid layers is to let Li metal (either in molten form or in bulk manner) react with organic solutions. For example, Yan *et al.*³⁵⁰ build an ionic-conductive film on a Li metal anode by immersing Li plates into the fluoroethylene carbonate solvent; the film displays a compact dual-layered structure with organic components (ROCO_2Li and ROLi) on the top and abundant inorganic components (Li_2CO_3 and LiF) on the bottom. Liu *et al.*¹²⁰ develop a spray quenching method to *in situ* fabricate an organic–inorganic composite SEI on Li metal, where the SEI film is composed on an organic matrix and

inorganic LiF and Li_3N nanoparticles embedding over it. Wang *et al.*³⁵¹ report another organic/inorganic hybrid SEI layer through codeposition of aromatic-based organosulfides and inorganic Li salts using poly(sulfur-random-1,3-diisopropenylbenzene) as an additive in an electrolyte. In this hybrid structure, the aromatic-based organic components with planar backbone conformation and π – π interaction can facilitate the formation of flat morphology and improve the toughness and flexibility; the inorganic components ($\text{Li}_2\text{S}/\text{Li}_2\text{S}_2$) provide Li-conductive pathways and necessary mechanical hardness. The as-formed durable SEI layer can effectively inhibit dendritic Li growth, enhancing Li deposition/dissolution CE (99.1% over 420 cycles) and Li–S battery cycling stabilities (1000 cycles).

Another approach to construct hybrid layers is to involve chemical or/and physical processes. To illustrate, Liu and co-workers report an interfacial layer consisting of $\text{SiO}_2@\text{PMMA}$ core–shell nanospheres using a combined method of surface polymerization and a slurry casting process.³⁵² Owing to the synergistic effect of SiO_2 and PMMA, this hybrid layer exhibits superior conduction of Li ions, good mechanical and thermal stabilities, and high mechanical flexibility, which are all key for irregular Li suppression and CE improvement. Besides, Cui's group use a doctor blade casting or drop casting method to afford a composite artificial SEI layer, consisting of a polymeric binder matrix and sub-100 nm Cu_3N nanoparticles tightly attached to it; furthermore, the Cu_3N nanoparticles can chemically react with Li metal beneath to form highly Li-ion-conducting Li_3N , which is beneficial for the uniform plating of Li metal.¹²⁰ In addition, Noked *et al.* employ a combined route of self-healing electrochemical polymerization (EP) and atomic layer deposition (ALD) to fabricate the hybrid layer, which contains an organic elastomer layer and an ALD inorganic layer.³⁵³ Under the synergistic impact of the dual-components, this hybrid layer is found feasible to accommodate mechanical and morphological changes associated with Li insertion/deinsertion.

4.3.2.3. Separator Modification. In a manner resembling protective layers over a Li metal anode, the separator plays an essential role in preventing penetration of irregular Li. As known, the penetration of the separator by irregular Li directly leads to an internal short-circuit or even raises safety concerns.

Hence, designing new separators or equipping commercial separators with enhanced mechanical strength is considered another alternative approach to adjust the stress generated on Li metal anodes.

Theoretically, dendrite suppression can be achieved if the shear modulus of the separator is larger than 7 GPa. For instance, a membrane consisting of poly(*p*-phenylene benzobisoxazole) nanofibers demonstrates a strong dendrite-suppression capability, owing to its ultimate strength of 525 MPa and Young's moduli of 20 GPa.³⁵⁴ Besides, a glass fiber separator coated with a graphene oxide nanosheet (GOn) presents ultrahigh mechanical stability (Young's modulus approaching 300 GPa) and superflexibility (bending modulus approaching 1 kT).³⁵⁵ Phase-field modeling demonstrates that a mechanically rigid GOn coating with a proper defect size (smaller than 25 nm) can physically block the anisotropic growth of Li (Figure 41), where high flexibility of the barrier layer used for suppression of irregular Li is beneficial to accommodate the morphological change and the stress induced by irregular Li.

4.3.3. External Applied Pressure Regulation. Apart from regulating stresses created inside the cell, tailoring the external pressure applied on the whole battery also influences the overall performance. In general, applying external pressure higher than the yield strength of bulk polycrystalline Li in a direction perpendicular to the cell stack can prolong the cycle life of Li metal cells;^{356,357} this is realized through confining Li growth and plastically deforming irregular Li to maintain a planar, low surface area morphology.⁴⁷ Dahn *et al.* investigate different anode-free NMC532//Cu pouch cells with constrained pressures between 75 and 2200 kPa.³⁵⁸ They find that increasing the initial average pressure from 75 to 2200 kPa is generally beneficial to the cycling performance and Li plating efficiency of anode-free cells. The pressure-dependent phenomenon is also observed in another anode-free cell using a dual-salt liquid electrolyte system.³⁵⁹ In this study, cells with 1 M LiPF₆ constrained under low pressure (~75 kPa) have a very poor capacity retention of 40% after 15 cycles; in contrast, the capacity retention can be improved to over 60% (after 50 cycles) when tested under a higher pressure of 1200 kPa.

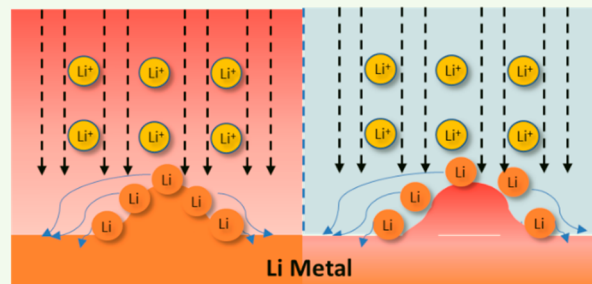
4.4. Temperature Field Regulation

The temperature field has a close relationship with the reaction kinetics of the processes, including the SEI formation and Li plating. Generally, elevating the temperature is feasible to improve Li plating behavior by enabling larger and lower density nuclei at the nucleation stage, a more stable/effective SEI layer, and a more steady/regular growth pattern as we have discussed in section 3.3.^{173,360} Within the safe range, increasing the working temperature of cells or inducing the self-heating of Li metal anode through elevating the plating current density are proven effective in promoting better cycling lifespans and Coulombic efficiency of the Li metal anode, as summarized in Figure 42. Conversely, to protect the Li metal anode at extremely low temperatures, high Li plating kinetics is demanded in the conditions, which would require the electrolyte to exhibit high ionic conductivity and low desolvation energy of Li⁺, and a uniform and robust SEI layer should also be formed on the anode surface.

4.4.1. High Working Temperature. Li plating/stripping behavior is greatly affected by electrolyte viscosity, ion distribution, interfacial state, etc., which are all strongly dependent on temperature. It has been demonstrated that higher temperature leads to lower nucleation density with larger

Temperature Field Regulation

Elevating Working Temperature Self-Heating Induced by High Current Density



Protection at low working temperature

Robust SEI Layer Low Desolvation Energy High Ionic Conductivity

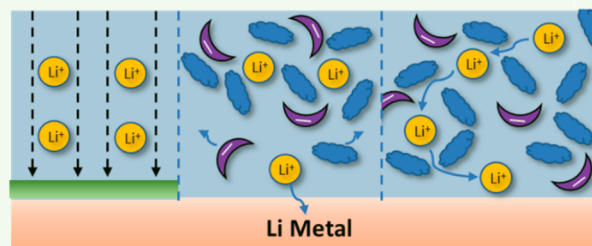


Figure 42. Overview of the available temperature field regulation strategies for stabilizing the Li metal anode.

deposit sizes due to the reduced surface migration barrier and accelerated ion diffusion.^{173,360} Therefore, directly elevating the cell working temperature at safe levels (*i.e.*, below any danger of electrolyte breakdown or thermal damage to the separator) is expected to promote better cycling lifespans and Coulombic efficiency of Li metal anode. For instance, in ether-based electrolytes (1 M LiTFSI in 1:1 vol/vol DOL/DME, with 1 wt % LiNO₃), the Cu//Li half-cell working at a high temperature of 60 °C enables the formation of a robust and stable SEI layer on the Li metal surface, which significantly improves the CE to an average value of 90–99.8% at the rate of 1 mA cm⁻² for 300 cycles.¹⁷⁴ In contrast, the CE rapidly decays to 75.9% after merely 75 cycles when working at 20 °C due to the soluble components of SEI formed in the conditions. Furthermore, the full cell composed of LiFePO₄ cathode and Li metal anode delivers superior rate capability with 131 mAh g⁻¹ capacity remaining at the high rate of 20 C when working at 60 °C in ether-based electrolyte, which is a significant improvement to 61 mAh g⁻¹ when working at 20 °C (Figure 43a,b).¹⁷⁴ This phenomenon has also been successfully implemented to improve the fast-charging ability of LIBs.³⁶¹

4.4.2. Self-Heating Induced by High Current Density.

Aside from directly applying a high working temperature for the cells, the temperature can also be elevated within the Li metal anode through increasing the operation rates (current densities) since it triggers a so-called self-heating effect. The self-heating effect has been used to heal the fatal Li irregular Li as well.¹⁶⁹ For example, Koratkar *et al.* observe the plating pattern absolutely recovered from irregular Li growth under a large current density (15 mA cm⁻²) and partially recovered under a relatively lower current density (9 mA cm⁻²), which are far beyond the prediction of the Sand's time model.¹⁶⁹ Later, they demonstrate

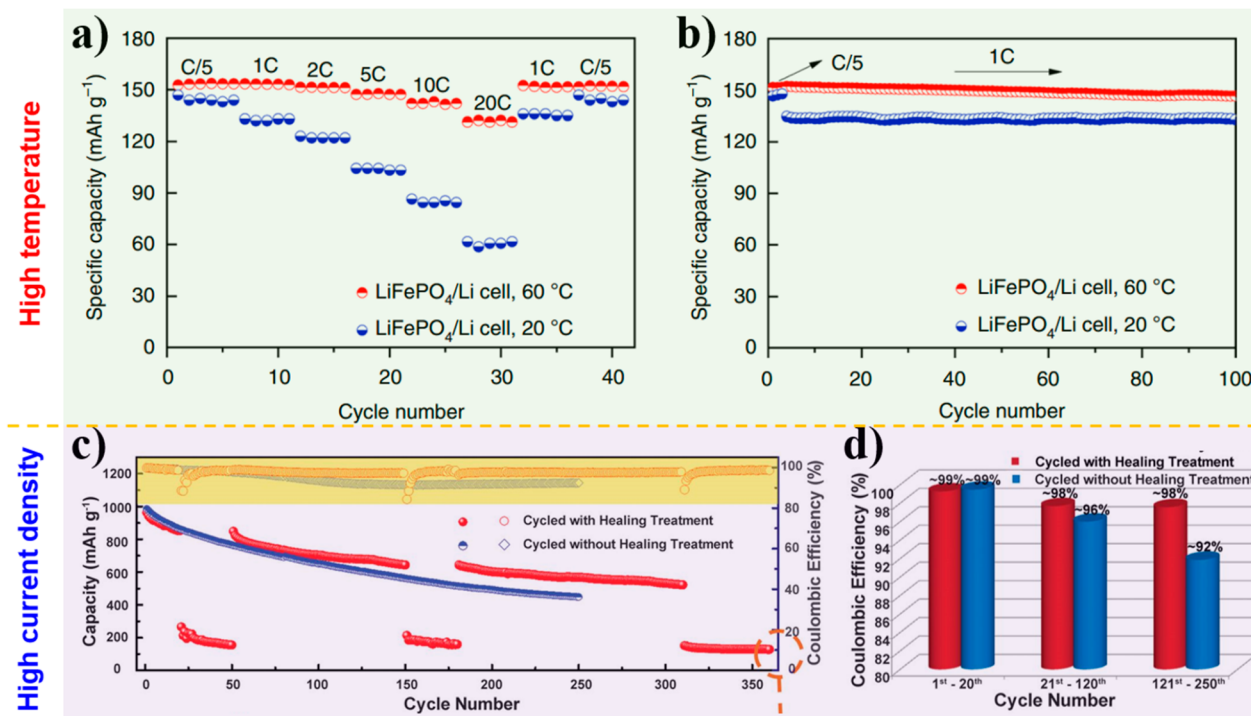


Figure 43. Influence of heating effect on cell performance. (a) Rate capability of LiFePO₄//Li cells cycled at various C-rates at 20 and 60 °C. (b) Long-term cycling of LiFePO₄//Li foil cells cycled at 0.2 C for the first three cycles and 1 C for the following cycles at 20 and 60 °C. Reproduced with permission from ref 174. Copyright 2019 Springer Nature. (c) Cycle stability and CE (highlighted in yellow) of Li–S batteries with and without periodic doses of healing treatment. Blue data points indicate performance of the baseline Li–S cell cycled at $\sim 0.75 \text{ mA cm}^{-2}$ without healing treatment. The red data points are for intermittent healing treatment (at current density of $\sim 9 \text{ mA cm}^{-2}$) applied between the 21st and 50th, 151st and 180th, and 311th and 360th cycles. For the remaining cycles, a current density of $\sim 0.75 \text{ mA cm}^{-2}$ was applied, which is identical to the baseline cell without healing. (d) Comparison of the average CE of the Li–S battery when operated at a current density of $\sim 0.75 \text{ mA cm}^{-2}$ with and without the healing treatment. Reproduced with permission from ref 169. Copyright 2018 AAAS.

that the phenomenon is closely related to the Joule heat (temperature) during cycling. With the cycling rate of 15 mA cm^{-2} , the temperature within cells rise to around 40–60 °C, where components like separator or electrolytes do not degrade and Li metal does not melt; meanwhile, the elevated temperature could dramatically increase the diffusion coefficient of Li⁺ in electrolytes as proven by the MD simulation (Figure 15f). With larger diffusion capability, more Li atoms would transfer from the tip to the valley between adjacent irregular Li particles favored by thermal dynamics (like Ostwald ripening) and then the irregular Li particles are supposed to fuse together to form a dense layer (Figure 15g).¹⁶⁹ Li–S cell performance using ether-based electrolyte (1 M LiTFSI in 1:1 vol/vol DOL/DME with 0.1 M LiNO₃) further demonstrated that periodic operation at high current densities ($\sim 9 \text{ mA cm}^{-2}$) for a limited duration is sufficient to heal the irregular Li, substantially improving the CE (Figure 43c,d), and enhancing the cycling stability relative to the performances of the battery under regular ($\sim 0.75 \text{ mA cm}^{-2}$ current density) operating conditions.¹⁶⁹ Furthermore, LIBs using a typical carbonate electrolyte (1 M LiPF₆ in 1:1 vol/vol EC/DEC) also shows a very long lifespan of 1000 cycles without an obvious capacity decay when tested at a high current density of 10 mA cm^{-2} , superior to that under a low current density.¹⁷⁸

4.4.3. Protection at Low Working Temperature. In practical situations, similar to commercial LIBs, LMBs may also be operated under low temperatures. Therefore, stabilizing the Li metal anode at low working temperatures is also important. In the electrolyte containing LiTFSI in DOL/DME with LiNO₃

additive, the rapid failure of the Li metal anode primarily originates from the thinner, chemically and structurally distinctive, and less resistive SEI in comparison to that formed at room temperature. Hence, the key to the stable/reversible Li metal in such severe conditions is to improve the quality of SEI through optimizing the composition of electrolytes.

McDowell *et al.* reported that the addition of fluoroethylene carbonate into ether-based electrolyte composed of 80 vol % DOL and 20 vol % DME could change the solvation structure of Li⁺, thus modifying the components and structure of the SEI layer at low temperatures.¹⁷⁶ Specifically, ¹⁷O NMR and MD calculations reveal that the cyclic carbonate additive would replace the DOL to enter the primary solvation shell of Li⁺; consequently, the SEI layer would be rich in both crystalline LiCO₃ and LiF instead of only LiF in pure ether containing electrolyte. The coexistence of Li₂CO₃ and LiF is believed to promote space charge accumulation and transport through the SEI, resulting in the large Li nuclei and improved Coulombic efficiency at low temperatures (-40°C and -60°C). Besides, Wang *et al.* tailored the SEI structure through decorating the Cu current collector with an electrochemically active monolayer (EAM) composed of 1,3-benzenedisulfonyl fluoride.³⁶² The EAM could significantly enhance the SEI passivation effect at -15°C by increasing the ratio of crystalline LiF to the LiCO₃ in the inner phase and an additional amorphous outer phase in comparison to that on the bare Cu current collector in the 1 M LiPF₆ in PC/FEC/ethyl 2,2,2-trifluoroethyl carbonate (8:1:1, v:v:v) with 10 wt % tris(pentafluorophenyl) borane, 5 wt % lithium tetrafluoroborate (LiBF₄), and 0.5 wt % lithium nitrate

Table 1. Merits and Limitations of Different Multiphysical Fields Regulation Strategies

multiphysical field regulation	classification	strategies	merits	limitations
reducing local reaction rate	planar conductive substrates with enhanced surface lithophilicity	uniform Li-ion flux around nuclei; even nucleation	massive electrolyte consumption; difficult to maintain the structural stability (3D Li substrates); inactive non-Li substrates decrease the volumetric/gravimetric energy density; vulnerable to be oxidized or etched (non-Li metallic substrates)	limited electrochemical-active sites
uniform and accelerated Li ⁺ diffusion	SEI engineering	uniform/rapid ion transportation within SEI film	narrow range of structure regulation (naturally formed SEI film); processing difficulties (artificial SEI film)	
ionic concentration field regulation	separator modification electrode layout design highly concentrated electrolytes external fields/forces	homogenizing Li-ion flux between Li metal anode and separator homogenizing the Li ⁺ concentration within the whole anode area more sufficient Li-ion source with suppressed concentration polarization, high transference number, strengthened SEI layer, reduced consumption of solvents redistribution of Li ions under the effect of Lorentz force and acoustics force	indirect way on homogenizing Li-ion flux near anode surface sacrifice of energy density; massive electrolyte consumption high cost, low ionic conductivity not applicable for real battery	strict dependence of additive types; poor CE high cost
homogenization of local electric field	electrostatic shielding effect limiting anionic migration (electrolyte tuning) adopting 3D conductive hosts	self-healing of uneven Li plating reduce space-charge effect and delay dendrite formation time	macroscopically surface-dominated distribution of electric field	
electric field regulation	redirection of macroscopic electric field internal stress regulation	homogenize local electric field around Li nuclei via lowering effective current density bottom-up Li plating spatially uniform Li plating side/back Li plating selective Li plating at defective sites LiX alloy anode soft substrates and electrode layout design	high space utilization; superior stability under high cycling capacity uniform Li nucleation/growth within the entire 3D host less damage to separator and less possibility of internal short circuit direct Li plating in designated defective sites minimized/unidirectional volume-strain release the internal tensile stress between plated Li metal	limited electrochemical active sites; poor high-current-density performance difficult to maintain plating pattern irregular Li metal morphology; poor cycling stability processing difficulties; narrow range of design narrow range of choices narrow range of choices
stress field regulation	external stress regulation external applied pressure regulation	SEI reinforcement artificial interface layer separator modification high packaging pressure	strengthen SEI film and minimize SEI breaking mechanical strong to block the penetration of irregular Li protuberance block the piercing of irregular Li protuberance delay irregular Li formation time	limited improvement poor mechanical stability; unable to prevent the dendrite initiation unable to prevent the irregular Li initiation; processing difficulties not applicable for real battery
temperature field regulation	high working temperature high working current density protection under low temperature (electrolyte engineering)	accelerated ion diffusion; lower nucleation density with larger deposit sizes self-healing of dendrites robust SEI, low desolvation energy and high ionic conductivity of electrolyte	high dependence to the electrolyte system; Limited conditions for application limited conditions for application poor Li ion migration kinetics; poor rate performance	

(LiNO_3). Furthermore, the EAM decorated Cu current collector allows for the much larger Li nuclei and extended cycle life of Li/LiCoO_2 full cell of 200 cycles at high capacity (2.0 mAh cm^{-2}) and high charging rate (45 min) conditions under the -15°C temperature.

In addition, the ionic conductivity and desolvation energy of Li^+ in electrolytes are the other critical factors that limit the kinetics of Li plating at low temperatures. In principle, both of them are closely correlated to the Li^+ solvation structure since the Li^+ move in the format of Li-solvent and it has to desolvate all the coordinated solvent before plating. A facile strategy to improve both factors is to utilize solvents that possess a low dielectric constant since the solvents would weakly bind with Li^+ in electrolytes. For instance, Fan *et al.* introduced the nonpolar solvent tetrafluoro-1-(2,2,2-trifluoroethoxy)ethane (D2) into the LiFSI-FEC/FEMC electrolyte, where the Li^+ solvation structure would be partially changed.³⁶³ Specifically, the Li^+ would still coordinate with the polar solvent in the primary shell, but the dipole–dipole interaction between the polar solvent molecules in the secondary shell would be interrupted by the nonpolar solvent D2. As a consequence, the electrolyte exhibits a superiorly high ionic conductivity of $10^{-2} \text{ mS cm}^{-1}$ and high transference number of 0.7 at an extreme temperature of -80°C . Similarly, Chen reported an all-fluorinated ester electrolyte composed of 1 M LiPF_6 in methyl 3,3,3-trifluoropionate (MTPP)/FEC (9:1), which delivered a high ionic conductivity of 0.75 mS cm^{-1} , far exceeding that of 1 M LiPF_6 EC/DEC electrolytes (0.005 mS cm^{-1}).³⁶⁴ The significant improvement could also be ascribed to the weaker binding energy for FEC-Li $^+$ than EC-Li $^+$.

Besides, adding electrochemical-inert diluents into HCEs could reduce the viscosity and improve ionic conductivity of the electrolytes as discussed in section 4.1.3.3. Now with the diluted HCEs, the high performance LMBs can be achieved even at extremely low temperature. For instance, the diluted HCEs-LiTFSI in 1:4 vol/vol EA/DCM is fabricated by adding diluent DCM into originally high concentration LiTFSI/EA mixtures. The derived electrolytes present superiorly high ionic conductivity (0.6 mS cm^{-1}), low viscosity (0.35 Pa s), and a wide electrochemical-stable potential range (0 to 4.85 V) at a low working temperature of -70°C .²⁹⁹

Meanwhile, liquid gaseous electrolytes also present intriguing potential enabling a high-performance Li metal anode at low temperatures.³⁶⁵ Meng *et al.* designed a cell prototype that stabilizes the hydrofluorocarbons (*i.e.*, fluoromethane (FM)) in the liquid state under a large pressure inside.³⁶⁶ The compressed liquid electrolyte exhibits a superiorly low freezing point of -142°C and high ionic conductivity of 1.1 mS cm^{-1} at -60°C . The Li/LiCoO_2 full cell based on the electrolyte merely retains 43.5% of room temperature capacity at -60°C at a rate of C/10. To improve the cycling efficiency of the Li metal, cosolvents, such as tetrahydrofuran (THF)³⁶⁷ and acetonitrile (AN)³⁶⁸ are added into the LiTFSI in FM electrolytes to tailor the solvation structure of Li^+ . MD simulation and Raman spectra results demonstrate that the cosolvents have stronger affinity than the FM solvent. Taking AN cosolvent as an example, the Li^+ solvation structure is not uniform in the concentrated 1.2 M LiTFSI and 1 M AN in the FM electrolyte.³⁶⁸ Part of Li^+ exists in large ionic aggregates, where FM, AN, and TFSI $^-$ are all in the solvation shell, while the other Li^+ are free of TFSI $^-$ in the solvation shell and diffuse in the format of $\text{e Li}^+ (\text{AN})_2(\text{FM})_n$ ($n = 2$ or 3). The free Li^+ are expected to present higher ionic conductivity and lower desolvation energy because of the

smaller size and fewer coordinators in the solvation sheath. Consequently, the electrolyte delivers an impressive ionic conductivity of 5.8 mS cm^{-1} and 4.8 mS cm^{-1} at -60°C and -78°C , respectively; the symmetric cell based on the electrolyte presents an impressive plating/stripping efficiency of 98.5% at low temperature (-60°C) at a current density of 0.5 mA cm^{-2} and 1 mAh cm^{-2} .

5. CONCLUSIONS AND PERSPECTIVES

The Li metal anode represents a key component for the next generation powerful batteries but challenged by the irregular Li growth, unstable SEI formation, huge volume change, along with low CE and poor cycling lifespan. In particular, the irregular Li formation issue remains an intractable conundrum for the commercialization of Li metal anodes. Over decades, a series of sophisticated models and elaborated experiments have been proposed to describe/investigate the evolution behavior of polymorphous Li and ultimately serve to guide the exploration of effective routes to delay/suppress/redirect irregular Li growth. In this review, we have summarized the formation mechanisms of three different types of irregular Li patterns in liquid electrolyte systems and elaborated the corresponding influencing factors from a new and more unitive perspective of multiphysical fields (involving the ionic concentration field, electric field, stress field, and temperature field), aiming to afford fresh and deeper insights to unveil Li metal evolution behavior. Notably, the boundaries between these physical fields overlap and are difficult to clearly differentiate, as they usually interact with each other in determining dynamic morphology and structural evolution of the Li metal anode (Figure 17). The as-proposed solutions for delaying/suppressing/redirecting irregular Li formation based on multiphysical field regulations have their own merits and limitations (Table 1), which need to be comprehensively considered for practical applications. Given the theoretical feasibility and the industrial compatibility of multiphysical field regulation strategies with current LIB fabrication chains, some of them are suggested for the most attention, such as electrolyte engineering, adopting thin surface coating, compositing Li metal with lightweight carbonaceous materials using the molten infusion method or a mechanical process, and employing a LiX alloy anode.

However, due to the harsh environment under industry-demanding levels, the evolution of Li metal is much more complicated and difficult to predict and manage, and there is still a long way to go forward for both fundamental study and future industrial commercialization. Here, we provide our perspectives with respect of Li metal anode in liquid electrolyte for better constructing safe and applicable LMBs.

- (1) The fundamental understanding of Li metal evolution based on practical conditions should be further explored. As mentioned in section 3, theoretical predictions for irregular Li growth are often based on the models with simplified cell parameters. In addition, the as-established theories only consider partial influencing factors but ignore some others that may also exert a significant effect on the Li evolution situation, especially after long-term cycling. For example, no models have been proposed with all multiphysical fields being considered, and the relationship between different influencing physic fields remains to be better connected.
- (2) Regarding the discussion of observed irregular Li deposits, detailed morphology of the Li metal (whisker-

- like, moss-like, tree-like, or mixed ones) shall be identified. Only by defining the morphology of irregular Li deposits, more accurate relationship between Li metal deposition conditions with irregular Li evolution mechanisms and the electrochemical performance of LMBs can be established. In addition, for the simulations of irregular Li evolution, it should also be clarified which type of irregular Li metal is used for the setup of computation models.
- (3) Despite of the most hazardous features for Li dendrites, it should be noted that the condition on Li dendrite formation is relatively harsher than the other two types of irregular Li structures (namely, Li whiskers and Li mosses). Hence, Li dendrites are not commonly observed in recent works and not the key bottleneck on the advancement of Li metal anode anymore. More attention should be moved on to suppress the evolution of whisker-like and moss-like Li deposits in practical applications.
- (4) Advanced nondestructive and operando techniques, such as cryo-electron microscopy, *in situ* TEM, and X-ray tomography, etc.,^{48,124,138,369–371} are highly encouraged to enlighten the dynamic morphological/structural evolution and then to establish the correlation with electrochemical performance. However, there is still a gap between reflected results from currently used operando techniques with real situations in practical cell conditions or the actual property of the Li metal.¹³⁹
- (5) In practical applications, the electrolyte amount in the commercial cell is very limited (<3.0 g Ah⁻¹)³⁷² with the consideration of saving preparation cost and improving the cell's energy density, while the electrolyte dosage in lab experiments is much higher. The limited electrolyte will easily result in the concentration polarization even under mild cycling conditions; thereafter, the interfacial reactions and mass transport will become uncontrollable, making it more possible for irregular Li growth.⁸⁵ Future research should pay more attention to the influence of the electrolyte amount.
- (6) The plating/stripping efficiency of the Li metal anode shall be further enhanced to achieve practical high-energy-density LMBs. Under the conditions of using an 80% excess of the Li metal source (including the Li⁺ ions provided from the cathode) to meet the cycling lifetime goal of over 500 cycles with a capacity retention of 80%, the expected Coulombic efficiency of the Li metal anode shall be larger than 99.8%.³⁷³ Unfortunately, most of reported results are still far behind this target. In addition, the artificial inflation of CE in Li metal batteries is a general phenomenon in all rechargeable metal batteries where an excess of the Li metal source and flood electrolyte are used, which needs to be considered when elaborating testing results. Standard protocols for measuring CEs in different coin cell configurations is urgently needed, in order to unravel the fundamental interrelations of those cells and apply CEs to estimate the range of cycle life for realistic high-energy LMBs.³⁷⁴ The main stumbling block for the improvement of CE lies in the deposition of an incompletely smooth Li metal even if it is not Li whisker, Li moss or Li dendrite, which can trigger the destruction of the SEI layer to some extent and then consume some of the Li source for the restoration of the SEI layer, thus leading to the deduction of CE to below 100%. For example, moss-like Li or the analogues look similar to planar Li metal, whereas its presence will alter the stability of the SEI layer and cause the deviation of CE. In addition, nonuniformity of Li metal evolution at the edge area of the electrode is more severe than that at the central area, due to the relatively higher roughness at the edge. This is because a higher roughness is more likely to induce the stress accumulation and therefore initiate irregular Li metal deposition (the “edge effect”). All of the above facts explain why CE can hardly reach 100%, and even “smooth” Li metal deposits are observed in some works. Therefore, minimizing the surface roughness of the Li metal anode during cycling would potentially maintain a high Li plating/stripping efficiency.
- (7) For research works based on host employment and modification, when evaluating the cycling efficiency of Li metal plating/stripping for the hosts, anode-free full cell systems are suggested. Conventionally, Li metal foil is used as the counter electrode in most publications; in this case, the Li metal source is excessively abundant and the CE are artificially inflated, as any loss of Li inventory (formation of SEI layer and “dead Li”) can be offset from the vast reservoir.³⁷⁵ In contrast, in an anode-free system (e.g., Cu//LFP system), Li metal source is limited since Li metal is directly plated from the cathode, thus making it a more suitable platform for a Coulombic efficiency study. Additionally, without using air and moisture sensitive Li metal, an anode-free battery is advantageous in energy density and cost over the conventional LMBs. Unfortunately, since there is no reservoir of fresh Li to replenish the cell during cycling and the influence of multiphysical fields will be more profound, the cycling performance is normally very poor. In this regard, vast strategies for stabilizing Li metal anodes can be transferred to the anode-free system.
- (8) More efforts should be made to evaluate the stability of as-modified Li metal anode in a full cell system and in the pouch cell configuration rather than the coin cell, which are closer to practical situations. Meanwhile, in these benchmarked full cells, it is better to use Li-free cathodes (such as the S cathode and O₂ cathode) to exclude the influence of an additional Li source extracted from the cathode, as discussed above. If Li-containing cathodes (e.g., LFP and LCO) are adopted, the N/P ratio shall be strictly controlled and need to be as low as possible (typically ≤ 3).³⁷² Whatever type of full cells are used, the ideal cathode capacity needs to be ≥ 3 mAh cm⁻² to meet the industry demand.
- (9) Air-stable, Li-containing metal anodes with long-term cycling stability are highly promising in reducing the preparation cost in real applications. Thus far, several breakthroughs have been made by converting air-sensitive Li metal into air-stable LiX alloy (X = Si, Sn, or Al)^{310,376} or passivating Li metal with air/water-proofing coatings,^{339,369} yet there is still a huge space to further simplify the fabrication process, reduce the materials cost with less inactive additives (e.g., graphene and CNT), and further improve the specific capacity of the as-composited anode.
- Multiphysical fields are fundamental and interrelated influencing factors for Li metal evolution behavior. The persistent multidisciplinary investigation is highly favorable for unveiling the polymorphous Li evolution mechanism and further inspiring feasible regulation strategies for delaying/redirectiong irregular Li formation, consequently

accelerating the practical application of high-energy density LMBs. Additionally, the multiphysical field knowledge and design principles of the modified Li metal anode can also potentially shed fresh light on other metal anodes, such as Na, K, Al, and Zn anodes, as they share similar electrochemical properties with the Li metal anode and are plagued by the irregular electrodeposit issue.^{156,253,377,378} The similarities include (1) high reactivity, particularly for Na and K metals. Similar to the Li metal, Na and K metals can react with most nonaqueous electrolytes, and a stable SIE is required to avoid parasitic side reactions between the electrolyte and the metal anodes. Despite Zn and Al metals being relatively stable in aqueous electrolytes, SEI may also exist when nonaqueous electrolytes are used. Therefore, the influence of SEI shall be considered when discussing their plating/stripping mechanisms. (2) Dramatic volume change. Metal anodes are host-free anodes, and their volume change can be dramatic under a 100% depth of discharge. This implies that the mechanical properties of metals will exert great influence on the polymorphs evolution. (3) Electron and ion-involved working mechanism. All metal anodes need both electronic and ionic suppliers/channels for an electrochemical redox reaction; therefore, the metal plating/stripping behaviors are closely associated with the metal ion concentration field and electric field around the metal anodes. In summary, the accumulation of multiphysical fields knowledge for LMBs could guide the development of other metal anode based batteries.

AUTHOR INFORMATION

Corresponding Authors

Huolin L. Xin – Department of Physics and Astronomy, University of California, Irvine, California 92697, United States;  orcid.org/0000-0002-6521-868X; Email: huolinx@uci.edu

Cheng Yang – Institute of Materials Research, Tsinghua Shenzhen International Graduate School, Tsinghua University, Shenzhen 518055, China;  orcid.org/0000-0003-2618-4787; Email: yang.cheng@sz.tsinghua.edu.cn

Feiyu Kang – Institute of Materials Research, Tsinghua Shenzhen International Graduate School and School of Materials Science and Engineering, Tsinghua University, Shenzhen 518055, China; Email: fykang@sz.tsinghua.edu.cn

Authors

Peichao Zou – Institute of Materials Research, Tsinghua Shenzhen International Graduate School, Tsinghua University, Shenzhen 518055, China; Department of Physics and Astronomy, University of California, Irvine, California 92697, United States;  orcid.org/0000-0003-0148-7482

Yiming Sui – Institute of Materials Research, Tsinghua Shenzhen International Graduate School, Tsinghua University, Shenzhen 518055, China

Houchao Zhan – Institute of Materials Research, Tsinghua Shenzhen International Graduate School, Tsinghua University, Shenzhen 518055, China

Chunyang Wang – Department of Physics and Astronomy, University of California, Irvine, California 92697, United States;  orcid.org/0000-0001-8461-3952

Hui-Ming Cheng – Shenzhen Geim Graphene Center, Tsinghua-Berkeley Shenzhen Institute and Tsinghua Shenzhen International Graduate School, Tsinghua University, Shenzhen 518055, China; Shenyang National Laboratory for

Materials Sciences, Institute of Metal Research, Chinese Academy of Sciences, Shenyang 110016, China;  orcid.org/0000-0002-5387-4241

Complete contact information is available at:
<https://pubs.acs.org/10.1021/acs.chemrev.0c01100>

Author Contributions

#P.Z. and Y.S. contributed equally to this work.

Notes

The authors declare no competing financial interest.

Biographies

Peichao Zou is currently a Postdoctoral Fellow at the University of California, Irvine (UCI) since 2019. He received his Ph.D. in Materials Science and Engineering from Tsinghua University in July 2019. He visited Nanyang Technological University (NTU, Singapore) as a joint cultivated postgraduate student in 2017. His research interests are focusing on field-induced synthesis and growth regulation of metallic micro/nanostructures for metal batteries and electrolytic water splitting applications. He has published over 40 peer-reviewed papers in *Chemical Reviews*, *Nature Communications*, *Energy & Environmental Science*, *Advanced Materials*, and *Advanced Functional Materials*, *Electrochemical Energy Reviews*, etc.

Yiming Sui received his B.Sc. degree in 2017 from Northeastern University, China, an M.Sc. degree in 2019 from the University of Washington, Seattle. Currently he is a Research Assistant at Tsinghua University in Professor Cheng Yang's lab. His research interests focus on developing high-performance electrode materials for secondary batteries like lithium-ion batteries, lithium-metal batteries, sodium-ion batteries, and so forth.

Houchao Zhan received his B.S. degree from Huazhong University of Science and Technology in 2018. He is currently a postgraduate student at Tsinghua Shenzhen International Graduate School under the supervision of Prof. Cheng Yang. His research interests focus on the preparation of nanomaterials and their application for batteries and supercapacitors.

Chunyang Wang is currently a Postdoctoral Fellow at the University of California, Irvine (UCI) since 2019. He received his Ph.D. from Shenyang National Laboratory for Materials Science (SYNL), Institute of Metal Research, Chinese Academy of Sciences (IMR, CAS) in June 2019. His research interests are focusing on the fundamental study of the structure and behavior of battery materials and nanometals/alloys using advanced transmission electron microscopy such as *in situ* TEM and electron tomography. He has published over 20 peer-reviewed papers in *Matter*, *Physical Review Letters*, *Nano Letters*, *Advanced Intelligent Systems*, etc.

Huolin Xin is an associate professor at UC Irvine. He graduated from the Physics Department of Cornell University in 2011 and joined the University of California, Irvine in 2018. Prior to becoming a professor at UCI, he worked at Brookhaven National Laboratory as a scientific staff member and a principal investigator from 2013 to 2018. He is an expert in developing novel materials for batteries, fuel cells, electrolyzers and future quantum technologies. He received the DOE Early Career Award and the UCI Distinguished Early-Career Faculty for Research in 2020, as well as the MRS Outstanding Young Investigator Award, the MSA Burton Medal, the Beall Innovation Award in Physical Science in 2021. Xin holds a strong track record in leading multidisciplinary studies. He's the lead PI in charge of managing a \$2.5-million DOE Vehicle Technology Office project on low-to-no-cobalt lithium-ion batteries. (For the battery industry, using cobalt is the equivalent of

buying blood diamonds.) Xin's published more than 270 peer-reviewed publications, and has co-authored more than 35 publications in *Science* and *Nature* sister journals. He was the Chair of the Microscopy and Microanalysis 2020 meeting, the annual society meeting of the Microscopy Society of America and the Microanalysis Society.

Hui-Ming Cheng is an Academician of Chinese Academy of Sciences, a Professor and Director of Advanced Carbon Research Division of Shenyang National Laboratory for Materials Science, Institute of Metal Research, the Chinese Academy of Sciences, and Professor of the Tsinghua Shenzhen International Graduate School, Tsinghua University. His research activities mainly focus on the synthesis, properties, and applications of carbon-based materials, energy storage materials, photocatalytic semiconducting materials, and high-performance bulk carbon materials. He has published over 350 peer-reviewed papers in *Nature*, *Science*, *Nature Materials*, *Nature Communications*, *Proceedings of the National Academy of Sciences U. S. A.*, *Advanced Materials*, *Journal of the American Chemical Society*, *Angewandte Chemie*, *Advanced Functional Materials*, *Advanced Energy Materials*, *ACS Nano*, etc. He has received several international and national awards, including the National Natural Science Award of China (second class) in 2006, the Charles E. Pettinos Award (American Carbon Society, USA) in 2010, and the Prize for Scientific and Technological Progress of Ho Leung Ho Lee Foundation in 2010. He is the Editor of *Carbon* and the Editor-in-Chief of *Energy Storage Materials*. Prof. Cheng is also the cochairman of the World Conference on Carbon in 2002 (Beijing) and 2011 (Shanghai).

Feiyu Kang is a world renowned scientist in carbon-based materials and energy storage materials, dedicated to the development of natural graphite deep processing technology and high safety rechargeable batteries. He has published more than 500 papers in academic journals and coauthored 6 monographs. He has filed more than 130 Chinese, U.S., and PCT patents. A total of 32 patented technologies have been transferred and applied, with the patent transfer fee and equity reaching over 88 million RMB. He won the second prize of National Technology Invention of China (ranking first), the third prize of National Technology Invention of China (ranking third), the first prize of two provincial and ministerial natural sciences (ranking first), the first prize of provincial and ministerial invention (ranking first), and the mayor's prize of the Shenzhen Science and Technology Award. He presides over the National Basic Research Program of China, two key projects of the National Science Foundation of China, and 863 projects of the Ministry of Science and Technology of China.

Cheng Yang received his Ph.D. in Chemistry from the Hong Kong University of Science and Technology in 2007. Then he worked as a postdoc in the Department of Mechanical Engineering, The Hong Kong University of Science and Technology and was a visiting research faculty in the School of Materials Science and Technology, Georgia Institute of Technology. He has been an Associate Professor at Tsinghua Shenzhen International Graduate School since 2011. His research group mainly focuses on the mechanism and fabrication methodology of hierarchical functional nanostructures under non-equilibrium thermodynamics conditions and their applications in functional devices. He has published over 100 peer-reviewed papers, including *Nature Communications* (2), *Advanced Materials* (3), *Energy & Environmental Science* (6), etc. and filed over 70 Chinese and U.S. patents, among which 6 were successfully transferred and applied in industry. He was awarded the China Invention & Innovation Award (first prize, ranked first), China Industry-University Research Cooperation Innovation Award (second prize, ranked second), Guangdong Science Foundation for Distinguished Young Scholars, Guangdong Distinguished Young Scholar Award, Guangdong Youth Science and Technology Award, and the New Scientist Award of Tsinghua University.

ACKNOWLEDGMENTS

The authors thank the Local Innovative and Research Teams Project of Guangdong Pearl River Talents Program (Grant 2017BT01N111), the Shenzhen Geim Graphene Center, the National Nature Science Foundation of China (Project No. S2061160482), the Guangdong Province Science and Technology Department (Project No. 2020A0505100014), the Shenzhen Government (Project No. JCYJ20170412171720306), and the Tsinghua Shenzhen International Graduate School Overseas Collaboration Project for financial support. Work done at the University of California, Irvine (UCI) is supported by the startup funding of H.L.X.

REFERENCES

- (1) Goodenough, J. B.; Kim, Y. Challenges for Rechargeable Batteries. *J. Power Sources* **2011**, *196*, 6688–6694.
- (2) Liu, C.; Massé, R.; Nan, X.; Cao, G. A Promising Cathode for Li-Ion Batteries: $\text{Li}_3\text{V}_2(\text{PO}_4)_3$. *Energy Stor. Mater.* **2016**, *4*, 15–58.
- (3) Kim, S. W.; Seo, D. H.; Ma, X.; Ceder, G.; Kang, K. Electrode Materials for Rechargeable Sodium-Ion Batteries: Potential Alternatives to Current Lithium-Ion Batteries. *Adv. Energy Mater.* **2012**, *2*, 710–721.
- (4) Tarascon, J. M.; Armand, M. Issues and Challenges Facing Rechargeable Lithium Batteries. *Nature* **2001**, *414*, 359–367.
- (5) Armand, M.; Tarascon, J. M. Building Better Batteries. *Nature* **2008**, *451*, 652–657.
- (6) Scrosati, B. Recent Advances in Lithium Ion Battery Materials. *Electrochim. Acta* **2000**, *45*, 2461–2466.
- (7) Sui, Y.; Liu, C.; Masse, R. C.; Neale, Z. G.; Atif, M.; AlSalhi, M.; Cao, G. Dual-Ion Batteries: The Emerging Alternative Rechargeable Batteries. *Energy Stor. Mater.* **2020**, *25*, 1–32.
- (8) Palacín, M. R. Recent Advances in Rechargeable Battery Materials: A Chemist's Perspective. *Chem. Soc. Rev.* **2009**, *38*, 2565–2575.
- (9) Dunn, B.; Kamath, H.; Tarascon, J.-M. Electrical Energy Storage for the Grid: A Battery of Choices. *Science* **2011**, *334*, 928–935.
- (10) Liu, C.; Neale, Z. G.; Cao, G. Understanding Electrochemical Potentials of Cathode Materials in Rechargeable Batteries. *Mater. Today* **2016**, *19*, 109–123.
- (11) Nitta, N.; Wu, F.; Lee, J. T.; Yushin, G. Li-Ion Battery Materials: Present and Future. *Mater. Today* **2015**, *18*, 252–264.
- (12) Choi, J. W.; Aurbach, D. Promise and Reality of Post-Lithium-Ion Batteries with High Energy Densities. *Nat. Rev. Mater.* **2016**, *1*, 16013.
- (13) Goodenough, J. B. Energy Storage Materials: A Perspective. *Energy Stor. Mater.* **2015**, *1*, 158–161.
- (14) Liang, Y.; Yao, Y. Positioning Organic Electrode Materials in the Battery Landscape. *Joule* **2018**, *2*, 1690–1706.
- (15) Lin, D.; Liu, Y.; Cui, Y. Reviving the Lithium Metal Anode for High-Energy Batteries. *Nat. Nanotechnol.* **2017**, *12*, 194–206.
- (16) Xu, W.; Wang, J.; Ding, F.; Chen, X.; Nasybulin, E.; Zhang, Y.; Zhang, J.-G. Lithium Metal Anodes for Rechargeable Batteries. *Energy Environ. Sci.* **2014**, *7*, 513–537.
- (17) Sand, H. J. S. On the Concentration at the Electrodes in a Solution, with Special Reference to the Liberation of Hydrogen by Electrolysis of a Mixture of Copper Sulphate and Sulphuric Acid. *Philos. Mag.* **1901**, *1*, 45–79.
- (18) Chazalviel, J. N. Electrochemical Aspects of the Generation of Ramified Metallic Electrodeposits. *Phys. Rev. A: At., Mol., Opt. Phys.* **1990**, *42*, 7355–7367.
- (19) Fleury, V.; Chazalviel, J. N.; Rosso, M.; Sapoval, B. The Role of the Anions in the Growth Speed of Fractal Electrodeposits. *J. Electroanal. Chem. Interfacial Electrochem.* **1990**, *290*, 249–255.
- (20) Bai, P.; Guo, J.; Wang, M.; Kushima, A.; Su, L.; Li, J.; Brushett, F. R.; Bazant, M. Z. Interactions between Lithium Growths and Nanoporous Ceramic Separators. *Joule* **2018**, *2*, 2434–2449.
- (21) Wang, X.; Zeng, W.; Hong, L.; Xu, W.; Yang, H.; Wang, F.; Duan, H.; Tang, M.; Jiang, H. Stress-Driven Lithium Dendrite Growth

- Mechanism and Dendrite Mitigation by Electroplating on Soft Substrates. *Nat. Energy* **2018**, *3*, 227–235.
- (22) Xu, R.; Cheng, X. B.; Yan, C.; Zhang, X. Q.; Xiao, Y.; Zhao, C. Z.; Huang, J. Q.; Zhang, Q. Artificial interphases for highly stable lithium metal anode. *Matter* **2019**, *1*, 317–344.
- (23) Zhang, H.; Eshetu, G. G.; Judez, X.; Li, C.; Rodriguez-Martínez, L. M.; Armand, M. Electrolyte Additives for Lithium Metal Anodes and Rechargeable Lithium Metal Batteries: Progress and Perspectives. *Angew. Chem., Int. Ed.* **2018**, *57*, 15002–15027.
- (24) Jin, S.; Jiang, Y.; Ji, H.; Yu, Y. Advanced 3D Current Collectors for Lithium-Based Batteries. *Adv. Mater.* **2018**, *30*, 1802014.
- (25) Guo, Y.; Li, H.; Zhai, T. Reviving Lithium-Metal Anodes for Next-Generation High-Energy Batteries. *Adv. Mater.* **2017**, *29*, 1700007.
- (26) Fang, C.; Wang, X.; Meng, Y. S. Key Issues Hindering a Practical Lithium-Metal Anode. *Trends Chem.* **2019**, *1*, 152–158.
- (27) Cheng, X.-B.; Zhang, R.; Zhao, C.-Z.; Zhang, Q. Toward Safe Lithium Metal Anode in Rechargeable Batteries: A Review. *Chem. Rev.* **2017**, *117*, 10403–10473.
- (28) Bai, P.; Li, J.; Brushett, F. R.; Bazant, M. Z. Transition of Lithium Growth Mechanisms in Liquid Electrolytes. *Energy Environ. Sci.* **2016**, *9*, 3221–3229.
- (29) Li, S.; Jiang, M.; Xie, Y.; Xu, H.; Jia, J.; Li, J. Developing High-Performance Lithium Metal Anode in Liquid Electrolytes: Challenges and Progress. *Adv. Mater.* **2018**, *30*, 1706375.
- (30) Liu, B.; Zhang, J.-G.; Xu, W. Advancing Lithium Metal Batteries. *Joule* **2018**, *2*, 833–845.
- (31) Liu, Y.; Cui, Y. Lithium Metal Anodes: A Recipe for Protection. *Joule* **2017**, *1*, 649–650.
- (32) Zhang, X.; Yang, Y.; Zhou, Z. Towards Practical Lithium-Metal Anodes. *Chem. Soc. Rev.* **2020**, *49*, 3040–3071.
- (33) Liu, D.-H.; Bai, Z.; Li, M.; Yu, A.; Luo, D.; Liu, W.; Yang, L.; Lu, J.; Amine, K.; Chen, Z. Developing High Safety Li-Metal Anodes for Future High-Energy Li-Metal Batteries: Strategies and Perspectives. *Chem. Soc. Rev.* **2020**, *49*, 5407–5445.
- (34) Zheng, J.; Kim, M. S.; Tu, Z.; Choudhury, S.; Tang, T.; Archer, L. A. Regulating Electrodeposition Morphology of Lithium: Towards Commercially Relevant Secondary Li Metal Batteries. *Chem. Soc. Rev.* **2020**, *49*, 2701–2750.
- (35) Takada, K. Progress and Prospective of Solid-State Lithium Batteries. *Acta Mater.* **2013**, *61*, 759–770.
- (36) Liu, S.; Xia, X.; Zhong, Y.; Deng, S.; Yao, Z.; Zhang, L.; Cheng, X.-B.; Wang, X.; Zhang, Q.; Tu, J. 3D TiC/C Core/Shell Nanowire Skeleton for Dendrite-Free and Long-Life Lithium Metal Anode. *Adv. Energy Mater.* **2018**, *8*, 1702322.
- (37) Fan, L.; Wei, S.; Li, S.; Li, Q.; Lu, Y. Recent Progress of the Solid-State Electrolytes for High-Energy Metal-Based Batteries. *Adv. Energy Mater.* **2018**, *8*, 1702657.
- (38) Cheng, X.; Zhao, C.; Yao, Y.; Liu, H.; Zhang, Q. Recent Advances in Energy Chemistry between Solid-State Electrolyte and Safe Lithium-Metal Anodes. *Chem.* **2019**, *5*, 74–96.
- (39) Mauger, A.; Armand, M.; Julien, C. M.; Zaghib, K. Challenges and Issues Facing Lithium Metal for Solid-State Rechargeable Batteries. *J. Power Sources* **2017**, *353*, 333–342.
- (40) Lu, J.; Chen, Z.; Pan, F.; Cui, Y.; Amine, K. High-Performance Anode Materials for Rechargeable Lithium-Ion Batteries. *Electrochim. Energy Rev.* **2018**, *1*, 35–53.
- (41) Trinh, N. D.; Lepage, D.; Ayme-Perrot, D.; Badia, A.; Dolle, M.; Rochefort, D. An Artificial Lithium Protective Layer that Enables the Use of Acetonitrile-Based Electrolytes in Lithium Metal Batteries. *Angew. Chem., Int. Ed.* **2018**, *57*, 5072–5075.
- (42) Peled, E. The Electrochemical Behavior of Alkali and Alkaline Earth Metals in Nonaqueous Battery Systems—The Solid Electrolyte Interphase Model. *J. Electrochem. Soc.* **1979**, *126*, 2047–2051.
- (43) Chou, C.-Y.; Kim, H.; Hwang, G. S. A Comparative First-Principles Study of the Structure, Energetics, and Properties of Li–M ($M = Si, Ge, Sn$) Alloys. *J. Phys. Chem. C* **2011**, *115*, 20018–20026.
- (44) Ferrese, A.; Newman, J. Mechanical Deformation of a Lithium-Metal Anode Due to a Very Stiff Separator. *J. Electrochem. Soc.* **2014**, *161*, A1350–A1359.
- (45) Schultz, R. P. *Lithium: Measurement of Young's Modulus and Yield Strength*; Fermi National Accelerator Laboratory: Batavia, IL, 2002.
- (46) Krauskopf, T.; Richter, F. H.; Zeier, W. G.; Janek, J. Physicochemical Concepts of the Lithium Metal Anode in Solid-State Batteries. *Chem. Rev.* **2020**, *120*, 7745–7794.
- (47) Xu, C.; Ahmad, Z.; Aryanfar, A.; Viswanathan, V.; Greer, J. R. Enhanced Strength and Temperature Dependence of Mechanical Properties of Li at Small Scales and Its Implications for Li Metal Anodes. *Proc. Natl. Acad. Sci. U. S. A.* **2017**, *114*, 57–61.
- (48) Zhang, L.; Yang, T.; Du, C.; Liu, Q.; Tang, Y.; Zhao, J.; Wang, B.; Chen, T.; Sun, Y.; Jia, P.; et al. Lithium Whisker Growth and Stress Generation in an In Situ Atomic Force Microscope–Environmental Transmission Electron Microscope Set-Up. *Nat. Nanotechnol.* **2020**, *15*, 94–98.
- (49) Greer, J. R.; Nix, W. D. Nanoscale Gold Pillars Strengthened through Dislocation Starvation. *Phys. Rev. B: Condens. Matter Mater. Phys.* **2006**, *73*, 245410.
- (50) Greer, J. R.; De Hosson, J. T. M. Plasticity in Small-Sized Metallic Systems: Intrinsic versus Extrinsic Size Effect. *Prog. Mater. Sci.* **2011**, *56*, 654–724.
- (51) Xiang, B.; Wang, L.; Liu, G.; Minor, A. M. Electromechanical Probing of Li/Li₂CO₃ Core/Shell Particles in a TEM. *J. Electrochem. Soc.* **2013**, *160*, A415–A419.
- (52) Masias, A.; Felten, N.; Garcia-Mendez, R.; Wolfenstein, J.; Sakamoto, J. Elastic, Plastic, and Creep Mechanical Properties of Lithium Metal. *J. Mater. Sci.* **2019**, *54*, 2585–2600.
- (53) Bridgman, P. W. The Effect of Tension on the Electrical Resistance of Certain Abnormal Metals. *Proc. Am. Acad. Arts Sci.* **1922**, *57*, 41–66.
- (54) Robertson, W. M.; Montgomery, D. J. Elastic Modulus of Isotopically-Concentrated Lithium. *Phys. Rev.* **1960**, *117*, 440–442.
- (55) Lee, G.; Kim, J.-Y.; Burek, M. J.; Greer, J. R.; Tsui, T. Y. Plastic Deformation of Indium Nanostructures. *Mater. Sci. Eng., A* **2011**, *528*, 6112–6120.
- (56) Barrett, C. S. X-Ray Study of the Alkali Metals at Low Temperatures. *Acta Crystallogr.* **1956**, *9*, 671–677.
- (57) Tang, Y.; Zhang, L.; Chen, J.; Sun, H.; Yang, T.; Liu, Q.; Huang, Q.; Zhu, T.; Huang, J. Electro-Chemo-Mechanics of Lithium in Solid State Lithium Metal Batteries. *Energy Environ. Sci.* **2021**, *14*, 602.
- (58) Gorgas, I.; Herke, P.; Schoeck, G. The Plastic Behaviour of Lithium Single Crystals. *Physica status solidi (a)* **1981**, *67*, 617–623.
- (59) Vuillemin, B.; Philippe, X.; Oltra, R.; Vignal, V.; Coudreuse, L.; Dufour, L.; Finot, E. SVET, AFM and AES Study of Pitting Corrosion Initiated on MnS Inclusions by Microinjection. *Corros. Sci.* **2003**, *45*, 1143–1159.
- (60) Morigaki, K.-i.; Ohta, A. Analysis of the Surface of Lithium in Organic Electrolyte by Atomic Force Microscopy, Fourier Transform Infrared Spectroscopy and Scanning Auger Electron Microscopy. *J. Power Sources* **1998**, *76*, 159–166.
- (61) Gireaud, L.; Grugeon, S.; Laruelle, S.; Yrieix, B.; Tarascon, J. M. Lithium Metal Stripping/Plating Mechanisms Studies: A Metallurgical Approach. *Electrochim. Commun.* **2006**, *8*, 1639–1649.
- (62) Liu, Y.; Liu, Q.; Xin, L.; Liu, Y.; Yang, F.; Stach, E. A.; Xie, J. Making Li-Metal Electrodes Rechargeable by Controlling the Dendrite Growth Direction. *Nat. Energy* **2017**, *2*, 17083.
- (63) Sethian, J. A.; Strain, J. Crystal Growth and Dendritic Solidification. *J. Comput. Phys.* **1992**, *98*, 231–253.
- (64) Li, H.; Li, Y.; Aljarb, A.; Shi, Y.; Li, L.-J. Epitaxial Growth of Two-Dimensional Layered Transition-Metal Dichalcogenides: Growth Mechanism, Controllability, and Scalability. *Chem. Rev.* **2018**, *118*, 6134–6150.
- (65) Cai, Z.; Liu, B.; Zou, X.; Cheng, H.-M. Chemical Vapor Deposition Growth and Applications of Two-Dimensional Materials and Their Heterostructures. *Chem. Rev.* **2018**, *118*, 6091–6133.

- (66) Wang, D.; Zhang, W.; Zheng, W.; Cui, X.; Rojo, T.; Zhang, Q. Towards High-Safe Lithium Metal Anodes: Suppressing Lithium Dendrites via Tuning Surface Energy. *Adv. Sci.* **2017**, *4*, 1600168.
- (67) Hull, C. M.; Switzer, J. A. Electrodeposited Epitaxial Cu (100) on Si (100) and Lift-Off of Single Crystal-Like Cu (100) foils. *ACS Appl. Mater. Interfaces* **2018**, *10*, 38596–38602.
- (68) Hwang, S.; Oh, I.; Kwak, J. Electrodeposition of Epitaxial Cu (111) Thin Films on Au (111) Using Defect-Mediated Growth. *J. Am. Chem. Soc.* **2001**, *123*, 7176–7177.
- (69) Uosaki, K.; Ye, S.; Naohara, H.; Oda, Y.; Haba, T.; Kondo, T. Electrochemical Epitaxial Growth of a Pt (111) Phase on an Au (111) Electrode. *J. Phys. Chem. B* **1997**, *101*, 7566–7572.
- (70) Steiger, J.; Richter, G.; Wenk, M.; Kramer, D.; Mönig, R. Comparison of the Growth of Lithium Filaments and Dendrites under Different Conditions. *Electrochim. Commun.* **2015**, *50*, 11–14.
- (71) Yoshimatsu, I.; Hirai, T.; Yamaki, J. i. Lithium Electrode Morphology during Cycling in Lithium Cells. *J. Electrochim. Soc.* **1988**, *135*, 2422.
- (72) Yurkiv, V.; Foroozan, T.; Ramasubramanian, A.; Shahbazian-Yassar, R.; Mashayek, F. Phase-Fiield Modeling of Solid Electrolyte Interface (SEI) Influence on Li Dendritic Behavior. *Electrochim. Acta* **2018**, *265*, 609–619.
- (73) Kushima, A.; So, K. P.; Su, C.; Bai, P.; Kuriyama, N.; Maebashi, T.; Fujiwara, Y.; Bazant, M. Z.; Li, J. Liquid Cell Transmission Electron Microscopy Observation of Lithium Metal Growth and Dissolution: Root Growth, Dead Lithium and Lithium Flotsams. *Nano Energy* **2017**, *32*, 271–279.
- (74) Chianelli, R. R. Microscopic Studies of Transition Metal Chalcogenides. *J. Cryst. Growth* **1976**, *34*, 239–244.
- (75) Steiger, J.; Kramer, D.; Mönig, R. Mechanisms of Dendritic Growth Investigated by In Situ Light Microscopy during Electrodeposition and Dissolution of Lithium. *J. Power Sources* **2014**, *261*, 112–119.
- (76) Steiger, J.; Kramer, D.; Mönig, R. Microscopic Observations of the Formation, Growth and Shrinkage of Lithium Moss during Electrodeposition and Dissolution. *Electrochim. Acta* **2014**, *136*, 529–536.
- (77) Wood, K. N.; Kazyak, E.; Chadwick, A. F.; Chen, K.-H.; Zhang, J.; Thornton, K.; Dasgupta, N. P. Dendrites and Pits: Untangling the Complex Behavior of Lithium Metal Anodes through Operando Video Microscopy. *ACS Cent. Sci.* **2016**, *2*, 790–801.
- (78) Kazyak, E.; Wood, K. N.; Dasgupta, N. P. Improved Cycle Life and Stability of Lithium Metal Anodes through Ultrathin Atomic Layer Deposition Surface Treatments. *Chem. Mater.* **2015**, *27*, 6457–6462.
- (79) Chang, H. J.; Ilott, A. J.; Trease, N. M.; Mohammadi, M.; Jerschow, A.; Grey, C. P. Correlating Microstructural Lithium Metal Growth with Electrolyte Salt Depletion in Lithium Batteries Using 7Li MRI. *J. Am. Chem. Soc.* **2015**, *137*, 15209–15216.
- (80) Tu, Z.; Choudhury, S.; Zachman, M. J.; Wei, S.; Zhang, K.; Kourkoutis, L. F.; Archer, L. A. Fast Ion Transport at Solid–Solid Interfaces in Hybrid Battery Anodes. *Nat. Energy* **2018**, *3*, 310–316.
- (81) Zou, P.; Wang, Y.; Chiang, S.-W.; Wang, X.; Kang, F.; Yang, C. Directing Lateral Growth of Lithium Dendrites in Micro-Compartimented Anode Arrays for Safe Lithium Metal Batteries. *Nat. Commun.* **2018**, *9*, 464.
- (82) Brandt, K. Historical Development of Secondary Lithium Batteries. *Solid State Ionics* **1994**, *69*, 173–183.
- (83) Whittingham, M. S. Lithium Batteries and Cathode Materials. *Chem. Rev.* **2004**, *104*, 4271–4302.
- (84) Wood, K. N.; Noked, M.; Dasgupta, N. P. Lithium Metal Anodes: Toward an Improved Understanding of Coupled Morphological, Electrochemical, and Mechanical Behavior. *ACS Energy Lett.* **2017**, *2*, 664–672.
- (85) Xiao, J. How Lithium Dendrites form in Liquid Batteries. *Science* **2019**, *366*, 426–427.
- (86) Rosso, M.; Brissot, C.; Teyssot, A.; Dollé, M.; Sannier, L.; Tarascon, J.-M.; Bouchet, R.; Lascaud, S. Dendrite Short-Circuit and Fuse Effect on Li/Polymer/Li Cells. *Electrochim. Acta* **2006**, *51*, 5334–5340.
- (87) Rosso, M.; Gobron, T.; Brissot, C.; Chazalviel, J. N.; Lascaud, S. Onset of Dendritic Growth in Lithium/Polymer Cells. *J. Power Sources* **2001**, *97*, 804–806.
- (88) Brissot, C.; Rosso, M.; Chazalviel, J. N.; Lascaud, S. Dendritic Growth Mechanisms in Lithium/Polymer Cells. *J. Power Sources* **1999**, *81*, 925–929.
- (89) Monroe, C.; Newman, J. Dendrite Growth in Lithium/Polymer Systems: A Propagation Model for Liquid Electrolytes under Galvanostatic Conditions. *J. Electrochim. Soc.* **2003**, *150*, A1377–A1384.
- (90) Tu, Z.; Nath, P.; Lu, Y.; Tikekar, M. D.; Archer, L. A. Nanostructured Electrolytes for Stable Lithium Electrodeposition in Secondary Batteries. *Acc. Chem. Res.* **2015**, *48*, 2947–2956.
- (91) Yang, C.-P.; Yin, Y.-X.; Zhang, S.-F.; Li, N.-W.; Guo, Y.-G. Accommodating Lithium into 3D Current Collectors with a Submicron Skeleton towards Long-Life Lithium Metal Anodes. *Nat. Commun.* **2015**, *6*, 8058.
- (92) Yun, Q.; He, Y.-B.; Lv, W.; Zhao, Y.; Li, B.; Kang, F.; Yang, Q.-H. Chemical Dealloying Derived 3D Porous Current Collector for Li Metal Anodes. *Adv. Mater.* **2016**, *28*, 6932–6939.
- (93) Yamaki, J.-i.; Tobishima, S.-i.; Hayashi, K.; Keiichi Saito; Nemoto, Y.; Arakawa, M. A Consideration of the Morphology of Electrochemically Deposited Lithium in an Organic Electrolyte. *J. Power Sources* **1998**, *74*, 219–227.
- (94) Pei, A.; Zheng, G.; Shi, F.; Li, Y.; Cui, Y. Nanoscale Nucleation and Growth of Electrodeposited Lithium Metal. *Nano Lett.* **2017**, *17*, 1132–1139.
- (95) Plieth, W. *Electrochemistry for Materials Science*; Elsevier: Amsterdam, The Netherlands, 2008.
- (96) Ely, D. R.; García, R. E. Heterogeneous Nucleation and Growth of Lithium Electrodeposits on Negative Electrodes. *J. Electrochim. Soc.* **2013**, *160*, A662–A668.
- (97) Ohring, M. *The Materials Science of Thin Films*; Academic Press: San Diego, CA, 2001.
- (98) Chen, X.; Chen, X.-R.; Hou, T.-Z.; Li, B.-Q.; Cheng, X.-B.; Zhang, R.; Zhang, Q. Lithiophilicity Chemistry of Heteroatom-Doped Carbon to Guide Uniform Lithium Nucleation in Lithium Metal Anodes. *Sci. Adv.* **2019**, *5*, eaau7728.
- (99) Li, N.; Zhang, K.; Xie, K.; Wei, W.; Gao, Y.; Bai, M.; Gao, Y.; Hou, Q.; Shen, C.; Xia, Z.; et al. Reduced-Graphene-Oxide-Guided Directional Growth of Planar Lithium Layers. *Adv. Mater.* **2020**, *32*, 1907079.
- (100) Zheng, J.; Zhao, Q.; Tang, T.; Yin, J.; Quilty, C. D.; Renderos, G. D.; Liu, X.; Deng, Y.; Wang, L.; Bock, D. C.; et al. Reversible Epitaxial Electrodeposition of Metals in Battery Anodes. *Science* **2019**, *366*, 645–648.
- (101) Yan, K.; Lu, Z.; Lee, H.-W.; Xiong, F.; Hsu, P.-C.; Li, Y.; Zhao, J.; Chu, S.; Cui, Y. Selective Deposition and Stable Encapsulation of Lithium through Heterogeneous Seeded Growth. *Nat. Energy* **2016**, *1*, 16010.
- (102) Zhang, R.; Chen, X.-R.; Chen, X.; Cheng, X.-B.; Zhang, X.-Q.; Yan, C.; Zhang, Q. Lithiophilic Sites in Doped Graphene Guide Uniform Lithium Nucleation for Dendrite-Free Lithium Metal Anodes. *Angew. Chem., Int. Ed.* **2017**, *56*, 7764–7768.
- (103) Li, K.; Hu, Z.; Ma, J.; Chen, S.; Mu, D.; Zhang, J. A 3D and Stable Lithium Anode for High-Performance Lithium–Iodine Batteries. *Adv. Mater.* **2019**, *31*, 1902399.
- (104) Okajima, Y.; Shibuta, Y.; Suzuki, T. A Phase-Fiield Model for Electrode Reactions with Butler–Volmer Kinetics. *Comput. Mater. Sci.* **2010**, *50*, 118–124.
- (105) Zhao, F.; Zhou, X.; Deng, W.; Liu, Z. Entrapping Lithium Deposition in Lithiophilic Reservoir Constructed by Vertically Aligned ZnO Nanosheets for Dendrite-Free Li Metal Anodes. *Nano Energy* **2019**, *62*, 55–63.
- (106) Yuan, L.-X.; Wang, Z.-H.; Zhang, W.-X.; Hu, X.-L.; Chen, J.-T.; Huang, Y.-H.; Goodenough, J. B. Development and Challenges of LiFePO₄ Cathode Material for Lithium-Ion Batteries. *Energy Environ. Sci.* **2011**, *4*, 269–284.

- (107) Cui, J.; Yao, S.; Ihsan-Ul-Haq, M.; Wu, J.; Kim, J. K. Correlation between Li Plating Behavior and Surface Characteristics of Carbon Matrix toward Stable Li Metal Anodes. *Adv. Energy Mater.* **2019**, *9*, 1802777.
- (108) Hou, T.-Z.; Chen, X.; Peng, H.-J.; Huang, J.-Q.; Li, B.-Q.; Zhang, Q.; Li, B. Design Principles for Heteroatom-Doped Nano-carbon to Achieve Strong Anchoring of Polysulfides for Lithium–Sulfur Batteries. *Small* **2016**, *12*, 3283–3291.
- (109) Liu, W.; Xia, Y.; Wang, W.; Wang, Y.; Jin, J.; Chen, Y.; Paek, E.; Mitlin, D. Pristine or Highly Defective? Understanding the Role of Graphene Structure for Stable Lithium Metal Plating. *Adv. Energy Mater.* **2019**, *9*, 1802918.
- (110) Shi, F.; Pei, A.; Vailionis, A.; Xie, J.; Liu, B.; Zhao, J.; Gong, Y.; Cui, Y. Strong Texturing of Lithium Metal in Batteries. *Proc. Natl. Acad. Sci. U. S. A.* **2017**, *114*, 12138–12143.
- (111) Huang, Z.; Zhou, G.; Lv, W.; Deng, Y.; Zhang, Y.; Zhang, C.; Kang, F.; Yang, Q.-H. Seeding Lithium Seeds towards Uniform Lithium Deposition for Stable Lithium Metal Anodes. *Nano Energy* **2019**, *61*, 47–53.
- (112) Wang, X.; Pawar, G.; Li, Y.; Ren, X.; Zhang, M.; Lu, B.; Banerjee, A.; Liu, P.; Dufek, E. J.; Zhang, J. G.; et al. Glassy Li Metal Anode for High-Performance Rechargeable Li Batteries. *Nat. Mater.* **2020**, *19*, 1339–1345.
- (113) Peled, E.; Straze, H. The Kinetics of the Magnesium Electrode in Thionyl Chloride Solutions. *J. Electrochem. Soc.* **1977**, *124*, 1030–1035.
- (114) Kanamura, K.; Tamura, H.; Shiraishi, S.; Takehara, Z. i. XPS Analysis of Lithium Surfaces Following Immersion in Various Solvents Containing LiBF₄. *J. Electrochem. Soc.* **1995**, *142*, 340–347.
- (115) Kanamura, K.; Shiraishi, S.; Takehara, Z. i. Electrochemical Deposition of Very Smooth Lithium Using Nonaqueous Electrolytes Containing HF. *J. Electrochem. Soc.* **1996**, *143*, 2187–2197.
- (116) Ein-Eli, Y.; McDevitt, S. F.; Laura, R. The Superiority of Asymmetric Alkyl Methyl Carbonates. *J. Electrochem. Soc.* **1998**, *145*, L1–L3.
- (117) Ein-Eli, Y. A New Perspective on the Formation and Structure of the Solid Electrolyte Interface at the Graphite Anode of Li-Ion Cells. *Electrochem. Solid-State Lett.* **1999**, *2*, 212–214.
- (118) Sun, C.; Liu, J.; Gong, Y.; Wilkinson, D. P.; Zhang, J. Recent Advances in All-Solid-State Rechargeable Lithium Batteries. *Nano Energy* **2017**, *33*, 363–386.
- (119) Fan, X.; Chen, L.; Borodin, O.; Ji, X.; Chen, J.; Hou, S.; Deng, T.; Zheng, J.; Yang, C.; Liou, S. C.; et al. Non-Flammable Electrolyte Enables Li-Metal Batteries with Aggressive Cathode Chemistries. *Nat. Nanotechnol.* **2018**, *13*, 715–722.
- (120) Liu, S.; Xia, X.; Deng, S.; Xie, D.; Yao, Z.; Zhang, L.; Zhang, S.; Wang, X.; Tu, J. In Situ Solid Electrolyte Interphase from Spray Quenching on Molten Li: A New Way to Construct High-Performance Lithium-Metal Anodes. *Adv. Mater.* **2019**, *31*, 1806470.
- (121) Cheng, X.-B.; Zhang, R.; Zhao, C.-Z.; Wei, F.; Zhang, J.-G.; Zhang, Q. A Review of Solid Electrolyte Interphases on Lithium Metal Anode. *Adv. Sci.* **2016**, *3*, 1500213.
- (122) Sacci, R. L.; Black, J. M.; Balke, N.; Dudney, N. J.; More, K. L.; Unocic, R. R. Nanoscale Imaging of Fundamental Li Battery Chemistry: Solid-Electrolyte Interphase Formation and Preferential Growth of Lithium Metal Nanoclusters. *Nano Lett.* **2015**, *15*, 2011–2018.
- (123) Aurbach, D.; Daroux, M. L.; Faguy, P. W.; Yeager, E. Identification of Surface Films Formed on Lithium in Propylene Carbonate Solutions. *J. Electrochem. Soc.* **1987**, *134*, 1611–1620.
- (124) Zhao, J.; Liao, L.; Shi, F.; Lei, T.; Chen, G.; Pei, A.; Sun, J.; Yan, K.; Zhou, G.; Xie, J.; et al. Surface Fluorination of Reactive Battery Anode Materials for Enhanced Stability. *J. Am. Chem. Soc.* **2017**, *139*, 11550–11558.
- (125) Li, Y.; Huang, W.; Li, Y.; Pei, A.; Boyle, D. T.; Cui, Y. Correlating Structure and Function of Battery Interphases at Atomic Resolution Using Cryoelectron Microscopy. *Joule* **2018**, *2*, 2167–2177.
- (126) Han, F.; Westover, A. S.; Yue, J.; Fan, X.; Wang, F.; Chi, M.; Leonard, D. N.; Dudney, N. J.; Wang, H.; Wang, C. High Electronic Conductivity as the Origin of Lithium Dendrite Formation within Solid Electrolytes. *Nat. Energy* **2019**, *4*, 187–196.
- (127) Winter, M. The Solid Electrolyte Interphase—the Most Important and the Least Understood Solid Electrolyte in Rechargeable Li Batteries. *Z. Phys. Chem.* **2009**, *223*, 1395–1406.
- (128) Lu, P.; Harris, S. J. Lithium Transport within the Solid Electrolyte Interphase. *Electrochem. Commun.* **2011**, *13*, 1035–1037.
- (129) Shen, Z.; Zhang, W.; Li, S.; Mao, S.; Wang, X.; Chen, F.; Lu, Y. Tuning the Interfacial Electronic Conductivity by Artificial Electron Tunneling Barriers for Practical Lithium Metal Batteries. *Nano Lett.* **2020**, *20*, 6606–6613.
- (130) Liu, W.; Lin, D.; Pei, A.; Cui, Y. Stabilizing Lithium Metal Anodes by Uniform Li-Ion Flux Distribution in Nanochannel Confinement. *J. Am. Chem. Soc.* **2016**, *138*, 15443–15450.
- (131) Cresce, A. v.; Russell, S. M.; Baker, D. R.; Gaskell, K. J.; Xu, K. In Situ and Quantitative Characterization of Solid Electrolyte Interphases. *Nano Lett.* **2014**, *14*, 1405–1412.
- (132) Shi, S.; Lu, P.; Liu, Z.; Qi, Y.; Hector Jr, L. G.; Li, H.; Harris, S. J. Direct Calculation of Li-Ion Transport in the Solid Electrolyte Interphase. *J. Am. Chem. Soc.* **2012**, *134*, 15476–15487.
- (133) Peled, E.; Golodnitsky, D.; Ardel, G. Advanced Model for Solid Electrolyte Interphase Electrodes in Liquid and Polymer Electrolytes. *J. Electrochem. Soc.* **1997**, *144*, L208–L210.
- (134) Christensen, J.; Newman, J. A Mathematical Model for the Lithium-Ion Negative Electrode Solid Electrolyte Interphase. *J. Electrochem. Soc.* **2004**, *151*, A1977–A1988.
- (135) Leung, K.; Jungjohann, K. L. Spatial Heterogeneities and Onset of Passivation Breakdown at Lithium Anode Interfaces. *J. Phys. Chem. C* **2017**, *121*, 20188–20196.
- (136) Ramasubramanian, A.; Yurkiv, V.; Foroozan, T.; Ragone, M.; Shahbazian-Yassar, R.; Mashayek, F. Lithium Diffusion Mechanism through Solid–Electrolyte Interphase in Rechargeable Lithium Batteries. *J. Phys. Chem. C* **2019**, *123*, 10237–10245.
- (137) Chen, X. R.; Yao, Y. X.; Yan, C.; Zhang, R.; Cheng, X. B.; Zhang, Q. A Diffusion–Reaction Competition Mechanism to Tailor Lithium Deposition for Lithium–Metal Batteries. *Angew. Chem., Int. Ed.* **2020**, *59*, 7743–7747.
- (138) He, Y.; Ren, X.; Xu, Y.; Engelhard, M. H.; Li, X.; Xiao, J.; Liu, J.; Zhang, J.-G.; Xu, W.; Wang, C. Origin of Lithium Whisker Formation and Growth under Stress. *Nat. Nanotechnol.* **2019**, *14*, 1042–1047.
- (139) Lu, Z.; Liang, Q.; Wang, B.; Tao, Y.; Zhao, Y.; Lv, W.; Liu, D.; Zhang, C.; Weng, Z.; Liang, J.; et al. Graphitic Carbon Nitride Induced Micro-Electric Field for Dendrite-Free Lithium Metal Anodes. *Adv. Energy Mater.* **2019**, *9*, 1803186.
- (140) Zheng, G.; Wang, C.; Pei, A.; Lopez, J.; Shi, F.; Chen, Z.; Sendek, A. D.; Lee, H.-W.; Lu, Z.; Schneider, H.; et al. High-Performance Lithium Metal Negative Electrode with a Soft and Flowable Polymer Coating. *ACS Energy Lett.* **2016**, *1*, 1247–1255.
- (141) Li, H.; Yamaguchi, T.; Matsumoto, S.; Hoshikawa, H.; Kumagai, T.; Okamoto, N. L.; Ichitsubo, T. Circumventing Huge Volume Strain in Alloy Anodes of Lithium Batteries. *Nat. Commun.* **2020**, *11*, 1584.
- (142) Abermann, R.; Koch, R. The Internal Stress in Thin Silver, Copper and Gold Films. *Thin Solid Films* **1985**, *129*, 71–78.
- (143) Spaepen, F. Interfaces and Stresses in thin Films. *Acta Mater.* **2000**, *48*, 31–42.
- (144) Chason, E.; Sheldon, B. W.; Freund, L. B.; Floro, J. A.; Hearne, S. J. Origin of Compressive Residual Stress in Polycrystalline Thin Films. *Phys. Rev. Lett.* **2002**, *88*, 156103.
- (145) Franks, J. Growth of Whiskers in the Solid Phase. *Acta Metall.* **1958**, *6*, 103–109.
- (146) Tu, K. N. Irreversible Processes of Spontaneous Whisker Growth in Bimetallic Cu–Sn Thin-Film Reactions. *Phys. Rev. B: Condens. Matter Mater. Phys.* **1994**, *49*, 2030–2034.
- (147) Sobiech, M.; Wohlschlögel, M.; Welzel, U.; Mittemeijer, E. J.; Hügel, W.; Seekamp, A.; Liu, W.; Ice, G. E. Local, Submicron, Strain Gradients as the Cause of Sn Whisker Growth. *Appl. Phys. Lett.* **2009**, *94*, 221901.

- (148) Ju, Z.; Nai, J.; Wang, Y.; Liu, T.; Zheng, J.; Yuan, H.; Sheng, O.; Jin, C.; Zhang, W.; Jin, Z.; et al. Biomacromolecules Enabled Dendrite-Free Lithium Metal Battery and Its Origin Revealed by Cryo-Electron Microscopy. *Nat. Commun.* **2020**, *11*, 488.
- (149) Chason, E.; Jadhav, N.; Pei, F.; Buchovecky, E.; Bower, A. Growth of Whiskers from Sn Surfaces: Driving Forces and Growth Mechanisms. *Prog. Surf. Sci.* **2013**, *88*, 103–131.
- (150) Harry, K. J.; Hallinan, D. T.; Parkinson, D. Y.; MacDowell, A. A.; Balsara, N. P. Detection of Subsurface Structures underneath Dendrites Formed on Cycled Lithium Metal Electrodes. *Nat. Mater.* **2014**, *13*, 69–73.
- (151) Harry, K. J.; Liao, X.; Parkinson, D. Y.; Minor, A. M.; Balsara, N. P. Electrochemical Deposition and Stripping Behavior of Lithium Metal across a Rigid Block Copolymer Electrolyte Membrane. *J. Electrochem. Soc.* **2015**, *162*, A2699–A2706.
- (152) Dollé, M.; Sannier, L.; Beaudoin, B.; Trentin, M.; Tarascon, J.-M. Live Scanning Electron Microscope Observations of Dendritic Growth in Lithium/Polymer Cells. *Electrochim. Solid-State Lett.* **2002**, *5*, A286–A289.
- (153) Jana, A.; Woo, S. I.; Vikrant, K. S. N.; García, R. E. Electrochemomechanics of Lithium Dendrite Growth. *Energy Environ. Sci.* **2019**, *12*, 3595–3607.
- (154) Zheng, G. Y.; Lee, S. W.; Liang, Z.; Lee, H.-W.; Yan, K.; Yao, H. B.; Wang, H. T.; Li, W. Y.; Chu, S.; Cui, Y. Interconnected Hollow Carbon Nanospheres for Stable Lithium Metal Anodes. *Nat. Nanotechnol.* **2014**, *9*, 618–623.
- (155) Tatsuma, T.; Taguchi, M.; Oyama, N. Inhibition Effect of Covalently Cross-Linked Gel Electrolytes on Lithium Dendrite Formation. *Electrochim. Acta* **2001**, *46*, 1201–1205.
- (156) Liu, H.; Cheng, X.-B.; Jin, Z.; Zhang, R.; Wang, G.; Chen, L.-Q.; Liu, Q.-B.; Huang, J.-Q.; Zhang, Q. Recent Advances in Understanding Dendrite Growth on Alkali Metal Anodes. *EnergyChem.* **2019**, *1*, 100003.
- (157) Jana, A.; García, R. E. Lithium Dendrite Growth Mechanisms in Liquid Electrolytes. *Nano Energy* **2017**, *41*, 552–565.
- (158) Ferrese, A.; Albertus, P.; Christensen, J.; Newman, J. Lithium Redistribution in Lithium-Metal Batteries. *J. Electrochem. Soc.* **2012**, *159*, A1615–A1623.
- (159) Ferrese, A.; Newman, J. Modeling Lithium Movement over Multiple Cycles in a Lithium-Metal Battery. *J. Electrochem. Soc.* **2014**, *161*, A948–A954.
- (160) Monroe, C.; Newman, J. The Effect of Interfacial Deformation on Electrodeposition Kinetics. *J. Electrochem. Soc.* **2004**, *151*, A880–A886.
- (161) Monroe, C.; Newman, J. The Impact of Elastic Deformation on Deposition Kinetics at Lithium/Polymer Interfaces. *J. Electrochem. Soc.* **2005**, *152*, A396–A404.
- (162) Wanakule, N. S.; Panday, A.; Mullin, S. A.; Gann, E.; Hexemer, A.; Balsara, N. P. Ionic Conductivity of Block Copolymer Electrolytes in the Vicinity of Order-Disorder and Order-Order Transitions. *Macromolecules* **2009**, *42*, 5642–5651.
- (163) Shen, X.; Zhang, R.; Shi, P.; Chen, X.; Zhang, Q. How Does External Pressure Shape Li Dendrites in Li Metal Batteries? *Adv. Energy Mater.* **2021**, *11*, 2003416.
- (164) Barai, P.; Higa, K.; Srinivasan, V. Lithium Dendrite Growth Mechanisms in Polymer Electrolytes and Prevention Strategies. *Phys. Chem. Chem. Phys.* **2017**, *19*, 20493–20505.
- (165) Shi, F.; Pei, A.; Boyle, D. T.; Xie, J.; Yu, X.; Zhang, X.; Cui, Y. Lithium Metal Stripping beneath the Solid Electrolyte Interphase. *Proc. Natl. Acad. Sci. U. S. A.* **2018**, *115*, 8529–8534.
- (166) Kasemchainian, J.; Zekoll, S.; Spencer Jolly, D.; Ning, Z.; Hartley, G.; Marrow, T.; Bruce, P. Critical Stripping Current Leads to Dendrite Formation on Plating in Lithium Anode Solid Electrolyte Cells. *Nat. Mater.* **2019**, *18*, 1105–1111.
- (167) Wang, M.; Wolfenstine, J. B.; Sakamoto, J. Temperature Dependent Flux Balance of the Li/Li₇Zn₃Zr₂O₁₂ Interface. *Electrochim. Acta* **2019**, *296*, 842–847.
- (168) Zhang, X. Q.; Chen, X.; Xu, R.; Cheng, X. B.; Peng, H. J.; Zhang, R.; Huang, J. Q.; Zhang, Q. Columnar Lithium Metal Anodes. *Angew. Chem., Int. Ed.* **2017**, *56*, 14207–14211.
- (169) Li, L.; Basu, S.; Wang, Y.; Chen, Z.; Hundekar, P.; Wang, B.; Shi, J.; Shi, Y.; Narayanan, S.; Koratkar, N. Self-Heating-Induced Healing of Lithium Dendrites. *Science* **2018**, *359*, 1513–1516.
- (170) Akolkar, R. Modeling Dendrite Growth during Lithium Electrodeposition at Sub-Ambient Temperature. *J. Power Sources* **2014**, *246*, 84–89.
- (171) Gao, X.; Zhou, Y.-N.; Han, D.; Zhou, J.; Zhou, D.; Tang, W.; Goodenough, J. B. Thermodynamic Understanding of Li-Dendrite Formation. *Joule* **2020**, *4*, 1864–1879.
- (172) Aryanfar, A.; Brooks, D. J.; Colussi, A. J.; Merinov, B. V.; Goddard, W. A., 3rd; Hoffmann, M. R. Thermal Relaxation of Lithium Dendrites. *Phys. Chem. Chem. Phys.* **2015**, *17*, 8000–8005.
- (173) Zhu, Y.; Xie, J.; Pei, A.; Liu, B.; Wu, Y.; Lin, D.; Li, J.; Wang, H.; Chen, H.; Xu, J.; et al. Fast Lithium Growth and Short Circuit Induced by Localized-Temperature Hotspots in Lithium Batteries. *Nat. Commun.* **2019**, *10*, 2067.
- (174) Wang, J.; Huang, W.; Pei, A.; Li, Y.; Shi, F.; Yu, X.; Cui, Y. Improving Cyclability of Li Metal Batteries at Elevated Temperatures and its Origin Revealed by Cryo-Electron Microscopy. *Nat. Energy* **2019**, *4*, 664–670.
- (175) Thenuwara, A. C.; Shetty, P. P.; McDowell, M. T. Distinct Nanoscale Interphases and Morphology of Lithium Metal Electrodes Operating at Low Temperatures. *Nano Lett.* **2019**, *19*, 8664–8672.
- (176) Thenuwara, A. C.; Shetty, P. P.; Kondekar, N.; Sandoval, S. E.; Cavallaro, K.; May, R.; Yang, C.-T.; Marbella, L. E.; Qi, Y.; McDowell, M. T. Efficient Low-Temperature Cycling of Lithium Metal Anodes by Tailoring the Solid-Electrolyte Interphase. *ACS Energy Lett.* **2020**, *5*, 2411–2420.
- (177) Adair, K. R.; Banis, M. N.; Zhao, Y.; Bond, T.; Li, R.; Sun, X. Temperature-Dependent Chemical and Physical Microstructure of Li Metal Anodes Revealed through Synchrotron-Based Imaging Techniques. *Adv. Mater.* **2020**, *32*, 2002550.
- (178) Hundekar, P.; Basu, S.; Pan, J.; Bartolucci, S. F.; Narayanan, S.; Yang, Z.; Koratkar, N. Exploiting Self-Heat in a Lithium Metal Battery for Dendrite Healing. *Energy Stor. Mater.* **2019**, *20*, 291–298.
- (179) Lee, Y.; Ma, B.; Bai, P. Concentration Polarization and Metal Dendrite Initiation in Isolated Electrolyte Microchannels. *Energy Environ. Sci.* **2020**, *13*, 3504–3513.
- (180) Jana, A.; Ely, D. R.; García, R. E. Dendrite-Separator Interactions in Lithium-Based Batteries. *J. Power Sources* **2015**, *275*, 912–921.
- (181) Wang, T.; Salvatierra, R. V.; Tour, J. M. Detecting Li Dendrites in a Two-Electrode Battery System. *Adv. Mater.* **2019**, *31*, 1807405.
- (182) Gu, Y.; Wang, W.-W.; He, J.-W.; Tang, S.; Xu, H.-Y.; Yan, J.-W.; Wu, Q.-H.; Lian, X.-B.; Zheng, M.-S.; Dong, Q.-F.; et al. Electrochemical Polishing of Lithium Metal Surface for Highly Demanding Solid-Electrolyte Interphase. *ChemElectroChem* **2019**, *6*, 181–188.
- (183) Gu, Y.; Wang, W.-W.; Li, Y.-J.; Wu, Q.-H.; Tang, S.; Yan, J.-W.; Zheng, M.-S.; Wu, D.-Y.; Fan, C.-H.; Hu, W.-Q.; et al. Designable Ultra-Smooth Ultra-Thin Solid-Electrolyte Interphases of Three Alkali Metal Anodes. *Nat. Commun.* **2018**, *9*, 1339.
- (184) Cheng, X.-B.; Yan, C.; Chen, X.; Guan, C.; Huang, J.-Q.; Peng, H.-J.; Zhang, R.; Yang, S.-T.; Zhang, Q. Implantable Solid Electrolyte Interphase in Lithium-Metal Batteries. *Chem.* **2017**, *2*, 258–270.
- (185) Krystian, M.; Pichl, W. Metallography of Alkali Metal Single Crystals. *Mater. Charact.* **2001**, *46*, 1–9.
- (186) Xiong, S.; Xie, K.; Diao, Y.; Hong, X. Properties of Surface Film on Lithium Anode with LiNO₃ as Lithium Salt in Electrolyte Solution for Lithium–Sulfur Batteries. *Electrochim. Acta* **2012**, *83*, 78–86.
- (187) Basile, A.; Bhatt, A. I.; O’Mullane, A. P. Stabilizing Lithium Metal Using Ionic Liquids for Long-Lived Batteries. *Nat. Commun.* **2016**, *7*, ncomms11794.
- (188) Tang, W.; Yin, X.; Chen, Z.; Fu, W.; Loh, K. P.; Zheng, G. W. Chemically Polished Lithium Metal Anode for High Energy Lithium Metal Batteries. *Energy Stor. Mater.* **2018**, *14*, 289–296.

- (189) Guo, F.; Wu, C.; Chen, H.; Zhong, F.; Ai, X.; Yang, H.; Qian, J. Dendrite-Free Lithium Deposition by Coating a Lithiophilic Heterogeneous Metal Layer on Lithium Metal Anode. *Energy Stor. Mater.* **2020**, *24*, 635–643.
- (190) Peng, Z.; Song, J.; Huai, L.; Jia, H.; Xiao, B.; Zou, L.; Zhu, G.; Martinez, A.; Roy, S.; Murugesan, V.; et al. Enhanced Stability of Li Metal Anodes by Synergetic Control of Nucleation and the Solid Electrolyte Interphase. *Adv. Energy Mater.* **2019**, *9*, 1901764.
- (191) Doyle, K. P.; Lang, C. M.; Kim, K.; Kohl, P. A. Dendrite-Free Electrochemical Deposition of Li–Na Alloys from an Ionic Liquid Electrolyte. *J. Electrochem. Soc.* **2006**, *153*, A1353–A1357.
- (192) Stark, J. K.; Ding, Y.; Kohl, P. A. Dendrite-Free Electrodeposition and Reoxidation of Lithium–Sodium Alloy for Metal-Anode Battery. *J. Electrochem. Soc.* **2011**, *158*, A1100–A1105.
- (193) Qiu, H.; Tang, T.; Asif, M.; Li, W.; Zhang, T.; Hou, Y. Stable Lithium Metal Anode Enabled by Lithium Metal Partial Alloying. *Nano Energy* **2019**, *65*, 103989.
- (194) Peng, Z.; Ren, F.; Yang, S.; Wang, M.; Sun, J.; Wang, D.; Xu, W.; Zhang, J.-G. A Highly Stable Host for Lithium Metal Anode Enabled by $\text{Li}_9\text{Al}_4\text{-Li}_3\text{N}$ -AlN Structure. *Nano Energy* **2019**, *59*, 110–119.
- (195) Yuan, H.; Nai, J.; Tian, H.; Ju, Z.; Zhang, W.; Liu, Y.; Tao, X.; Lou, X. W. An Ultrastable Lithium Metal Anode Enabled by Designed Metal Fluoride Spansules. *Sci. Adv.* **2020**, *6*, eaaz3112.
- (196) Park, J.; Jeong, J.; Lee, Y.; Oh, M.; Ryou, M.-H.; Lee, Y. M. Micro-Patterned Lithium Metal Anodes with Suppressed Dendrite Formation for Post Lithium-Ion Batteries. *Adv. Mater. Interfaces* **2016**, *3*, 1600140.
- (197) Lee, Y.-S.; Lee, J. H.; Choi, J.-A.; Yoon, W. Y.; Kim, D.-W. Cycling Characteristics of Lithium Powder Polymer Batteries Assembled with Composite Gel Polymer Electrolytes and Lithium Powder Anode. *Adv. Funct. Mater.* **2013**, *23*, 1019–1027.
- (198) Seong, I. W.; Hong, C. H.; Kim, B. K.; Yoon, W. Y. The Effects of Current Density and Amount of Discharge on Dendrite Formation in the Lithium Powder Anode Electrode. *J. Power Sources* **2008**, *178*, 769–773.
- (199) Kim, J. S.; Yoon, W. Y.; Yi, K. Y.; Kim, B. K.; Cho, B. W. The Dissolution and Deposition Behavior in Lithium Powder Electrode. *J. Power Sources* **2007**, *165*, 620–624.
- (200) Kong, S.-K.; Kim, B.-K.; Yoon, W.-Y. Electrochemical Behavior of Li-Powder Anode in High Li Capacity Used. *J. Electrochem. Soc.* **2012**, *159*, A1551–A1553.
- (201) Ryou, M.-H.; Lee, Y. M.; Lee, Y.; Winter, M.; Bieker, P. Mechanical Surface Modification of Lithium Metal: Towards Improved Li Metal Anode Performance by Directed Li Plating. *Adv. Funct. Mater.* **2015**, *25*, 834–841.
- (202) Liu, H.; Cheng, X.-B.; Xu, R.; Zhang, X.-Q.; Yan, C.; Huang, J.-Q.; Zhang, Q. Plating/Stripping Behavior of Actual Lithium Metal Anode. *Adv. Energy Mater.* **2019**, *9*, 1902254.
- (203) Chen, Y.; Yue, M.; Liu, C.; Zhang, H.; Yu, Y.; Li, X.; Zhang, H. Long Cycle Life Lithium Metal Batteries Enabled with Upright Lithium Anode. *Adv. Funct. Mater.* **2019**, *29*, 1806752.
- (204) Liang, Z.; Yan, K.; Zhou, G.; Pei, A.; Zhao, J.; Sun, Y.; Xie, J.; Li, Y.; Shi, F.; Liu, Y. Composite Lithium Electrode with Mesoscale Skeleton via Simple Mechanical Deformation. *Sci. Adv.* **2019**, *5*, eaau5655.
- (205) Cheng, X.-B.; Hou, T.-Z.; Zhang, R.; Peng, H.-J.; Zhao, C.-Z.; Huang, J.-Q.; Zhang, Q. Dendrite-Free Lithium Deposition Induced by Uniformly Distributed Lithium Ions for Efficient Lithium Metal Batteries. *Adv. Mater.* **2016**, *28*, 2888–2895.
- (206) Lu, L. L.; Ge, J.; Yang, J. N.; Chen, S. M.; Yao, H. B.; Zhou, F.; Yu, S.-H. Free-Standing Copper Nanowire Network Current Collector for Improving Lithium Anode Performance. *Nano Lett.* **2016**, *16*, 4431–4437.
- (207) Chi, S.-S.; Liu, Y.; Song, W.-L.; Fan, L.-Z.; Zhang, Q. Prestoring Lithium into Stable 3D Nickel Foam Host as Dendrite-Free Lithium Metal Anode. *Adv. Funct. Mater.* **2017**, *27*, 1700348.
- (208) Jin, S.; Sun, Z.; Guo, Y.; Qi, Z.; Guo, C.; Kong, X.; Zhu, Y.; Ji, H. High Areal Capacity and Lithium Utilization in Anodes Made of Covalently Connected Graphite Microtubes. *Adv. Mater.* **2017**, *29*, 1700783.
- (209) Titirici, M.-M.; White, R. J.; Brun, N.; Budarin, V. L.; Su, D. S.; del Monte, F.; Clark, J. H.; MacLachlan, M. J. Sustainable Carbon Materials. *Chem. Soc. Rev.* **2015**, *44*, 250–290.
- (210) Raji, A.-R. O.; Villegas Salvatierra, R.; Kim, N. D.; Fan, X.; Li, Y.; Silva, G. A. L.; Sha, J.; Tour, J. M. Lithium Batteries with Nearly Maximum Metal Storage. *ACS Nano* **2017**, *11*, 6362–6369.
- (211) Wang, J.; Wang, H.; Xie, J.; Yang, A.; Pei, A.; Wu, C.-L.; Shi, F.; Liu, Y.; Lin, D.; Gong, Y.; et al. Fundamental Study on the Wetting Property of Liquid Lithium. *Energy Stor. Mater.* **2018**, *14*, 345–350.
- (212) Zhang, R.; Cheng, X.-B.; Zhao, C.-Z.; Peng, H.-J.; Shi, J.-L.; Huang, J.-Q.; Wang, J.; Wei, F.; Zhang, Q. Conductive Nanostructured Scaffolds Render Low Local Current Density to Inhibit Lithium Dendrite Growth. *Adv. Mater.* **2016**, *28*, 2155–2163.
- (213) Cheng, Y.; Ke, X.; Chen, Y.; Huang, X.; Shi, Z.; Guo, Z. Lithiophobic-Lithiophilic Composite Architecture through Co-Deposition Technology toward High-Performance Lithium Metal Batteries. *Nano Energy* **2019**, *63*, 103854.
- (214) Jin, C.; Sheng, O.; Lu, Y.; Luo, J.; Yuan, H.; Zhang, W.; Huang, H.; Gan, Y.; Xia, Y.; Liang, C.; et al. Metal Oxide Nanoparticles Induced Step-Edge Nucleation of Stable Li Metal Anode Working under an Ultrahigh Current Density of 15 mA cm^{-2} . *Nano Energy* **2018**, *45*, 203–209.
- (215) Zhang, Y.; Luo, W.; Wang, C.; Li, Y.; Chen, C.; Song, J.; Dai, J.; Hitz, E. M.; Xu, S.; Yang, C.; et al. High-Capacity, Low-Tortuosity, and Channel-Guided Lithium Metal Anode. *Proc. Natl. Acad. Sci. U. S. A.* **2017**, *114*, 3584–3589.
- (216) Hafez, A. M.; Jiao, Y.; Shi, J.; Ma, Y.; Cao, D.; Liu, Y.; Zhu, H. Stable Metal Anode Enabled by Porous Lithium Foam with Superior Ion Accessibility. *Adv. Mater.* **2018**, *30*, 1802156.
- (217) Jin, C.; Sheng, O.; Luo, J.; Yuan, H.; Fang, C.; Zhang, W.; Huang, H.; Gan, Y.; Xia, Y.; Liang, C.; et al. 3D Lithium Metal Embedded within Lithiophilic Porous Matrix for Stable Lithium Metal Batteries. *Nano Energy* **2017**, *37*, 177–186.
- (218) Chen, K.-H.; Sanchez, A. J.; Kazyak, E.; Davis, A. L.; Dasgupta, N. P. Synergistic Effect of 3D Current Collectors and ALD Surface Modification for High Coulombic Efficiency Lithium Metal Anodes. *Adv. Energy Mater.* **2019**, *9*, 1802534.
- (219) Yang, C.; Yao, Y.; He, S.; Xie, H.; Hitz, E.; Hu, L. Ultrafine Silver Nanoparticles for Seeded Lithium Deposition toward Stable Lithium Metal Anode. *Adv. Mater.* **2017**, *29*, 1702714.
- (220) Singh, A.; Lutz, L.; Ong, G. K.; Bustillo, K.; Raoux, S.; Jordan-Sweet, J. L.; Milliron, D. J. Controlling Morphology in Polycrystalline Films by Nucleation and Growth from Metastable Nanocrystals. *Nano Lett.* **2018**, *18*, 5530–5537.
- (221) Huang, S.; Zhang, W.; Ming, H.; Cao, G.; Fan, L.-Z.; Zhang, H. Chemical Energy Release Driven Lithiophilic Layer on 1 m² Commercial Brass Mesh toward Highly Stable Lithium Metal Batteries. *Nano Lett.* **2019**, *19*, 1832–1837.
- (222) Ye, H.; Xin, S.; Yin, Y.-X.; Li, J.-Y.; Guo, Y.-G.; Wan, L.-J. Stable Li Plating/Stripping Electrochemistry Realized by a Hybrid Li Reservoir in Spherical Carbon Granules with 3D Conducting Skeletons. *J. Am. Chem. Soc.* **2017**, *139*, 5916–5922.
- (223) Lin, D.; Liu, Y.; Liang, Z.; Lee, H.-W.; Sun, J.; Wang, H.; Yan, K.; Xie, J.; Cui, Y. Layered Reduced Graphene Oxide with Nanoscale Interlayer Gaps as a Stable Host for Lithium Metal Anodes. *Nat. Nanotechnol.* **2016**, *11*, 626–632.
- (224) Luo, L.; Wu, J.; Luo, J.; Huang, J.; Dravid, V. P. Dynamics of Electrochemical Lithiation/Delithiation of Graphene-Encapsulated Silicon Nanoparticles Studied by In-situ TEM. *Sci. Rep.* **2014**, *4*, 3863.
- (225) Mukherjee, R.; Thomas, A. V.; Datta, D.; Singh, E.; Li, J.; Eksik, O.; Shenoy, V. B.; Koratkar, N. Defect-Induced Plating of lithium Metal within Porous Graphene Networks. *Nat. Commun.* **2014**, *5*, 3710.
- (226) Yuan, W.; Zhou, Y.; Li, Y.; Li, C.; Peng, H.; Zhang, J.; Liu, Z.; Dai, L.; Shi, G. The Edge- and Basal-Plane-Specific Electrochemistry of a Single-Layer Graphene Sheet. *Sci. Rep.* **2013**, *3*, 2248.
- (227) Meng, Q.; Deng, B.; Zhang, H.; Wang, B.; Zhang, W.; Wen, Y.; Ming, H.; Zhu, X.; Guan, Y.; Xiang, Y.; et al. Heterogeneous Nucleation

- and Growth of Electrodeposited Lithium Metal on the Basal Plane of Single-Layer Graphene. *Energy Stor. Mater.* **2019**, *16*, 419–425.
- (228) Song, Q.; Yan, H.; Liu, K.; Xie, K.; Li, W.; Gai, W.; Chen, G.; Li, H.; Shen, C.; Fu, Q.; et al. Vertically Grown Edge-Rich Graphene Nanosheets for Spatial Control of Li Nucleation. *Adv. Energy Mater.* **2018**, *8*, 1800564.
- (229) Zhai, P.; Wang, T.; Yang, W.; Cui, S.; Zhang, P.; Nie, A.; Zhang, Q.; Gong, Y. Uniform Lithium Deposition Assisted by Single-Atom Doping toward High-Performance Lithium Metal Anodes. *Adv. Energy Mater.* **2019**, *9*, 1804019.
- (230) Liu, Y.; Qin, X.; Zhang, S.; Huang, Y.; Kang, F.; Chen, G.; Li, B. Oxygen and Nitrogen Co-Doped Porous Carbon Granules Enabling Dendrite-Free Lithium Metal Anode. *Energy Stor. Mater.* **2019**, *18*, 320–327.
- (231) Liu, L.; Yin, Y.-X.; Li, J.-Y.; Wang, S.-H.; Guo, Y.-G.; Wan, L.-J. Uniform Lithium Nucleation/Growth Induced by Lightweight Nitrogen-Doped Graphitic Carbon Foams for High-Performance Lithium Metal Anodes. *Adv. Mater.* **2018**, *30*, 1706216.
- (232) Liu, H.; Chen, X.; Cheng, X.-B.; Li, B.-Q.; Zhang, R.; Wang, B.; Chen, X.; Zhang, Q. Uniform Lithium Nucleation Guided by Atomically Dispersed Lithiophilic CoNx Sites for Safe Lithium Metal Batteries. *Small Methods* **2019**, *3*, 1800354.
- (233) Xu, J.; Mahmood, J.; Dou, Y.; Dou, S.; Li, F.; Dai, L.; Baek, J.-B. 2D Frameworks of C₂N and C₃N as New Anode Materials for Lithium-Ion Batteries. *Adv. Mater.* **2017**, *29*, 1702007.
- (234) Noked, M.; Soffer, A.; Aurbach, D. The Electrochemistry of Activated Carbonaceous Materials: Past, Present, and Future. *J. Solid State Electrochem.* **2011**, *15*, 1563.
- (235) Verma, P.; Maire, P.; Novák, P. A Review of the Features and Analyses of the Solid Electrolyte Interphase in Li-Ion Batteries. *Electrochim. Acta* **2010**, *55*, 6332–6341.
- (236) Peled, E.; Menkin, S. Review—SEI: Past, Present and Future. *J. Electrochem. Soc.* **2017**, *164*, A1703–A1719.
- (237) Pu, J.; Li, J.; Shen, Z.; Zhong, C.; Liu, J.; Ma, H.; Zhu, J.; Zhang, H.; Braun, P. V. Interlayer Lithium Plating in Au Nanoparticles Pillared Reduced Graphene Oxide for Lithium Metal Anodes. *Adv. Funct. Mater.* **2018**, *28*, 1804133.
- (238) Li, J.; Zou, P.; Chiang, S. W.; Yao, W.; Wang, Y.; Liu, P.; Liang, C.; Kang, F.; Yang, C. A Conductive-Dielectric Gradient Framework for Stable Lithium Metal Anode. *Energy Stor. Mater.* **2020**, *24*, 700–706.
- (239) Li, Q.; Zhu, S. P.; Lu, Y. Y. 3D Porous Cu Current Collector/Li-Metal Composite Anode for Stable Lithium-Metal Batteries. *Adv. Funct. Mater.* **2017**, *27*, 1606422.
- (240) Liang, Z.; Lin, D.; Zhao, J.; Lu, Z.; Liu, Y.; Liu, C.; Lu, Y.; Wang, H.; Yan, K.; Tao, X.; et al. Composite Lithium Metal Anode by Melt Infusion of Lithium into a 3D Conducting Scaffold with Lithiophilic Coating. *Proc. Natl. Acad. Sci. U. S. A.* **2016**, *113*, 2862–2867.
- (241) Zhang, H.; Liao, X.; Guan, Y.; Xiang, Y.; Li, M.; Zhang, W.; Zhu, X.; Ming, H.; Lu, L.; Qiu, J.; et al. Lithiophilic-Lithiophobic Gradient Interfacial Layer for a Highly Stable Lithium Metal Anode. *Nat. Commun.* **2018**, *9*, 3729.
- (242) Zhang, R.; Chen, X.; Shen, X.; Zhang, X.-Q.; Chen, X.-R.; Cheng, X.-B.; Yan, C.; Zhao, C.-Z.; Zhang, Q. Coralloid Carbon Fiber-Based Composite Lithium Anode for Robust Lithium Metal Batteries. *Joule* **2018**, *2*, 764–777.
- (243) Wang, L.; Zhu, X.; Guan, Y.; Zhang, J.; Ai, F.; Zhang, W.; Xiang, Y.; Vijayan, S.; Li, G.; Huang, Y.; et al. ZnO/Carbon Framework Derived from Metal-Organic Frameworks as a Stable Host for Lithium Metal Anodes. *Energy Stor. Mater.* **2018**, *11*, 191–196.
- (244) Fan, L.; Li, S.; Liu, L.; Zhang, W.; Gao, L.; Fu, Y.; Chen, F.; Li, J.; Zhuang, H. L.; Lu, Y. Enabling Stable Lithium Metal Anode via 3D Inorganic Skeleton with Superlithiophilic Interphase. *Adv. Energy Mater.* **2018**, *8*, 1802350.
- (245) Wang, L.; Zhang, L.; Wang, Q.; Li, W.; Wu, B.; Jia, W.; Wang, Y.; Li, J.; Li, H. Long Lifespan Lithium Metal Anodes Enabled by Al₂O₃ Sputter Coating. *Energy Stor. Mater.* **2018**, *10*, 16–23.
- (246) Niu, C.; Pan, H.; Xu, W.; Xiao, J.; Zhang, J.-G.; Luo, L.; Wang, C.; Mei, D.; Meng, J.; Wang, X.; et al. Self-Smoothing Anode for Achieving High-Energy Lithium Metal Batteries under Realistic Conditions. *Nat. Nanotechnol.* **2019**, *14*, 594–601.
- (247) Tantratian, K.; Cao, D.; Abdelaziz, A.; Sun, X.; Sheng, J.; Natan, A.; Chen, L.; Zhu, H. Stable Li Metal Anode Enabled by Space Confinement and Uniform Curvature through Lithiophilic Nanotube Arrays. *Adv. Energy Mater.* **2020**, *10*, 1902819.
- (248) Zhao, Y.; Zheng, K.; Sun, X. Addressing Interfacial Issues in Liquid-Based and Solid-State Batteries by Atomic and Molecular Layer Deposition. *Joule* **2018**, *2*, 2583–2604.
- (249) Alpen, U. V. Li3N: A promising Li ionic conductor. *J. Solid State Chem.* **1979**, *29*, 379–392.
- (250) Wu, M.; Wen, Z.; Liu, Y.; Wang, X.; Huang, L. Electrochemical Behaviors of a Li₃N Modified Li Metal Electrode in Secondary Lithium Batteries. *J. Power Sources* **2011**, *196*, 8091–8097.
- (251) Ma, G.; Wen, Z.; Wu, M.; Shen, C.; Wang, Q.; Jin, J.; Wu, X. A Lithium Anode Protection Guided Highly-Stable Lithium–Sulfur Battery. *Chem. Commun.* **2014**, *50*, 14209–14212.
- (252) Zhou, Y.; Zhang, X.; Ding, Y.; Bae, J.; Guo, X.; Zhao, Y.; Yu, G. Redistributing Li-Ion Flux by Parallelly Aligned Holey Nanosheets for Dendrite-Free Li Metal Anodes. *Adv. Mater.* **2020**, *32* (38), 2003920.
- (253) Wei, S.; Choudhury, S.; Tu, Z.; Zhang, K.; Archer, L. A. Electrochemical Interphases for High-Energy Storage Using Reactive Metal Anodes. *Acc. Chem. Res.* **2018**, *51*, 80–88.
- (254) Xiang, J.; Cheng, Z.; Zhao, Y.; Zhang, B.; Yuan, L.; Shen, Y.; Guo, Z.; Zhang, Y.; Jiang, J.; Huang, Y. A Lithium-Ion Pump Based on Piezoelectric Effect for Improved Rechargeability of Lithium Metal Anode. *Adv. Sci.* **2019**, *6*, 1901120.
- (255) Ramadoss, A.; Saravananakumar, B.; Lee, S. W.; Kim, Y.-S.; Kim, S. J.; Wang, Z. L. Piezoelectric-Driven Self-Charging Supercapacitor Power Cell. *ACS Nano* **2015**, *9*, 4337–4345.
- (256) Song, R.; Jin, H.; Li, X.; Fei, L.; Zhao, Y.; Huang, H.; Lai-Wa Chan, H.; Wang, Y.; Chai, Y. A Rectification-Free Piezo-Supercapacitor with a Polyvinylidene Fluoride Separator and Functionalized Carbon Cloth Electrodes. *J. Mater. Chem. A* **2015**, *3*, 14963–14970.
- (257) Xue, X.; Deng, P.; Yuan, S.; Nie, Y.; He, B.; Xing, L.; Zhang, Y. CuO/PVDF Nanocomposite Anode for a Piezo-Driven Self-Charging Lithium battery. *Energy Environ. Sci.* **2013**, *6*, 2615–2620.
- (258) Xing, L.; Nie, Y.; Xue, X.; Zhang, Y. PVDF Mesoporous Nanostructures as the Piezo-Separator for a Self-Charging Power Cell. *Nano Energy* **2014**, *10*, 44–52.
- (259) Xue, X.; Wang, S.; Guo, W.; Zhang, Y.; Wang, Z. L. Hybridizing Energy Conversion and Storage in a Mechanical-to-Electrochemical Process for Self-Charging Power Cell. *Nano Lett.* **2012**, *12*, 5048–5054.
- (260) Ryou, M.-H.; Lee, D. J.; Lee, J.-N.; Lee, Y. M.; Park, J.-K.; Choi, J. W. Excellent Cycle Life of Lithium-Metal Anodes in Lithium-Ion Batteries with Mussel-Inspired Polydopamine-Coated Separators. *Adv. Energy Mater.* **2012**, *2*, 645–650.
- (261) Liu, W.; Mi, Y.; Weng, Z.; Zhong, Y.; Wu, Z.; Wang, H. Functional Metal-Organic Framework Boosting Lithium Metal Anode Performance via Chemical Interactions. *Chem. Sci.* **2017**, *8*, 4285–4291.
- (262) Nie, L.; Li, Y.; Chen, S.; Li, K.; Huang, Y.; Zhu, Y.; Sun, Z.; Zhang, J.; He, Y.; Cui, M.; et al. Biofilm Nanofiber-Coated Separators for Dendrite-Free Lithium Metal Anode and Ultrahigh-Rate Lithium Batteries. *ACS Appl. Mater. Interfaces* **2019**, *11*, 32373–32380.
- (263) Tu, Z.; Kambe, Y.; Lu, Y.; Archer, L. A. Nanoporous Polymer-Ceramic Composite Electrolytes for Lithium Metal Batteries. *Adv. Energy Mater.* **2014**, *4*, 1300654.
- (264) Shang, H.; Zuo, Z.; Dong, X.; Wang, F.; Lu, F.; Zheng, H.; Li, K.; Li, Y. Efficiently Suppressing Lithium Dendrites on Atomic Level by Ultrafiltration Membrane of Graphdiyne. *Mater. Today Energy* **2018**, *10*, 191–199.
- (265) Zhi, J.; Li, S.; Han, M.; Chen, P. Biomolecule-Guided Cation Regulation for Dendrite-Free Metal Anodes. *Sci. Adv.* **2020**, *6*, eabb1342.
- (266) Chen, H.; Pei, A.; Wan, J.; Lin, D.; Vilá, R.; Wang, H.; Mackanic, D.; Steinrück, H.-G.; Huang, W.; Li, Y.; et al. Tortuosity Effects in Lithium-Metal Host Anodes. *Joule* **2020**, *4*, 938–952.

- (267) Fan, L.; Zhuang, H. L.; Zhang, W.; Fu, Y.; Liao, Z.; Lu, Y. Stable Lithium Electrodeposition at Ultra-High Current Densities Enabled by 3D PMF/Li Composite Anode. *Adv. Energy Mater.* **2018**, *8*, 1703360.
- (268) Matsuda, S.; Kubo, Y.; Uosaki, K.; Nakanishi, S. Insulative Microfiber 3D Matrix as a Host Material Minimizing Volume Change of the Anode of Li Metal Batteries. *ACS Energy Lett.* **2017**, *2*, 924–929.
- (269) Liang, Z.; Zheng, G.; Liu, C.; Liu, N.; Li, W.; Yan, K.; Yao, H.; Hsu, P.-C.; Chu, S.; Cui, Y. Polymer Nanofiber-Guided Uniform Lithium Deposition for Battery Electrodes. *Nano Lett.* **2015**, *15*, 2910–2916.
- (270) Suo, L.; Xue, W.; Gobet, M.; Greenbaum, S. G.; Wang, C.; Chen, Y.; Yang, W.; Li, Y.; Li, J. Fluorine-Donating Electrolytes Enable Highly Reversible 5-V-Class Li Metal Batteries. *Proc. Natl. Acad. Sci. U. S. A.* **2018**, *115*, 1156–1161.
- (271) Stone, H. A.; Stroock, A. D.; Ajdari, A. Engineering Flows in Small Devices: Microfluidics Toward a Lab-on-a-Chip. *Annu. Rev. Fluid Mech.* **2004**, *36*, 381–411.
- (272) Dydek, E. V.; Bazant, M. Z. Nonlinear Dynamics of Ion Concentration Polarization in Porous Media: The Leaky Membrane Model. *AICHE J.* **2013**, *59*, 3539–3555.
- (273) Dydek, E. V.; Zaltzman, B.; Rubinstein, I.; Deng, D. S.; Mani, A.; Bazant, M. Z. Overlimiting Current in a Microchannel. *Phys. Rev. Lett.* **2011**, *107*, 118301.
- (274) Delgado, A. V.; González-Caballero, F.; Hunter, R. J.; Koopal, L. K.; Lyklema, J. Measurement and Interpretation of Electrokinetic Phenomena. *J. Colloid Interface Sci.* **2007**, *309*, 194–224.
- (275) Suo, L.; Hu, Y.-S.; Li, H.; Armand, M.; Chen, L. A New Class of Solvent-in-Salt Electrolyte for High-Energy Rechargeable Metallic Lithium Batteries. *Nat. Commun.* **2013**, *4*, 1481.
- (276) Qian, J.; Henderson, W. A.; Xu, W.; Bhattacharya, P.; Engelhard, M.; Borodin, O.; Zhang, J.-G. High Rate and Stable Cycling of Lithium Metal Anode. *Nat. Commun.* **2015**, *6*, 6362.
- (277) Fan, X.; Chen, L.; Ji, X.; Deng, T.; Hou, S.; Chen, J.; Zheng, J.; Wang, F.; Jiang, J.; Xu, K.; et al. Highly Fluorinated Interphases Enable High-Voltage Li-Metal Batteries. *Chem.* **2018**, *4*, 174–185.
- (278) Piao, N.; Ji, X.; Xu, H.; Fan, X.; Chen, L.; Liu, S.; Garaga, M. N.; Greenbaum, S. G.; Wang, L.; Wang, C.; et al. Countersolvent Electrolytes for Lithium-Metal Batteries. *Adv. Energy Mater.* **2020**, *10*, 1903568.
- (279) Chen, S.; Zheng, J.; Mei, D.; Han, K. S.; Engelhard, M. H.; Zhao, W.; Xu, W.; Liu, J.; Zhang, J.-G. High-Voltage Lithium-Metal Batteries Enabled by Localized High-Concentration Electrolytes. *Adv. Mater.* **2018**, *30*, 1706102.
- (280) Wang, H.; Matsui, M.; Kuwata, H.; Sonoki, H.; Matsuda, Y.; Shang, X.; Takeda, Y.; Yamamoto, O.; Imanishi, N. A Reversible Dendrite-Free High-Areal-Capacity Lithium Metal Electrode. *Nat. Commun.* **2017**, *8*, 15106.
- (281) Ueno, K.; Murai, J.; Ikeda, K.; Tsuzuki, S.; Tsuchiya, M.; Tataro, R.; Mandai, T.; Umebayashi, Y.; Dokko, K.; Watanabe, M. Li⁺ Solvation and Ionic Transport in Lithium Solvate Ionic Liquids Diluted by Molecular Solvents. *J. Phys. Chem. C* **2016**, *120*, 15792–15802.
- (282) Ueno, K.; Murai, J.; Moon, H.; Dokko, K.; Watanabe, M. A Design Approach to Lithium-Ion Battery Electrolyte Based on Diluted Solvate Ionic Liquids. *J. Electrochem. Soc.* **2017**, *164*, A6088–A6094.
- (283) Doi, T.; Shimizu, Y.; Hashinuchi, M.; Inaba, M. Dilution of Highly Concentrated LiBF₄/Propylene Carbonate Electrolyte Solution with Fluoroalkyl Ethers for 5-V LiNi_{0.5}Mn_{1.5}O₄ Positive Electrodes. *J. Electrochem. Soc.* **2017**, *164*, A6412–A6416.
- (284) Qin, L.; Xiao, N.; Zheng, J.; Lei, Y.; Zhai, D.; Wu, Y. Localized High-Concentration Electrolytes Boost Potassium Storage in High-Loading Graphite. *Adv. Energy Mater.* **2019**, *9*, 1902618.
- (285) Huang, A.; Liu, H.; Manor, O.; Liu, P.; Friend, J. Enabling Rapid Charging Lithium Metal Batteries via Surface Acoustic Wave-Driven Electrolyte Flow. *Adv. Mater.* **2020**, *32*, 1907516.
- (286) Shen, K.; Wang, Z.; Bi, X.; Ying, Y.; Zhang, D.; Jin, C.; Hou, G.; Cao, H.; Wu, L.; Zheng, G.; et al. Magnetic Field–Suppressed Lithium Dendrite Growth for Stable Lithium-Metal Batteries. *Adv. Energy Mater.* **2019**, *9*, 1900260.
- (287) Wang, A.; Deng, Q.; Deng, L.; Guan, X.; Luo, J. Eliminating Tip Dendrite Growth by Lorentz Force for Stable Lithium Metal Anodes. *Adv. Funct. Mater.* **2019**, *29*, 1902630.
- (288) Enze, L. The Application of a Surface Charge Density Distribution Function to the Solution of Boundary Value Problems. *J. Phys. D: Appl. Phys.* **1987**, *20*, 1609–1615.
- (289) Enze, L. The Distribution Function of Surface Charge Density with Respect to Surface Curvature. *J. Phys. D: Appl. Phys.* **1986**, *19*, 1–6.
- (290) Aurbach, D. Review of Selected Electrode–Solution Interactions which Determine the Performance of Li and Li Ion Batteries. *J. Power Sources* **2000**, *89*, 206–218.
- (291) Aurbach, D.; Zinigrad, E.; Cohen, Y.; Teller, H. A Short Review of Failure Mechanisms of Lithium Metal and Lithiated Graphite Anodes in Liquid Electrolyte Solutions. *Solid State Ionics* **2002**, *148*, 405–416.
- (292) Sadiku, M. N. *Elements of Electromagnetics*; Oxford University Press, 2014.
- (293) Ding, F.; Xu, W.; Graff, G. L.; Zhang, J.; Sushko, M. L.; Chen, X.; Shao, Y. Y.; Engelhard, M. H.; Nie, Z. M.; Xiao, J.; et al. Dendrite-Free Lithium Deposition via Self-Healing Electrostatic Shield Mechanism. *J. Am. Chem. Soc.* **2013**, *135*, 4450–4456.
- (294) Ding, F.; Xu, W.; Chen, X.; Zhang, J.; Shao, Y.; Engelhard, M. H.; Zhang, Y.; Blake, T. A.; Graff, G. L.; Liu, X.; et al. Effects of Cesium Cations in Lithium Deposition via Self-Healing Electrostatic Shield Mechanism. *J. Phys. Chem. C* **2014**, *118*, 4043–4049.
- (295) Goodman, J. K. S.; Kohl, P. A. Effect of Alkali and Alkaline Earth Metal Salts on Suppression of Lithium Dendrites. *J. Electrochem. Soc.* **2014**, *161*, D418–D424.
- (296) Wu, B.; Liu, Q.; Mu, D.; Xu, H.; Wang, L.; Shi, L.; Gai, L.; Wu, F. Suppression of lithium dendrite growth by introducing a low reduction potential complex cation in the electrolyte. *RSC Adv.* **2016**, *6*, S1738–S1746.
- (297) Tikekar, M. D.; Archer, L. A.; Koch, D. L. Stability Analysis of Electrodeposition across a Structured Electrolyte with Immobilized Anions. *J. Electrochem. Soc.* **2014**, *161*, A847–A855.
- (298) Zuo, T. T.; Wu, X. W.; Yang, C. P.; Yin, Y. X.; Ye, H.; Li, N. W.; Guo, Y. G. Graphitized Carbon Fibers as Multifunctional 3D Current Collectors for High Areal Capacity Li Anodes. *Adv. Mater.* **2017**, *29*, 1700389.
- (299) Luo, W.; Zhang, Y.; Xu, S. M.; Dai, J. Q.; Hitz, E. M.; Li, Y. J.; Yang, C. P.; Chen, C. J.; Liu, B. Y.; Hu, L. B. Encapsulation of Metallic Na in an Electrically Conductive Host with Porous Channels as a Highly Stable Na Metal Anode. *Nano Lett.* **2017**, *17*, 3792–3797.
- (300) Wang, A.; Zhang, X.; Yang, Y.-W.; Huang, J.; Liu, X.; Luo, J. Horizontal Centripetal Plating in the Patterned Voids of Li/Graphene Composites for Stable Lithium-Metal Anodes. *Chem.* **2018**, *4*, 2192–2200.
- (301) Zou, P.; Chiang, S.-W.; Li, J.; Wang, Y.; Wang, X.; Wu, D.; Nairan, A.; Kang, F.; Yang, C. Ni@Li₂O Co-axial Nanowire based Reticular Anode: Tuning Electric Field Distribution for Homogeneous Lithium Deposition. *Energy Stor. Mater.* **2019**, *18*, 155–164.
- (302) Hong, B.; Fan, H.; Cheng, X.-B.; Yan, X.; Hong, S.; Dong, Q.; Gao, C.; Zhang, Z.; Lai, Y.; Zhang, Q. Spatially Uniform Deposition of Lithium Metal in 3D Janus Hosts. *Energy Stor. Mater.* **2019**, *16*, 259–266.
- (303) Liu, Y. Y.; Lin, D. C.; Liang, Z.; Zhao, J.; Yan, K.; Cui, Y. Lithium-Coated Polymeric Matrix as a Minimum Volume-Change and Dendrite-Free Lithium Metal Anode. *Nat. Commun.* **2016**, *7*, 10992.
- (304) Pu, J.; Li, J.; Zhang, K.; Zhang, T.; Li, C.; Ma, H.; Zhu, J.; Braun, P. V.; Lu, J.; Zhang, H. Conductivity and Lithiophilicity Gradients Guide Lithium Deposition to Mitigate Short Circuits. *Nat. Commun.* **2019**, *10*, 1896.
- (305) Zheng, H.; Zhang, Q.; Chen, Q.; Xu, W.; Xie, Q.; Cai, Y.; Ma, Y.; Qiao, Z.; Luo, Q.; Lin, J.; Wang, L.; Qu, B.; Sa, B.; Peng, D.-L. 3D Lithiophilic–Lithiophobic–Lithiophilic Dual-Gradient Porous Skeleton for Highly Stable Lithium Metal Anode. *J. Mater. Chem. A* **2020**, *8*, 313–322.
- (306) Cao, Z.; Li, B.; Yang, S. Dendrite-Free Lithium Anodes with Ultra-Deep Stripping and Plating Properties Based on Vertically

- Oriented Lithium-Copper-Lithium Arrays. *Adv. Mater.* **2019**, *31*, 1901310.
- (307) Zou, P.; Chiang, S. W.; Zhan, H.; Sui, Y.; Liu, K.; Hu, S.; Su, S.; Li, J.; Kang, F.; Yang, C. A Periodic “Self-Correction” Scheme for Synchronizing Lithium Plating/Stripping at Ultrahigh Cycling Capacity. *Adv. Funct. Mater.* **2020**, *30*, 1910532.
- (308) Higashi, S.; Lee, S. W.; Lee, J. S.; Takechi, K.; Cui, Y. Avoiding Short Circuits from Zinc Metal Dendrites in Anode by Backside-plating Configuration. *Nat. Commun.* **2016**, *7*, 11801.
- (309) Sun, C.; Wu, T.; Wang, J.; Li, W.; Jin, J.; Yang, J.; Wen, Z. Favorable Lithium Deposition Behaviors on Flexible Carbon Microtube Skeleton Enable a High-performance Lithium Metal Anode. *J. Mater. Chem. A* **2018**, *6*, 19159–19166.
- (310) Zhao, J.; Zhou, G.; Yan, K.; Xie, J.; Li, Y.; Liao, L.; Jin, Y.; Liu, K.; Hsu, P. C.; Wang, J.; et al. Air-stable and freestanding lithium alloy/graphene foil as an alternative to lithium metal anodes. *Nat. Nanotechnol.* **2017**, *12*, 993–999.
- (311) Wang, S. H.; Yin, Y. X.; Zuo, T. T.; Dong, W.; Li, J. Y.; Shi, J. L.; Zhang, C. H.; Li, N. W.; Li, C. J.; Guo, Y.-G. Stable Li Metal Anodes via Regulating Lithium Plating/Stripping in Vertically Aligned Microchannels. *Adv. Mater.* **2017**, *29*, 1703729.
- (312) Zhang, W.-J. Lithium insertion/extraction mechanism in alloy anodes for lithium-ion batteries. *J. Power Sources* **2011**, *196*, 877–885.
- (313) Jin, S.; Ye, Y.; Niu, Y.; Xu, Y.; Jin, H.; Wang, J.; Sun, Z.; Cao, A.; Wu, X.; Luo, Y.; et al. Solid-Solution-Based Metal Alloy Phase for Highly Reversible Lithium Metal Anode. *J. Am. Chem. Soc.* **2020**, *142*, 8818–8826.
- (314) Dologlou, E. Self-Diffusion in Solid Lithium. *Glass Phys. Chem.* **2010**, *36*, 570–574.
- (315) Kong, L. L.; Wang, L.; Ni, Z. C.; Liu, S.; Li, G. R.; Gao, X. P. Lithium–Magnesium Alloy as a Stable Anode for Lithium–Sulfur Battery. *Adv. Funct. Mater.* **2019**, *29*, 1808756.
- (316) Yang, C.; Xie, H.; Ping, W.; Fu, K.; Liu, B.; Rao, J.; Dai, J.; Wang, C.; Pastel, G.; Hu, L. An Electron/Ion Dual-Conductive Alloy Framework for High-Rate and High-Capacity Solid-State Lithium-Metal Batteries. *Adv. Mater.* **2019**, *31*, 1804815.
- (317) Yurkiv, V.; Foroozan, T.; Ramasubramanian, A.; Shahbazian-Yassar, R.; Mashayek, F. The Influence of Stress Field on Li Electrodeposition in Li-Metal Battery. *MRS Commun.* **2018**, *8*, 1285–1291.
- (318) Sun, Z.; Jin, S.; Jin, H.; Du, Z.; Zhu, Y.; Cao, A.; Ji, H.; Wan, L. J. Robust Expandable Carbon Nanotube Scaffold for Ultrahigh-Capacity Lithium-Metal Anodes. *Adv. Mater.* **2018**, *30*, 1800884.
- (319) Yoo, D. J.; Elabd, A.; Choi, S.; Cho, Y.; Kim, J.; Lee, S. J.; Choi, S. H.; Kwon, T. W.; Char, K.; Kim, K. J.; et al. Highly Elastic Polyrotaxane Binders for Mechanically Stable Lithium Hosts in Lithium-Metal Batteries. *Adv. Mater.* **2019**, *31*, 1901645.
- (320) Chen, J.; Zhao, J.; Lei, L.; Li, P.; Chen, J.; Zhang, Y.; Wang, Y.; Ma, Y.; Wang, D. Dynamic Intelligent Cu Current Collectors for Ultrastable Lithium Metal Anodes. *Nano Lett.* **2020**, *20*, 3403–3410.
- (321) Liu, K.; Kong, B.; Liu, W.; Sun, Y.; Song, M.-S.; Chen, J.; Liu, Y.; Lin, D.; Pei, A.; Cui, Y. Stretchable Lithium Metal Anode with Improved Mechanical and Electrochemical Cycling Stability. *Joule* **2018**, *2*, 1857–1865.
- (322) Aurbach, D.; Gamolsky, K.; Markovsky, B.; Gofer, Y.; Schmidt, M.; Heider, U. On the Use of Vinylene Carbonate (VC) as an Additive to Electrolyte Solutions for Li-Ion Batteries. *Electrochim. Acta* **2002**, *47*, 1423–1439.
- (323) Sato, K.; Zhao, L.; Okada, S.; Yamaki, J.-i. LiPF₆/Methyl Difluoroacetate Electrolyte with Vinylene Carbonate Additive for Li-Ion Batteries. *J. Power Sources* **2011**, *196*, 5617–5622.
- (324) Burns, J. C.; Petibon, R.; Nelson, K. J.; Sinha, N. N.; Kassam, A.; Way, B. M.; Dahn, J. R. Studies of the Effect of Varying Vinylene Carbonate (VC) Content in Lithium Ion Cells on Cycling Performance and Cell Impedance. *J. Electrochem. Soc.* **2013**, *160*, A1668–A1674.
- (325) McMillan, R.; Slegr, H.; Shu, Z. X.; Wang, W. Fluoroethylene Carbonate Electrolyte and Its Use in Lithium Ion Batteries with Graphite Anodes. *J. Power Sources* **1999**, *81*, 20–26.
- (326) Heine, J.; Hilbig, P.; Qi, X.; Niehoff, P.; Winter, M.; Bieker, P. Fluoroethylene Carbonate as Electrolyte Additive in Tetraethylene Glycol Dimethyl Ether based Electrolytes for Application in Lithium Ion and Lithium Metal Batteries. *J. Electrochem. Soc.* **2015**, *162*, A1094–A1101.
- (327) Zhang, X.-Q.; Cheng, X.-B.; Chen, X.; Yan, C.; Zhang, Q. Fluoroethylene Carbonate Additives to Render Uniform Li Deposits in Lithium Metal Batteries. *Adv. Funct. Mater.* **2017**, *27*, 1605989.
- (328) Liu, Q. C.; Xu, J. J.; Yuan, S.; Chang, Z. W.; Xu, D.; Yin, Y. B.; Li, L.; Zhong, H. X.; Jiang, Y. S.; Yan, J. M.; et al. Artificial Protection Film on Lithium Metal Anode toward Long-Cycle-Life Lithium-Oxygen Batteries. *Adv. Mater.* **2015**, *27*, 5241–5247.
- (329) Aurbach, D.; Pollak, E.; Elazari, R.; Salitra, G.; Kelley, C. S.; Affinito, J. On the Surface Chemical Aspects of Very High Energy Density, Rechargeable Li–Sulfur Batteries. *J. Electrochem. Soc.* **2009**, *156*, A694.
- (330) Song, J.-H.; Yeon, J.-T.; Jang, J.-Y.; Han, J.-G.; Lee, S.-M.; Choi, N.-S. Effect of Fluoroethylene Carbonate on Electrochemical Performances of Lithium Electrodes and Lithium-Sulfur Batteries. *J. Electrochem. Soc.* **2013**, *160*, A873.
- (331) Lu, Y. Y.; Tu, Z. Y.; Archer, L. A. Stable Lithium Electrodeposition in Liquid and Nanoporous Solid Electrolytes. *Nat. Mater.* **2014**, *13*, 961–969.
- (332) Li, T.; Zhang, X.-Q.; Shi, P.; Zhang, Q. Fluorinated Solid-Electrolyte Interphase in High-Voltage Lithium Metal Batteries. *Joule* **2019**, *3*, 2647–2661.
- (333) Wang, D.; Luan, C.; Zhang, W.; Liu, X.; Sun, L.; Liang, Q.; Qin, T.; Zhao, Z.; Zhou, Y.; Wang, P.; et al. Zipper-Inspired SEI Film for Remarkably Enhancing the Stability of Li Metal Anode via Nucleation Barriers Controlled Weaving of Lithium Pits. *Adv. Energy Mater.* **2018**, *8*, 1800650.
- (334) Liu, K.; Pei, A.; Lee, H. R.; Kong, B.; Liu, N.; Lin, D.; Liu, Y.; Liu, C.; Hsu, P. C.; Bao, Z.; et al. Lithium Metal Anodes with an Adaptive “Solid-Liquid” Interfacial Protective Layer. *J. Am. Chem. Soc.* **2017**, *139*, 4815–4820.
- (335) Liu, F.; Xiao, Q.; Wu, H. B.; Shen, L.; Xu, D.; Cai, M.; Lu, Y. Fabrication of Hybrid Silicate Coatings by a Simple Vapor Deposition Method for Lithium Metal Anodes. *Adv. Energy Mater.* **2018**, *8*, 1701744.
- (336) Bai, M.; Xie, K.; Yuan, K.; Zhang, K.; Li, N.; Shen, C.; Lai, Y.; Vajtai, R.; Ajayan, P.; Wei, B. A Scalable Approach to Dendrite-Free Lithium Anodes via Spontaneous Reduction of Spray-Coated Graphene Oxide Layers. *Adv. Mater.* **2018**, *30*, 1801213.
- (337) Liu, Y.; Tzeng, Y.-K.; Lin, D.; Pei, A.; Lu, H.; Melosh, N. A.; Shen, Z.-X.; Chu, S.; Cui, Y. An Ultrastrong Double-Layer Nanodiamond Interface for Stable Lithium Metal Anodes. *Joule* **2018**, *2*, 1595–1609.
- (338) Yan, K.; Lee, H. W.; Gao, T.; Zheng, G.; Yao, H.; Wang, H.; Lu, Z.; Zhou, Y.; Liang, Z.; Liu, Z.; et al. Ultrathin Two-Dimensional Atomic Crystals as Stable Interfacial Layer for Improvement of Lithium Metal Anode. *Nano Lett.* **2014**, *14*, 6016–6022.
- (339) Shen, X.; Li, Y.; Qian, T.; Liu, J.; Zhou, J.; Yan, C.; Goodenough, J. B. Lithium Anode Stable in Air for Low-Cost Fabrication of a Dendrite-Free Lithium Battery. *Nat. Commun.* **2019**, *10*, 900.
- (340) Zhu, B.; Jin, Y.; Hu, X.; Zheng, Q.; Zhang, S.; Wang, Q.; Zhu, J. Poly(dimethylsiloxane) Thin Film as a Stable Interfacial Layer for High-Performance Lithium-Metal Battery Anodes. *Adv. Mater.* **2017**, *29*, 1603755.
- (341) Kim, J. Y.; Kim, A. Y.; Liu, G.; Woo, J. Y.; Kim, H.; Lee, J. K. Li₄SiO₄-Based Artificial Passivation Thin Film for Improving Interfacial Stability of Li Metal Anodes. *ACS Appl. Mater. Interfaces* **2018**, *10*, 8692–8701.
- (342) Kozen, A. C.; Lin, C.-F.; Pearse, A. J.; Schroeder, M. A.; Han, X.; Hu, L.; Lee, S.-B.; Rubloff, G. W.; Noked, M. Next-Generation Lithium Metal Anode Engineering via Atomic Layer Deposition. *ACS Nano* **2015**, *9*, 5884–5892.
- (343) Pang, Q.; Liang, X.; Shyamsunder, A.; Nazar, L. F. An In Vivo Formed Solid Electrolyte Surface Layer Enables Stable Plating of Li Metal. *Joule* **2017**, *1*, 871–886.

- (344) Han, X.; Gong, Y.; Fu, K. K.; He, X.; Hitz, G. T.; Dai, J.; Pearse, A.; Liu, B.; Wang, H.; Rubloff, G.; et al. Negating Interfacial Impedance in Garnet-Based Solid-State Li Metal Batteries. *Nat. Mater.* **2017**, *16*, 572.
- (345) Gao, Y.; Zhao, Y.; Li, Y. C.; Huang, Q.; Mallouk, T. E.; Wang, D. Interfacial Chemistry Regulation via a Skin-Grafting Strategy Enables High-Performance Lithium-Metal Batteries. *J. Am. Chem. Soc.* **2017**, *139*, 15288–15291.
- (346) Sun, Y.; Zhao, Y.; Wang, J.; Liang, J.; Wang, C.; Sun, Q.; Lin, X.; Adair, K. R.; Luo, J.; Wang, D.; et al. A Novel Organic “Polyurea” Thin Film for Ultralong-Life Lithium-Metal Anodes via Molecular-Layer Deposition. *Adv. Mater.* **2019**, *31*, 1806541.
- (347) Lopez, J.; Pei, A.; Oh, J. Y.; Wang, G.-J. N.; Cui, Y.; Bao, Z. Effects of Polymer Coatings on Electrodeposited Lithium Metal. *J. Am. Chem. Soc.* **2018**, *140*, 11735–11744.
- (348) Liang, X.; Pang, Q.; Kochetkov, I. R.; Sempere, M. S.; Huang, H.; Sun, X.; Nazar, L. F. A Facile Surface Chemistry Route to a Stabilized Lithium Metal Anode. *Nat. Energy* **2017**, *2*, 17119.
- (349) Lee, J.-I.; Shin, M.; Hong, D.; Park, S. Efficient Li-Ion-Conductive Layer for the Realization of Highly Stable High-Voltage and High-Capacity Lithium Metal Batteries. *Adv. Energy Mater.* **2019**, *9*, 1803722.
- (350) Yan, C.; Cheng, X. B.; Tian, Y.; Chen, X.; Zhang, X. Q.; Li, W. J.; Huang, J. Q.; Zhang, Q. Dual-Layered Film Protected Lithium Metal Anode to Enable Dendrite-Free Lithium Deposition. *Adv. Mater.* **2018**, *30*, 1707629.
- (351) Li, G.; Huang, Q.; He, X.; Gao, Y.; Wang, D.; Kim, S. H.; Wang, D. Self-Formed Hybrid Interphase Layer on Lithium Metal for High-Performance Lithium-Sulfur Batteries. *ACS Nano* **2018**, *12*, 1500–1507.
- (352) Liu, W.; Li, W.; Zhuo, D.; Zheng, G.; Lu, Z.; Liu, K.; Cui, Y. Core-Shell Nanoparticle Coating as an Interfacial Layer for Dendrite-Free Lithium Metal Anodes. *ACS Cent. Sci.* **2017**, *3*, 135–140.
- (353) Kozen, A. C.; Lin, C.-F.; Zhao, O.; Lee, S. B.; Rubloff, G. W.; Noked, M. Stabilization of Lithium Metal Anodes by Hybrid Artificial Solid Electrolyte Interphase. *Chem. Mater.* **2017**, *29*, 6298–6307.
- (354) Hao, X.; Zhu, J.; Jiang, X.; Wu, H.; Qiao, J.; Sun, W.; Wang, Z.; Sun, K. Ultrastrong Polyoxazole Nanofiber Membranes for Dendrite-Proof and Heat-Resistant Battery Separators. *Nano Lett.* **2016**, *16*, 2981–2987.
- (355) Foroozan, T.; Soto, F. A.; Yurkiv, V.; Sharifi-Asl, S.; Deivanayagam, R.; Huang, Z.; Rojaee, R.; Mashayek, F.; Balbuena, P. B.; Shahbazian-Yassar, R. Synergistic Effect of Graphene Oxide for Impeding the Dendritic Plating of Li. *Adv. Funct. Mater.* **2018**, *28*, 1705917.
- (356) Wilkinson, D. P.; Blom, H.; Brandt, K.; Wainwright, D. Effects of Physical Constraints on Li Cyclability. *J. Power Sources* **1991**, *36*, 517–527.
- (357) Hirai, T.; Yoshimatsu, I.; Yamaki, J. i. Influence of Electrolyte on Lithium Cycling Efficiency with Pressurized Electrode Stack. *J. Electrochem. Soc.* **1994**, *141*, 611–614.
- (358) Louli, A. J.; Genovese, M.; Weber, R.; Hames, S. G.; Logan, E. R.; Dahn, J. R. Exploring the Impact of Mechanical Pressure on the Performance of Anode-Free Lithium Metal Cells. *J. Electrochem. Soc.* **2019**, *166*, A1291–A1299.
- (359) Weber, R.; Genovese, M.; Louli, A. J.; Hames, S.; Martin, C.; Hill, I. G.; Dahn, J. R. Long Cycle Life and Dendrite-Free Lithium Morphology in Anode-Free Lithium Pouch Cells Enabled by a Dual-Salt Liquid Electrolyte. *Nat. Energy* **2019**, *4*, 683–689.
- (360) Guo, Y.; Li, D.; Xiong, R.; Li, H. Investigation of the Temperature-Dependent Behaviours of Li Metal Anode. *Chem. Commun.* **2019**, *55*, 9773–9776.
- (361) Yang, X.-G.; Liu, T.; Gao, Y.; Ge, S.; Leng, Y.; Wang, D.; Wang, C.-Y. Asymmetric Temperature Modulation for Extreme Fast Charging of Lithium-Ion Batteries. *Joule* **2019**, *3*, 3002–3019.
- (362) Gao, Y.; Rojas, T.; Wang, K.; Liu, S.; Wang, D.; Chen, T.; Wang, H.; Ngo, A. T.; Wang, D. Low-Temperature and High-Rate-Charging Lithium Metal Batteries Enabled by an Electrochemically Active Monolayer-Regulated Interface. *Nat. Energy* **2020**, *5*, 534–542.
- (363) Fan, X.; Ji, X.; Chen, L.; Chen, J.; Deng, T.; Han, F.; Yue, J.; Piao, N.; Wang, R.; Zhou, X.; Xiao, X.; Chen, L.; Wang, C. All-Temperature Batteries Enabled by Fluorinated Electrolytes with Non-Polar Solvents. *Nat. Energy* **2019**, *4*, 882–890.
- (364) Holoubek, J.; Yu, M.; Yu, S.; Li, M.; Wu, Z.; Xia, D.; Bhaladhare, P.; Gonzalez, M. S.; Pascal, T. A.; Liu, P.; Chen, Z. An All-Fluorinated Ester Electrolyte for Stable High-Voltage Li Metal Batteries Capable of Ultra-Low-Temperature Operation. *ACS Energy Lett.* **2020**, *5*, 1438–1447.
- (365) Gupta, A.; Manthiram, A. Designing Advanced Lithium-Based Batteries for Low-Temperature Conditions. *Adv. Energy Mater.* **2020**, *10*, 2001972.
- (366) Rustomji, C. S.; Yang, Y.; Kim, T. K.; Mac, J.; Kim, Y. J.; Caldwell, E.; Chung, H.; Meng, Y. S. Liquefied Gas Electrolytes for Electrochemical Energy Storage Devices. *Science* **2017**, *356*, eaal4263.
- (367) Yang, Y.; Davies, D. M.; Yin, Y.; Borodin, O.; Lee, J. Z.; Fang, C.; Olgun, M.; Zhang, Y.; Sabrina, E. S.; Wang, X.; Rustomji, C. S.; Meng, Y. S. High-Efficiency Lithium-Metal Anode Enabled by Liquefied Gas Electrolytes. *Joule* **2019**, *3*, 1986–2000.
- (368) Yang, Y.; Yin, Y.; Davies, D. M.; Zhang, M.; Mayer, M.; Zhang, Y.; Sabrina, E. S.; Wang, S.; Lee, J. Z.; Borodin, O.; Rustomji, C. S.; Meng, Y. S. Liquefied Gas Electrolytes for Wide-Temperature Lithium Metal Batteries. *Energy Environ. Sci.* **2020**, *13*, 2209–2219.
- (369) Sun, F.; Zhou, D.; He, X.; Osenberg, M.; Dong, K.; Chen, L.; Mei, S.; Hilger, A.; Markötter, H.; Lu, Y.; et al. Morphological Reversibility of Modified Li-Based Anodes for Next-Generation Batteries. *ACS Energy Lett.* **2020**, *5*, 152–161.
- (370) Ren, X. C.; Zhang, X. Q.; Xu, R.; Huang, J. Q.; Zhang, Q. Analyzing Energy Materials by Cryogenic Electron Microscopy. *Adv. Mater.* **2020**, *32*, 1908293.
- (371) Chen, Y.; Wang, Z.; Li, X.; Yao, X.; Wang, C.; Li, Y.; Xue, W.; Yu, D.; Kim, S. Y.; Yang, F.; et al. Li metal Deposition and Stripping in A Solid-State Battery via Coble Creep. *Nature* **2020**, *578*, 251–255.
- (372) Niu, C.; Lee, H.; Chen, S.; Li, Q.; Du, J.; Xu, W.; Zhang, J.-G.; Whittingham, M. S.; Xiao, J.; Liu, J. High-Energy Lithium Metal Pouch Cells with Limited Anode Swelling and Long Stable Cycles. *Nat. Energy* **2019**, *4*, 551–559.
- (373) Adams, B. D.; Zheng, J.; Ren, X.; Xu, W.; Zhang, J.-G. Accurate Determination of Coulombic Efficiency for Lithium Metal Anodes and Lithium Metal Batteries. *Adv. Energy Mater.* **2018**, *8*, 1702097.
- (374) Xiao, J.; Li, Q.; Bi, Y.; Cai, M.; Dunn, B.; Glossmann, T.; Liu, J.; Osaka, T.; Sugiura, R.; Wu, B.; et al. Understanding and Applying Coulombic Efficiency in Lithium Metal Batteries. *Nat. Energy* **2020**, *5*, 561–568.
- (375) Genovese, M.; Louli, A. J.; Weber, R.; Hames, S.; Dahn, J. R. Measuring the Coulombic Efficiency of Lithium Metal Cycling in Anode-Free Lithium Metal Batteries. *J. Electrochem. Soc.* **2018**, *165*, A3321–A3325.
- (376) Zhao, J.; Lee, H.-W.; Sun, J.; Yan, K.; Liu, Y. Y.; Liu, W.; Lu, Z. D.; Lin, D. C.; Zhou, G. M.; Cui, Y. Metallurgically Lithiated SiO_x Anode with High Capacity and Ambient Air Compatibility. *Proc. Natl. Acad. Sci. U. S. A.* **2016**, *113*, 7408–7413.
- (377) Shin, J.; Lee, J.; Park, Y.; Choi, J. W. Aqueous Zinc Ion Batteries: Focus on Zinc Metal Anodes. *Chem. Sci.* **2020**, *11*, 2028–2044.
- (378) Blanc, L. E.; Kundu, D.; Nazar, L. F. Scientific Challenges for the Implementation of Zn-Ion Batteries. *Joule* **2020**, *4*, 771–799.